The influence of dynamic response characteristics on traumatic brain injury

Andrew Post

Thesis submitted to the Faculty of Graduate and Postdoctoral Studies in partial fulfillment of the requirements for a doctoral degree in Human Kinetics

Human Kinetics

Faculty of Health Sciences

University of Ottawa

Abstract

Research into traumatic brain injury (TBI) mechanisms is essential for the development of methods to prevent its occurrence. One of the most common ways to incur a TBI is from falls, especially for the young and very old. The purpose of this thesis was to investigate how the acceleration loading curves influenced the occurrence of different types of TBI, namely: epidural hematoma, subdural hematoma, subarachnoid hemorrhage, and contusion. This investigation was conducted in three parts. The first study conducted reconstructions of 20 TBI cases with varying outcomes using MADYMO, Hybrid III, and finite element methodologies. This study provided a dataset of threshold values for each of the TBI injuries measured in parameters of strain and stress. The results of this study indicated that using a combined reconstructive approach produces results which are in keeping with the literature for TBI. The second study examined how the characteristics of the loading curves which were produced from each reconstruction influenced the outcome using a principal components analysis. It was found that the duration of the event accounted for much of the variance in the results, followed with the acceleration components. Different curve characteristics also accounted for differing amounts of variance in each of the lesion types. Study 3 examined how the dynamic response of the impact influenced where in the brain a subdural hematoma (SDH) could occur. It was found that the largest magnitudes of acceleration produced SDH in the parietal lobe, and the lowest in the occipital lobe. Overall this thesis examined the mechanism of injury for TBI using a large dataset with methodologies which complement each other's limitations. As a result in depth information of the nature of TBI was attained and information provided which may be used to improve future protection and standard development.

Acknowledgements

First, I would like to thank my supervisor, Dr. Blaine Hoshizaki. His guidance and advice throughout this process was without peer and his presence was equally essential whenever there were issues to which I could not find a solution. I would also like to thank Dr. Michael Gilchrist for not only giving his time and advice selflessly but also his hospitality for my many visits to the University College Dublin. Finally, I must thank Dr. Manuel Forero Rueda, who received my stream of questions without complaint throughout the years and without whom I certainly would not have completed this dissertation.

I would like to thank the Neurotrauma Impact Science Laboratory team of undergraduate and graduate students with whom I have had the pleasure of working with over the years. More specifically, Phil, Evan, Marshall, Anna, Clara, Lauren, Katrina, Scott, Genille, and Leslie. You have all challenged me to be better at what I do, made the laboratory a place I enjoyed every day (even when equipment broke), and influenced me in many ways. Without all of you this process would have been a much more difficult and painful experience instead of one of the best times of my life.

Thank you to my family, in particular my parents and sister, whose constant support was invaluable to the completion of this degree. Also, thank you Oro for getting me away from my desk for a walk when I needed a break.

Finally I must thank my wife, Shaunna, for her constant support and objective opinion throughout my studies. Her selfless help with my writing by proof reading manuscripts with information she probably wished she didn't need or want to know was priceless. Without her I would not have been able to be who I am today. Last, but not least, thank you Olivia, for showing me the great enjoyment that can be had in the smallest things. Those are the truly most important accomplishments in life.

Table of Contents

List of abbreviations

AIS	Abbreviated Injury Scale
CG	Centre of Gravity
CSDM	Cumulative Strain Damage Measure
CNS	Central Nervous System
CSF	Cerebro Spinal Fluid
CT	Computed Tomography
DAI	Diffuse Axonal Injury
DTI	Diffuse Tensor Imaging
EDH	Epidural Hematoma
FAA	Federal Aviation Administration
FE	Finite Element
FEA	Finite Element Analysis
FEM	Finite Element Model
GAMBIT	Generalized Acceleration Model for Brain Injury Threshold
GCS	Glasgow Coma Scale
GSI	Gadd Severity Index
HIC	Head Injury Criterion
HIP	Head Impact Power
HITs	Head Impact Telemetry system
ICP	Intracranial Pressure
ISO	International Standards Organization
MADYMO	Mathematical Dynamic Models
MRI	Magnetic Resonance Imaging
mTBI	mild Traumatic Brain Injury
NASA	National Aeronautics and Space Administration
NDT	Neutral Density Targets
NHTSA	National Highway Traffic Safety Administration
SAE	Society of Automotive Engineers
SAH	Subarachnoid Hemorrhage
SDH	Subdural Hematoma
SIMon	Simulated Injury monitor
TBI	Traumatic Brain Injury
UCDBTM	University College Dublin Brain Trauma Model
WSTC	Wayne State Tolerance Curve
WSUHIM	Wayne State University Head Injury Model

PART I

Chapter 1

Introduction

Traumatic brain injuries (TBI) contribute to a high degree of mortality and morbidity in society. The costs of these injuries are high, both in lost productivity and care facilities for those no longer able to care for themselves. In the United States, there are approximately 1.7 million cases of traumatic brain injuries every year (Sosin et al., 1996). While Canadian statistics in this area are not complete, it can be assumed that the number of traumatic brain injuries in Canada to be roughly 170,000 per year. In addition, 150,000 Canadians are likely to suffer nonfatal traumatic brain injuries that will not require hospital treatment (CIHI, 2006). Of these injuries there would likely be associated effects including sick days and rehabilitation which can create costs in excess of 10 billion dollars a year (CAN). The elderly and children are the most likely to experience a traumatic brain injury, with falls being the most common cause of injury (Styrke et al., 2007). Of all injuries, brain trauma has the singular distinction of having the highest rates of morbidity and mortality (Centres for Disease Control and Prevention, 1997). As a result, a great deal of research has been undertaken to help prevent these injuries from occurring. Recently, much attention has been paid to brain injuries due to their serious effects on the nervous system and the repercussions to the quality of life of the injured person.

Traumatic brain injuries (TBI) occur when the head is subject to either a rapid acceleration or deceleration, leading to irreversible shearing or deformation of brain tissue or vasculature (Viano et al., 1989). These traumatic brain injuries can be defined by the following categories: contusions, intercranial bleeds, and diffuse axonal injuries (DAI). These occur in daily events, such as falls, sports, and more frequently in car accidents. Research involving the prevention of traumatic brain injuries generally focuses on the mechanism governing their creation (Viano et al., 1989). Once the mechanism of injury has been identified a threshold value based upon a dependent variable describing the event could be established (King et al., 2003). These thresholds or tolerance metrics are then used to create pass/fail criteria for standards to govern the development of safer cars, helmets, and play structures (King et al., 2003, Kleiven, 2007).

Currently the primary tolerance metrics being used to develop protective head equipment are peak resultant linear acceleration and integrations of peak acceleration time histories (Hoshizaki and Brien, 2004). Peak resultant linear acceleration was developed as an injury metric based upon intracranial pressure research with animals (Gurdjian and Gurdjian, 1975). However, the correlation of peak resultant linear acceleration to actual injury was low, which led to the development of integrations of the acceleration time curve of an impact. The Gadd Severity Index and Head Injury Criterion were among the first attempts to link the time histories of linear acceleration curves to injury (Hoshizaki and Brien, 2004). These integrations were adopted by many standards organizations, but research has shown that they too are limited when correlated with head injury (Goldsmith, 1981). The lack of correlation of tolerance levels based solely on kinematic descriptors to injury has led researchers to use advanced computational modeling to simulate the effects of three-dimensional motion on brain deformation.

Recent research investigating metrics of brain injury has employed the use of finite element modeling (FEM) (Horgan and Gilchrist, 2003; Willinger and Baumgartner, 2003a/b; Zhang et al., 2004; Kleiven, 2007). When used in conjunction with injury research this technique allows for investigations into brain deformation based tolerance criteria (King et al., 2003). Due to the lack of correlation of peak resultant accelerations to brain injury, this method is seen as a suitable alternative because it uses the acceleration time histories and its interaction with the brain tissue characteristics to determine the resulting brain deformations (Forero Rueda et al., 2011; Post and Hoshizaki, 2012). While it is generally accepted that the brain deformation response to an impact should be measured to develop the appropriate tolerance criteria, it is currently unknown how the characteristics of the dynamic response contributes to the location and severity of the stresses and strains which are related to brain injury. Earlier work undertaken by the author has demonstrated that different shaped curves with the same peak values in linear and rotational acceleration produce different magnitudes in brain deformation (Post et al., 2012). This supports work identifying low correlations of peak acceleration to brain deformation metrics (Oeur et al., 2011).

To investigate the influence of dynamic response characteristics on brain injury, reconstructions of clinically documented traumatic brain injuries have been undertaken. Such reconstructions allow the investigation of the influence of linear and rotational acceleration time histories (peak, slope, duration etc) on brain deformation metrics (King et al., 2003). Brain injury reconstruction research could not only provide more data on traumatic brain injury thresholds, but also on how the brain deformations are related to impact kinematics. Brain injury research will provide a better understanding of how brain deformations occur and potentially how to reduce the risk and severity of brain injuries using improved helmet, car, and playground designs.

This thesis investigated brain anatomy with respect to modeling the brain and brain injuries. The relationship between neural damage, brain tissue deformation, and the kinematic response to an impact will be discussed. Current injury metrics will be examined and the limitations of these measures discussed. The low correlation of current injury metrics will be investigated as will the pros and cons of finite element modeling as a measure for predicting the risk of brain injury. Finally, the use and application of medical imaging with respect to injury reconstructions will be examined as an aid to establishing location specific injury thresholds.

1.1 Epidemiology of Head Injuries

Of all injuries incurred to the body, head injuries are those that have the highest incidence of death and long term disability. The Canadian Institute for Health Information (CIHI, 2006) showed the number of people admitted to trauma hospitals with severe head injuries as determined by the abbreviated injury scale (AIS) rose by 46% between 2000 and 2004. In 2003/04 of all cases, youth (up to 24 years) had the highest proportion of hospitalizations due to traumatic brain injuries (TBI) representing 30% of all cases (4966 patients) with the elderly (65+) second with 29% of reported cases. The largest proportion of these injuries have been associated with falls (45%) followed by motor vehicle accidents (36%) and assaults (9%). When examined by age group the young and old (40%, 76%) have the highest incidence of brain injury incurred by falling. In the adult population the majority of head injuries are incurred through motor vehicle accidents followed closely by falls.

In the United States there are approximately 1.7 million incidents of traumatic brain injury every year. Over 1.5 million Americans are thought to suffer nonfatal traumatic brain injuries each year which do not require hospitalization (Sosin et al., 1996). Overall, 34% of all injury deaths in the United States are caused by some form of TBI (Centres for Disease Control and Prevention, 1997). The direct and indirect cost of TBI in the United States has been estimated at $60 billion in the year 2000.

Other countries report similar rates of traumatic brain injuries. Sweden reported 354 TBI incidents per 100000 people, with the median age being 23 years. The most common injury event was falls at 55% of all cases followed by motor vehicle accidents (30%). Falls were associated with the highest percentage of TBI for children and the elderly. Of all these cases 34 had intracranial hemorrhage (8% of all those injured) with increasing presentation with increasing age (Styrke et al., 2007). In the UK traffic accidents were responsible for 40% of all TBI cases, with about a third of those suffering permanent disability (Brooks et al., 1997; Viano et al., 1997). The socio-economic costs for traffic accidents in the European Union in 1999 were estimated to be in excess of 160 billion euro (European Transport Safety Council, 1999).

These large numbers of people affected by TBI has not gone unnoticed by the countries in which they occur. In the United States a report from the National Institute of Health (1999) TBI was declared a major health problem in society and efforts need to be made to reduce its incidence and increase identification. The World Health Organization (WHO) arrived at a similar conclusion, identifying mild traumatic brain injury as an important public health problem requiring more research (Cassidy et al., 2004). The research assigned to this area must focus on predicting brain injuries and how they occur so that they can be prevented from happening in the future.

1.2 The Anatomy of the Brain

The brain is one of nature’s most complex organs. It is responsible for thought processes and regulating body functions and for this reason, when injured can cause a high rate of morbidity and mortality. For finite element models of the human head and brain, all the essential structures must be represented. This is no easy feat as the brain is a highly complex system that behaves in a non-linear fashion when under stress. To achieve a valid brain finite element model, modelers must consider the many parts of the brain and how they interact to form a whole. The following section will discuss the anatomy of the brain with respect to modeling and brain injury.

The brain is enveloped within a protective casing of bone known as the skull and is composed of several different complex parts. The male brain is on average 1600g while the female brain averages 1450g, however in terms of brain size by body weight the proportions are equal. The brain can be classified to have three primary parts: i) the cerebrum; ii) the cerebellum; and iii) the brain stem (Marieb, 1998). The cerebrum is composed of two cerebral hemispheres and is the most superior part of the brain. The hemispheres account for 83% of the total brain mass and are the most visible parts of the intact brain. The surfaces of the cerebral hemispheres are marked with ridges called 'gyri' and furrows referred to as sucli. Deeper chasms in the brain tissue are referred to as fissures and are often used as important anatomical landmarks such as the longitudinal fissure and transverse fissure (Marieb, 1998). These fissures act to separate the two cerebral hemispheres with the fibrous bundle known as the corpus callosum, which is the only attachment. Each hemisphere of the cerebrum is composed of grey matter and white matter (Marieb, 1998). The grey matter is the most superficial tissue and is referred to as the cerebral cortex. This tissue consists of neuron cell bodies, dendrites, and unmyelinated axons. This layer is normally only 2 – 4 mm thick, but due to the sulci and gyri has a large surface area (Figure 1).

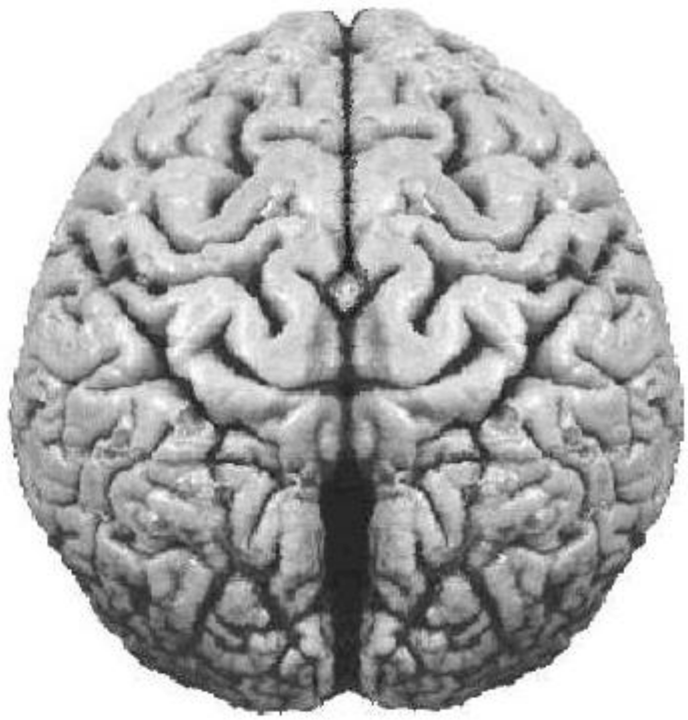

Figure 1. Top view of the human brain showing the longitudinal fissure separating the cerebral hemispheres and the gyri and sulci of the cerebrum (from Horgan, 2005)

The cerebral cortex accounts for roughly 40% of the total brain mass. Functionally, the cerebral cortex contains three areas: i) motor areas; ii) sensory areas; and iii) association areas. Motor areas control voluntary motor functions, sensory areas provide conscious awareness of sensation, and association areas act to integrate diverse information for action. Deep to the grey matter is the cerebral white matter. This matter provides communication between cerebral areas, the cerebral cortex, and lower central nervous system (CNS) centers (Figure 2). White matter is composed of myelinated fibers bundled into large tracts (Marieb, 1998). These tracts are defined by the direction they run in and are known as either commissural, association, or projection. Comissures connect corresponding areas of the two cerebral hemispheres which allows them to function as a coordinated unit. Association fibers transmit impulses within a single hemisphere. Projection fibers are fibers entering the cerebral hemispheres from lower brain or cord centers, and fibers leaving the cortex to travel to lower areas. They tie the cortex to the remainder of the nervous system as well as the receptors and effectors of the body. Of the three types of fibers, projection is the only type to run vertically; commissures and association fibers run horizontally (Marieb, 1998). The cerebral cortices are subdivided into frontal lobes, parietal lobes, temporal lobes, and occipital lobes. Each area is associated with certain functions. The frontal lobe is associated with reasoning, planning, speech and motor functions. The parietal lobes interpret sensory information and integrate that information. The temporal lobes process auditory information and visual information if processed by the occipital lobes (Figure 3).

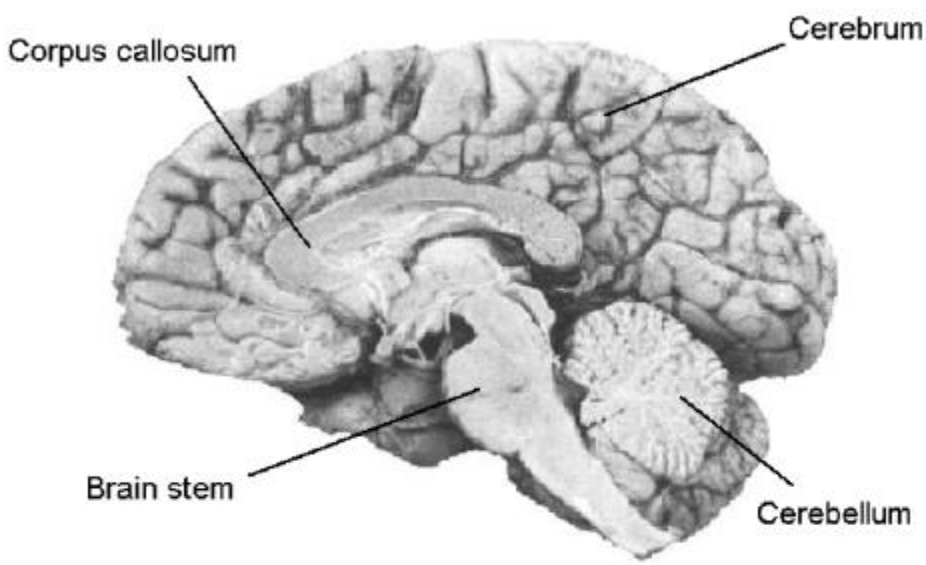

Figure 2. Sagittal slice showing the major components of the brain (From Horgan, 2005)

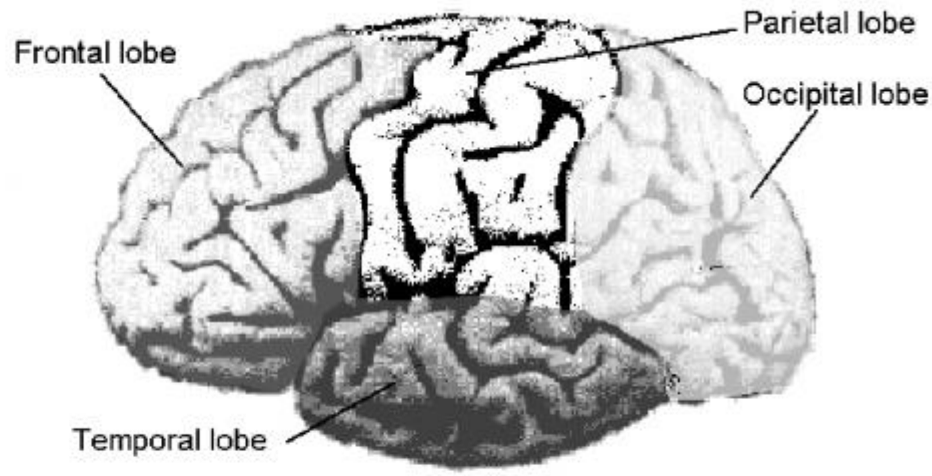

Figure 3. Lateral view of the brain showing the different lobes (from Horgan, 2005).

The cerebellum is the second largest part of the brain, accounting for around 11% of the total brain mass (Figure 2). It is located in the posterior cranial fossa of the skull, under the occipital lobes and is separated from them by the tentorium cerebelli and the transverse cerebral fissure. Like the cerebrum, the cerebellum has a thin outer cortex of grey matter, internal white matter, and small deeply situated pockets of grey matter. The cerebellum acts to coordinate body movements, maintaining muscle tone, posture, and equilibrium. It also plays a major role in skilled motions (Marieb, 1998).

The brain stem is located at the base of the skull where the spinal cord enters the cranial cavity. Like the spinal cord, it is formed of deep grey matter that is surrounded by white matter fiber tracts. The brain stem is composed of three parts: the midbrain, the pons, and the medulla oblongata. The brain stem is known to produce the rigidly programmed automatic behaviours necessary for survival and relays messages between the spinal cord and the cerebrum (Marieb, 1998).

The brain also has spaces referred to as ventricles that are continuous with each other and the central canal of the spinal cord. These hollow ventricular spaces are filled with cerebrospinal fluid (CSF). There are four ventricles and they are all interconnected: the lateral ventricles, the third ventricle and the fourth ventricle. Cerebrospinal fluid is formed in the ventricles, fills them and moves through the lateral and median apertures into the subarachnoid space. The lateral ventricles are large C shaped membranes that pass through all the lobes of the cerebral hemisphere. The sizes of the ventricles are small but can vary. The amount of CSF volume in the ventricles and brain/spinal spaces is normally around 130 ml with 20 ml contained specifically inside the ventricles (Marieb, 1998). The volume of CSF is normally found in the lateral ventricles with the third and fourth ventricles carrying only around 2 ml of the 20 ml.

1.21 The Meninges

The meninges are three connective tissue membranes that lie just external to the central nervous system organs (Figure 4). They serve four primary functions: i) to cover and protect the CNS; ii) protect blood vessels and enclose the venous sinuses; iii) contain cerebrospinal fluid; and iv) form partitions within the skull. From the external layer to the internal layer, the meninges are the dura mater, arachnoid and pia mater (Marieb, 1998).

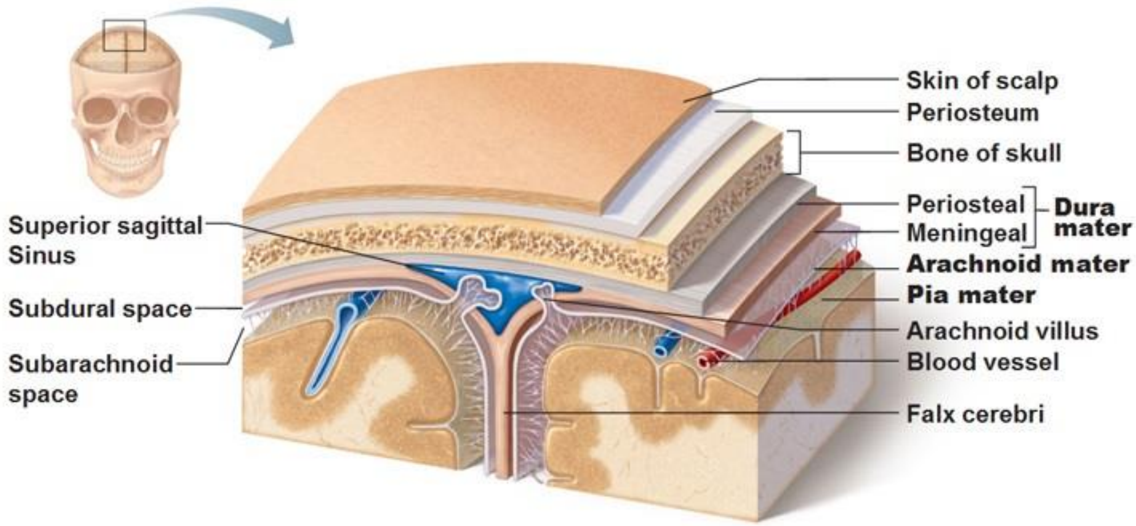

Figure 4. Layers of the meninges (see Antranik.org)

The strongest of the meninges is the dura mater. It has a double membrane with the inelastic periosteal layer attached to the inner surface of the skull and a meningeal layer forming the external covering of the brain. The brain’s dural layers are fused together except in certain areas where they enclose the dural sinuses which collect venous blood from the brain and direct it down into the jugular vein in the neck (Marieb, 1998). In several locations the dura forms flat septa which attaches to the skull which helps to limit the movement of the brain relative to the cranium. The dural septa are known as the falx cerebri, the falx cerebelli, and the tentorium. The falx cerebri is a large fold that dips into the longitudinal fissure between the cerebral hemispheres. The falx cerebelli continues inferiorly from the posterior falx cerebri and forms a midline partition that runs along the vermis of the cerebellum (Marieb, 1998). The tentorium is a near horizontal fold which extends into the transverse fissure between the cerebral hemispheres and the cerebellum.

The arachnoid mater is the middle meninx which is a loose brain covering which never dips into the sulci. It is separated from the dura mater by a narrow cavity called the subdural space. Beneath the arachnoid mater is the subarachnoid space which has weblike extensions which span the gap and secure the membrane to the underlying pia mater (Marieb, 1998). The subarachnoid space is filled with CSF and contains the largest blood vessels to the brain. These blood vessels are susceptible to damage due to the fine elastic properties of the arachnoid mater (Figure 5).

The pia mater is composed of fine connective tissue with many small blood vessels. It is the only meninx to be tightly adhered to the brain, and follows its entire surface. The small arteries which enter the brain tissue carry a sheath of pia mater with them.

The cerebrospinal fluid is located in the brain and spinal cord and forms a protective cushion that gives some buoyancy to the central nervous system organs. The CSF effectively reduces the brain weight by around 97% and also serves to prevent the brain from crushing under its own weight. Once produced, the cerebrospinal fluid moves freely about the ventricles. The CSF serves an additional purpose of protecting the brain and spinal cord from traumatic injury and, along with blood, nourishes the brain. In adults the total CSF volume is around 150 ml, which is replaced every 3 to 4 hours (Marieb, 1998).

This overview of the anatomy of the brain shows how different parts of the brain have different functions and locations. These parts also have different properties. Accurate descriptions of the properties and characteristics of these tissues are essential for the successful creation of an accurate finite element model.

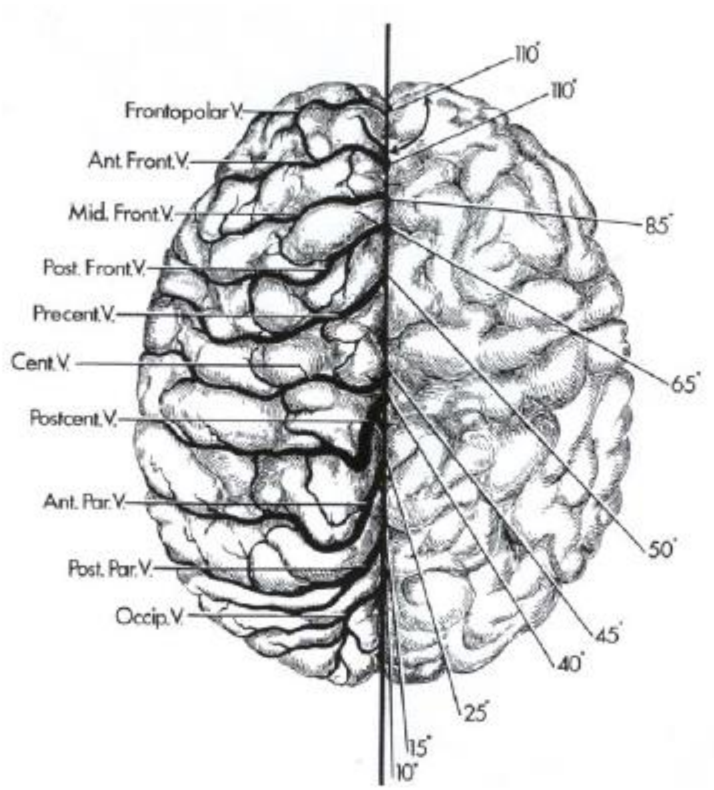

Figure 5. Superior view of the brain showing the main bridging veins and average angles at which the veins enter the sinus on the right (reproduced from Oka et al., 1985)

1.3 Traumatic and Mild Traumatic Brain Injuries

The importance of the brain in regulating body functions and thought processes makes brain injury a high risk to disability and death. Brain injuries can result from either a direct or indirect impact to the head (Viano et al., 1989). Both of these scenarios can cause a high linear and/or rotational acceleration that is the root cause of brain injuries. Brain injuries can be subdivided into focal and diffuse brain injuries. Focal injuries are those brain injuries that are large enough to be seen on medical imaging devices. These injuries are commonly the result of severe translations that cause the brain to lag behind the skull and create stresses on the structures that tether the brain to the cranium resulting in hematoma (Viano et al., 1989). These motions can also cause the brain to bump against the bony protuberances within the skull causing contusions. Focal injuries are categorized into brain contusion and hematoma, of which there are several types. Diffuse injuries are normally the result of head rotation and by definition affect a diffuse volume of tissues in the brain. These injuries are generally only visible microscopically and rarely appear on standard medical imaging devices. As such the data on this type of injury tends to be from postmortem dissections and staining techniques. The mild traumatic brain injury, also known as concussion, is one type of diffuse brain injury. Diffuse axonal injury is the most severe type of diffuse brain injury and commonly results in severe disability and death. It is important to have an understanding of the structures damaged when a brain injury occurs to put the brain injury research into context. The following section discusses focal and diffuse traumatic brain injuries including contusions, hematomas, concussion and diffuse axonal injury.

1.31 Focal injury

Contusion

Contusions are often described as bruises to the brain. Several mechanisms are proposed as resulting in this injury (see Chapter 2). There are two types of contusion, the coup and the contrecoup. The coup contusion occurs below the impact site and the contrecoup contusions occur at a location distal and often diametrically opposite to the initial impact (Gurdjian et al., 1968). The contusion can produce a wide variety of symptoms depending on the location of the brain damage. For example, cortical contusion patients normally remain conscious however brain stem contusions can cause symptoms ranging from unconsciousness to coma depending on severity.

Hematomas

Hematomas (or bleeds) occur when there is damage to the brain vasculature resulting in regions of high pressure from the accumulating blood (Kleiven, 2003). The presence of large amounts of blood can compress the brain tissue and cause severe tissue damage and death. Intracranial hematomas are classed as epidural, subdural, subarachnoid, and intracerebral.

Epidural hematoma

Epidural hematoma is the presence of bleeding above the dura layer and underneath the skull. The source of this bleeding can be venous or arterial in nature. The most common cause of an epidural hematoma is a skull fracture. This results in a build-up of blood within the cranial cavity creates a dangerous increase in pressure and damage to the dural layer (Marieb, 1998).

Subdural hematoma

Subdural hematoma (SDH) occurs when there is a build-up of blood below the dural layer. They are usually a result of tears to the bridging veins which empty into the venous sinuses. The tearing of these veins is often a result of relative brain skull motions resulting from mechanical loading. Small amounts of blood created in this way may be reabsorbed, but larger hematomas mix with the cerebrospinal fluid and this added fluid volume causes a dramatic increase in pressure upon the cerebrum. There are different classifications of subdural hematoma, with acute SDHs requiring attention within 24 hours of the incident, and chronic requiring medical intervention within 11 days of the incident (Marieb, 1998).

Subarachnoid hemorrhage

A subarachnoid hemorrhage is bleeding into the subarachnoid space, which is the area between the arachnoid membrane and the pia mater (Marieb, 1998). This injury can occur spontaneously, but also occurs in response to a blow to the head.

Intracerebral hematoma

Intracerebral hematoma is localized blood volumes found throughout the cerebrum. These types of hematoma are attributed to pressure gradients throughout the cranial cavity (Marieb, 1998).

1.32 Diffuse brain injury

Diffuse brain injuries are separated into two types: concussion (mTBI) and diffuse axonal injury (DAI). These types of injuries are termed 'diffuse' due to the large volumes of distribution of the stresses and strains which cause brain damage and subsequent clinical injury. These types of injury can occur at various levels of energy and have been thought to be caused primarily by rotations (Holbourn, 1943; Gennarelli et al., 1983; Meaney and Smith, 2011). These rotations result in a widespread area of damage over a volume of the brain as opposed to specific locations as would be the case with focal brain injuries.

Mild traumatic brain injury (mTBI)

On the continuum of diffuse brain injury the mTBI, commonly referred to as concussion, would be considered the mildest form. Concussion is defined as a post-traumatic brain dysfunction often characterized by unconsciousness, visual impairment, and disturbance of equilibrium and memory (Levin et al., 2012). This type of injury is thought to occur primarily through rotations and has been found to be commonplace in contact sporting events. These rotations in combination with linear motion create diffuse stresses and strains to brain tissue resulting in transient local deformations leading to symptoms of concussion (Holbourn, 1943). The neural damage often appears to be temporary in nature, but can result in long term debilitating symptoms (McKee et al., 2010). Recently there has been some evidence to suggest that although there appears to be little mechanical damage, there are physiological responses to concussion which can cause long term degeneration of brain tissue (Omalu et al., 2005; McKee et al., 2010; Gavett et al., 2011; Shively et al., 2012). This research has led to concussion becoming an issue which needs to be resolved in sport through better helmet design and adjustments to rules (King et al. 2003; Forero Rueda et al., 2011; Post and Hoshizaki 2012).

Diffuse axonal injury (DAI)

Diffuse axonal injury is a diffuse injury which is identifiable by widespread damage to the white matter axons in the brain stem, cerebellum, and cerebral hemispheres. This damage is thought to be caused primarily through rotations that contribute to a shearing effect on the axons of white matter causing interruption of brain function (Smith and Meaney, 2011). Due to the microscopic nature of this injury it has been difficult to identify outside of autopsy; however recent developments in diffusion tensor imaging (DTI) MRI imaging has offered a method to track damage in the white matter tracts in the brain (Bigler, 2001). This injury is thought to be present in 50% of all head injury cases, and is responsible for 35% of deaths in head injury patients (Meaney et al., 1994). Of all brain injuries, DAI has been found to have the highest rate of mortality at 65%, with subdural hematoma second at 47% (Gennarelli, 1983). The symptoms of DAI can vary from short losses of consciousness to deep coma and death (Bandak, 1994).

1.4 Summary

Brain injuries are a complex and difficult area of research. The brain itself is a complicated structure with many levels of complexity not yet fully understood, especially on a physiological level. As a result, the mechanisms causing brain injuries are complex and difficult to quantify due to the nature of the kinematics of the injurious event. It is also difficult to quantify TBI progression post impact in terms of physiology and recovery. Great effort has been undertaken in order to reduce the risk of injury by setting injury thresholds used in helmet standard development (Hoshizaki and Brien, 2004). However due to the complex nature of brain injury there is much more research required. The identification of more appropriate injury metrics in addition to the development of more accurate thresholds defining the risk brain injury has yet to be accomplished. Such values and variables would be invaluable in the development of protective strategies to decrease the risk and severity of these injuries.

1.5 Thesis Objectives

The objectives of this thesis are as follows:

Study 1

1. To establish a methodology that can be used to reconstruct traumatic brain injuries from falls.

2. To examine thresholds of injury for different traumatic brain injury lesions.

3. To examine the existence of a continuum of injury within the context of different types of traumatic brain injury lesions.

Study 2

1. To examine the influence of different characteristics of acceleration loading curves on the occurrence of different traumatic brain injury lesions.

Study 3

1. To examine how the kinematics of the event influences the presence of subdural hematoma in different lobes of the brain.

Chapter 2

Mechanisms of Brain Injury

A part of this section has been published in:

Post A and Hoshizaki TB. (2012). Mechanisms of brain impact injuries and their prediction: A review. Trauma, 14(4), 327-349.

Understanding the mechanism of injury for brain trauma is very important in the development of prevention technologies and to establish rules in sport to prevent the impacts which increase the risk of brain injuries. Human variability and the inability to measure these injury mechanisms directly requires the investigation of brain injury using animal, physical, and numerical modeling techniques in an attempt to understand the underlying mechanics of the injury. Several researchers have published review articles concerning brain injury mechanisms, notably King et al., (2003) and Hardy et al. (1994). Viano et al. (1989) summarized these and other works and described the mechanisms of brain injury: i) direct brain contusion from skull deformation at the point of contact; ii) brain contusion from movements of the brain against rough and irregular interior skull surfaces or from the side opposite the impact; iii) brain deformation in response to pressure gradients and motions relative to the skull, resulting in stress in the tissues and iv) intracerebral hematoma from movement of the brain relative to its dural envelope, resulting in tears of connecting blood vessels (Viano et al., 1989).

The following sections will describe the past and current research on mechanisms of brain injury. The discussion will begin with an overview on the mechanism of injury which creates brain contusions, followed by an examination of the effect of intracranial pressure on brain damage. This discussion will lead into the effects of linear acceleration and rotational acceleration on skull/brain relative motions and how finite element modeling has led to a new understanding of injury mechanisms.

2.1 Contusions and hematomas resulting from skull deformation and brain motion

Direct brain contusion was identified by Viano et al. (1989) as the result of either local skull deformation or movements of the skull against the rough and irregular interior skull surfaces from contact. Historically, contusions have been associated with the in bending of bone at the impact site, intracranial pressure, and skull/brain relative motions (Courville, 1950; Gurdjian and Gurdjian, 1975). Impact contusions are normally a product of a localized mechanical response either at the loading site (coup) or areas distal to that loading site (contrecoup) (Bandak and Eppinger, 1994). The skull deformation theory for brain contusion is related specifically to the coup site, as the contrecoup site has been thought to be produced through intracranial pressures and relative skull/brain movements (Gurdjian and Lissner, 1944). A direct impact to the skull produces local stress areas, causing a slight in bending of the skull bones that 'slap' the brain tissue directly underneath (Gurdjian and Gurdjian, 1975). The amount of this deformation of tissue underneath the impacted skull can create injurious strains to brain tissue as well as to cerebral blood vessels. The area of damage to the underlying brain may also spread laterally from the impact site. The rebound from this elastic deformation of the skull as it returns to its original position can cause the dura to separate from the skull which can result in epidural hematomas (Gurdjian and Gurdjian, 1975).

The mechanism of injury and the influencing factors contributing to the presence of intracerebral hematoma (ICH) are similar to those for brain contusions (Gennarelli and Thibault, 1982; Gurdjian and Gurdjian, 1980). From this research, it has been suggested that there is a continuum of brain motion-induced head injury; where contusions occur at lower magnitudes of skull/brain motion and ICH occur at higher magnitudes (Gennarelli et al., 1971; Gennarelli et al., 1972). In fact, animal impacts have shown that, unlike contusions, only high linear or rotational accelerations and rapid rates of onset are responsible for this type of injury (Gennarelli, 1983). Intracerebral hematomas normally occur in three different locations: i) the extradural space (epidural hematoma); ii) the subdural space (subdural hematoma) and iii) within the brain (Adams et al., 1980; Gurdjian and Gurdjian, 1980). Subdural (SDH) and epidural hematoma (EDH) are created by relative skull/brain motion which causes shear strains on the parasagittal bridging veins tethering the free floating brain to the skull (Kleiven, 2003). If the veins rupture, a hematoma accrues within the cranial cavity, creating a potentially fatal amount of pressure on the brain (Adams et al., 1983; Bradshaw et al., 2001a; Kleiven, 2003). Due to the directional material characteristics of these vessels, the orientation and location of the impact vector can also be influential in the creation of a SDH (Kleiven, 2003). Hematomas can also be found within the brain tissue itself post-impact. Small tears and hemorrhages are often found at interfaces between the grey and white matter in the direction of the force that was applied (Gurdjian and Gurdjian, 1975). In support of this theory, researchers used non-impact linear and rotational accelerations on monkeys to investigate brain injury (Gennarelli et al., 1971; Adams et al., 1981). They found that when undergoing linear or rotational translations, SDHs could be created in the absence of any physical impact (Gennarelli et al., 1971; Adams et al., 1981).

2.2 Intracranial pressure gradients produced from direct impact

Intracranial pressure is the pressure inside the skull and therefore brain tissue and CSF. This mechanism is measured using units of pressure in Pascals. Research using animal and cadaver models has shown brain deformation from an impact to be associated with increased intracranial pressures, a product of linear translations (acceleration) (Haddad et al., 1955; Gurdjian et al., 1966b; Thomas et al., 1966; Unterharnscheidt and Sellier, 1966; Unterharnscheidt and Higgins, 1969), and strains which have been correlated to rotational acceleration (Hodgson et al., 1983; Kleiven, 2003; Zhang et al., 2006). The theory of pressure gradients resulting from impacts is thought to be one of the primary factors in the development of focal brain injury (Ommaya and Gennarelli, 1974). The inertia of the brain pushing up against the impact site as it lags behind the faster moving skull creates an area of high pressure and at the distal site; this translation of the brain within the skull creates a corresponding area of negative pressure (Gurdjian and Gurdjian, 1975). The resulting pressure gradient creates shear stresses that result in local deformation of brain tissue (Thomas et al., 1967; Gurdjian et al., 1968). This is especially important with respect to brain stem damage from impact, as the relative resistance of brain motion in this area causes a concentration of potentially damaging stress and strain (Gurdjian and Lissner, 1961; Gurdjian and Gurdjian, 1975; Hodgson et al., 1983). In one of the first investigations of pressure gradients using dogs, Gurdjian and Lissner showed that post-impact, areas of high pressure formed at the coup site and low pressure areas occurred at the contrecoup site (1944). From this, they suggested that a gradient of pressure between the two sites produced injurious dynamic stresses in the brain tissue (Gurdjian and Lissner, 1944). Furthering this research, intracranial pressure (ICP) was linked to acceleration magnitudes and durations to head injury by inducing concussive impacts on dogs (Gurdjian et al., 1953). In a physical model approach to the investigation of pressure gradients, Thomas et al. made use of gel-filled skulls (1967). Using sensors to detect the brain dynamics during impact, acceleration, and pressure were found to be positively correlated. They showed that pressure gradients did exist and that both acceleration and compression were influential in this mechanism (Thomas et al., 1967). Supporting the theory of pressure being linked to acceleration, Kopecky and Ripperger (1969) used a fluid-filled cylinder impact model to investigate pressure gradients. They found that positive and negative pressures are a function of acceleration. In further investigations into this phenomenon, Kenner and Goldsmith used a distilled water-filled sphere to investigate pressure waves from an impact. They found a compression wave at the site of impact and a tensile wave at the location opposite to impact confirming the existence of a pressure gradient (Kenner and Goldsmith, 1972).

Positive pressure theory accounts for coup injuries when the head is impacted and contrecoup injuries received when falling. Lindenburg (1960) helped develop this theory; his pathological findings suggested a thinning of cerebro spinal fluid between the brain and dura at the contrecoup site, which would indicate an increase in pressure at that location during a fall. Edberg et al. (1963) used a gel-based physical model to simulate skull impacts and found positive pressures at the impact site and negative pressures at the contrecoup site. Further analysis of pressure during falling revealed that the pressures are reversed as the brain lags the motion of the skull (negative pressure at impact site, positive pressure at opposite site) which was later confirmed by Dawson et al. (1980) and Yanagida et al. (1989).

While positive pressure has been suggested as influential in this mechanism of injury the effect of negative pressure in the creation of contusions has also been investigated (Hardy et al., 1994). Areas of negative pressure are thought to cause bubbles of gas to appear in the brain tissue and cause damage when they collapse due to local area stresses and strains. Negative pressure has also been linked with cavitation theory. Gross (1958) was the first proponent of the cavitation theory of brain injury. Using half-filled fluid filled glass flasks as human head surrogates he showed that by accelerating the flasks downwards cavitation in the fluid was produced. When a similar experiment was conducted with a completely full and sealed flask a pressure gradient was formed from the impacted end of the tube to the non-impacted end, which Gross (1958) applied in theory to explain the commonly seen coup and contrecoup injury sites. If the tube received a hard enough blow the tensile force would exceed the tensile strength of the fluid, which would then tear apart and produce temporary cavities. These cavities would form in areas of negative pressure normally found in areas opposite to the impact site and their collapse could potentially be violent enough to cause brain injury. Cavitation was also thought to create local vacuum cavities in the brain, and once these cavities collapse the neural tissue would receive damaging strains (Denny-Brown and Russell, 1941; Gross, 1958; Lubock and Goldsmith, 1980).

The theory of negative pressure causing brain contusion has not been widely accepted. Suh et al. (1972) found that when impacting a fluid-filled spherical shell, negative pressure regions were not located at the contrecoup site. Other researchers found that negative pressure did not contribute to injury when impacting animal models such as rabbits and Macaques (Stalhammar, 1975a; Stalhammar, 1975b; Stalhammar and Olsson, 1975; Nuscholtz et al., 1984). Nuscholtz et al. (1984) concluded from their research that cavitation was not a mechanism of injury for contusion, but that head and neck position during impact was of greater importance. More recently finite element modeling of impacts has shown a low correlation between negative pressure and brain injury in pigs (Miller et al., 1998).

The research countering the negative pressure and cavitation theory to coup and contrecoup injuries led to a re-evaluation of commonly held theories on the mechanism of injury for contusions (Gurdjian and Gurjian, 1975). Building upon Courville’s (1950) review of contusion, Gurdjian and Gurdjian impacted dogs and monkeys to show that surface contrecoup contusions most likely result from relative movements of the brain against bony prominences on the interior of the skull (Gurdjian, 1970; Gurdjian and Gurdjian, 1975). They also stated that if cavitation theory was correct, the contusions would be present in the occipital poles of the hemispheres for frontal impacts, which is not the case (Gurdjian and Gurdjian, 1975). In their review of acute head injury, Gurdjian and Gurdjian (1980) identified that cavitation was easier to create experimentally than by using human material. They felt this was due to the high relative amounts of energy needed to induce negative pressure injury in animals with brains that are 4 or 5 times smaller than human (Gurdjian and Gurdjian, 1980). Another problem is that experimentally researchers use silicone gel and/or water to simulate the brain masses in their models, which have different viscosities than brain tissue and would thus react differently under loading scenarios (Holbourn, 1943; Gurdjian and Gurdjian, 1980). This large body of research has led to the conclusion that cavitation theory is an unlikely contributor to the development of contrecoup injuries (Gurdjian and Gurdjian, 1980).

2.3 Rotation causing skull/brain relative motions

The theory that the rotation of the head and not linear translation causes brain injury was first championed by Holbourn in 1943. Two primary concepts as to how rotations cause injury to the brain exist: i) the inability of the brain to rotate within the skull causes injurious focal point shear stresses and strains (Hardy et al., 1994; Bradshaw and Morfey, 2001) and ii) diffuse shearing of brain tissue, normally located at zones of change in density due to differing inertial properties, causes focal and diffuse injuries (Ommaya and Gennarelli, 1974; Yoganandan et al., 2008).

The restriction of brain motion from an impact is greatest at the anterior fossa, which may explain why the majority of brain injuries are located there regardless of the impact site (Ommaya and Gennarelli, 1974). Other brain structures can also create injurious local strains in resistance to rotation such as the falx and tentorium (Li et al., 2007). Using a brain model that defined brain matter as homogeneous and incompressible, Holbourn (1943) investigated this theory. Under the assumption that shear stresses and strains were the most likely source of injury, he found that rotation was a far greater influence to injury than linear translations (Holbourn, 1943). Gurdjian et al. (1968) supported this theory through direct impacts to monkeys; they concluded that injurious strains developed in the brain resulted from differences in the material properties of the tissues and the transmission of forces through them. This theory was further investigated by Unterharnsheidt and Higgins (1969) who induced non-impact pure rotational accelerations to squirrel monkeys. They found that the monkeys suffered subdural hematoma, torn bridging veins, and brain lesions, supporting the theory that rotation alone could induce severe brain injury (Unterharnscheidt and Higgins, 1969).

Further studies on monkeys and pure head rotation were undertaken using a special device to induce controlled non-impact linear and rotational accelerations of the animals' heads (Gennarelli et al., 1972; Gennarelli et al., 1979; Adams et al., 1981; Gennarelli et al., 1981; Adams et al., 1983). The results indicated that by adjusting the rotational acceleration pulses, DAI, and acute subdural hematoma could be created (Gennarelli et al., 1979). Subdural hematoma was created by shorter duration, higher magnitude rotational accelerations, and DAI was produced by longer duration, lower magnitude coronal rotations. Investigation into mTBI showed that non-contact linear acceleration did not produce concussion, but that non-contact translations and rotations can cause concussive injury in animals (Gennarelli et al., 1971; Gennarelli et al., 1972). Gennarelli et al. (1983) and Adams et al. (1983) also found that DAI severity was influenced by impact location, with sagittal head motions being the most severe. This extensive rotational acceleration work on monkeys yielded pathological results very close to those that would be expected for human injuries (Adams et al., 1981; Adams et al., 1983). As such, researchers concluded that the occurrance of human head injury could be influenced by rotational acceleration (Gennarelli et al., 1972; Zhang et al., 2001).

Further research into diffuse injuries created by blunt trauma by Ommaya and Gennarelli (1974) indicated that damaging strains through inertial loading decreases in magnitude from the surface of the brain to the centre of the brain. At low levels of rotational inertial loading, the damage caused by shear strain does not extend into the cortex. The level of injurious damage to the brain tissues appeared to depend upon the material and structural properties of these tissues (Ommaya, 1968; Ommaya and Hirsch, 1971). Finally, in their review of the mechanisms of concussion and diffuse injury, they concluded that the results of an impact depend largely upon the manner in which the mechanical properties of the multi-component, anisotropic, inhomogeneous brain tissue behave, as well as the effect of the location of bony prominences, dural partitions, vascular anatomy and sources of tissue interfaces with different densities (Ommaya and Gennarelli, 1974).

More recent research into the effect of rotational acceleration was conducted by two groups. Zhang et al. (2006) analyzed the effect of linear and rotational acceleration in isolation using their finite element model (FEM) of the human head and found it was rotation that highly influenced the levels of strain and not linear translations. Yoganandan et al. (2008) used a FEM of the human head and demonstrated that the shape of rotational acceleration pulses had a significant effect on the strains of the brain, far more than linear translations. Other FEM research simulating head impacts by Fijalkowski et al. (2009) and Bradshaw et al. (2001) also identified rotation as the main contributor of injurious levels of strain.

2.4 Combined linear and rotational acceleration theories

While it has been shown that intracranial pressure-induced strains are largely dependent upon linear accelerations resulting from impact and that tensile strains from brain motion are dependent on rotational acceleration, no reported cases exist outside the laboratory setting where they occur in isolation. This has led to theories suggesting that brain injuries occur through a combination of elastic deformation of the skull, positive and negative pressures and inertial brain lag from linear and rotational accelerations (Gurdjian and Gurdjian, 1975). This premise is supported by researchers arguing that if injury was solely dependent upon rotation, the acceleration levels would need to be impossibly high to induce injury. Assuming a combination of rotation and intracranial pressures influenced by linear acceleration as the source of the injuries is more plausible (Ommaya et al., 1967; Ommaya and Hirsch, 1971; Ommaya et al., 1971; Ono et al., 1980).

Recent work using physical and numerical modeling supports the early work conducted by Gennarelli et al. (1983) and Adams et al. (1983). Analyses using finite element modeling have supported the early animal and cadaver research. Zhou et al. (1995) employed an FEM of the human head to show that coup and contrecoup injuries are pressure induced, while brain stem injuries appear to be produced by shear strain. This shear strain is likely influenced by the unique material properties of the brain stem, and the geometrical constraints in that region of the brain. Bandak and Eppinger (1994) used their FEM of the human brain to show that both rotational and linear accelerations can cause strain damage to the brain. These numerical modeling approaches have the added benefit of more accurately representing the human tissue responses to an impact in that they have geometries and characteristics closer to the human than previous animal models.

2.5 Finite element modeling of mechanism of injury

Past approaches to investigating the mechanism and thresholds of traumatic brain injury have included the use of animal, cadaver, and physical models (Hardy et al., 1994). More recently mathematical models have been used; however, each of these models has had limited success (Voo et al., 1996). The cadaver studies lacked the living response of a human being during impact. The material properties of cadaver tissue are not similar to those of living tissue, nor are the mechanical responses under various loading conditions (Prange et al., 2002). Animal research has the benefit of using live animals for the recreation of specific mechanisms of brain injury, and the modeling of that injury, but lacks the geometry of the human brain (Ommaya et al., 1967). This discrepancy is important, especially in the identification of likely areas of contusion which have been postulated to be due to brain skull relative motion in which the brain contacts bony prominences inside the skull (Gurdjian and Gurdjian, 1976). Another important limitation is that animal thresholds cannot be expanded to humans due to differences in size, structure, and material properties of the brain tissue without assumptions. The use of physical human head surrogates is a more recent approach to the study of traumatic brain injury. These systems, normally comprised of a metal headform and skin, are reliable and repeatable; however, their drawback is in the area of omni-directional validity. Although the use of accelerometers allow some correlation to be made to brain injury (King et al., 1995), the motion of these head forms does not represent the complex tissue-level injury mechanisms which damage the brain.

Detailed numerical modeling techniques offer a potential solution to the limitations of these research methods. The currently used finite element (FE) modeling approach has given scientists the ability to simulate brain injury scenarios on skull/brain systems that are accurate in geometry, anatomy, and material properties (Table 1 and 2). The use of FE modeling, in conjunction with more conventional areas of research, may provide insight into the mechanisms and tolerance levels of brain injury (Yang et al., 2006).

Kenner and Goldsmith (1972) developed one of the earliest FE models for use in brain injury research. Under direct impact conditions, their model compared the response of an axisymmetric thin spherical shell model with the response of an aluminum shell. They found that the thin spherical shell model predicted strains 20% higher than those of the aluminum shell (Kenner and Goldsmith, 1972).

Following the work of Kenner and Goldsmith (1972), another FE model of the human head was published (Chan, 1974). Chan used an axisymmetric model with the head represented as an ellipsoid and the skull and brain represented as a viscoelastic material. The FE model was used to examine the effect of large shear stress on cerebral blood vessels and brain matter. The model was impacted directly with forces of varying durations and amplitudes causing internal shear deformation as well as negative contrecoup intracranial pressures which were calculated. Both shear strain and pressure were found to be important factors in the production of a brain injury (Chan, 1974).

Ward and Thompson (1975) developed a three-dimensional linear elastic model of the brain, complete with dura folds, ventricles and brain stem, for a direct frontal impact. This model did not include the skull and cerebral spinal fluid (CSF), as it employed a roller-supported linear spring system to simulate the tethering of the brain to the skull. This model was validated against experimental data from measurements of brain stem motion resulting from direct impacts to a cadaver head. While results indicated that a model without the falx and tentorium could not predict brain stem motion accurately, this model was capable of accurately predicting the intracranial pressure response data in the cerebrum from Nahum et al.'s (1977) frontal cadaver head impacts, which has become a standard validation for FE models.

In 1980, Nahum et al. developed a model that could be used to simulate a lateral impact for measurement of subdural pressures. Using six cadavers (1 emblamed, 5 unembalmed), the model predictions were compared with the measured cadaver responses. However, embalmed tissue would likely differ from unembalmed tissues in their response. Nahum et al. (1980) noted that the lateral impact predictions of the model did not match those of the front and occipital areas as closely.

The following year, the same group examined the effects of lateral impacts on cadavers with and without helmets, reporting the linear and rotational accelerations and subdural pressures (Nahum et al., 1981). The model showed an indistinct pressure gradient for a lateral impact when compared with a frontal impact. The authors felt this was due to the combination of components of linear acceleration that are not experienced during a direct frontal impact. Nahum et al. (1980) also reported that the falx and tentorium appeared to play an important role in compartmentalizing brain motion inside the skull. Furthermore, the responses of different cadavers were compared. The experimentally obtained pressure responses between two cadavers were very different, indicating single tests on cadavers have a high degree of biological variation (Nahum et al., 1980).

In summarizing FE modeling, Ward (1982) suggested that the brain should not be modeled as an incompressible structure, but rather with a reduced integration scheme. Ward used a reduced integration scheme for the volumetric component of the model and a full integration scheme for the shear component, with a nearly incompressible material characteristic assigned to the brain. Ward concluded that brain models could predict brain stresses and displacements if the anatomy was correct (presence of dura folds, falx, tentorium and foramen magnum). The author also concluded that: (i) stresses and strains in the brain lagged those of the skull; (ii) coup and contrecoup contusions were caused by pressure associated with translational acceleration; (iii) subdural hematomas were caused by high shear strains; (iv) the incidence and length of concussion were related to the magnitude of brain response; and (v) the largest shear strains were predicted along the skull/brain interface, brainstem, and cerebellum (Ward, 1982).

In the early nineties, Ruan et al. (1993) created a three-dimensional FE model of the human head based upon Shugar's (1975) head geometry to explore the correlation between the Head Injury Criterion (HIC) and brain injury. The head model was complex including the scalp, three layered skull, CSF, dura mater, falx, and brain. The brain and scalp were defined as viscoelastic materials, while the remainder of the head was defined as elastic that was based upon cadaver skull and brain material tests. Data from Nahum et al. (1977) were used to partially validate the model. Under a direct impact, the simulation indicated a correlation between HIC and intracranial pressure, as well as head acceleration and intracranial pressure (Ruan et al., 1993).

Shortly after Ruan et al. (1993), Zhou et al. (1995) developed a three-dimensional FE model of the human head to evaluate the effect of using homogeneous brain parameters versus inhomogeneous brain parameters for frontal and sagittal plane impacts. The model included the scalp, skull, dura, falx, tentorium, pia, CSF, venous sinuses, ventricles, cerebrum (grey and white matter), cerebellum, brains stem and parasagittal bridging veins, and was validated against Nahum et al.'s (1977) intracranial pressure data from cadavers. The simulation results indicated the importance of differentiating between grey and white matter as well as including ventricles in the head model. Both homogeneous and inhomogeneous head models predicted nearly the same intracranial pressure response, but different shear stress response. The results indicated that coup and contrecoup injuries are related to pressure, and that brain stem injuries are caused by shear stress and strain. The authors also postulated that the level of strain in the genu (anterior end of the corpus callosum) could be used as a predictor of diffuse axonal injury (DAI). Analysis of the parasagittal bridging veins showed that the bridging veins at the central part of the superior sagittal sinus were at the highest risk of impact induced rupture. Also, the bridging veins could endure higher tensile strains for a frontal impact due to the rebound of the brain (Zhou et al., 1995). The authors felt this could be significant as a mechanism of injury for subdural hematoma, as direction can play a major role in the incidence of brain injury (Gennarelli et al., 1987).

To improve the prediction of DAI, Bandak and Eppinger (1994) developed a FE model of the head from CT scans to evaluate a new strain based damage measure. The FE model of the head included the skull, dura mater, falx, CSF and brain. The material definitions were elastic or viscoelastic, with the brain considered as being linear, homogeneous and isotropic, and the skull considered as a rigid structure. The new measurement was termed the cumulative strain damage measure (CSDM) and was based on maximum principal strain which has been associated with the mechanism of injury producing DAI (Meaney and Thibault, 1990). The CSDM was calculated from strain tensors obtained by integrating the rate of deformation tensor while accounting for large deformations. The authors tested their model using three-dimensional kinematic simulations. A total of 36 simulations were conducted in an attempt to isolate the kinematic effect most likely to produce DAI. The results indicated that the CSDM was associated with rotational accelerations; anterior and posterior rotations produced higher results. The authors noted that this research does not confirm the appropriateness of using the CSDM as a measurement of

DAI and that further experiments to reconstruct well defined head injury cases with pathology data would be necessary (Bandak and Eppinger, 1994).

One year later, DiMasi et al. (1995) were assessing car crashworthiness by combining the use of a Hybrid III equipped with a 3-2-2-2 (Padgaonkar,et al., 1975) accelerometer array with FE modeling. They used the Hybrid III dummy system installed in cars and crashed them into a series of pillars. The linear and rotational acceleration output was then used to drive the model. Basic in geometry and parts, the model was comprised of a skull-like enclosure, soft deformable interior component to represent the brain, and a representation of the dura mater forming the falx. The results indicated that pure rotational acceleration was more influential in inducing strain and translational acceleration was more influential in producing high HIC values. The authors concluded that for car crashes, HIC alone was insufficient for the evaluation of brain damage as it does not account for the influence of rotational acceleration in the mechanism of injury (DiMasi et al., 1995).

In 1996, Turquier et al. (1996) used a FE head model developed by Willinger et al. (1995) to evaluate validation procedures using cadaver test data. The purpose was to test the model parameters related to the skull and subarachnoid space. The model was linear elastic, isotropic, and homogeneous in nature, and included the brain, subarachnoid space, tentorium, and falx (Willinger at al., 1995). Upon simulation of the cadaver experiments (Trosseille et al., 1992) in the modeling software, the authors found a similar but not identical response to the experiments. The authors noted oscillations in the simulation not seen in the experiments, which affected results. Also, good agreement between simulation and experiment was found only in terms of acceleration, not pressure. These findings led the authors to believe that correct boundary conditions chosen for the FE model are essential for accurate reproduction of cadaver based validations (Turquier et al., 1996).

Claessens et al. (1997) created a FE model of the human head in an effort to assess the importance of the geometric detail of the brain components and their interface conditions under impact loads. The authors developed a three-dimensional FE model from CT scans and used data from Nahum et al.'s (1977) experiments for validation. The model was composed of hexahedral elements, with the skull and brain represented as homogeneous and isotropic, with linear elastic material behaviour. Once the validation was complete, three conditions under translational impact were examined: (i) the effect of varying Young's Modulus; (ii) the effect of varying the skull/brain interface; and (iii) the incorporation of additional anatomical details, such as the meninges and how they affect the results. The results indicated that the higher Young's Modulus results in lower pressure at the coup and contrecoup regions, with no oscillations as seen in the other two conditions. The lower Young's Modulus resulted in a higher pressure in the frontal and foramen regions. Adjusting the skull/brain interface produced pressures with a lower amplitude in the coup and contrecoup sites for the sliding condition. For Von Mises stress, the free condition led to a much later peak with similar amplitude. The research also indicated that adding the falx and tentorium prevented the compression of underlying structures such as the cerebellum and brain stem. These additional structures led to a decrease in maximum pressure in the coup and contrecoup regions. For Von Mises stress, high values are seen in the cerebrum at the interface locations of the falx, but the cerebellum is more or less stress free. Based on these results, the authors concluded that the characteristics and constitutive properties of brain tissue and the skull/brain interface definition are essential for correct simulations. They also suggested that the modeling of brain structure geometry such as the falx and tentorium should take a lower priority to these factors in the development of a head model. Claessens et al. (1997) also identified that in this research only translational impacts were conducted and the effect of rotational impacts on these conditions must be explored as well.

In the late nineties, Al-Bsharat et al. (1999) developed a head FE model to evaluate the influence of different boundary conditions on the skull/brain interface. The original model used solid elements with a low shear modulus to represent the CSF and, as with preceding studies, was validated using intracranial pressure data from Nahum et al. (1977). The original model did not represent the skull/brain motion accurately; however, further testing revealed that by modeling a sliding interface between the brain and skull (between pia and arachnoid) layers, agreement was reached between simulation and experimental data from cadaver impacts measured using a high speed x-ray system.

In 2001, Zhang et al. developed a highly complex model to compensate for the perceived limitations of FE simulations up to that point. The authors identified that validations of previous models were limited to frontal intracranial pressure response, and therefore, the effectiveness of the simulations was also limited. To account for this, a very finely meshed FE model of the human head was developed for impact research; a model with a total of 314,500 elements. The model was comprised of the scalp, three layered skull, dura, falx, tentorium, pia mater layer, sagittal sinus, transverse sinus, CSF, hemispheres of the cerebrum with distinct grey and white matter, cerebellum, brainstem, lateral ventricles, third ventricle, and bridging veins. The material definitions used were isotropic, with different material characteristics for the different brain parts as per Zhou et al. (1995). The intracranial and ventricular pressure validation data was taken from Nahum et al. (1977) and Trosseille et al.'s (1992) cadaver experiments. The relative brain motion validation was conducted by comparing the simulation results to previous cadaver impacts that measured skull/brain relative movement using a high speed x-ray system King et al., 1999; Hardy et al., 2001).

Following the extensive validation, a variety of impacts were simulated using the FE model. The stability test used peak linear accelerations of 200 g and peak rotational acceleration of 12,000 rad/s^2, which were chosen due to their association with brain injury (Gurdjian et al. 1963; Ommaya et al. 1967). The model was subject to varying magnitudes of linear and rotational acceleration to test its robustness in a wide range of applications. The validation results indicated good agreement between the simulation and the experimental cadaver measurements for intracranial pressure (with some discrepancy), and brain motion. The discrepancies in the pressure data resulted from geometrical differences among cadavers and imprecise reporting of the location of the experimental pressure transducers in the original experiment. Finally, the authors concluded that while the model underwent rigorous validation, not enough was known about brain impact mechanics for the validations to be complete. More research would be needed in brain responses to impact and real world head injury cases would need to be simulated and validated before FE models could be used as a tool to aid in the development of strategies to prevent brain injury (Zhang et al., 2001).

Kleiven and Hardy (2002) developed a FE model of the human head for the purpose of investigating how the characteristics of the model could influence the results of a brain injury simulation. The model included the scalp, skull, brain, meninges, CSF, and parasagittal bridging veins, with hyperelastic and viscoelastic material definitions. The authors tested the simulation under three different skull and brain interfaces: (i) a tied interface, including the CSF; (ii) a sliding interface that allowed separation between the skull and brain; and (iii) a sliding interface with no separation, which allowed for sliding in the tangential direction and transfer of tension and compression in the radial direction. Three different brain stiffness parameters were also tested, with values encompassing the published brain tissue parameters. Each condition was tested against Nahum et al. (1977) for intracranial pressure differences and against Hardy et al. (2001) for relative skull/brain motion. The results indicated that intracranial pressure response is dependent on the skull/brain interface condition and less dependent on the parameters of the brain tissue. The tied interface including CSF produced results closest to the experimental results. However, the brain motion for low magnitude impacts was insensitive to skull/brain interface condition. The model and experimental tests had smaller relative motion for a lateral impact than for a frontal or occipital impact. Adjusting the shear properties of the brain tissue produced a difference in localized brain motion response, with the average published values producing the closest correlation to experimental data. As a result of this research, the authors concluded that lower shear properties should be used to predict local brain response and that further investigation into the effects of brain tissue shear properties for prediction of brain skull motion is needed (Kleiven and Hardy, 2002).

Horgan and Gilchrist (2003) developed a FE model for simulating head impacts incurred during pedestrian accidents. They conducted a parametric study to investigate the effects of bulk and shear modulus of the brain and CSF on the simulation response. A variety of mesh densities, element formulations and model types were investigated and compared to Nahum et al.'s (1977) cadaver data. The FE model was comprised of a scalp, three layered skull, dura, CSF, pia, falx, tentorium, cerebral hemispheres, cerebellum, and brain stem. A linearly viscoelastic material model with a large deformation theory was used to model the brain tissue. The results of the parametric study indicated that the short term shear modulus of the brain had the largest effect on the intracranial pressure and on the Von Mises stress response. The bulk modulus had the largest effect on the contrecoup pressure when the CSF was modeled using a coupled node definition. The mesh density investigation indicated that a coarsely meshed model could be used to simulate investigations of pressure response and a finer mesh would be needed for detailed investigations. When simulating identical impact scenarios with different FE models, the authors found that the modeling of the CSF and skull thickness must be carefully considered to reach the correct pressure distribution. The authors suggested that the physical properties of the head being impacted should be scaled to the model for best correlations (Horgan and Gilchrist, 2003).

A year later, Horgan and Gilchrist (2004) created six different versions of their model to test the influence of different configurations on pressure and skull/brain motion response. The six models created were: (i) the baseline model (Horgan and Gilchrist, 2003); (ii) the baseline model differentiating between grey and white matter; (iii) a model with three elements through the thickness of CSF; (iv) a model simulating a sliding brain skull boundary condition; (v) a projection mesh model, which also differentiated between grey and white matter; and (vi) a morphed model. All models were tested following the cadaver impact method used by Trosseille et al. (1992) and Hardy et al. (2001) and the intracranial pressure and brain skull movement responses were compared. The results of the simulations indicated little difference in the intracranial pressure response between the six models used. In fact, when compared to Hardy et al.'s (2001) cadaver experiments, little difference was found between the models, leading the authors to conclude that the improvements over the baseline model may not have been warranted (Horgan and Gilchrist, 2004).

Ho and Kleiven (2007) used a complete three-dimensional model of the human head to evaluate the effect of brain vasculature on impact response. Three different FE models of the brain were used: (i) one without vasculature; (ii) one with linear elastic vessels and; (iii) one with non-linear elastic vessels. The amount of vasculature included in the models was determined from three-dimensional angioplasties. A 10,000 rad/s^2 rotational and a 100 g translational semi-sinusoidal impact was simulated over 5 ms for each of the models in the sagittal plane. The results indicated that the effect of vasculature on maximum principal strain is minimal. The brain stem showed a small increase in strain, which the authors felt was a result of larger vessels in the region propagating strain into deeper parts of the brain stem. In conclusion, the authors felt the inclusion of vasculature would be useful to study the effect of acute subdural hematoma, where failure could be predicted by measuring the strain on the vasculature. However, including the vasculature when investigating the mechanism of other brain injuries is not necessary (Ho and Kleiven, 2007).

Li et al. (2007) used a head FE model to determine the influence of the falx on localized brain strains associated with brain injury from a lateral impact. The model used was a simplified two dimensional linear viscoelastic model, consisting of rigid skull, rigid falx, CSF, and cerebrum. The model was validated through comparisons to experimental temporal motion and strain data from a physical model (Bradshaw et al., 2001a). A pulse of 7,800 rad/s^2 with a 4.5 ms duration was applied laterally to two versions of the model, one with a rigid falx and one with a flexible falx. The results indicated that the strains in the cerebral vertex for the flexible falx condition were greater than those with the rigid falx. In the corpus callosum, the region of strain was similar between the two conditions, with the flexible falx showing a slightly delayed response. The maximum principal strain at the postcentral sulcus was lower for the flexible falx. In conclusion the flexibility of the falx has significant effect on maximum principal strain and on the regional brain responses (Li et al., 2007).

Yoganandan et al. (2008) analyzed the influence of acceleration and deceleration pulses on brain strains using a two dimensional FE model of the human head to investigate the mechanism of brain injury. The model was developed based on a physical model used by Bradshaw et al. (2001a) to evaluate acute subdural hematoma and DAI for coronal head impacts. The FE model was impacted under three conditions: (i) acceleration pulse of 4.5 ms, 7,800 rad/sec^2 ii) deceleration only pulse of 20 ms, 1.4 rad/sec^2; (iii) biphasic acceleration and deceleration pulse; and (iv) biphasic deceleration and acceleration pulse. The results indicated that peak principal strains increased with increasing separation time interval for both biphasic pulses, with the first pulse being dominant with increasing separation time. For pure acceleration and deceleration pulse conditions the strain regions were all similar; however, the biphasic conditions resulted in strains which were region and pulse shape specific. The corpus callosum incurred the highest strains for all profiles, with acceleration-deceleration pulses producing the greatest strains. The authors attributed these differences in brain response to geometry, material properties of the brain and the type of loading condition (Yoganandan et al., 2008).

Ho and Kleiven (2009) followed their effect of vasculature research with an investigation into the effect of sulci on traumatic brain injury using FE modeling. Two FE models of the human head were created from medical images consisting of the skull, CSF, pia mater, falx, tentorium, gray matter, white matter and brainstem. One model had detailed sulci geometry and the second had smooth brain geometry. A 10,000 rad/s^2 sinusoidal pulse, with a 5 ms duration was simulated due to its association as a possible threshold value for DAI (Marguiles and Thibault, 1992). The translational pulse had a peak value of 100 g. The results indicated that the strain and strain rate of the brain tissue during an impact was reduced in many regions for the FE model with sulci. This was especially apparent when the pulses were applied in the sagittal plane. The strain distribution across the brain tissue was also altered with the inclusion of the sulci, which indicated that the sulci have a function as an overall motion constraint. These findings would suggest that it is important to include sulci in future FE models (Ho and Kleiven, 2009). Many advances in FE modeling have occurred over the past three decades (Tables 1, 2). From the early days of simple geometrical head representations, FE modeling research has focused mainly on the how the various parameters describing the nature of the skull and brain can influence the validity of its predictions. Geometric detail has become more accurate due to the improved MRI and CT scans upon which they are based; however, the tissue material properties and their influence on brain motion has proven to be a more difficult problem to solve. The role of the falx and tentorium as structures that influence brain motion was originally established in 1975 by Ward and Thompson, and has since been confirmed (Claessens et al., 1997; Li et al., 2007).

Finite element head research was furthered when a comparison of frontal and lateral cadaver head impacts to simulation results showed that the direction of impact affects the intracranial response (Nahum et al., 1981). The following year, Ward reported that all brain anatomies should be present (falx, tentorium, foramen magnum and dura folds) if correct brain stresses and displacements were to be predicted (Ward, 1982). Decades later Ho and Kleiven (2007, 2009) did further research on the effect of including the geometry of the brain sulci and brain vasculature which determined that including the sulci was influential on brain responses but that including the vasculature was not. Zhou et al. (1995) built upon the research by Ward (1982) by suggesting that the brain should not be modeled as a homogeneous structure. They created an FE of the brain separating grey and white matter, resulting in a layer of precision to predictions. Claessens et al. (1997) followed this work by examining the effect of FE brain model material characteristics and skull/brain interface on a simulation. They found that the simulation results were very sensitive to these parameters, leading others to investigate the influence of the brain skull interface more closely. One group found that a sliding interface matched cadaver experiments closely (Al-Bsharat et al., 1999), while another discovered that a tied brain skull interface was the best match to validation data (Kleiven and Hardy, 2002).

Table 1. Historical listing of finite element models 1972 – 1995

Components	Validation method	Main Conclusions	References
axi-symmetric thin spherical shell model	n/a	predicted 20% higher strains in the skulll than in similar aluminum spherical shell	Kenner and Goldsmith (1972)
visco-elastic prolate ellipsoid shell and core	n/a	both shear strain and reduced pressure equally important in brain injury	Chan (1974)
fluid-filled nested spherical shells	n/a	predicted reduction in brain pressure due to helmet	Khalil et al., (1974); Khalil and Hubbard (1977)
		model without falx cerebri and tentorium could not predict the brainstem deflections correctly (1975)	Ward and Thompson (1975, 1982); Nahum et al. (1977, 1979)
3-D linear elastic model: Cerebrum; cerebellum; brain stem; ventricles; dura folds (half brain model)	against data from static measurements of the brainstem during flexion and extension of the head, as well as experimentally determined mode shapes and natural frequencies: Was able to predict the intracranial pressure using data from Nahum's test #37	**(A)** Brain models could predict brain stresses or displacements if the model included the dura folds, falx, tentorium, foramen magnum and effective compressibility. **(B)** stresses and strains developped in the brain lagged those in the skull **(C)** coup and contrecoup contusions were caused by pressure associated with translational acceleration **(D)** subdural hematomas were caused by high shear strains **(E)** occurance and duration of concussion were related to magnitude of brain response **(F)** largest shear strains were predicted along the brain skull interface, brainstem and cerebellum	Ward and Thompson (1982)
Same as above, full 3D for lateral impact	Compared to 9 cadaver experiments (4 embalmed, 5 non)	Model predictions did not fit the cadaver responses well for lateral imapcts.	Nahum et al., (1980)
Same as above, full 3D for lateral impact	one pressurized Cadaver	linear and angular acceleration along with subdural pressures reported	Nahum et al., (1981)
3D, Scalp, a three-layered skull, cerebral spinal fluid (CSF), dura mater, falx cerebri, and brain//linear viscoelastic for brain and scalp	Validated against Nahum et al. (1977) acceleration, impact force, intracranial pressure.	for direct impact HIC and intracranial pressure were correlated, as were head acceleration and intracranial pressure	Ruan et al. (1993); Ruan and Prasad (1994)
included skull and brain with simplified geometry	n/a	higher strain for windshield impact compared to A-pillar impact	DiMasi et al. (1995)

Table 2. Historical listing of finite element models 1995-2003

Components	Validation method	Main Conclusions	References
scalp, skull, dura, falx, tentorium, pia, CSF, venous sinuses, ventricles, cerebrum (grey and white matter), cerebellum, brain stem, and parasagittal bridging veins….the first to use differing properties for white and grey matter	Validated against intracranial pressure in Nahum et al. (1977).	Large variations were observed in shear stress distriubtion patters, and the intracranial pressure was not affected by the change in properties	Zhou et al. (1995)
Skull, falx, tentorium, subarachnoid space, cerebrum, brainstem	Validated agaisnt epidural data from Trosseille et al. (1992)	Analysis of contemproary validation techniques led to conclusion that FE model boundary conditions must be accurate for model validity	Turquier et al. (1996); Willinger et al. (1995)
skull, brain, face	Attempted validation against Nahum et al. (1977), failed due to couple brain and skull interface	concluded that the junction between the brain and skull was somewhere between the rigid coupling and free interface that was simulated	
skull, falx cerebri, tentorium, cerebrum, cerebellum, and brainstem	Matched gel experimental results to model predictions.	Model predicted maximum shear strain 10 times that reported by Bandak and Eppinger (1994) for the same laoding condition. This was attirbuted to low shear modulus and strain softening effect for model simulations	Claessens et al (1997); Brands et al. (2002)
scalp, three-layered skull, dura, falx, tentorium, pia, CSF, venous sinuses, ventricles, cerebrum, (gray and white matter), cerebellum, brain stem, and parasagittal bridging veins	Validated against intracranial pressure and other 'reasonable' peak pressures in Nahum et al. (1977). The brain/skull displacements were still well below those reported by King et al. (1999).	Adding a sliding interface between brain and skull (interface between pia and arachnoid) matched displacement measures froma high speed x ray system. Intracranial pressure validation was successful. Matched time histories coup and contrecoup pressures for #37, and peak values from other tests.	Al-Bsharat et al. (1999)
The scalp, skull with an outer table, diploe, and inner table, dura, falx cerebri, tentorium, pia, sagittal sinus, transverse sinus, CSF, hemispheres of the cerebrum with distinct white and gray matter, cerebellum, brainstem, lateral ventricles, third ventricles, and bridging veins	Validated against Nahum et al. (1977) and Trosseille et al. (1992) intracranial and ventricular pressure data. Relative displacement data between brain and skull by King et al. (1999) and Hardy et al. (2001) and facial impact data by Nyquist et al. (1986) and Allsop et al. (1988)	The model predicted higher positive pressures and larger localized skull deformation at the impact site for lateral impacts. Lateral impact also induced higher localized shear stress in the core regions of the brain. If shear deformation is considered to be an injury indicator for diffuse injuries, a high shear stress due to a lateral impact indicates the head would have a decreased tolerance to shear deformation in the lateral impact	Zhang et al. (2001)
Scalp, skull, brain, meninges, CSF, bridging veins, brainstem, spinal cord, cervical vertebrae	n/a	Relative brain skull motions were affected by material properties. The average shear properties reported by Donnelly and Medige (1997) matched experimental data reported by Hardy et al (2001a) best. Use of a tied interface resulted in best correlation between emasured and predicted intracranial pressure.	Kleiven and Hardy (2002)
Skull, brain, dura-CSF, falx, bridging veins	n/a	Established the cumulative strain damage measure as a possible indicator for brain injury	Bandak and Eppinger (1994); Takhounts et al. (2003)
cerebrum, cerebellum, brainstem, intracranial membranes (falx and tentorium), pia, CSF, dura, three-layered skull and facial bone	Validated against Nahum et al. (1977) pressure and time histories, Hardy et al. (2001) for brain motion. Also validated against real world injury events.	Parametric study indicating that varying the shear modulus had a large influence on intracranial pressure and Von-Mises response; varying bulk modulus had large effect on contrecoup pressure	Horgan and Gilchrist (2003)

Horgan and Gilchrist (2003) continued research into the effects of brain parameters on simulation results and confirmed that the brain parameters were very influential. In 2001, Zhang et al. developed a model which matched the most complex validations, agreeing with intracranial pressure and brain motion data from cadaver experiments. This was an important investigation because the validation of the FE model is crucial to the accuracy and validity of brain injury research. Current validation procedures include comparison the intracranial pressure response of the brain from a frontal impact to a cadaver head (Nahum et al., 1977), cadaver brain displacement data (Hardy et al., 2001), and occasionally real world scenarios. Several models have achieved this level of validation, but as with determining the material definitions of brain tissue, there is much research left to be conducted before a truly accurate and fully validated brain FE model can be established. Data for these validations are limited as much of it is conducted on cadaveric tissue. Also, most of this validation data is from single impacts in a single vector, limiting the applicability of these validations to impacts to other areas of the head (Nahum et al., 1982). In conclusion, including accurate anatomy and material properties of the human brain in a FE model of the human head is essential to the accuracy of any simulation. Also, having fully three-dimensional impact data including intracranial responses would be ideal to achieve a full validation.

2.6 Summary

Mechanisms of injury for the skull and brain are undoubtedly linked to some amount of injurious deformation of tissue. Using methods such as FE modeling and animal models to study brain injury, the mechanisms have been described in many ways by a variety of researchers, but Viano et al. (1989) offered four possible mechanisms based on a review of previous literature which were: i) direct brain contusion from skull deformation at the point of contact; ii) brain contusion from movements of the brain against rough and irregular interior skull surfaces or from the side opposite the impact; iii) brain deformation in response to pressure gradients and motions relative to the skull, resulting in stress in the tissues and iv) intracerebral hematoma from movement of the brain relative to its dural envelope, resulting in tears of connecting blood vessels. While each mechanism is supplied as a separate entity, upon further examination they have commonalities. It could be deduced that all brain injuries are linked in some form to either translational or rotational skull/brain motions and could be quantified by measuring brain deformation (Kleiven, 2007). It would seem that all mechanisms investigated are the result of either impact induced or impulsive brain deformation. The loading characteristics, when described using three-dimensional kinematics, can then be quantified through measurement of corresponding engineering variables. However, such variables have yet to be identified. Recently through the use of finite element modeling it has become possible to measure brain deformation by simulating head impacts with many output variables such as intracranial pressure and brain strains (Zhang et al., 2001). This allows for a more complete description of the resulting brain deformation from mechanical loading and possibly an avenue to discover a dependent variable which is highly correlated to injury. This association of mechanical variable to brain injury has been attempted in the past with limited some success (Gadd, 1966; Versace, 1971). The following section will discuss the advancement of prediction of brain injury from linear acceleration through to measurement of brain stresses and strains through use of finite element modeling.

Chapter 3

Head Injury Predictors

A part of this section has been published in:

Post A and Hoshizaki TB. (2012). Mechanisms of brain impact injuries and their prediction: A review. Trauma, 14(4), 327-349.

The mechanisms of brain trauma previously described have one variable in common; a certain amount of measurable deformation or stress of the brain tissue past the point of recovery resulting in permanent deformation and injury. The amount of loading quantified using deformation based dependent variables would indicate the threshold the brain tissue has to injury. Identifying these tolerances to injury would allow for improvements in protective devices and design of structures. It could also aid in the creation of better rules for sport to eliminate risky situations likely to cause a specific type of loading to the head and brain. However as there are many mechanisms of injury it is difficult to identify a singular level of tolerance for brain injury.

When injury thresholds are being created many different factors must be accounted for. To establish an injury criterion, the input, output, and all system variables must be considered (O'Donoghue, 1999). In the creation of an impact induced deformation the characteristics of the applied force are the input variables. These variables would be represented as inbound velocity, mass, location, direction, and magnitude. The mechanical output from these variables would be deformation of the brain and the rate of stress and strain of tissue. Other factors which are known to influence the input and output are geometries of the head, constitutive properties as well as age, sex, health, and intoxication (Horgan, 2005).

These variables make the creation of a specific tolerance curve for brain injury difficult. Some researchers have made some simplifications to these assumptions to help establish tolerance curves for specific types of injuries (Zhang et al., 2004; Kleiven, 2007). Research in this area has focused on linear acceleration as a measure of injury as it has been linked with the creation of potentially injurious pressure gradients in the skull (Thomas et al., 1966). However the low correlation linear acceleration has had with brain injury led to integrations of the acceleration time curve to account for other aspects of the injurious pulse (Gadd, 1966; Versace, 1971). Rotational acceleration has also been proposed as an important factor in injury, and as a result has been suggested as an important measure (Holbourn, 1943). More recently finite element modeling has created an opportunity to measure the outcome of simulated impacts in brain tissue deformation characteristics such as stress and strain (King et al., 2003).

The following section will discuss these parameters and how they apply to the creation of tolerance limits for brain injury. The discussion will begin with commonly used medical scales such as the abbreviated injury scale and move on to engineering metrics such as linear and rotational acceleration. Attempts to interpret the effect of linear and rotational acceleration curve shape using integrations will be covered and their limitations, which will lead to the currently proposed solutions involving finite element modeling. Finally, the status of the literature concerning accident reconstruction and injury threshold levels will be discussed.

3.1 Abbreviated Injury Scale (AIS)

As far back as 1943, injury scales have attempted to classify the severity of all sorts of injuries for medical purposes (Petrucelli et al., 1981). Following several other injury scale attempts, the abbreviated injury scale (AIS) was developed by a group of engineers, physicians, and researchers who recognized the need of a uniformly accepted injury scale to classify injuries (Petrucelli et al., 1981). The need for this scale was driven by automotive crash investigation and research. The original AIS were patterned on the General Motors Collision Performance and Injury Report in 1969 and were later published in 1971 (AMA committee on Medical Aspects of Automotive Safety, 1971). The scale was based upon the analysis of 75 motor vehicle related injuries and was further validated through dissemination and use by other medical practitioners. The AIS is an empirical scale that assigns a value to the severity of the observed injury. It uses a numerical modeling method to rank anatomical injury by severity and thus does not describe any consequence of the injury such as mental or physical disabilities. The index ranges from 0 to 6, with 0 = no injury, 1 = minor injury, 2 = moderate injury, 3/4 = serious/severe injury, 5/6 = critical/fatal injury. For head injury, AIS values of 0 to 3 would constitute neck or back injury and minor concussion, and 4 to 6 would be concussion and cerebellar lesions. There is a section of the AIS which deals specifically with head injury based upon the level of consciousness (Glasgow Coma Scale) and duration of coma which is normally used in a clinical setting.

The AIS and other scales in use by medical practitioners assign a value based upon observed anatomical damage. When these types of scales are used in conjunction with injury reconstruction research in the attempt to identify mechanical variable thresholds a lack of correlation to injury occurs (Willinger and Baumgartner, 2003b). This problem arises because different lesion types can produce a similar AIS score. This difficulty was identified by Willinger and Baumgartner (2003b) when they attempted to correlate AIS scores with engineering parameters through injury reconstructions. They felt that the low correlations (0.3 to 0.6) of engineering parameter with AIS made comparison with this score unacceptable, but when the reconstructions were separated by lesion type some correlation of parameter to lesion occurred.

3.2 Kinematic predictors of injury

3.21 Linear Acceleration

Linear acceleration has been linked to brain motion causing intracranial pressure differences within the cranium due to relative brain skull motion (Thomas et al., 1966; Gurdjian et al., 1966b). Gurdjian et al.'s (1961; 1966b) early work measuring intracranial pressure changes from impacts on animals was amongst the first to attempt to find a correlative parameter to brain damage. They discovered that pressure changes could be a possible mechanism of injury as they would cause damaging shear stresses to brain tissue. This pressure is a result of deformation of the skull and its acceleration after an impact, and therefore if the kinematics of the event were monitored, risk of injury could be evaluated (Gurdjian et al., 1961). The correlation of linear acceleration to intracranial pressure and therefore levels of injury was further confirmed by Nuscholtz et al. (1987) with blunt impact experiments on adult Macaque monkeys.

The use of linear acceleration as an injury metric has been successful to date, with protective technologies created to reduce this variable resulting in the reduction in focal injuries such as skull fracture and TBI in sport (Hoshizaki and Brien, 2004). While there has been a reduction in focal injuries, the prevalence of diffuse injury such as concussion has yet to be resolved. The inability of protective devices to influence the occurrence of this phenomenon may be a result of a lack of measurement of rotational kinematics associated with impact.

3.22 Rotational Acceleration

The influence of rotational acceleration on the creation of head injury lies in the principle that the three-dimensional kinematics of the head after an impact influences the deformation characteristics of brain tissue and thus injury. Holbourn (1943) was one of the first proponents of the rotational theory to brain injury citing that any change in the head velocity from an impact can be analyzed in vectors of linear and rotational acceleration. He contested that linear acceleration could not cause compressive injury due to the incompressible nature of the brain and that rotational acceleration was the sole cause of brain damage. This conclusion was based upon the fundamental assumption that the brain tissue is largely damaged through shear strains to neuronal tissues and as such all injuries could be assessed through the rotational kinematics of the head (Holbourn, 1943).

Experiments by Gennarelli et al. (1981) underscored the importance of rotational acceleration in the production of injury. Using a device that could elicit a rotational acceleration dominant motion with minimal linear accelerations to the heads of monkeys they created a wide range of injury, from concussion and intracerebral hematoma to death (Gennarelli et al., 1981; Adams et al., 1981). The same rotational acceleration inducing device was used to examine the effect of direction on brain injury in monkeys (Gennarelli et al., 1983). It was found through this study that the direction of the rotation is also influential on the resulting injury, not just its severity but also type of brain lesion (Gennarelli et al., 1983).

More recent work using finite element modeling of the human head to assess the influence of kinematics on brain deformation has been undertaken. Forero Rueda et al. (2011) analyzed injurious events to equestrian jockeys and found that rotational acceleration was highly correlated with stress and strain in the brain while linear acceleration had a lower correlation. In an evaluation of head injury criteria, Kleiven (2006) also found that rotational acceleration had high correlation with peak strains in his head injury model.

Rotational acceleration has only recently started to be considered as an important descriptor of head impact events. While it has been shown to be influential in the creation of brain injury in the absence of linear acceleration it is unlikely that an event producing linear or rotational acceleration in isolation could ever occur. It has also been shown that injuries are facilitated by the combined loading of both linear and rotational accelerations (Meaney and Smith, 2011). It is for this reason that for a full description of an injurious event the complete three-dimensional kinematics must be represented to be able to evaluate the brain tissue response to the event.

3.3 Injury Criterion

3.31 Integrations, GSI and HIC

While peak linear acceleration was found to be correlated with pressure and skull fracture, the influence of the acceleration time curve was also found to be important (Gurdjian et al., 1966a). Using animal and cadaver impact data an acceleration-time tolerance curve was developed. This curve is commonly known as the Wayne State Tolerance Curve (WSTC) (SAE J885a). This curve exemplified that high accelerations could be tolerated for short durations while lower accelerations could be tolerated for longer durations. This relationship was confirmed by Ono et al. (1980) with the development of the human head impact tolerance curve (Japan head tolerance curve).

In an attempt to create a value that could easily be applied to the development of head protective devices in the automotive industry the Gadd severity index was developed (Gadd, 1966). This severity index is an extension of the WSTC and is represented thus:

$$GSI = \int_{t_0}^{t} \vec{a}^{2.5} dt$$

where a is the response function (acceleration), 2.5 is a weighting factor and t is time. The value of n = 2.5 was an approximation of the slope of a log-log plot of the WSTC. The weighting factor was included to give greater influence to high levels of response to injury and lower levels would have less influence on the creation of an injury. This integral was viewed as an improvement upon using peak values for prediction as it incorporated differing curve shapes and eliminated the importance of different sections of the pulse as the whole event was incorporated in the solution. A value of 1000 was used as a proposed injury threshold based on data from Wayne State, the FAA, and NASA. Very long duration pulses (50 ms) were considered inconsequential in this equation as head impacts are normally less than 15 ms.

In an attempt to improve upon the GSI a head injury criterion (HIC) was suggested by Versace (1971) and was adopted by the NHTSA for standard testing in the automotive industry. The HIC is calculated by selecting the time range for the integration for the linear acceleration pulse measured at the centre of gravity of the head and is calculated thus:

$$HIC = (t - t_0) \left[\left(\frac{1}{t - t_0} \right) \int_{t_0}^{t} \vec{a}\,(t)\,dt \right]^{2.5}$$

A tolerance value of 1000 was also suggested for the HIC for injury. The time limits in use can vary but the recommended limits are 36ms (NHTSA) and 15 ms (ISO).

These integrations have some limitations and assumptions. The limitations associated with the HIC and GSI show how difficult it is to measure the mechanisms of head injury and link them to an injury metric. Nahum and Smith (1976) used impacts to cadavers to correlate the severity of brain injury to GSI or HIC. The results of these impacts showed that HIC had some correlation to brain trauma. Later, Newman (1980) identified that correlation of linear acceleration time curves measured at the centre of gravity of an anthropometric test dummy and its time dependence on injury was in fact unfounded. The limitations of GSI and HIC for longer time durations were brought into perspective as well as the methods of the original cadaver tests. Also, treating the human head as a rigid body is erroneous. These arguments were supported by research attempting to correlate AIS to function of HIC where no relationship was found (Newman, 1980).

In an attempt to link HIC to injury parameters, Prasad and Mertz (1985) produced risk curves for the criterion to head injury. They produced a linear curve showing HIC values between 0 and 3000 to percentage of people who would correspondingly be at risk of injury from 1% to 99%. From this a HIC of 1000 corresponded to 16% risk of brain injury, and a value of 1500 indicated a risk greater than 50% for 15 ms duration. From this data they suggested that the HIC be limited to 15 ms for best use in the automotive industry.

3.32 GAMBIT

The first threshold criterion that attempted to include both rotational and linear acceleration was Newman's (1986) Generalized Head Acceleration Model for Brain Injury Threshold (GAMBIT). The validity of this integration was tested against all known head injury databases in which the three-dimensional kinematics were reported. The GAMBIT is calculated thus:

$$G(t) = \left[\left(\frac{a(t)}{a_c}\right)^n + \left(\frac{\alpha(t)}{\alpha_c}\right)^m\right]^{1/S}$$

where a(t) and α(t) refer to the instantaneous value of translational and rotational acceleration respectively and *n*, *m*, and *S* are empirical constants selected to fit the available data. This calculation differs from previous integrations in that it does not attempt to assign a limit for a particular AIS score. The GAMBIT assigns a critical value in linear and rotational acceleration beyond which injury would occur (a_c and α_c). This calculation would predict an injury if the value of G goes beyond 1.

3.33 Head Impact Power (HIP)

The head impact power (HIP) injury metric was developed by Newman et al. (1999, 2000a/b) from 24 American football impact events, in which concussion was reported in nine impact events. The theory behind this injury metric was that if the rate of change of kinetic energy passes some critical value, a brain injury would occur. This was the first injury calculation to include six degrees of motion (three linear/three rotational) and sensitivity characteristics to relate change of kinetic energy to injury. For the development of this metric reconstructive analysis of head to head impacts were used. The three-dimensional kinematic parameters of the impacts were reconstructed from game videos and then used for a laboratory reconstruction of the event using Hybrid III anthropometric test dummies. Each case was then analyzed using commonly applied injury metrics such as peak linear and rotational acceleration, GSI, HIC, GAMBIT as well as the newly formed HIP:

$$HIP = \left(m\vec{a_x}\int\vec{a_x}dt\right) + \left(m\vec{a_y}\int\vec{a_y}dt\right) + \left(m\vec{a_z}\int\vec{a_z}dt\right)$$
$$+ \left(I\vec{\alpha_x}\int\vec{\alpha_x}dt\right) + \left(I\vec{\alpha_y}\int\vec{\alpha_y}dt\right) + \left(I\vec{\alpha_z}\int\vec{\alpha_z}dt\right)$$

where the HIP is the head impact power and the frame of reference is that for the head, a_x, a_y and a_z are the linear acceleration components along the three axes and α_x, α_y and α_z are the rotational acceleration components. The values for the human head are those of the 50% Hybrid III dummy head form. The reconstructions indicated that there was a 50% chance of mTBI at 12.8 kW. Using the above equation they were able to incorporate directional sensitivities but the values for the coefficients were not known.

Upon further analysis of their results from the impacts it was found that impact velocity had no correlation with the creation of mTBI. From the assessment using the integrative techniques it was found that those calculations incorporating both linear and rotational acceleration had the highest correlation to injury (GAMBIT and HIP) (Newman et al., 2000a).

While the concept of the HIP was sound, the data upon which it was based had limitations. The position of the cameras, frame rates and zoom settings contributed to significant error for the initial laboratory reconstruction parameters. Newman himself calculated these errors to be in excess of 20% (Newman et al., 2005). The exact impact vector producing the injury to the brain is difficult to ascertain and approximations were used for the contact area for the Hybrid III reconstructions. These assumptions can lead to significant error as it has been shown through research conducted by Walsh et al. (2011) small variations in impact vector can lead to significantly different head-form dynamic responses.

3.34 Limitations to currently used injury metrics

Goldsmith (1981) discussed the limitations to the use of a single value to describe the entirety of all the mechanisms of brain injury. He identified that it is unlikely that one parameter could describe the tolerance limits for head injury for all populations. This is especially true for comparisons across the young to the very old, where it has been documented that the material characteristics of brain tissue can change dramatically (Prange et al., 2002). Goldsmith agreed with Newman's concept that rigid body mechanics was not a suitable choice for a system of deformable components such as the head and brain, especially under a dynamic loading scenario. Goldsmith also concluded that it would be erroneous to use an integration metric based solely upon peak resultant linear acceleration when rotational acceleration has been identified as a likely contributor to the mechanism of brain injury. This hypothesis has been supported by researchers establishing that linear and rotational motions influence different brain deformation parameters such as intracranial pressure (linearly dependent) and shear stress and strain (rotationally dependent) (Kleiven, 2007; Forero Rueda et al., 2011; Meaney and Smith, 2011). Due to the low correlations of peak linear and rotational accelerations to injury type it has been suggested that injurious brain tissue deformations are likely a product of all aspects of the linear and rotational acceleration time histories (King et al., 2003). If this theory is correct, the nature of these time histories would influence not only the severity but also the location of injurious brain deformations.

The brain material characteristics and how they respond in an impact scenario is also influential on the location and severity of brain damage (Prange et al., 2002). This relationship is not represented by current peak value based injury metrics. It has been documented that each brain material (grey matter, white matter etc) has different characteristics and anisotropic behaviour. As a result of these differences it is likely that each material would be affected differently by the three-dimensional linear and rotational motions resulting from an impact. This theory would suggest that there may not be a 'continuum' of brain injury, but rather certain brain injuries would be highly influenced by linear motions and others by rotational motions, which has been suggested for focal and diffuse injury creation.

As a result, it may be concluded that more accurate reconstructions and modeling techniques would be required if a suitable injury metric could be established. The first step would be to research the brain deformation response under three-dimensional linear and rotational acceleration loads. This type of injury research could account for some of the limitations associated with using peak values and integrations of linear acceleration variables. Through the use of finite element modeling the combined effects of linear and rotational acceleration can be measured. It is that deformation which can be represented using a dependent variable which could be used as an injury metric. This would in part address the need to differentiate between mechanical and physiological damage to the CNS as well as determine what the brain deformation tolerance levels are as opposed to measuring acceleration values.

3.4 Proposed Brain Deformation Based Injury Metrics

Finite element modeling offers a possible solution to many of the limitations that arise when peak variable or integrations of three-dimensional rigid body motions are used. This technique allows for the approximate material properties and geometry of the head and brain to be represented under a three-dimensional impact loading scenario. This permits the calculation of how linear and rotational acceleration influence the deformation of brain tissue and contribute to brain injury. This response is also influenced by the vector and location of the impact and in so doing addresses many of the limitations which make the use of integrations such as the HIC and GSI questionable. While finite element modeling offers this complex analysis of brain deformation to impact, there are many dependent variables which can be used to describe the nature of these deformations for the purpose of establishing a threshold.

3.41 Strain

The most commonly used measure of brain deformation is strain. Strain is defined as the change in dimension divided by its original dimension, of which there are three types. Tensile and shear are the most likely types of strain that will cause injury to brain tissue. A third type of strain is compressive strain, which is thought to not be as influential in brain injury as the first two, but important in the production of crushing injuries such as skull fracture. Tensile strain occurs when a piece of tissue is stretched along its axis. With respect to central nervous system tissues, tensile strains may not result in mechanical failure before signs of signal interruption begin to appear (Bain and Meaney, 2001). This phenomenon makes it difficult for anatomists to describe the failure tolerances of brain tissues, especially in relation to reversible injuries such as mild traumatic brain injury (mTBI) (Meaney and Smith, 2011). Shear strain occurs when opposite forces act across a tissue, moving it in opposite directions. This means that when the tolerance limit to shear for a tissue is exceeded, the tissue will separate. This is a common mechanism of injury for brain tissue due to rotation (Ommaya and Gennarelli, 1974; Meaney and Smith, 2011). The output from head impact simulations are typically characterized in terms of tensile strain, more specifically maximum principal strain.

3.42 Maximum Principal Strain

Maximum principal strain is defined as the elongation of a tissue along one of the principal axes relative to its original length (Silva, 2006). The use of this dependent variable is a result of its correlation to mechanical failure in anatomical testing. It is commonly used to signify brain deformation in finite element modeling simulations for head injury. The limitations to this measurement technique are that it takes the largest value of elongation along the principal axis as its sole measurement. This could cause a scenario where the largest value may not be representative of the mechanism of injury. The equation for maximum principal strain is represented thus:

$$\varepsilon 1, 2 = \frac{\varepsilon_x + \varepsilon_y + \varepsilon_z}{3} \pm \frac{\sqrt{2}}{3}\sqrt{(\varepsilon_x - \varepsilon_y)^2 + (\varepsilon_y - \varepsilon_z)^2 + (\varepsilon_z - \varepsilon_x)^2}$$

where ε is strain.

3.43 Von Mises Stress

Von Mises stress is a calculation used for complicated loading scenarios (Silva, 2006). In layman's terms, it takes the various tensors involved in the stress of a structure and gives a result in uniaxial stress which can be compared to the literature (Silva, 2006). This calculation is used to sum the various stress tensors involved in the failure of a structure and reports it in units of stress. This has been widely used by researchers as it accounts for the different directions of stress upon an element. The equation for von Mises stress is represented thus:

$$\sigma = \sqrt{0.5\left[(\sigma_x - \sigma_y)^2 + (\sigma_y - \sigma_z)^2 + (\sigma_z - \sigma_x)^2\right]} + \sqrt{+3\left(\tau_{xy}^2 + \tau_{yz}^2 + \tau_{zx}^2\right)}$$

where σ corresponds to normal stress values and τ corresponds to the shear stress values.

3.44 Intracranial Pressure

This parameter was originally thought to cause brain injury from research on cadavers and dogs conducted by Gurdjian and Gurdjian (1976) and others (Thomas et al., 1966). While it has been theorized to cause local deformations of brain tissue during and after an impact the direct measurement of these pressures and gradients are uncommon. This parameter is used in injury threshold research, since intracranial pressure changes normally result from impacts to the head (Kleiven, 2007).

$$P = F/A$$

where P is pressure, F is force, and A is the area.

3.45 Cumulative Strain Damage Measure

The cumulative strain damage measure (CSDM) was developed by Bandak and Eppinger (1994) to account for the large areas of deformation incurred in the creation of DAI. The development of this measure was based upon the assumption that DAI and other diffuse injuries present themselves after a volume of neural tissue is exposed to an injurious level of strain. This accumulation of strain damage was calculated by Bandak and Eppinger (1994) by measuring the volume of the brain which had experienced strain past a certain level. Through testing on finite element models of the human brain it was found this measure was highly influenced by rotational acceleration and that anterior-posterior rotations were more dangerous in the creation of DAI than medial-lateral rotations. While this measurement appears to have some use in identifying diffuse injuries it is not as widely used in the assessment of focal injuries. It does however put forward a sound theory that instead of measuring stress and strain in one element, as is the case for maximum principal strain and Von Mises stress, that a volume of brain tissue should be considered.

$$Q_{ij}^{n+1} = \{D_{ik}^{n} W_{kj}^{n+1/2} + D_{jk}^{n} W_{ki}^{n+1/2}\}\ \Delta t^{n+1/2}$$

where Q_{ij} are the components of the rotational transformation of D_{ij} from the configuration at t^n to that at t^{n+1}, W is the asymmetric part of the velocity gradient tensor.

3.46 Strain rate

Strain rate is the rate of change of strain with respect to time. Due to the viscoelastic nature of brain tissue, it has been proposed that this variable would be important to the creation of a traumatic brain injury (King et al., 2003). Anatomical research describing the characteristics of brain tissue have to date reported both strain dependence and non-strain dependence depending on the structure (Monson et al., 2003; Darvish and Crandall, 2001; Hrapko et al., 2006). From this research it would seem that the bridging veins and other vascular tissues may not be strain rate dependent, but the more densely packed neural tissue may be. This area needs further investigation through reconstructions to establish a correlation to injury for this variable.

$$E = \varepsilon/t$$

where ε is the deformation of the object in strain and t is the time.

3.47 Product of Strain and Strain Rate

The use of the product of strain and strain rate was first proposed by King et al., (2003). This metric was based upon work done by Hardy et al. (2001) and Newman et al. (1999). From these data the authors identified a need to assess injury by brain deformation as opposed to rigid body kinematic based predictors. Under the assumption that the mechanism of injury for concussion is linked to strain rate some injury reconstructions were attempted (King et al., 2003). They discovered that the product of strain and strain rate had the highest correlation to mTBI followed by strain rate. Kleiven (2007) also used real world reconstructions to assess the correlation of the product of strain and strain rate with positive results.

$$\text{Product of strain and strain rate} = \varepsilon \bullet \varepsilon / t$$

where ε is strain and t is time.

Chapter 4

Injury threshold research

A part of this section has been published in:

Post A and Hoshizaki TB. (2012). Mechanisms of brain impact injuries and their prediction: A review. Trauma, 14(4), 327-349.

Injury threshold research attempts to link the mechanism of injury to an engineering variable that could then be used as a tool in prediction. Currently, thresholds have been proposed using kinematics based variables as well as variables describing brain deformation from FE analyses. Kinematic based reconstructions typically describe a head injury incident using resultant linear and rotational acceleration (Zhang et al., 2004; Fréchède and McIntosh, 2009). In finite element analysis brain deformation characteristics attempt to describe the injury (Zhang et al., 2004; Kleiven, 2007). These brain deformations can then be compared to existing anatomical thresholds for injury risk analyses. However, establishing tissue tolerances are difficult as different types of brain tissue are hypothesized to have different thresholds for injury (Morrison et al., 2003). In addition, human tissue characteristics vary from individual to individual; however, the following section covers what is currently understood regarding parameters involving tolerance limits of central nervous system tissue for the purpose of predicting human brain injury.

Applying threshold values attained from animal and cadaver experiments to living humans is difficult and as a result current methods attempt to correlate mechanical stress thresholds to mechanisms of injury using real world brain injury scenarios (Willinger and Baumgartner, 2003a/b; Zhang et al., 2004; Kleiven, 2007). Kleiven (2007) and Zhang et al. (2004) reconstructed filmed NFL football impacts resulting in concussion and nonconcussions using physical models inside a laboratory and used the resulting linear and rotational accelerations as input for an FEA of the head to describe the regions of stress and strain to the brain (Zhang et al., 2004; Kleiven, 2007). Willinger and Baumgartner (2003a) used a similar method, but the data set included motorcycle accidents as well as the NFL football reconstructions. The tolerances from the NFL reconstructions must be taken as estimated thresholds as the parameters surrounding the reconstructions contained around 20% error in the resulting head impact kinematics due to camera perspective errors and incorrect impact vectors (Newman et al., 2005).

4.1 Kinematic tolerance values

Before the advent of finite element modeling to show tissue deformation, thresholds for injury were based upon the linear and rotational acceleration responses of the head or head form to impact. For reconstructions of the NFL football impacts, linear and rotational acceleration values of 66, 82 and 106 g and 4600, 5900 and 7900 rad/s^2 were reported for a 25%, 50% and 80% chance of mTBI respectively (Zhang et al., 2004). However, Zhang et al.'s (2004) research disagrees with previous cadaver impact research, which indicated a threshold of 4,500 rad/s^2 for SDH (Lowenhielm, 1974a/b).

Relative points of comparison in the literature could be drawn from animal studies scaled to human head geometry (Ommaya et al., 1967). From primate mTBI data, values of 80 g were considered below threshold for concussion while values above 90 g and 1,800 rad/s^2 resulted in concussion and up to 16,000 rad/s^2 for DAI (Gurdjian et al., 1966a; Ommaya et al., 1967; Margulies and Thibault, 1992). Impact tests on volunteers found that a human could withstand values between 2,700 rad/s^2 for normal volunteers and around 16,000 rad/s^2 for boxers (Ewing, 1975; Pincemaille et al., 1989). The boxing data are much higher than previous data as a result of the use of sensors attached to the helmet; helmet response was typically greater than that of the head as a result of increased motions from the impact. Other data from instrumented helmets found 81, 103 and 82-146 g for thresholds of mTBI for collegiate football players (Duma et al., 2005; Brolinson et al., 2006; Schnebel et al., 2007) but are limited due to the sampling frequencies and helmet movement errors that affect this collection methodology. Finally, numerical models were employed to simulate Australian football impacts and found linear and rotational acceleration thresholds of 103 g and 8,020 rad/s^2 (Fréchède and McIntosh, 2009).

The low correlation that linear and rotational acceleration has to brain injury type has made the use of thresholds based on rigid body head kinematics difficult (Kleiven, 2007). This has led to the development of finite element models of the human brain to show how an impact quantified in the linear and rotational acceleration responses causes brain deformation (King et al., 2003). With this area of research, scientists have defined tolerances by kinematics as well as brain strain, stress and shear responses to impact (King et al., 2003). Tables 3 and 4 show the suggested thresholds to date based on accident reconstructions.

Table 3. Linear acceleration based thresholds from reconstructions

Lesion Type	Threshold	Measurement method	Reference
mTBI	82 g for 50% chance	Laboratory reconstruction	Zhang et al. (2004)
mTBI	One case at 81 g	Instrumented helmets	Duma et al. (2005)
mTBI	Three cases, range 55 - 136 g	Instrumented helmets	Brolinson et al. (2006)
mTBI	range of 82-146 g	Instrumented helmets	Schnebel et al. (2007)
mTBI	103 g mean peak	Dynamic modelling	Fréchède and McIntosh (2009)
Subdural Hematoma	range of 192 - 234 g	Motorcyle reconstruction	Willinger and Baumgartner (2003b)

Table 4. Rotational acceleration based thresholds from reconstructions

Lesion Type	Threshold	Measurement method	Reference
mTBI	5,900 rad/s² for 50% chance	Laboratory reconstruction	Zhang et al. (2004)
mTBI	range of 11,482 - 14,860 rad/s²	Motorcylce reconstruction	Willinger and Baumgartner (2003b)
mTBI	8,020 rad/s² mean peak	Dynamic modelling	Fréchède and McIntosh (2009)
no lesion	up to 2,700 rad/s²	Human Volunteers	Ewing (1975)
no lesion	up to 16,000 rad/s²	Human boxers	Pincemaille et al. (1989)
Subdural Hematoma	4,500 rad/s² for low end	Cadaver impacts	Lowenhielm (1974a)
mTBI	7,500 rad/s² for 99% chance	Scaled from primate impacts	Ommaya et al. (1967)
mild DAI	16,000 rad/s² for low end	Adult brain review	Ommaya et al. (2002)

4.2 Anatomic tissue tolerances

Chalupnik et al. (1971) were among the first to investigate the stress-strain behaviour of human cerebral blood vessels. They obtained 28 cerebral arteries from autopsy that were then perfused to the point of normal physiological pressures and stretched axially to failure at strain rates from 0.001 to 50 s^{-1}. The results indicated no rate dependence and reported the largest stress at 20 MPa and 0.2 strain.

Lovenhielm (1974b) investigated the failure characteristics of human parasagittal bridging veins at varying strain rates. The results indicated a dependence of ultimate elongation on rate of strain, decreasing from 70% to 20% for rates varying from 1 s^{-1} to 1000 s^{-1}, with the largest dependence on rate below 100 s^{-1}. Stress was also found to increase for the same region of strain rate, although there was some variation in results.

Lee and Haut (1989) analyzed the effect of strain rate on the parasagittal bridging veins of cadavers. One hundred thirty nine bridging veins were removed from the cadavers and stretched by a hydraulic testing machine beyond failure at a low rate (0.1 to 2.5 s^{-1}) and at a high rate (100 to 250 s^{-1}). The results indicated that strain rate had no effect on failure and that the average point of tensile failure (strain) was 0.51 to 0.55.

Margulies and Thibault (1992) proposed a tolerance criterion based on animal, physical, and analytical model experiments to determine the kinematics involved in diffuse axonal injury in the primate. From previous experiments scaled to human geometry and tissue properties, the critical strain value for moderate to severe DAI was found to be between 0.05 and 0.10.

Bain and Meaney (2000) examined tissue level thresholds for white matter axonal damage in guinea pigs. They stretched adult male guinea pig optic nerves to 8 levels of displacement (1.0 mm to 8.0 mm) and ran experiments to assess the amount of functional disruption. From this animal study, the results indicated three strain-based thresholds for morphological injury to the white matter: (i) Liberal – 0.34 strain, above which all nerves are predicted to have injury; (ii) Conservative – 0.14 strain, the strain below which no nerves exhibited injury; and (iii) Optimal – 0.21 strain, which is a value chosen to optimize sensitivity and specificity. The values for electrophysical impairment were: (i) Liberal – 0.28; (ii) Conservative – 0.13; and (iii) Optimal – 0.18. However, these values lose some validity when being applied to human tissue tolerance levels.

Monson et al. (2003) conducted research investigating the axial mechanical properties of human cerebral blood vessels. Eighteen cerebral arteries and fourteen veins were obtained from the cortical surface of the temporal lobe of human subjects during surgery. The vessels were then stretched at two rates: a low rate (0.01 to 0.26 s^{-1}) and a high rate (211 to 524 s^{-1}). Failure of the vessels occurred around 0.31 strain. Overall, the authors reached the following conclusions from the testing protocol: (i) the longitudinal stress-stretch behaviour of human cerebral blood vessels is usually characterized by an initial toe phase, followed by a linear phase until failure; (ii) cortical arteries are stiffer than cortical veins and at failure carry approximately twice as much stress at half the stretch; and (iii) strain rate over a range of more than four orders of magnitude has little effect on the mechanical failure properties of human cerebral arteries and veins (Monson et al., 2003).

Cater et al. (2006) studied the temporal development of hippocampal cell death in a rat animal model. Using a tissue based injury model, the authors developed a predictive function for hippocampal cell death evolution of 4 days in response to controlled tissue deformation. Rat hippocampal tissue cultures were subjected to measured deformations of 0.05 to 0.5 strain and strain rate of 0.1 to 50 s^{-1}. The results indicated that cell death was dependent on amount of strain, but not strain rate.

Table 5. Listing of measured brain tissue tolerances from anatomical testing

Injury Threshold Value	Tissue Type	Method	Reference
20 Mpa stress, 0.2 strain, no dependence on strain rate	Cerebral blood vessels	Cerebral cadaver arteries	Chalupnik et al. (1971)
Documented strain rate dependence of tissue	Parasagittal Bridging veins	Cadaver bridging veins	Lowenhielm (1974)
0.51 to 0.55 strain, no dependence on strain rate	Parasagittal Bridging veins	Cadaver bridging veins	Lee and Hault (1989)
0.05 to 0.10 strain	General to brain tissue	Analytical tissue model based on animal and physical models	Margulies and Thibault (1992)
0.1	White matter axons	Squid axon stretch	Thibault (1993)
0.19 strain, 6-11 kPa Von Mises stress and 0.8-1.0 kJ/m^3 strain energy density for contusions	Cortex	Cadaver tissue	Schreiber (1997)
8-16 kPa for DAI	CNS tissue	Sheep model	Anderson et al. (1999)
0.14 to 0.34 strain	White matter axons	Male guinea pig optic nerve stretch	Bain and Meaney (2000)
0.31 strain, no dependence on strain rate	Cerebral blood vessels	Human cerebral blood vessels from surgery	Monson et al. (2003)
Documented no dependence on strain rate	Hippocampal tissue culture	Rat hippocampal tissue culture deformation	Cater et al. (2006)

Overall, research into the mechanisms of injury for traumatic brain injury has shown that damage to neuronal tissues are caused by deformations and stresses as a result of combined loading of linear and rotational acceleration (Viano et al., 1989; Kleiven, 2007). These linear and rotational loading curves cause compression, tension, and shearing in different directions and locations of the brain (Gurdjian and Webster, 1947). The response of tissue to anatomical testing methods also suggests that they are sensitive to rates and direction of loading. Strain dependent nature of tissue has been studied by Nicolle et al. (2004) who observed neural tissue behaves differently at high frequency when compared to low frequency of loading for high speed impacts such as those causing brain injury. The method of loading brain tissue for tolerance testing has also been documented to produce varying failure rates as previously shown (Table 5). Also, Arbogast and Margulies (1998) and Donnelly and Medige (1997) demonstrated that brain material response was dependent on loading rate, particularly in the brainstem.

In summary, current brain material tolerances have been developed from two primary sources: animal tissue and cadaver tissue research (Table 5). Developing brain material threshold values from animal studies allows for more invasive procedures on living organisms, but lacks some level of applicability to human tissue. The cadaver tissue tolerance data benefits from being human tissue, but the issue of how different recently dead brain tissue is from living brain tissue remains in question. A review of current brain tissue tolerance research reveals that strain is highly correlated with mechanical tissue failure. There continues to be debate over the usefulness of strain rate in predicting tissue failure as well as compression because of the brains' high bulk modulus. Research has also shown that the nature of brain tissue is viscoelastic and anisotropic. The areas of brain tissue, for example grey matter vs white, hippocampus vs cortex, also display different response properties when loaded in different directions (Prange et al., 2002). The directional response of brain tissue has been shown to exist nearly 30 years ago by Gennarelli et al.'s (1987) work on monkeys. Kleiven (2003) has also demonstrated that the brain is more susceptible to subdural hematoma in certain directions. These variations in material characteristics of the brain tissue will have direct implications on how easily it is damaged, and to date there has been little research into the sensitivities of these tissues from a reconstructive perspective.

4.3 Tolerance limits for brain injury developed through reconstructions and finite element modeling

Finite element modeling allows for the use of tissue response parameters to describe the effect of an impact to the head. Anatomical tissue testing allows for the comparison of simulation results with mechanical tolerances measured in units of stress or strain. There has been work conducted by researchers doing reconstructive work on real life impacts examining the relationship between impact kinematics, variables such as maximum principal strain, Von Mises stress, intracranial pressure, and brain injury.

Willinger and Baumgartner (2003a) used their FE head model to explore possible brain injury thresholds using data from motorcycle accidents, American football head injuries and pedestrian head impacts (64 total head injuries). The FE model consisted of the face, cranium, scalp, brain, CSF, falx and tentorium, and was validated through cadaver impacts (Nahum et al., 1977; Trosseille et al., 1992). The motorcycle head impacts were replicated at a drop test facility by modifying the impact parameters until helmet damage could be replicated. The American football head injuries were reconstructed using video recordings of players' relative positions, velocities of impact, impact location, and simulated using Hybrid III dummy systems (Pellman et al., 2003; Newman et al., 2005). The non-helmeted pedestrian impacts were simulated using an analytical model predicting their kinematics before impacting car windscreens, developed from data acquired at the scene of the accident. The authors investigated the intracerebral pressure response, Von Mises stress, and global strain energy of the CSF in comparison to location and type of neurological lesion. The results revealed the Von Mises stress tolerance limit for a 50% chance of moderate or severe brain injury as 18 kPa to 38 kPa and subdural hematoma was 5.5 J for global strain energy in the CSF. Overall, the authors found that Von Mises stress was found to be the best predictor for brain injury.

In a study on brain injury tolerances, Willinger and Baumgartner (2003b) used a novel Bimass headform coupled with a FE model of the human head to reconstruct motorcycle accidents. The physical head surrogate used for reconstruction was a modified Hybrid III headform, with a mass to represent the brain attached to the skull with a damped spring system, to simulate brain skull motion. Thirteen motorcycle accidents were reconstructed in two ways: (i) on a drop tower from the data describing the accident with the new Bimass headform and (ii) the output from a standard Hybrid III three-dimensional time history was used to as input to the FE model developed at Université Louis Pasteur (Willinger and Baumgartner, 2003a). The FE model indicated a threshold for concussion at a Von Mises stress of approximately 20 kPa, and subdural hematoma thresholds at 4 J of strain energy in the CSF layer (Willinger and Baumgartner, 2003b).

Zhang et al. (2004) used the highly complex and extensively validated Wayne State Brain Injury Model to evaluate mild traumatic brain injury (mTBI) impacts incurred during American football games. The FE model consisted of the scalp, skull, dura, falx tentorium, pia, venous sinuses, CSF, lateral and third ventricles, cerebrum (gray and white matter), cerebellum, brain stem and parasagittal bridging veins, and was validated using cadaver data. Twenty four helmet to helmet impacts were reconstructed using on-field video data to identify the impact velocity and site (Newman et al., 2005). The impacts were then recreated using helmeted Hybrid III headforms on a guided wire drop rig with similar impact locations and velocities. The authors note that the estimated error of the entire process was around 11.3% to 20% (Newman et al., 2005). The intracranial pressure response of the model showed coup and contrecoup patterns, but the location of peak pressures did not correlate well with sites of concussive brain injury. However, the resulting magnitude of pressure did reflect the severity of impact. Pressure response was found to be highly influenced by translational acceleration and shear strains highly affected by rotational acceleration. The threshold injury analysis showed that shear stress levels for 25%, 50% and 80% chance of mild traumatic brain injury (mTBI) were 6.0, 7.8, and 10 kPa respectively. The shear strain thresholds incurred from the reconstruction were 0.14, 0.19, and 0.24 for 25%, 50%, and 80% chance of mTBI respectively. For kinematic correlations, the model indicated that a translational acceleration at the centre of gravity of 66, 82 and 106 g and rotational accelerations of 4,600, 5900, and 7900 rad/s^2 would lead to a 25%, 50%, and 80% chance of mTBI. For the integrated response variables, a HIC value of 151, 240, and 369 corresponded to the 25%, 50% and 80% chance of mTBI. The authors noted that their values were lower than many found in the literature, likely a result of the primarily lateral and frontal-lateral reconstructions, known to have a lower tolerance to impact (Gurdjian et al., 1963; Kleiven, 2003). This is an area that needs further research as more real-world brain injury data becomes available.

In 2005, Franklyn et al. used simulated car crash scenarios with known AIS outcomes to test the validity of two finite element models of the human head. The FE models used were the simulated injury monitor (SIMon) and the more refined and complete model developed at Wayne State University (WSUHIM) (Zhou et al., 1995). Real world car crash scenarios were reconstructed in the laboratory with similar impact mechanics as the actual event. All crush dimensions of the cars were recorded by SAE J224 Collision Deformation Classification profile and the change in velocity (Δv) calculated by CRASH3. Four cases were chosen for reconstruction based upon the relative simplicity of the reconstructive process. One AIS 0 (minor), 4 (severe) and 5 (critical) case were reconstructed and one multiple AIS case was simulated. The reconstruction involved impacting cars into structures with Hybrid III crash test dummies in the appropriate car seat with a Hybrid III headform equipped with a 3-2-2-2 accelerometer array for full 3D capture of the resulting kinematics. The linear and rotational accelerations from the reconstructions were then applied through the centre of gravity of each FE head model and comparisons were made to the medical AIS reports. The results of both FE models indicated that they were not able to reliably predict the resulting injuries found in the medical reports. In some cases, they were able to predict one type of injury but not another for the same reconstruction. These difficulties are likely a result of variations in the FE model parameters and the reconstructive process. While the models may be partially validated, the validation is direction specific and may lose some validity when the brain is impacted in different directions in such extreme ways. The material characteristics of the model and the parameters describing the material responses are also approximate. The reconstructive process in car crash scenarios is very difficult. There are a number of variables that must be controlled to get an accurate dynamic response for the impact. As a result it is unlikely that the reconstructions produced a linear and rotational acceleration response that could be used as input for validation. As such, while the research conducted showed an interesting methodology but there was too many variables that were not controlled and this was reflected by the lack of predictive abilities by both FE models.

Kleiven (2006) used a validated FE model (Kleiven and Hardy, 2002) to evaluate the sensitivity of kinematic head injury criteria to different impact vectors. A secondary purpose of the research was to investigate the effect of the kinematic dependent variables on intracranial strains associated with brain injury. Nine acceleration pulses were applied, pure translational and pure rotational, to the centre of gravity of the head in the posterior/anterior, superior/inferior and lateral vectors. The rotational acceleration pulses were sinusoidal with an amplitude of 10-11.6 krad/s^2 with a duration of 5 ms, and a peak rotational velocity of 25-29 rad/s (within the range of DAI suggested by Marguiles and Thibault, 1992), which gives a Head Impact Power (HIP) of 4.3 kW. The translational pulses were sinusoidal with an amplitude of 794 m/s^2 (80 g), and a duration of 5 ms, which results in a HIC of 52 and HIP of 4.3 kW. Maximum principal strain was chosen as the predictor for central nervous system (CNS) injuries based on its association with DAI (Marguiles and Thibault, 1992). The results indicated that HIC was unable to predict purely rotational impulses, while HIP and peak change in velocity require scaling to account for changes in direction. Pure rotational impulses and peak change in rotational velocity show best correlation with strain in the FE model. Finally, the authors found that for pure translational impulses, HIC and HIP showed the best correlation with the strain levels in the FE model.

Kleiven (2007) evaluated 58 National Football League head impact cases using an FE model of the human head in an attempt to identify the best brain injury predictor. The data for the 58 cases was the same as was used by Willinger and Baumgartner (2003b), and the data collection method as outlined by Newman et al. (2005). The author used the Kleiven and Hardy (2002) model, and the output from the reconstruction in linear and rotational acceleration was used in the model. Eight tissue level injury predictors were evaluated for correlation to brain injury for six different regions, encompassing the cerebrum to the whole brain. Ten kinematic-based predictors were also investigated for correlation to injury in addition to tissue level dependent variables such as strain and pressure. The results of the FE simulation revealed a 50% probability of concussion for maximum principal strain with a value of 0.21 in the corpus callosum and 0.26 in the grey matter. These values are different from previous research that has indicated these strain magnitudes to be associated with contusions and DAI (Bain and Meaney, 2000). For strain rate, a 50% probability of concussion was found at a value of 48.5 s^{-1}. The product of strain and strain rate also showed an association with injury with a 50% probability value of 10.1 s^{-1}, which is lower than previous reported values (Viano and Lovsund, 1999). The cumulative strain damage measure predicted a 47% chance of concussion in the white matter when 55% of the brain had endured a strain of 0.1, which is close to previous values reported by Takhounts et al. (2003). A 50% chance of concussion was found to be 8.4 kPa for Von Mises stress, which is in agreement with Zhang et al. (2004) but lower than that proposed by Willinger and Baumgartner (2003b), likely due to the inclusion of more severe injuries in their reconstructions. Strain energy density indicated a 50% chance of concussion threshold at 2.1 kJ/m^3. The magnitude of maximum and minimum pressure indicated a 50% chance of concussion in the grey matter of 65.8 kPa, which is in agreement with Zhang et al. (2004) (90 kPa) but considerably lower than Ward et al. (1979) (183 kPa). For negative pressure a 50% chance of injury was found to be 55.1 kPa in the white matter. The authors felt that this may not be a suitable predictor for injury as negative pressure theories are based upon cavitation, which has been discounted as a mechanism of injury in previous research (Hardy et al. 1994, Gurdjian and Gurdjian, 1976). When analyzing kinematic head data, translational acceleration had the highest correlation with pressure and rotational acceleration with strain. A high correlation with mTBI was found for the HIC, and when used in conjunction with peak change in rotational velocity, showed the best correlation with injury. The author made the following conclusions: (i) the maximum pressure in the grey matter showed the highest significance in statistical correlation with concussion; (ii) for reconstructions, a known injury pattern in the brain correlated well with contours of maximum principal strain, while pressure did not; (iii) rotational kinematics are the most influential factor for intracranial deformations; (iv) translational kinematics are the most influential factor for intracranial pressures; (v) correlation was found between resultant rotational acceleration and resultant peak change in velocity with maximum strain in the brain and (vi) a linear combination of HIC and peak change in rotational velocity showed highest correlation with maximum principal strain. In conclusion, the author notes that the description of the NFL impacts is not sufficient to adequately reconstruct the head injury cases, as the reported brain injuries did not have medical images with which to correlate any injury.

More recently Takhounts et al. (2008) modified their SIMon finite element head model in an attempt to improve its accuracy for use in car crash scenarios. The model was morphed to match a generalized head geometry and the number of elements and the refinement of the mesh was increased. Using this model they analyzed a series of dynamics responses from concussive impacts recorded by the head impact telemetry system (HITS) during American football league games. The resulting dynamic responses measured by the hits system varied from 19 g to 135 g for linear and 668 rad/s^2 to 9922 rad/s^2 for rotational acceleration. The brain deformation metrics used were maximum principal stress and strain. The maximum principal stress was found to have low correlation to injury, which was consistent with the incompressible characteristics of the model. The maximum principal strain varied from 0.076 to 0.921, which are well in excess of any currently postulated concussive thresholds (Zhang et al., 2004; Kleiven 2007). The majority of the values were about 50% strain, which would indicate a traumatic brain injury according to most anatomical threshold research (Lee and Hault, 1989; Monson et al., 2003). In their discussion, the authors discuss this discrepancy and attribute the results to the model being relatively ‘soft’ in material characteristics. While this may be true, errors in the input parameters may also have contributed to the discrepancies. The HITS system has its sensors attached to the inside of the helmet and calculates its’ linear and rotational accelerations from algorithms based upon the accelerometers relative locations. This system overlooks several aspects of impact mechanics; firstly the helmet is not rigid which changes the relative location of the accelerometers to each other, the accelerometers move in relation to the head, and the sampling speed of these accelerometers are low for direct head impacts (1 kHz). This system also has not been validated for measurement of rotational acceleration. It is possible the results of this study are in error not only as a result of modeling issues but also because of the errors found in the dynamic response produced by these helmet based reconstructions.

Table 6. Listing of thresholds for mTBI from reconstructions using a combination of physical headforms and FE modeling

mTBI Threshold value (50% chance)	Dependent variable	Location	Reference
0.21	Max. Principal Strain	Corpus Callosum	Kleiven (2007)
0.26	Max. Principal Strain	Grey Matter	Kleiven (2007)
0.19	Max. Principal Strain	Grey Matter	Zhang et al. (2004)
48.5 s^{-1}	Strain rate	Grey Matter	Kleiven (2007)
10.1 s^{-1}	Product of Strain and Strain rate	Grey Matter	Kleiven (2007)
2.1 kJ/m^3	Strain Energy Density	Grey Matter	Kleiven (2007)
5.5 J	Global Strain Energy	CSF	Willinger and Baumgartner (2003)
0.1	CSDM	White Matter	Kleiven (2007)
8.4 kPa	Von Mises Stress	Corpus Callosum	Kleiven (2007)
7.8 kPa	Von Mises Stress	Brain Stem	Zhang et al. (2004)
18 kPa	Von Mises Stress	Brain	Willinger and Baumgartner (2003)
65.8 kPa	Intracranial Pressure	Grey Matter	Kleiven (2007)
90.0 kPa	Intracranial Pressure	Grey Matter	Zhang et al. (2004)

4.4 Summary

Kleiven (2007), Zhang et al., (2004), and Willinger and Baumgartner (2003a/b) are the primary researchers currently investigating brain injury thresholds by reconstructing brain injury accidents. These researchers have collectively established certain brain tolerance criteria (Table 6), but lack complete agreement for any level of injury, which may imply a brain injury continuum instead of an exact threshold value. In addition, the authors of this research all use Pellman et al.'s (2003) research of concussive American football impacts. These reconstructive data are at best in error 11.3% from the video camera analyses, while the simulations showed errors of 17% for linear and 25% for resultant rotational acceleration (Newman et al., 2005). Other researchers have attempted to use a telemetry system to collect reconstruction data, which lacks validation for rotational kinematics. As a result the impact vector may not have been reproduced accurately with these reconstruction methods and could lead to different linear and rotational acceleration responses. Also, effective impact mass has not been adequately established, which would be influenced by the contractile state of the players' muscles involved in the injury scenario. All of these sources of variability contribute to the difficulty of having an accurate reconstruction of the event and call into question the validity of the output. A possible method to account for the varied reconstructive parameters (velocity, mass, location) would be to take a grid of all likely impact characteristic combinations and then plot the dynamic responses incurred (Kendall et al., 2012). This method could produce a window of possible response for each reconstruction, instead of having one value laden with uncontrolled or not understood levels of error.

While these reconstruction procedures have their limitations, the use of Mathematical Dynamic Models (MADYMO) and finite element modeling of the human brain also have their own. The MADYMO simulations use anthropometric dummy models which are based upon human kinematics but do not represent exact human parameters (O'Riordan et al., 2003). These models are used to simulate the kinematics of an impact and use the resulting head motions to drive finite element modeling processes (Doorly, 2007). The accuracy of these simulations depends upon the accuracy of the report forms and the representations of the impact surfaces within the simulated environment. In addition the human models used are validated for pedestrian impacts with cars and may not be accurate for use in sporting impacts. Finally, the models used in MADYMO simulations do not have muscle activation algorithms and thus the kinematics of the fall or collision may not be accurate to the event. Finite element models of the human brain also have limitations. The geometry of the brain can vary in the population and thus can be a source of variability when applied to injury reconstructions. The material properties assigned to the various parts of the model are normally derived from cadaver tissue testing that can have some differences with in vivo tissues in terms of impact response (Zhang et al., 2001). In addition, the description of the tissue response is based upon rheological tests that are dependent on rate of loading which can have varying results depending on how the test parameters are applied (Rashid et al., 2012a/b). Finally, the validation procedures for the finite element models of the human brain may not be directly applicable (pressure and brain motion for specific regions of the cerebrum) to the nature of the investigations for which the models are being used.

Kleiven (2007) comments on these discrepancies and acknowledges the limitations of physical and finite element model reconstructions in the attempt to establish injury threshold criteria for the brain. However, Kleiven and others have identified that this limitation may be in part overcome if endpoint medical images of the injured area were available for all injury scenarios to allow for comparison and backwards validation of the reconstructive parameters used (Zhang et al., 2004; Kleiven, 2007). Unfortunately in all these studies, there was no validation of the reconstructive procedures or the sample size was small. Further research in this area, preferably with medical scans and accurate reconstructions would be advantageous in establishing a continuum of brain injury, or possibly specific brain injury thresholds.

Research involving anatomical tissue has demonstrated brain structures are viscoelastic and anisotropic (Prange et al., 2002). Therefore it would be reasonable to expect the different regions of brain tissue and anatomic parts of the brain to behave differently under different loading scenarios. It could also be proposed that these different brain regions would have different thresholds for injury. This research demonstrates why simple peak linear and rotational acceleration measurements lack prediction for brain injury as they don't take into account the response of the brain tissue to such loads. Brain deformation metrics are seen by researchers as dependent variables that would be more closely associated with injury (King et al., 2003); however the correct variable to use for any particular type of injury has yet to be established. In addition, the influence of the linear and rotational acceleration curve characteristics on brain tissue deformation metrics has yet to be ascertained. With more accurate reconstructions and finite element models of the human brain these questions may be addressed.

Researchers have attempted to link engineering parameters to brain injury with limited success. What currently exists as thresholds are rough guidelines based upon research with accepted limitations in their methodologies. Kleiven (2007) and King et al. (2003) both identify that the reconstructions were limited, and that using medical imaging would aid in eliminating some of the limitations surrounding their injury threshold research. Medical imaging would allow for the positive identification of regions of injury for comparison to finite element modeling solutions. This would permit regions of deformation in the model to be compared to the region of injury in the medical images, allowing for a direct measurement of dependent variables in that volume. However, a reconstructive process must be established that accounts for the variability in mass, velocity, and impact location. Also, a reconstructive process that supplies a window of response could be used in conjunction with modeling to account for continuums of possible reconstructive possibilities and modeling responses. This protocol could allow for region specific brain deformations to be measured as well as supply a validation for the reconstructive process when compared to the literature. In addition, this method could further evaluate the finite element model's characteristics as well as further the understanding of reconstructive parameters.

Chapter 5

Medical Imaging in Brain Injury Research

Medical imaging is commonly used in the clinical assessment of traumatic brain injuries. Its use to date has been largely as a qualitative diagnostic tool to identify the presence of hematomas and other abnormalities in the brain for purposes of surgical intervention. New approaches have recently been developed to allow for the scientific quantitative use of medical imaging techniques such as computer tomography (CT) and magnetic resonance imaging (MRI) (Bigler, 2001; Basser and Jones, 2002, Sundgren et al., 2004). With these new imaging techniques it has become possible to make use of the scans to further validate brain injury reconstructions by enabling the correlation of injury metric to injury site. There are three primary medical imaging techniques used by biomechanical researchers, the CT, MRI and diffusion tensor MRI (DT-MRI). Computed tomography (CT) is a method that takes 2D x-ray slices of the object and uses digital geometry processing to generate a three-dimensional image. This method is commonly used to identify brain injury volumes such as intracerebral bleeds and contusions (Bigler, 2001). Magnetic resonance imaging (MRI) uses the property of nuclear magnetic resonance to visualize detailed internal structures by means of a powerful magnet. The tissue contrast available with this technique makes it preferable to CT imaging when it comes to analyzing the brain and other complicated structures (Basser and Jones, 2002). Diffusion weighted imaging (DT-MRI/ DTI) is used to show the diffusivity of water molecules in biological tissues. This allows for the examination of microstructures of the brain tissue such as white matter tracts (Sundgren et al., 2004). This increased capacity to examine tissue structures of the brain makes the use of DTI preferable for diffuse brain injury analyses.

This section will discuss the use of medical imaging as a new tool to identify regions of interest in accident reconstructions. The examination of these protocols will cover preliminary work on rats and more recent work on humans. Finally, it will cover tractography to help identify areas of diffuse axonal injury for examination using finite element modeling.

5.1 Medical imaging in accident reconstruction

Brain injury reconstructions have been attempted by re-creating a given impact using a combination of physical and FE models to find parameters which describe the brain deformations. One of the limitations often associated with this research is that there is no end point medical image with which to compare the finite element modeling output. This means that the exact location of stress or strain causing the subdural hematoma or contusion cannot be accounted for. With the advances in medical imaging it is now possible to draw comparisons between medical imaging and finite element modeling of the brain. There have been relatively few studies which have utilized this technique, but there has been some research in rats and some limited reconstructions with humans.

5.11 Quantitative MRI analysis of impact to rats

The use of animals to examine the links between mechanism of injury and brain deformation parameters allows for in depth understanding of injury characteristics. Mao et al., (2010) used rats to associate levels of strain to neuronal cell death by location in the brain. This research inferred a relationship between maximum principal strain and cell death in the human. There has been some research using quantitative MRI techniques to evaluate impacts to rats. Colgan et al. (2010a) used rats to evaluate the influence of controlled cortical impact on brain volume changes. The rats' brains were directly impacted at what were identified as ‘mild’ and ‘severe’ velocities and depths of penetration with the intracranial pressure (ICP) monitored by MRI over a period of 5 hours. The 5 hour time period was chosen to reflect the average time taken from the injurious event to hospital admittance (Breen et al., 2000). The MRI results indicated an increase in ICP and a reduction in CSF in the cranium. This increase in pressure caused reduced blood flow similar to the response in human patients who have suffered a TBI (Steiner and Andrews, 2006). In addition, the mild impacts were slower to manifest injurious symptoms when compared to the more severe impacts. This led the authors to conclude that it is possible to develop an intervention that may help prevent neuronal loss before the mild injury produces more deleterious secondary effects.

Direct cortical impact techniques have limitations that have implications for human reconstructions. Firstly, the rate at which the indentor impacts the brain tissue and other mechanical variables can influence the results. More importantly, the authors note that the anisotropy of neural tissue fibers (preferential orientation) with respect to the impact vector will have an influence on the injury severity and the volume of brain tissue affected (Mao et al., 2010).

5.12 Human focal brain injury reconstruction with use of medical imaging

There is a paucity of research using medical imaging for accident reconstructions. O’Riordan et al. (2003) used medical imaging as an aid to MADYMO reconstructions of brain injury incidents. The computational model was used to simulate 4 different brain injury (as identified by CT scan) scenarios in an attempt to identify the dynamic response in terms of linear and rotational acceleration response in relation to the injury. As a result of the limitation in number, age, location, and type of injuries, no attempt was made to correlate the resultant peaks in linear and rotational acceleration to brain injury. The authors concluded that using this type of combined FE and MADYMO injury simulation would be useful in creating improved reconstructive parameters for use as input to more refined finite element models.

Doorly and Gilchrist (2006) used two of O'Riordan et al.'s (2003) reconstructions with CT scans and MADYMO inputs to examine the brain injury event using a finite element model of the human brain. The cases chosen were of a young boy (11 years old) and an elderly lady (76 years old), both injured as a result of a fall. The MADYMO reconstruction resulted in peak resultant linear and rotational accelerations of 366 g and 36 krad/s^2 for the boy and 236 g and 33 krad/s^2 for the elderly lady. These curves were then used as input conditions for the FEA, which produced results in brain deformation for both cases (see table 7). The authors felt that the boy did not suffer the severe injuries (e.g. subarachnoid hemorrhage, contusion) normally associated with the magnitude of input kinematics due to the relatively compliant nature of the developing cranium. Following a sensitivity analysis, the authors identified that slight differences in head position and body characteristics in MADYMO for the fall simulation can lead to different output parameters for the impact. This is also evidenced by work done by Horgan (2005) who used the same two falling incidents to apply the newly created University College Dublin Brain Trauma Model (UCDBTM) to a real world injury event. For the 11 year old boy the linear acceleration was found to be 584 g and rotational acceleration of 20 krad/s^2 and 308 g and 44 krad/s^2 for the 76 year old elderly lady. This led to variations in FEA results as can be seen in table 7. These results identify the need for accurate representations of reconstructive parameters and the influence that impact characteristics can have on output (Walsh et al., 2010). With respect to brain injury parameters, Doorly and Gilchrist (2006) reported that strain rate and the product of strain and strain rate appeared to be good predictors for the boy's injuries.

Table 7. The brain deformation parameters from Doorly and Gilchrist (2006) and Horgan (2005) reconstructions.

	Doorly and Gilchrist values (2006)				Horgan values (2005)			
	Injury area		Highest value		Injury area		Highest value	
Parameter	Boy	Lady	Boy	Lady	Boy	Lady	Boy	Lady
Von Mises Stress (kPa)	11.2	7.8	15.2	16.7	3.2	6.0	12.67	18.8
Strain	0.32	0.25	0.34	0.48	0.07	0.2	0.3	0.28
Strain rate (s^{-1})	103	96.6	107	100	11.8	30	71.6	57.7
Strain X Strain rate (s^{-1})	18.7	12.7	26.9	24.7	0.48	2.4	19.5	20

In his 2007 paper, Kleiven used a finite element model of the human brain in conjunction with medical images to reconstruct a motorcross accident. The rider in this simulation was impacted to the head by the front fender of another bike and then impacted the ground with his head. The resulting CT images indicated the presence of several intracerebral hematomas in the brain. Using finite element analysis, Kleiven reconstructed the accident and found that maximum principal strain patterns successfully identified the injured regions as shown by the CT scans. The pressure distribution, which Kleiven found in a series of reconstructions to be linked to concussion, did not follow the injury pattern. The strain levels at maximum for the two largest hematomas were 0.3 and 0.4, which is known to be close to the levels expected for mechanical failure of cerebral veins and arteries (Lowenheilm, 1974a; Lee and Haut, 1989; Monson et al., 2003). These results led Kleiven to conclude that maximum principal strain in this case successfully predicted the presence of intracerebral hematoma. However, as identified by O'Riordan et al. (2003), Kleiven acknowledges that results using finite element modeling are dependent upon the quality of the reconstruction, which in the case of the motorcross incident was relatively inaccurate.

Both authors identify that it would be ideal to use a refined reconstructive process in conjunction with medical images to identify injury locations to further research in the area of injury metrics.

5.13 Medical imaging use for diffuse injuries

Studies by Kleiven (2007), Doorly and Gilchrist (2006), and O'Riordan et al. (2003) use either CT or MRI data to identify locations of focal brain injuries for accident reconstruction but not for diffuse injury identification. A possible reason for this is that to date neither CT nor MRI has been able to identify regions of the brain which have incurred diffuse injuries such as concussion and diffuse axonal injury. Recently a new method of medical imaging (diffuse tensor imaging) has been developed that allows for the examination of the white matter tracts inside the brain where diffuse axonal injury is thought to occur. Research by Colgan et al. (2010b) used a novel DTI protocol to identify the directionality of white matter tracts to improve the complexity of the University College Dublin Brain Trauma Model. By tracking the diffusion of water, Colgan et al. (2010b) identified the location of white matter neuronal fibers whose disruption is thought to be associated with diffuse axonal injury. In 2010, Singh et al. identified regions of interest in the brain tissue of DAI patients using a similar method to Colgan et al. (2010b). Using a 'normal' DT MRI scan as a baseline for comparison for injured DAI patients, Singh et al. successfully identified regions where the white matter tracts were disrupted. This methodology of quantitatively comparing a 'normal' scan to an injured scan was accomplished in a statistically rigorous manner that has applications for future DAI research. This methodology, along with Colgan et al.'s (2010b) allows for the identification of regions of disruption of neuronal fibers associated with DAI. These regions could then be compared to FEA reconstructions for relative levels of brain deformation that would allow association to injury metrics.

5.2 Summary

The use of medical imaging for biomechanical brain injury reconstruction in humans is rarely used. This is likely a result of the difficulty in attaining quality CT and DT-MRI scans of reconstructable injuries as well as the cost involved in the number of scans that would be necessary to create a statistically powerful data set. The potential benefit of using CT/MRI scans to aid in the reconstructive process has been identified by previous authors (Kleiven, 2007). The scans would allow for the correlation of reconstructive brain deformation based outputs to location and type of brain lesion. This would permit further validation of the model and the reconstructive processes. To date, this type of correlation has not been accomplished other than a few cases that were used primarily to identify a possible use of finite element modeling as opposed to the development of a statistically valid approach.

Chapter 6

Finite Element Model – University College Dublin Brain Trauma Model

6.1 Model development

The model used in this research was developed in Dublin, Ireland by Horgan and Gilchrist (2003) and is known as the University College Dublin Brain Trauma Model (UCDBTM). The geometric parameters of the model were from a male cadaver as determined by medical imaging techniques (Horgan and Gilchrist, 2003; Horgan and Gilchrist, 2004; Horgan, 2005). The male head selected was not that of a 50% male but was chosen based on the quality of the medical imaging scans. The head and brain finite element model was comprised of ten parts: the scalp, skull (cortical and trabecular bone), pia, falx, tentorium, cerebrospinal fluid (CSF), grey and white matter, cerebellum, and brain stem (Table 8). The scalp was modeled using shell elements, cortical and trabecular bone with brick elements of varying thickness, the dura with membrane elements, CSF with brick elements, pia with membrane elements, falx and tentorium with shell elements and the cerebrum, cerebellum and brain stem with brick elements. The CSF layer was modeled using solid elements with a high bulk modulus and low shear modulus to allow a sliding boundary condition between the interfaces of the CSF and brain. The algorithm allowed no spaces between the pia and the CSF layer. For the sliding surfaces a friction coefficient of 0.2 was used (Miller et al., 1998). The fluid present between the falx and the brain and between the tentorium, cerebrum, and cerebellum also had the same fluid algorithm. In total, the brain model was comprised of 26,000 elements. The depth of the CSF layer was 1.3 mm to simulate the norm for the average adult male. For this thesis, a modified version of the

UCDBTM, which was created by Doorly (2005), was used to run the simulations. The updated UCDBTM had a denser mesh for the CSF and the skull was removed as all inputs to the model were conducted through the reference point at the centre of gravity of the model.

6.11 Material Properties

The response of the model is highly dependent on its material properties and characteristics (Bandak and Eppinger, 1994). Biological tissues display typically nonlinear behaviours as opposed to linear behaviours in response to loading. When the material is under compression it will generate larger stresses for smaller and smaller strain increments as the body deforms. This behaviour also includes a rate dependent effect when applying loading or unloading, which is referred to as viscoelasticity. Linear elastic behaviour occurs when the behaviour in loading and unloading of the material is proportional and the response is instantaneous.

Previous finite element models of the brain have adopted linear elastic material constitutive laws (Shugar and Katona, 1975; Ward and Thompson, 1975). However, the current model uses the parameters used by Mendis et al. (1995) and Kleiven and Von Holst (2002) which are nonlinear viscoelastic material law under large deformation. A hyperelastic material model was used for the brain in shear in conjunction with a viscoelastic material property. The hyperelastic law was given by:

$$C_{10}(t) = 0.9C_{01}(t) = 620.5 + 1930e^{-t/0.008} + 1103e^{-t/0.15} \text{ (Pa)}$$

where C_{10} and C_{01} are the temperature-dependent material parameters, and t is time in seconds. The compressive behaviour of the brain was considered elastic. The shear modulus parameters were determined from a logarithmic plot (Horgan, 2005):

$$G(t) = G_\infty + (G_0 - G_\infty)e^{-\beta t}$$

where G_∞ is the long term shear modulus, G_0 is the short term shear modulus and β is the decay factor (Horgan and Gilchrist, 2003). As fluid has a high bulk modulus and zero resistance to shear, the CSF layer was modeled using solid elements with a low shear modulus as was used in other research (Ruan, 1993; Zhou et al., 1995; Kang et al., 1997; Hu et al., 1998; Gilchrist and O'Donoghue, 2000; Gilchrist et al., 2001).

The characteristics of brain tissue are those approximated from cadaveric and scaled animal anatomical testing. This is a necessary limitation of models because *in vi*vo human brain material parameters do not exist. Cadaver tissue properties are not exactly the same as living tissue, and while *in vivo* testing can be done on animals, the lack of a good scaling law makes use of these data questionable (Horgan, 2005). Variation can also be created by changes in material properties with age. These limitations to anatomical testing has resulted in there not being a definitive or generally accepted value for the properties of brain tissue, however cadaver tissue represents the closest fit to living human tissue characteristics (Horgan, 2005). From the cadaver testing it has been found that the different parts of brain tissue were heterogeneous as well as having unique geometric arrangement of neural fibers. The material properties for the bone, scalp and intracranial membranes were taken from the literature (Ruan, 1993; Willinger et al., 1995; Zhou et al., 1996; Kleiven and von Holst, 2002) with the values presented in table 8. The weight of the model was scaled to the dimensions of Nahum et al. (1977) which resulted in a brain mass of 1.422 kg. Inertial properties are I_{yy} = 1795 kg.mm^2, I_{zz} = 1572 kg.mm^2 and I_{xx} = 1315 kg.mm^2, and are similar to those of Kleiven and von Holst (2002).

Table 8. Finite element model material properties

Material	Young's modulus (MPa)	Poisson's ratio	Density (kg/m³)
Scalp	16.7	0.42	1000
Cortical Bone	15000	0.22	2000
Trabecular Bone	1000	0.24	1300
Dura	31.5	0.45	1130
Pia	11.5	0.45	1130
Falx	31.5	0.45	1140
Tentorium	31.5	0.45	1140
CSF	15000	0.5	1000
Grey Matter	Hyperelastic	0.49	1040
White Matter	Hyperelastic	0.49	1040

6.2 Validation of the Model

Validation of the model was accomplished through comparisons with intracranial pressure data from Nahum et al. (1977) and Trosseille et al.'s (1992) cadaver impact tests. Brain motion was validated using data from Hardy et al.'s (2001) research. Further validations were compared real world brain injury events to assess the viability of the model for use in injury assessment (Horgan, 2005; Doorly 2007).

6.21 Intracranial Pressure from a Translational Impact

The model was validated by simulating the cadaver head impacts conducted by Nahum et al. (1977) and comparing the time histories of the experiment against the FE simulations. For the simulation, the head was rotated forwards at 45 degrees to the Frankfort plane and a frontal impact was delivered in an anterior to posterior direction through the centre of mass. The load curve was semi sinusoidal with a peak of 7,000 N and duration of 6 ms. A free boundary condition was assumed in the simulation as the neck would be unlikely to affect the results of so brief an impact (Ruan, 1993). Figure 6 shows the pressure time history of the response of the simulation in comparison to the experiment #37 of Nahum et al.'s (1977) cadaver experiments.

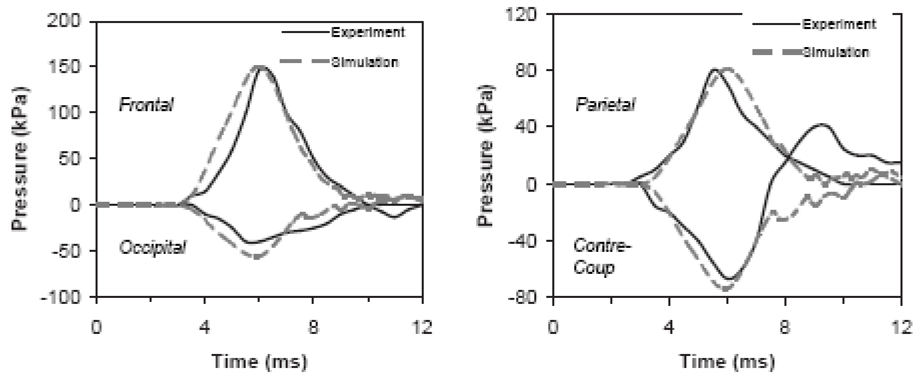

Figure 6. Comparison of the intracranial pressure time histories of Nahum et al. (1977), and the simulation prediction. (with permission from Horgan, 2005)

The results from Nahum et al. (1977) were based upon pressure transducers placed in regions of the head, unlike the simulation where the response is full field data. The comparisons were selected in the same locations as Nahum et al.'s (1977) transducers: the coup (frontal) site, the parietal site, the occipital site, and the contrecoup site. The correlation showed good agreement between the cadaver experiments and the simulation results. The maximum values, shape of the response and duration of effect all matched well at the specified locations. The only exception was the contrecoup site showed some oscillations from negative to positive pressure late in the impact for the experiments where the simulation trace decays to zero (Horgan, 2005).

6.22 Intracranial Pressure from a Combined Rotational and Translational Acceleration Impact

Following the Nahum et al. (1977) comparisons, a more complicated validation using Trosseille et al.'s (1992) cadaver impacts was conducted. Trosseille et al. (1992) measured the intracranial pressure for an impact which had both linear and rotational components. The repressurized cadaver had a 12-accelerometer array affixed to its skull in the occipital region to allow for three-dimensional kinematic measurement of the head motion. Pressure transducers were placed in the subarachnoid space and in the ventricles to measure both intracranial and ventricular pressures. The cadavers were then suspended in a sitting position and impacted with a 23.4 kg impactor at 7.0 m/s in the antero-posterior direction in the facial area. The resulting data showed the dynamic response of the cadaver in the three translational and rotational acceleration components at the centre of gravity (CG) of the head. Intracranial pressures were measured in the frontal and occipital lobes and ventricular pressures in the lateral and third ventricles.

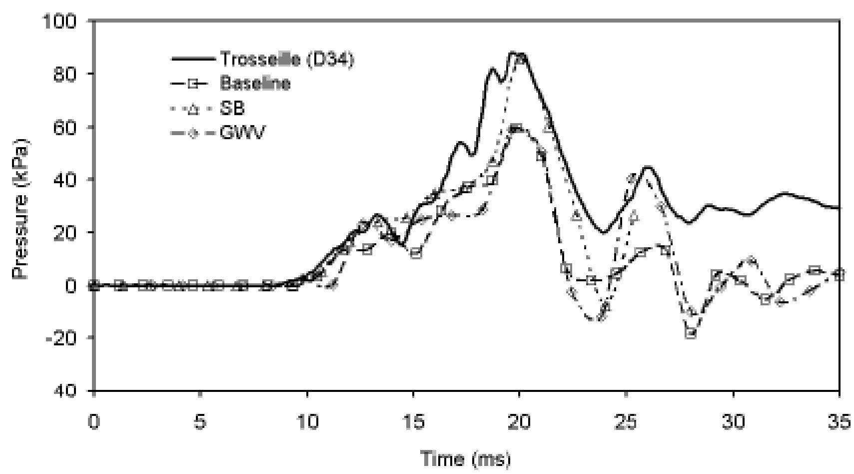

Figure 7. Comparison of frontal pressure for Trosseille et al.'s (1992) experiments and the finite element model (SB - Sliding boundary) (with permission from Horgan, 2005)

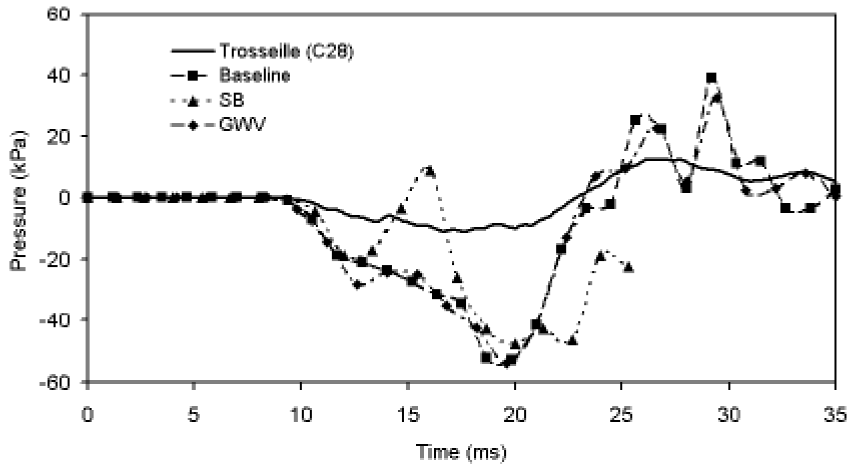

Figure 8. Comparison of occipital pressure for Trosseille et al.'s (1992) experiments and the finite element model (SB - Sliding Boundary) (with permission from Horgan, 2005)

Figures 7 and 8 show the comparison between the sliding boundary baseline model and the cadaver experiments conducted by Trosseille et al. (1992). The shape, trends and duration of pressure pulse agreed with the experimental results in the frontal lobe region. The magnitude of the predicted pressure was similar to the experimental values for the frontal region but not accurately predicted in the occipital region.

6.23 Brain Displacement Validation

Research conducted by Hardy and Kleiven (2002) produced vectorized brain displacement data for different regions of the brain during an impact that was used for validations of the model (Hardy et al., 2001; Hardy and Kleiven, 2002). In Hardy's experiments neutral density targets (NDT) with similar density to the brain tissue were inserted in columns into the brain. The head was then fixed to a sled device and struck by either an impactor or by moving the head into an object at a preset velocity. Upon impact the trajectories of the NDTs were monitored using high-speed X-ray radiography. The same impact conditions were simulated using the UCDBTM with the relative displacements of the

NDTs predicted numerically and compared to the experimental data (Figure 9, 10). Upon comparison the resulting displacements of the simulation were similar to the experimental results (Horgan, 2005).

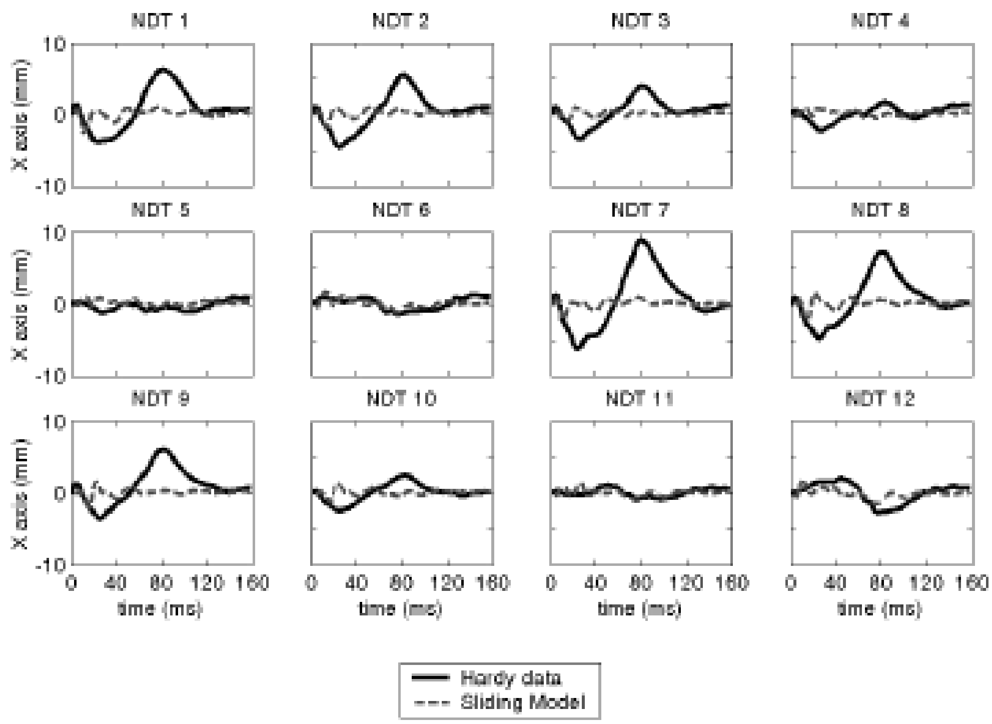

Figure 9. Model response compared to the experimental displacement (x direction) (with permission from Horgan, 2005)

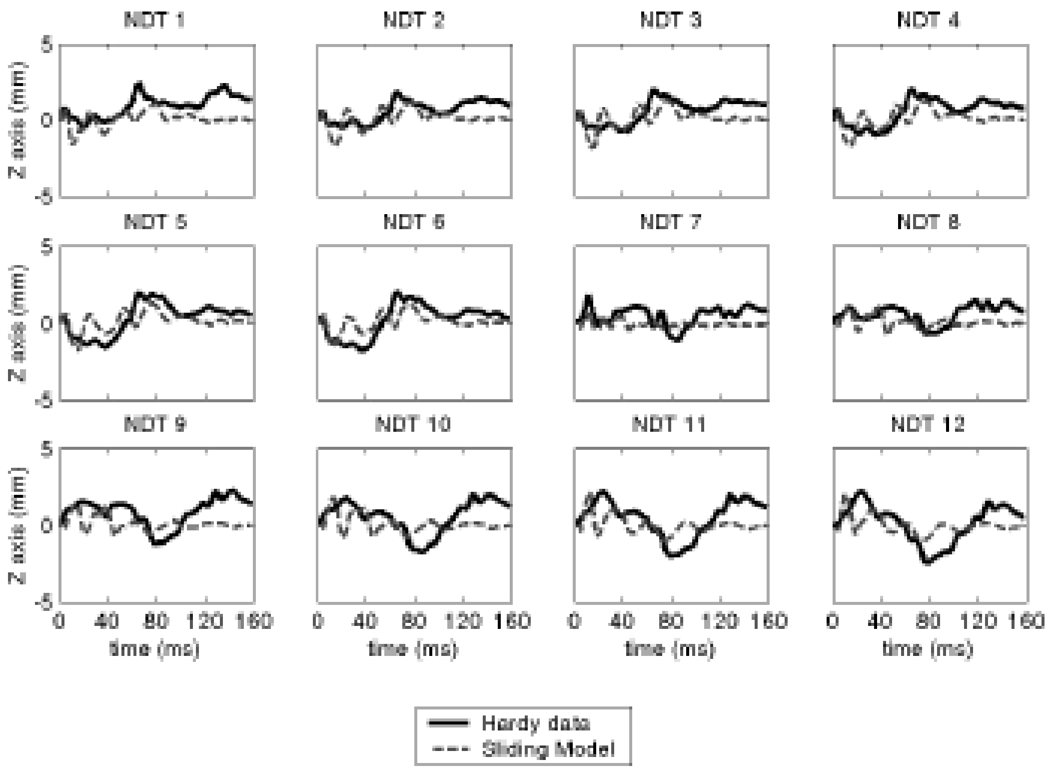

Figure 10. Model response compared to the experimental displacements (z direction) (with permission from Horgan, 2005)

In conclusion, the UCDBTM showed good pressure response when compared with a translational cadaver impact but a poorer correlation with sensor data from more complicated loading scenarios. This was likely a result of the assumptions (e.g. material, boundary conditions, geometry) that are necessary during model construction that may not be accurate to actual anatomical responses. There are further limitations associated with assumptions based on model geometry and the types of material properties used. Continued research is required to improve these parameters (Horgan, 2005).

PART II – Three Studies

Study1

Analysis of brain deformation from falls resulting in traumatic brain injury

Andrew Post[1] PhD, T. Blaine Hoshizaki[1] PhD, Michael D. Gilchrist[2,1] PhD, Susan Brien[3,1] MD, Michael Cusimano[4] MD, and Shawn Marshall[5] MD

Human Kinetics, University of Ottawa, Ottawa, Canada[a]

School of Mechanical & Materials Engineering, University College Dublin, Dublin, Ireland[b]

Hull Hospital, Gatineau, Canada[c]

St. Michael's Hospital, Toronto, Canada[d]

Ottawa General Hospital, Ottawa, Canada[e]

Key Words: Traumatic brain injury; biomechanics; subdural hematoma, contusion, subarachnoid hemorrhage; epidural hematoma

Running Title: Analysis of TBI in Humans

Abstract

Object: The purpose of this study is to reconstruct traumatic brain injury events (Subdural/epidural hematoma, contusion, subarachnoid hemorrhage, parenchymal hemorrhage) using a combination of Hybrid III anthropometric dummy, MADYMO simulations and finite element modeling in order to examine brain deformation based metrics linked to traumatic brain injury. This brain deformation will be measured using known metrics in regions of the brain identified by medical imaging. *Methods:* Twenty fall reconstructions were conducted using a monorail drop rig and finite element modeling of the human brain. *Results:* The brain deformation metrics for the TBI lesions produced from the falls were consistent with the values found in the literature. The results indicated no significant difference for any metric between the TBI lesion types which is likely a result of human variability. However, when using a rank ordering (low response to high) of the brain deformation metrics the following hierarchy presented itself: subdural hematoma, contusion, subarachnoid hemorrhage, epidural hematoma and parenchymal hemorrhage. This order was further reinforced by the number of lesions found for the reconstructions, with subdural hematoma being present the most often and parenchymal the least. *Conclusions*: It was concluded that the reconstructions were consistent with the values found in the literature for TBI. Also, a continuum of brain deformation response was suggested: subdural hematoma, contusion, subarachnoid hemorrhage, epidural hematoma, and parenchymal hemorrhage.

Introduction

Traumatic brain injuries (TBI) contribute to a high degree of mortality and morbidity in society. The costs of these injuries are high, both in lost productivity of the individual and care burden for those no longer able to care for themselves. In the United States, there are an estimated 1.7 million cases of traumatic brain injuries every year[37]. While Canadian statistics in this area are not complete, it can be estimated that 170,000 traumatic brain injuries per year occur in Canada. In addition, 150,000 Canadians are likely to suffer nonfatal traumatic brain injuries that will not require hospital treatment[37]. The elderly and children are the most likely to experience a traumatic brain injury, with falls being the most common cause[38]. Of all injuries, brain trauma has the singular distinction of having the highest morbidity and mortality[31]. As a result, a great deal of research has been undertaken to help reduce the severity and frequency of head injuries. Recently much attention has been paid to brain injuries due to their serious effects on the nervous system and the repercussions to the quality of life of the injured person.

Much of the research has focused on finding injury metrics which could be used to predict the type and presence of concussion or traumatic brain injury. Early work focused on relationships between peak resultant linear acceleration and pressure gradients in the skull or integrations of linear acceleration loading curves such as the Gadd Severity Index (GSI) and Head Injury Criterion (HIC)[18]. From these early works, the motor industry adopted the HIC as the preferred method of evaluation to determine likelihood of brain injury[39]. However, as the knowledge surrounding the mechanism of brain injury progressed, these metrics were identified as having low correlations with actual brain injury[12]. The issue lies primarily with the assumptions of evaluating all head injuries by linear acceleration alone and ignoring the influence of rotational accelerations, which have been identified as influential in the creation of brain lesions[14,44]. Other researchers have attempted to remedy this omission by including the effects of rotation and inertia of the head in predictive equations but have met with similarly low correlations to brain injury[29,30]. As a result of the difficulties of linking the dynamic response of head impacts to brain injury it has been suggested by several authors that characterizing the deformation of brain material in response to linear and rotational accelerations would be a more effective method of predicting brain injury and thus provide new opportunities to improve upon protective technologies[8,20,21].

Several researchers have used finite element (FE) modeling to investigate risk of injury based on brain deformation metrics. Zhang et al[45] and Kleiven[21] used sporting impacts reconstructed using Hybrid III dummies and finite element modeling to investigate metrics that may be useful in predicting the occurrence of concussion. Willinger and Baumgartner[42] also used a similar methodology and dataset with extra data from motorcycle crashes and pedestrian impacts. Both sets of researchers suggested several metrics that may have some relationship to concussion, with von Mises stress, maximum principal strain, strain rate, and product of strain and strain rate seemingly the most predictive.

Similar methods have been used in TBI research, with the added benefit that the lesions are detectable through standard medical imaging methods[21]. This method has a benefit that concussive research does not in that the finite element modeling can look at the specific regions of the brain that was injured. This allows for the measurement of brain deformations in the regions of the brain which were injured, instead of global brain response which is the case for concussion research. This also allows for the examination of the different types of TBI lesions and where they occur. Medical imaging has been used by a couple researchers with limited sample sizes, likely due to the difficulty in attaining high quality MRI or CT scans. Horgan[15] (2005) and Doorly and Gilchrist[6] used mathematical dynamical modeling (MADYMO) in conjunction with the University College Dublin Brain Trauma Model (UCDBTM) to reconstruct traumatic brain injuries for an elderly lady and a young boy sustained from falling. This method allowed for the estimation of the falling scenario in a virtual environment, accounting for approximate body position and head location at point of impact. The MADYMO process also allowed for the impact surfaces and geometries to be represented in the simulation. The output of the reconstructive process was examined by highest peak value and the average value incurred at the injury area in the FE model as designated by the medical imaging. Overall, Doorly and Gilchrist[6] found that the product of strain and strain rate appeared to be good predictors of the boys injuries (Table 1). These examinations of TBI have focused on examining predictive variables for the lesions found in the medical scans. The results have been limited somewhat by the small sample sizes of the research. Also, there has been no attempt to examine the differences in response produced by the events leading to different types of TBI lesions such as contusion, subdural hematoma and so on. If a hierarchy of response could be elucidated between the different types of TBI lesion could be found it would add a new dimension to the understanding of the mechanisms behind this type of injury.

Table 1: The brain deformation metrics from reconstructions using medical imaging

	Doorly and Gilchrist values (2006)				Horgan values (2005)			
	Injury area		Highest value		Injury area		Highest value	
Parameter	Boy	Lady	Boy	Lady	Boy	Lady	Boy	Lady
Von Mises Stress (kPa)	11.2	7.8	15.2	16.7	3.2	6.0	12.67	18.8
Strain	0.32	0.25	0.34	0.48	0.07	0.2	0.3	0.28
Strain rate (s^{-1})	103	96.6	107	100	11.8	30	71.6	57.7
Strain X Strain rate (s^{-1})	18.7	12.7	26.9	24.7	0.48	2.4	19.5	20

The purpose of this study is to reconstruct traumatic brain injury events using a combination of Hybrid III anthropometric dummy, MADYMO simulations, and finite element modeling in order to examine brain deformation based metrics related to different types of TBI lesions. From this analysis a continuum/hierarchy of response for the following TBI lesions may be elucidated: contusion, subdural hematoma, epidural hematoma, subarachnoid hemorrhage, and parenchymal hemorrhage.

Methodology

Twenty non-fatal real life incidents were selected by physicians at the Hull hospital in Gatineau (QC), Canada, the Ottawa General Hospital in Ottawa (ON), Canada, and the National Department of Neurosurgery at Beaumont Hospital, Dublin, Ireland who incurred one of the following TBI lesions: contusion, subdural hematoma (SDH), epidural hematoma (EDH), or subarachnoid hemorrhage (SAH). Each subject signed and informed consent form and all procedures met with ethical approvals. The cases were separated into easily reconstructable falls with clearly defined CT or MRI scans showing one of the target TBI lesions. The brain injury CT and MRI assessments were conducted by the radiologists and neurosurgeons at the source hospital. For each case, the medical imaging was conducted within 24 hours of the incident. In addition to the CT and MRI imaging, many of the lesions were later confirmed through ensuing surgical interventions. For the laboratory reconstructions, the impact parameters describing the falling event were established from witness reports and hospital accident report forms. This information established the start parameters for the computer and physical model simulations and contained information such as: impact vector, location of the impact on the head, velocity of impact, and impact surface.

To accomplish the reconstruction of the TBI event both MAthematic DYnamic MOdels (MADYMO) and Hybrid III anthropometric dummies were used. The MADYMO simulation was used to recreate the fall so that the impact head velocity could be ascertained. The Hybrid III anthropometric dummy headform was then dropped using a monorail to conduct the impacts. Mathematic Dynamic Models output has been used in Doorly (2007) and other research that have conducted reconstructions for the purposes of examining brain injuries such as TBI and concussion. While MADYMO is suitable for these analyses, the Hybrid III was used in this research as it allowed more control over impact location identification and the actual impact surface could be used instead of simulated. The ellipsoid model also lacks certain geometrical details in comparison to the Hybrid III which may influence the results. While both methods are suitable for brain injury research, and both have limitations, the Hybrid III was chosen for this research. As the monorail drop tower was used to reconstruct the falling incidents, only the vertical drop velocity could be used for the physical model simulations. This differs from reality somewhat as when a person falls there would be some component of translational and rotational velocity in other axes which are not accounted for in this research, as a result it is likely that the results may under-estimate the brain responses. The three-dimensional acceleration loading curves generated from the instrumented Hybrid III impacts were then used in the University College Dublin Brain Trauma Model (UCDBTM) to conduct the brain deformation analyses.

MADYMO reconstructions

Mathematic dynamic models is a tool which is commonly used to conduct reconstructions of falling incidents in a human population. This particular tool is quite powerful because it has a large database of human body models, which includes a series of ellipsoid pedestrian models, which were used in this research [32]. These pedestrian models were validated using a variety of impactors whose intention was to determine the risk to pedestrians from vehicle impacts. In the case of this research, the MADYMO simulations were used to reconstruct the falling motions based on the initial and final body positions of each subject as described in the injury report forms. From this simulation an approximation of the final kinematics of the head as it contacts the ground can be gained[1,6].

For each case which incurred a TBI lesion, an appropriately sized ellipsoid pedestrian model was chosen which was closest to the dimensions of the human subject[5]. The ellipsoid pedestrian model was then placed in a simulated environment constructed to be similar to the environment in which the individual fell (Figure 1). As there can be some variation from injury reports from eyewitnesses, a sensitivity analysis was conducted on each fall. In this sensitivity analysis, several simulations were conducted which represented a variety of likely joint angles and body positions[1,7]. From this sensitivity analysis, the fastest and slowest head impact velocity was determined. As the lowest velocity was considered to be the lower boundary of these TBI events, it was used for the ensuing physical and finite element model reconstructions (Table 2).

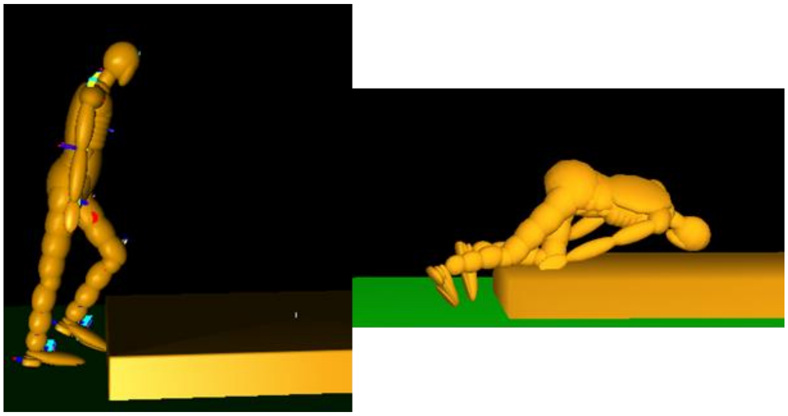

Figure 1. Example MADYMO simulation for a trip up a step and a forehead impact; (left) initial walking position; (right) position prior to impact.

Table 2. Impact velocities (lower boundaries) for each case from MADYMO simulations

Case #	Velocity (m/s)	Impact Surface	TBI Lesion
1	3.0 - 4.0	Concrete	Subdural Hematoma
2	4.7 - 5.2	Concrete	Subdural Hematoma
3	5.1 - 6.1	Concrete	Subdural Hematoma; Epidural Hematoma; Contusion
4	4.1 - 5.4	Concrete	Subarachnoid Hemorrhage
5	3.9 - 6.2	Wood	Subdural Hematoma; Subarachnoid Hemorrhage
6	2.2 - 3.3	Carpet	Subdural Hematoma
7	3.9 - 6.2	Concrete	Subdural Hematoma; Subarachnoid Hemorrhage; Contusion
8	3.3 - 4.8	Concrete	Subdural Hematoma
9	4.8 - 6.2	Concrete	Subdural Hematoma; Subarachnoid Hemorrhage;
10	3.6 - 4.9	Concrete	Subarachnoid Hemorrhage; Contusion
11	3.7 - 5.8	Concrete	Subdural Hematoma; Contusion
12	3.6 - 4.8	Concrete	Epidural Hematoma
13	4.8 - 6.2	Wood	Subdural Hematoma
14	3.8 - 6.0	Concrete	Subdural Hematoma; Contusion
15	4.8 - 5.8	Concrete	Parenchymal Hemorrhage; Contusion
16	5.1 - 5.6	Concrete	Subdural Hematoma
17	4.5 - 4.8	Concrete	Subdural Hematoma
18	3.5 - 4.2	Concrete	Subdural Hematoma
19	4.7 - 5.1	Concrete	Subdural Hematoma
20	5.4 - 6.1	Metal bar	Subdural Hematoma

Laboratory reconstruction

The falling reconstructions of each incident were carried out by guided monorail device equipped with a Hybrid III head and neck form.

Monorail

To simulate falling impacts, a monorail was used (Figure 2). The monorail consisted of a 4.7 m long rail to which the drop carriage was attached. The drop carriage runs along the rails on ball bushings to reduce the effects of friction on velocity and was released by a pneumatic piston. A Hybrid III 50% headform and neck was attached to the drop carriage to allow for measurement of three-dimensional impact characteristics. The impact velocity was measured using a photoelectric time gate placed within 0.02 m of the impact.

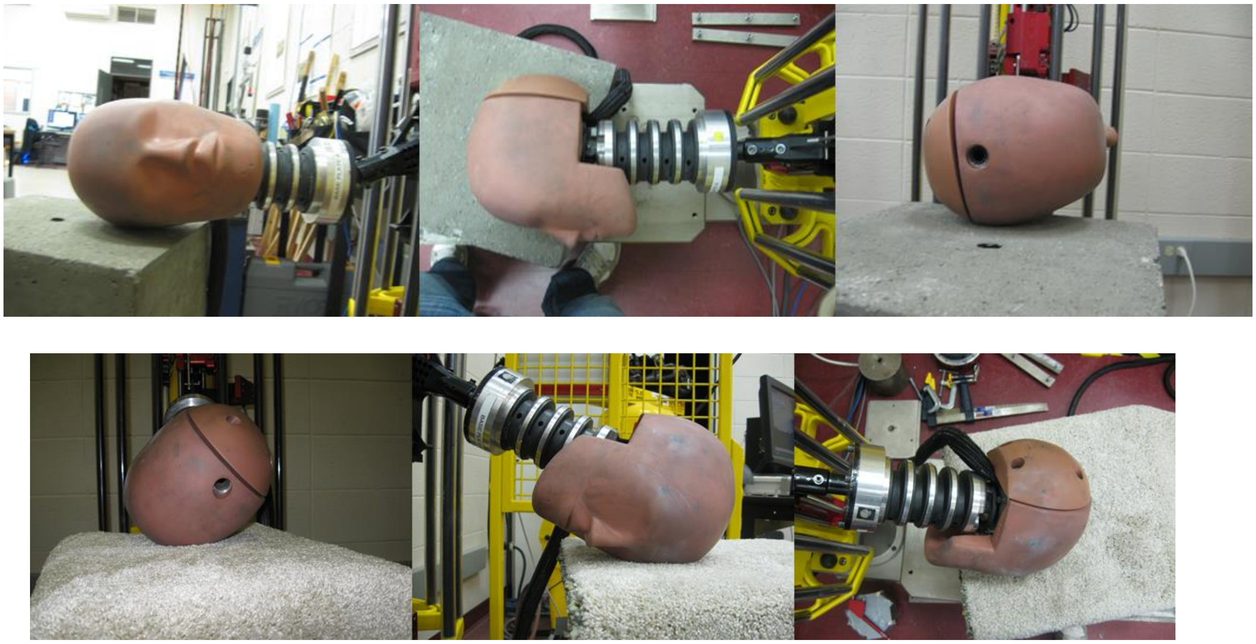

Figure 2. Monorail reconstruction of a fall using the Hybrid III headform; (top) fall to concrete; (Bottom) fall onto carpet with underlay on a concrete anvil.

The anvil at the base of the monorail was composed of steel. The top of the anvil was changed to represent the surface the head contacted as described by the report describing the incident (Table 2). The base of the monorail was 0.67 m high, 0.30 m wide, and 0.38 m deep and was fixed to the floor using 6 concrete bolts. The 4.7 meter vertical track was bolted to the wall and the ceiling to minimize movement of the system and background noise or vibration.

Hybrid III

A 50th percentile adult headform (mass 4.54 ± 0.01kg) and neck was instrumented for measurement of three-dimensional kinematics according to Padgaonkar's 3-2-2-2 accelerometer array[34] (Figure 2). The x-axis was defined as facing forward from the head centre of gravity, the y-axis to the left of the head and the z-axis vertically upwards. The accelerometers used were Endevco 7264C-2KTZ-2-300.

Laboratory reconstruction procedure

Upon identification of a brain injury case suitable for reconstruction, the parameters from the injury reports were reviewed and utilized to identify starting points for the laboratory reconstructions. In the case of these reconstructions, the Hybrid III 50% headform was affixed to the monorail and dropped from the appropriate height to obtain the falling impact velocity that was determined by the MADYMO reconstructions. For each reconstruction, three trials were conducted per velocity identified through the MADYMO reconstructions. This led to between six and nine trials per injury reconstruction as there were consistently at least two to three different possible impact velocities. The impact surface was matched to the accident impact surface and thus its characteristics. The impact site was identified from images of the impact location on the subject and the location of swelling on the CT/MRI scans (Figure 3).

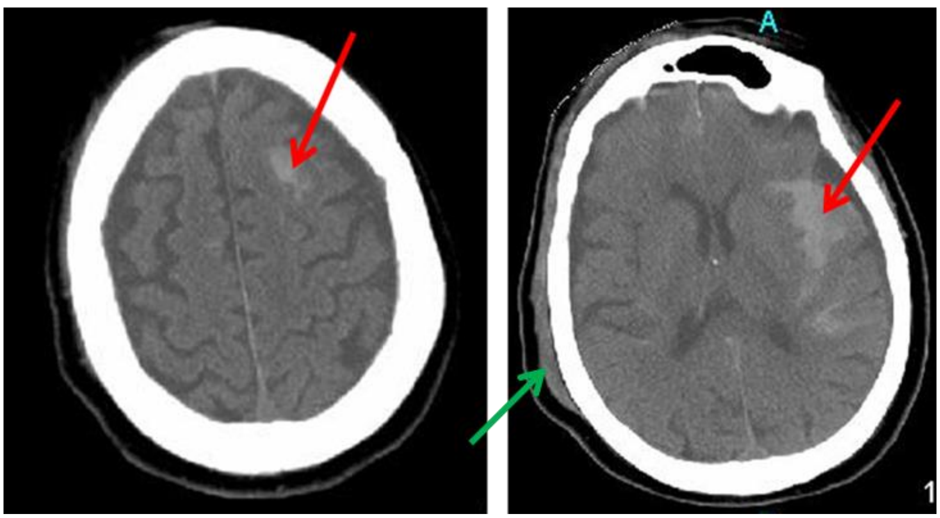

Figure 3. Medical images showing: (left) contusion, and (right) subarachnoid hemorrhage (red arrows). Impact site indicated by green arrow.

The accelerometer data channels were sampled at 20 kHz and recorded using DTS TDAS PRO software. All data were filtered with a SAE J211 class 1000 filter. Each reconstruction provided a three-dimensional description of the head kinematics of the impact event. The resulting x, y and z linear and rotational acceleration curves were captured and then used for the finite element model simulations. The loading curves were applied to the UCDBTM at the centre of mass of the model.

Finite element model (UCDBTM)

The model used in this research was developed in Dublin and is known as the University College Dublin Brain Trauma Model (UCDBTM). The geometric parameters of the model was from a male cadaver as determined by medical imaging techniques[15,16,17]. The head and brain finite element model was comprised of ten parts: the scalp, skull (cortical and trabecular bone), pia, falx, tentorium, cerebrospinal fluid (CSF), grey and white matter, cerebellum and brain stem. The scalp was modeled using shell elements, cortical and trabecular bone with brick elements of varying thickness, the dura with membrane elements, CSF with brick elements, pia with membrane elements, falx and tentorium with shell elements and the cerebrum, cerebellum and brain stem with brick elements. The CSF layer was modeled using solid elements with a high bulk modulus and a low shear modulus to create a sliding boundary condition between the interfaces of the CSF and brain. The algorithm allowed no spaces between the pia and the CSF layer. For the sliding surfaces a friction coefficient of 0.2 was used[26]. The fluid present between the falx and the brain and between the tentorium, cerebrum and cerebellum also had the same fluid algorithm. In total, the brain model was comprised of approximately 26,000 hexahedral elements.

The current model uses the parameters used by Mendis et al[25] and Kleiven and von Holst[22] which are nonlinear viscoelastic material law under large deformation. A hyperelastic material model was used for the brain in shear in conjunction with the viscoelastic material property. The hyperelastic law was given by:

$$C_{10}(t) = 0.9C_{01}(t) = 620.5 + 1930e^{-t/0.008} + 1103e^{-t/0.15} \text{ (Pa)}$$

where C_{10} and C_{01} are the temperature-dependent material parameters, and t is time in seconds. The compressive behaviour of the brain was considered elastic. The shear characteristics of the viscoelastic behaviour of the brain were expressed by:

$$G(t) = G_\infty + (G_0 - G_\infty)e^{-\beta t}$$

where G_∞ is the long term shear modulus, G_0 is the short term shear modulus and β is the decay factor[16]. As fluid has a high bulk modulus and zero resistance to shear, the CSF layer was modeled using solid elements with a low shear modulus as was used in other research[10,11,19,35,46] to simulate the sliding interaction between the brain and skull.

The characteristics of brain tissue are those approximated from cadaveric and scaled animal anatomical testing. The material properties for the brain and skull were taken from the literature[22,35,43,46] and the values are shown in tables 3 and 4. The model was validated against Nahum et al's[28] cadaver impacts measuring cranial pressures and Hardy et al's[13] research of brain motion. Further validations of the model for brain injury research was conducted using real life incidents by Doorly and Gilchrist[5] and Post et al[33] and were found to be in good agreement with the values in the literature for TBI lesions from falls.

Table 3. Finite element model material properties

Material	Young's modulus (MPa)	Poisson's ratio	Density (kg/m³)
Scalp	16.7	0.42	1000
Cortical Bone	15000	0.22	2000
Trabecular Bone	1000	0.24	1300
Dura	31.5	0.45	1130
Pia	11.5	0.45	1130
Falx	31.5	0.45	1140
Tentorium	31.5	0.45	1140
CSF	Water	0.5	1000
Grey Matter	Hyperelastic	0.49	1060
White Matter	Hyperelastic	0.49	1060

Table 4. Material characteristics of the brain tissue used for the UCDBTM

	Shear Modulus (kPa)			
Material	G_0	G_∞	Decay Constant (s^{-1})	Bulk Modulus (GPa)
White Matter	12.5	2.5	80	2.19
Grey Matter	10	2	80	2.19
Brain Stem	22.5	4.5	80	2.19
Cerebellum	10	2	80	2.19

Region of interest identification

The CT and MRI scans of each subject were assessed by board certified radiologists and neurosurgeons at the hospital to identify the type of lesion and the location of the damage[4,5,21,33]. The CT/MRI images were then compared to the UCDBTM and a suitable region of the model was selected to represent the region of interest (ROI) of the injured area (Figures 4, 5, and 6). The FE model was also scaled to the closest dimensions of the brain of the subject[22].

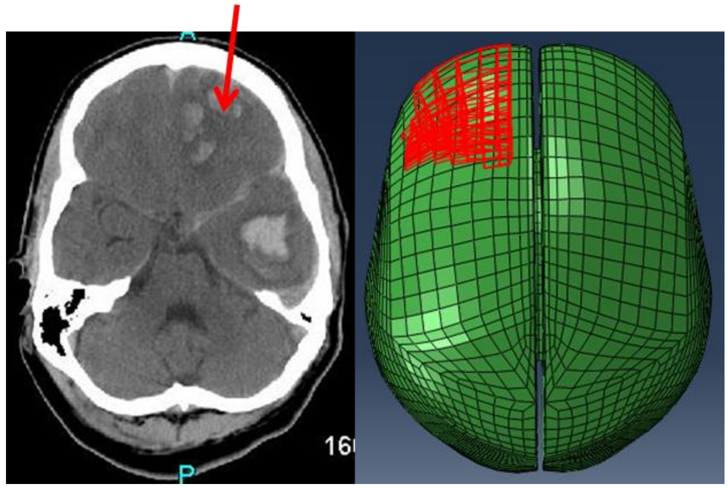

Figure 4. UCDBTM region of interest representing the region of the frontal subarachnoid hemorrhage (red)

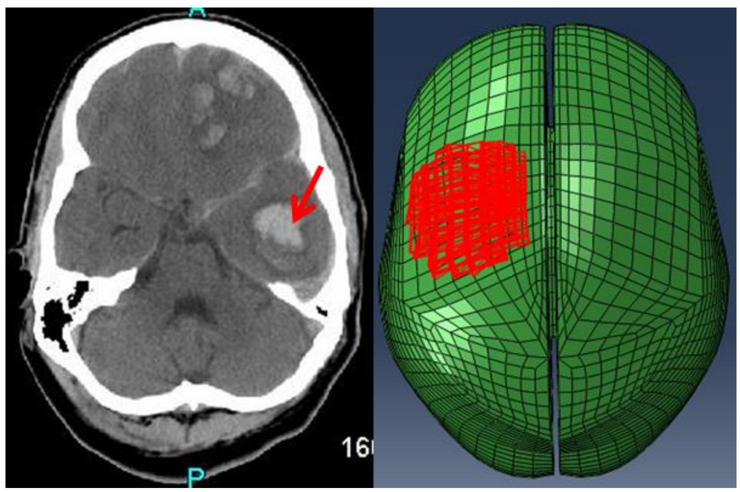

Figure 5. UCDBTM region of interest representing the region of the temporal subarachnoid hemorrhage (red)

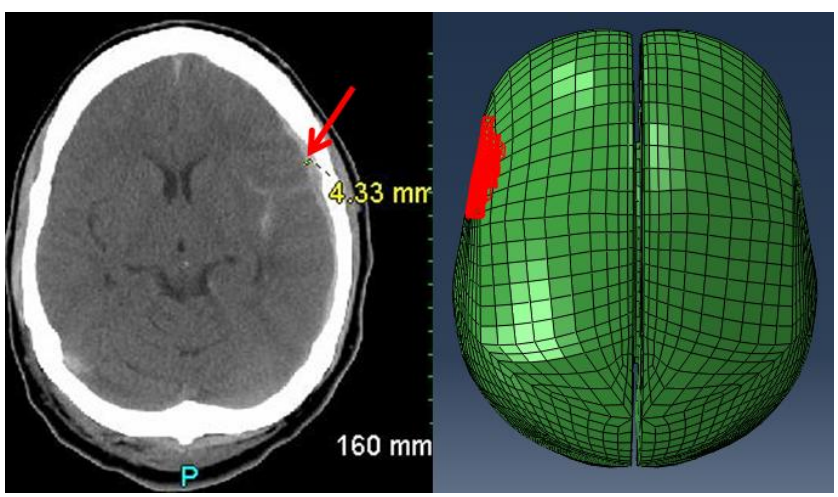

Figure 6. UCDBTM region of interest representing the region of the subdural hematoma (red)

The brain tissue deformation parameters

The brain tissue parameters chosen for this study were maximum principal strain (MPS), von Mises stress (VMS), max shear strain, max shear stress, max strain rate, max product of strain and strain rate and intracranial pressure. These variables were chosen based upon previous research which has used these parameters to describe brain injuries[21,42,45]. The peak magnitude in the ROI as represented by the element experiencing the largest deformation was used for analysis. In addition, an average value that was calculated across all elements at the point of largest deformation in the ROI was determined for MPS and VMS. The results were grouped by brain lesion to identify continuums of injury which may exist within each brain deformation metric. Statistical comparisons between lesion type (contusion, subdural hematoma, epidural hematoma, subarachnoid hemorrhage) was conducted using analysis of variance (ANOVA). A t-test was also used to determine if the outcome measures of the ROI differed significantly from the response of the cerebrum for peak values. Average values were also compared by t-test for maximum principal strain and von Mises stress.

Results

The results of the fall reconstructions are presented in tables 5 through 9.The results of the ANOVA showed no statistical difference between the lesion types from the reconstructions ($p > 0.05$) and as a result trends were analyzed. From the corridor of response, the lower boundary values were used for these analyses. The t-tests were run for each lesion type in comparison with cerebrum responses. The results indicated that the majority of the lesion responses differed significantly from the cerebrum responses[4]. In many cases the values of the cerebrum were larger than those in the region of interest identified and were located along the tentorium or falx cerebri. An ordering (based on lowest magnitude of response) of the TBI lesions as measured by each brain deformation metric is presented in table 10. From this table, a rank ordering was accomplished, with a value of '1' was assigned to the TBI lesion with the lowest magnitude for that metric, '2' to the next lowest and so on. For example, for pressure (Pa), SAH would have a value of '1', SDH '2', contusion '3', EDH '4', and parenchymal hemorrhage '5'. This ranking was conducted for each metric and added up to analyze how the TBI lesions ranked over all the metrics measured. Using this method, the following continuum based on lowest response was found: SDH, contusion (including parenchymal), SAH, and EDH.

Table 5. Brain deformation metrics found for the contusion region of interest

	Pressure (Pa)	MPS	VMS (Pa)	Shear stress (Pa)	Shear strain	Strain rate (s^{-1})	Product of strain and strain rate	Average MPS	Average VMS
MAX	2360697	0.577	20106	10740	1.14	141.3	79.3	0.208	5991
MIN	271901	0.196	6471	2701	0.216	36.3	8.7	0.067	2355
Average	810523	0.336	11311	5465	0.555	72.4	27.1	0.114	3583
Stdev	529826	0.117	4017	2514	0.266	35.7	22.5	0.049	1193

Table 6. Brain deformation metrics found for the epidural hematoma region of interest

	Pressure (Pa)	MPS	VMS (Pa)	Shear stress (Pa)	Shear strain	Strain rate (s^{-1})	Product of strain and strain rate	Average MPS	Average VMS
MAX	706114	0.328	11238	5038	0.540	72.9	23.9	0.111	4049
MIN	386426	0.250	9906	4326	0.338	26.9	6.7	0.084	3622
Average	548081	0.293	10731	4756	0.448	53.7	16.3	0.100	3909
Stdev	169254	0.033	561	280	0.096	21.3	7.8	0.012	157

Table 7. Brain deformation metrics found for the parenchymal hemorrhage region of interest

	Pressure (Pa)	MPS	VMS (Pa)	Shear stress (Pa)	Shear strain	Strain rate (s^{-1})	Product of strain and strain rate	Average MPS	Average VMS
MAX	788407	0.309	10084	4554	0.466	43.8	13.5	0.114	3933
MIN	754568	0.296	9750	4455	0.455	35	10.7	0.104	3590
Average	767546	0.304	9876	4500	0.462	40.2	12.2	0.108	3725
Stdev	18245	0.007	181	50	0.006	4.6	1.4	0.006	183

Table 8. Brain deformation metrics found for the subarachnoid hemorrhage region of interest

	Pressure (Pa)	MPS	VMS (Pa)	Shear stress (Pa)	Shear strain	Strain rate (s^{-1})	Product of strain and strain rate	Average MPS	Average VMS
MAX	2013397	0.474	19157	10702	0.867	222.9	104.3	0.146	6540
MIN	157600	0.260	9294	4132	0.341	17.3	4.5	0.081	2775
Average	696526	0.365	12988	6326	0.585	79.8	33.3	0.113	4590
Stdev	421981	0.082	3197	2096	0.155	68.9	33.7	0.017	1257

Table 9. Brain deformation metrics found for the subdural hematoma region of interest

	Pressure (Pa)	MPS	VMS (Pa)	Shear stress (Pa)	Shear strain	Strain rate (s^{-1})	Product of strain and strain rate	Average MPS	Average VMS
MAX	1643120	0.491	16444	10782	0.765	142.3	69.9	0.252	8782
MIN	168295	0.200	6154	2569	0.246	22.2	4.4	0.061	2428
Average	797444	0.327	10794	4903	0.476	71.6	25.9	0.131	4398
Stdev	347602	0.086	3100	1875	0.127	37.4	19.0	0.037	1346

Table 10. Rank ordering of lesion by brain deformation metric using minimum threshold values

	Pressure (Pa)		MPS		VMS (Pa)
SAH	157600	Contusion	0.196	Subdural	6154
Subdural	168295	Subdural	0.2	Contusion	6471
Contusion	271901	Epidural	0.25	SAH	9294
Epidural	386426	SAH	0.26	Parenchymal	9750
Parenchymal	754568	Parenchymal	0.296	Epidural	9906
	Shear stress (Pa)		**Shear Strain**		**Strain rate (s^{-1})**
Subdural	2569	Contusion	0.216	SAH	17.3
Contusion	2701	Subdural	0.246	Subdural	22.2
SAH	4132	Epidural	0.338	Epidural	26.9
Epidural	4326	SAH	0.341	Parenchymal	35
Parenchymal	4455	Parenchymal	0.455	Contusion	36.3
	Product (s^{-1})		**AVG MPS**		**AVG VMS (Pa)**
Subdural	4.44	Contusion	0.069	Contusion	2422
SAH	4.498	Subdural	0.079	Subdural	2865
Epidural	6.725	SAH	0.083	SAH	3152
Contusion	8.736	Epidural	0.089	Parenchymal	3725
Parenchymal	10.71	Parenchymal	0.108	Epidural	3835

Case by case analysis by deformation metric

The results of the individual reconstructions are presented in this section (Figures 7 through 15). The parenchymal hemorrhage result is reported as a contusion, as a parenchymal hemorrhage is a specification of a particular type of contusion.

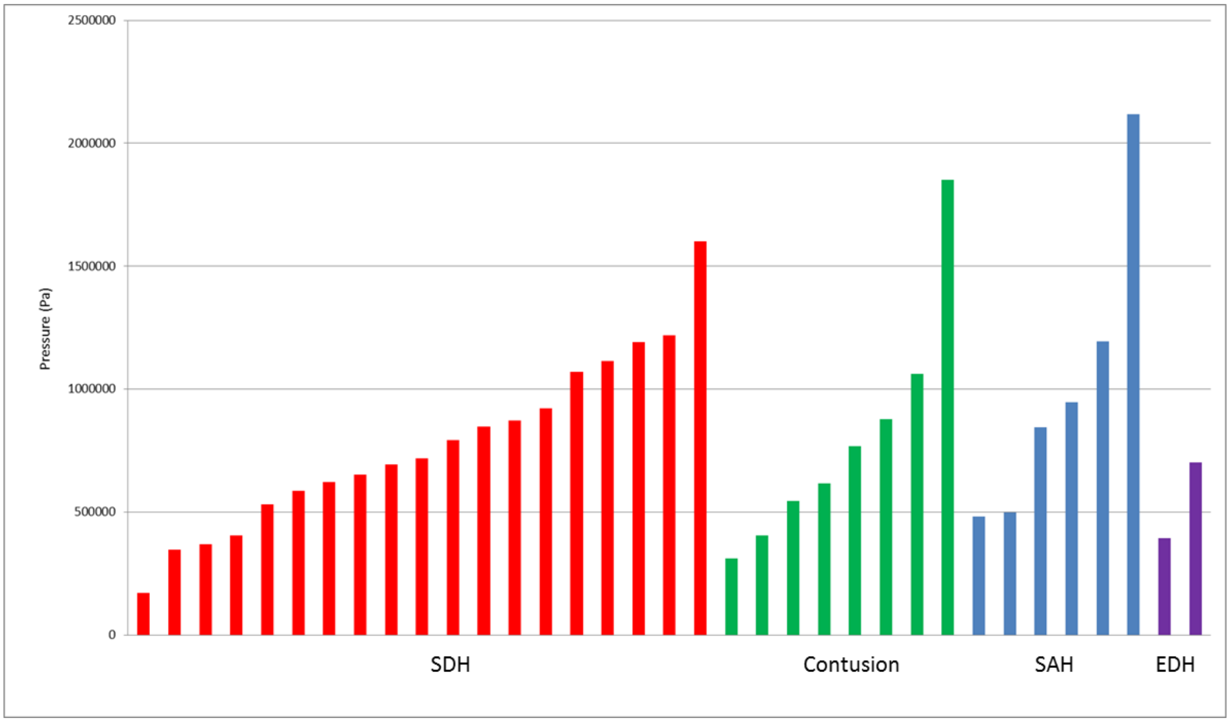

Figure 7. Case by case pressure (SDH = subdural hematoma; SAH = subarachnoid hemorrhage; EDH = epidural hematoma)

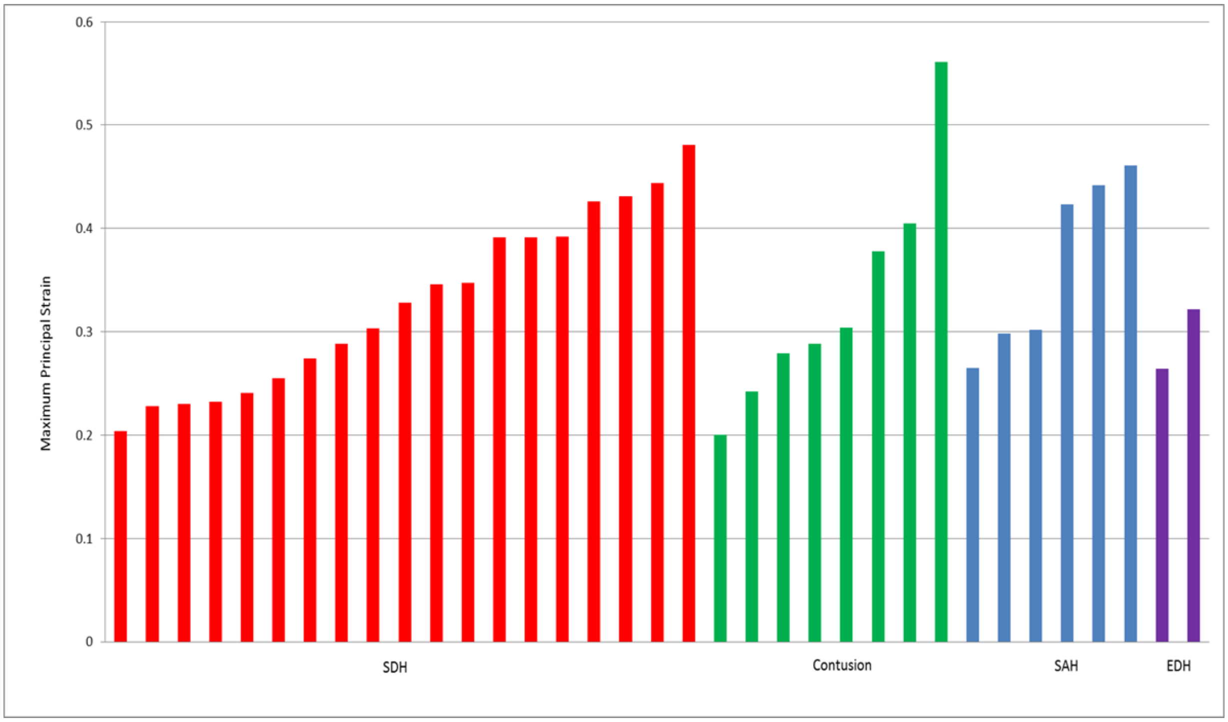

Figure 8. Case by case maximum principal strain (SDH = subdural hematoma; SAH = subarachnoid hemorrhage; EDH = epidural hematoma)

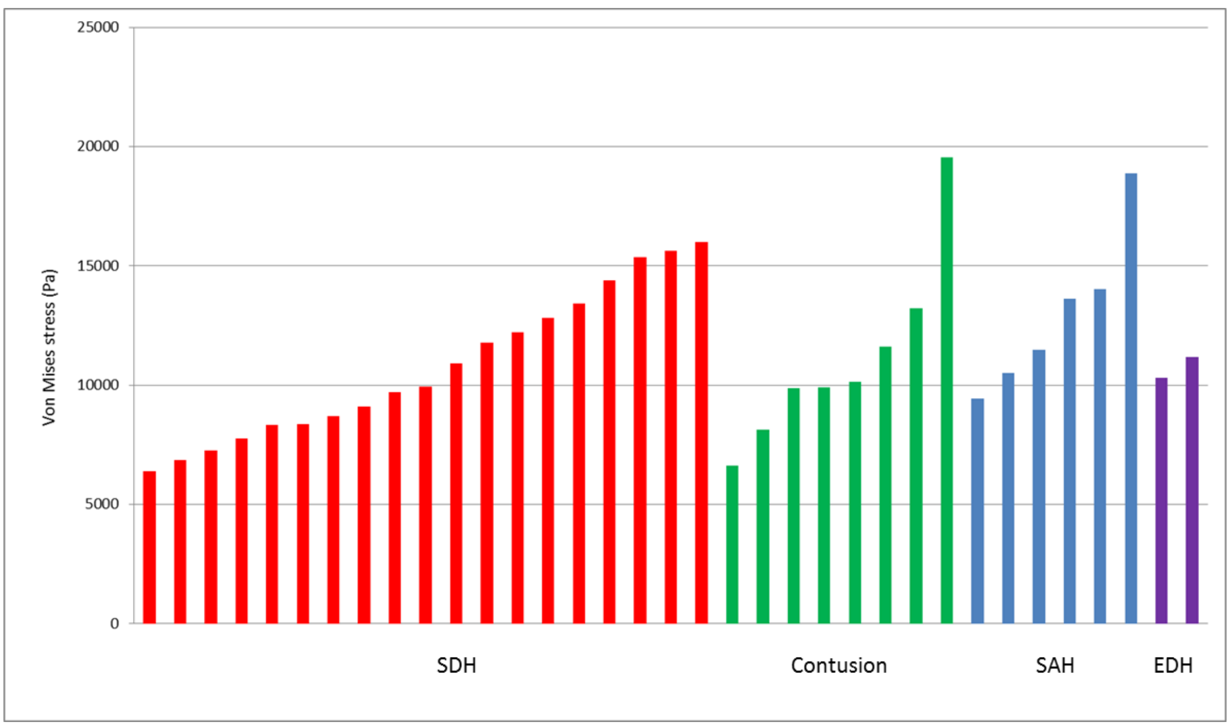

Figure 9. Case by case von Mises stress (SDH = subdural hematoma; SAH = subarachnoid hemorrhage; EDH = epidural hematoma)

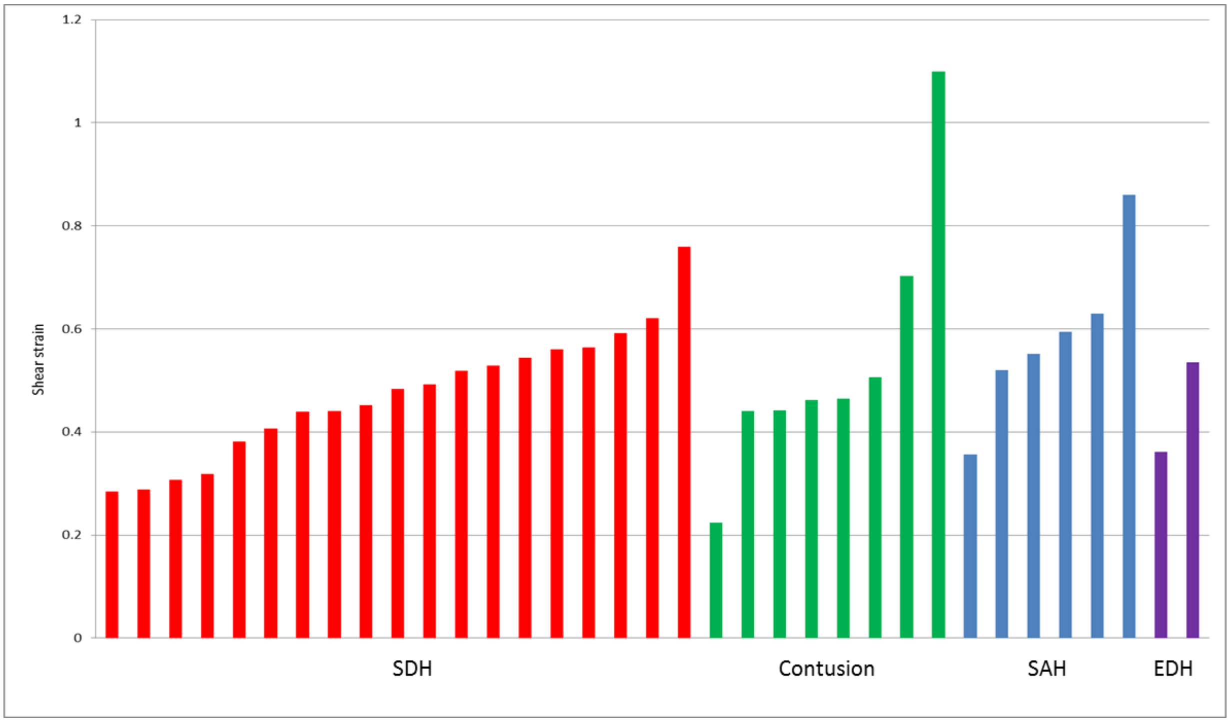

Figure 10. Case by case shear strain (SDH = subdural hematoma; SAH = subarachnoid hemorrhage; EDH = epidural hematoma)

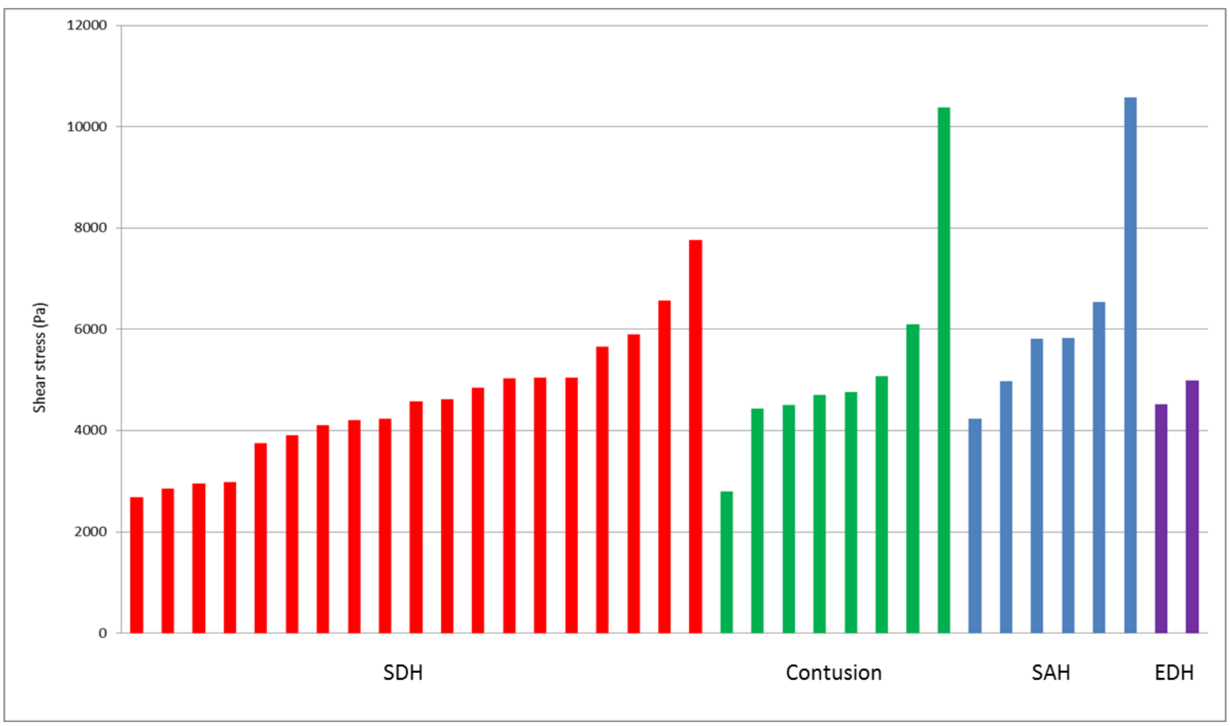

Figure 11. Case by case shear stress (SDH = subdural hematoma; SAH = subarachnoid hemorrhage; EDH = epidural hematoma)

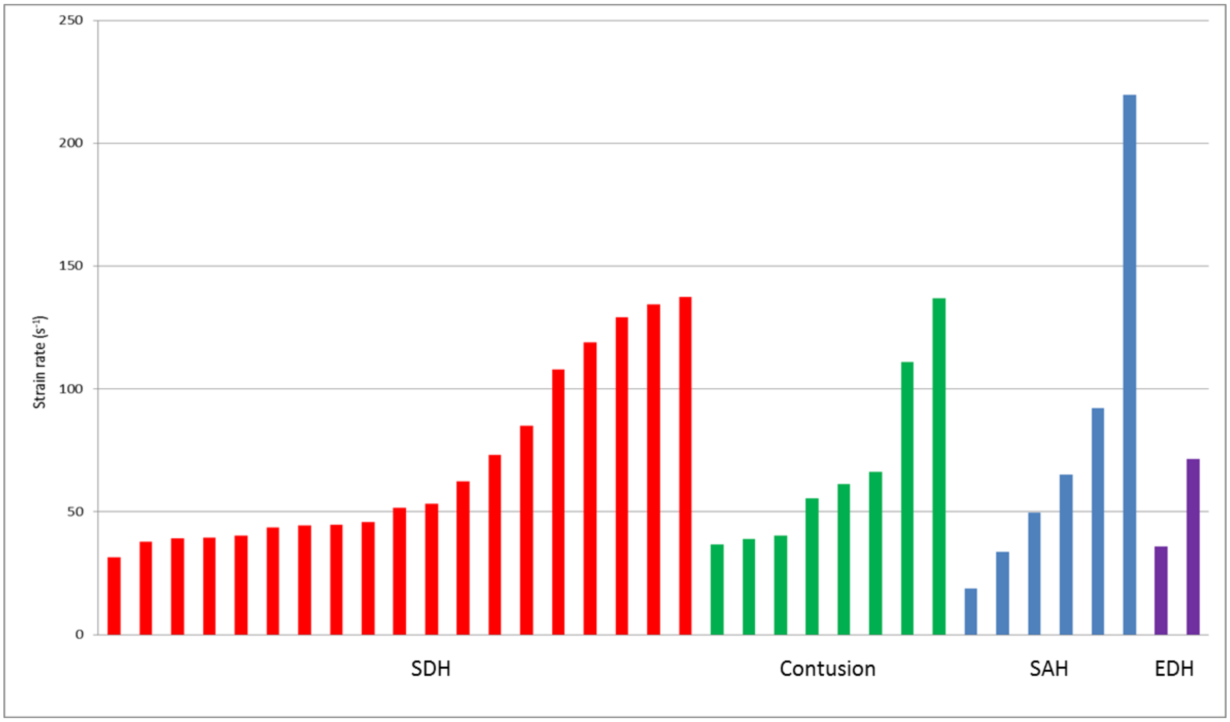

Figure 12. Case by case strain rate (SDH = subdural hematoma; SAH = subarachnoid hemorrhage; EDH = epidural hematoma)

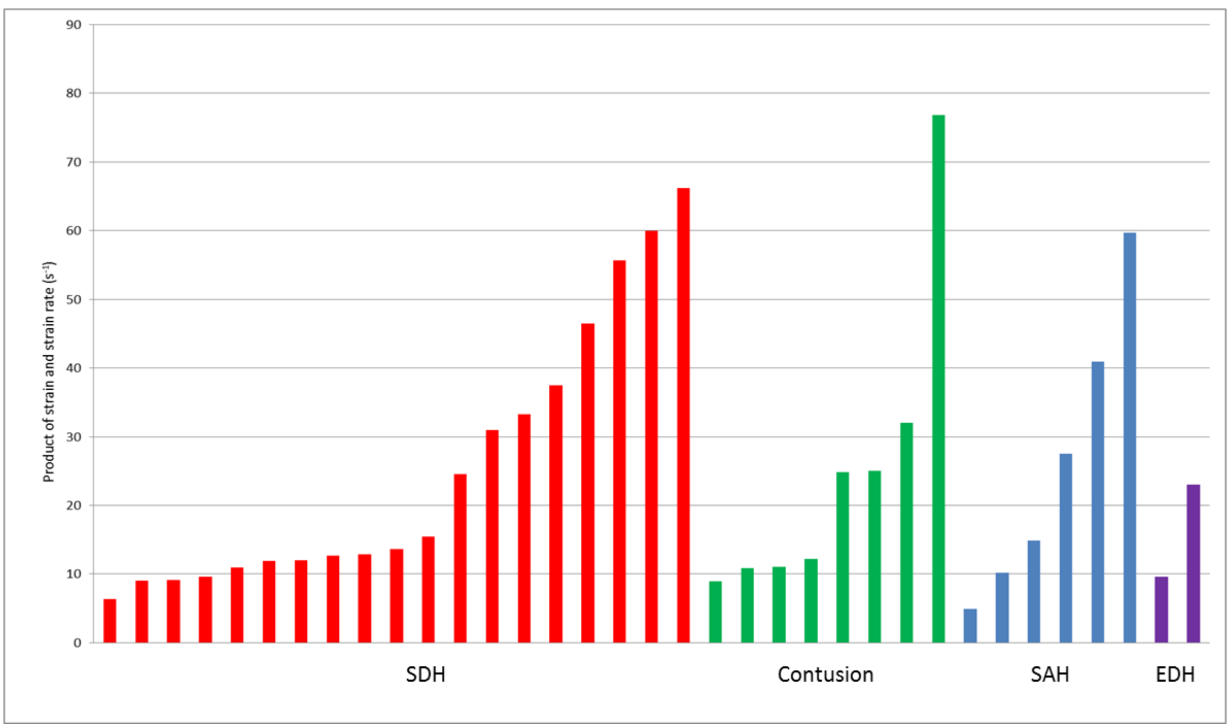

Figure 13. Case by case product of strain and strain rate (SDH = subdural hematoma; SAH = subarachnoid hemorrhage; EDH = epidural hematoma)

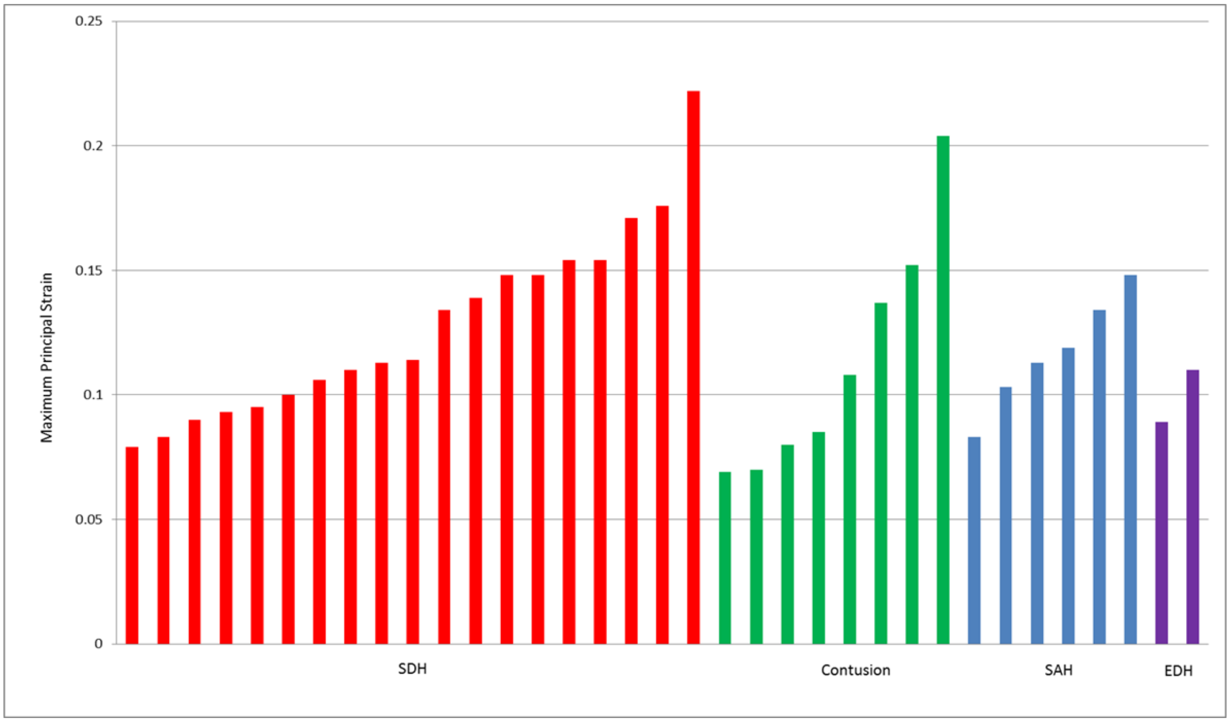

Figure 14. Case by case average maximum principal strain (SDH = subdural hematoma; SAH = subarachnoid hemorrhage; EDH = epidural hematoma)

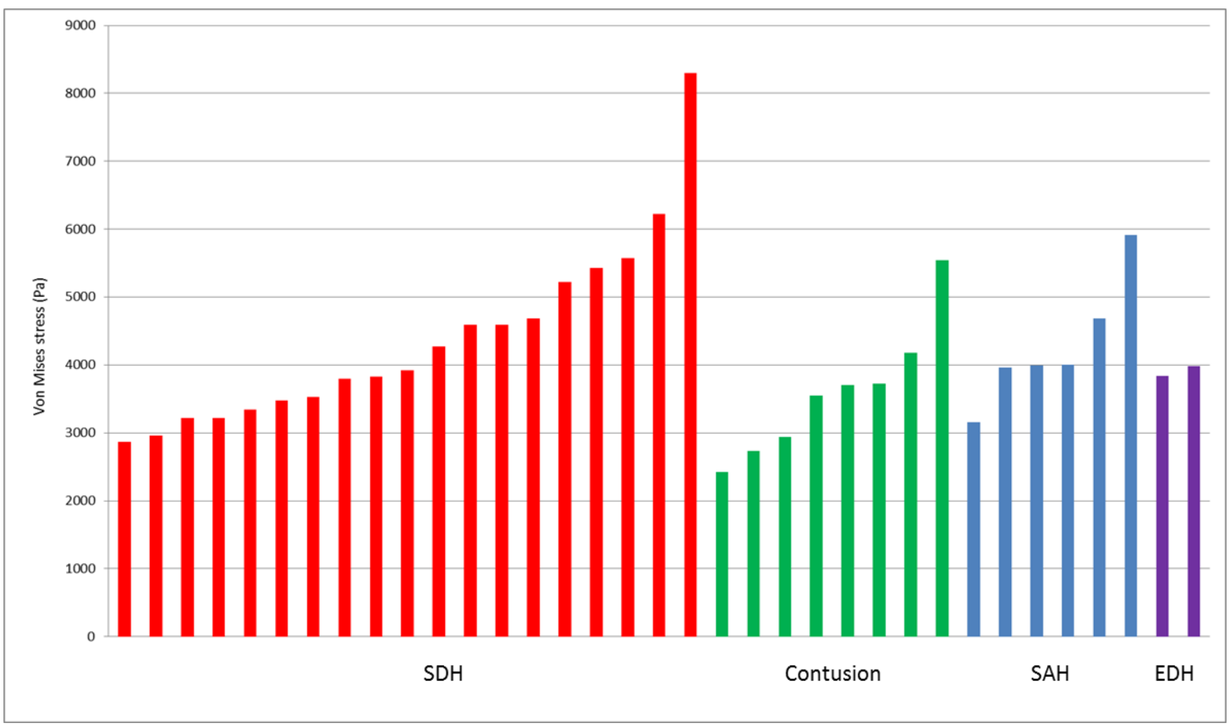

Figure 15. Case by case average von Mises stress (SDH = subdural hematoma; SAH = subarachnoid hemorrhage; EDH = epidural hematoma)

Discussion

To the author's knowledge this is the first time a comperehensive analysis of different TBI lesions using brain deformation metrics has been conducted. Unlike most TBI research, this work has examined the continuum of TBI lesions as separate entities as opposed to lumping them into one broad category. Upon examination of the literature for similar studies researching TBI (Tables 11 through 14), Doorly's[4] work was the closest in methodology and purpose to the current research. Zhang et al[45], Willinger and Baumgartner[43], and Kleiven[21] also conducted similar physical to finite element modeling brain injury simulations, however the intended area of research was mTBI (Table 15). The mTBI data does however help establish a possible lower boundary upon which to frame the current results. In comparison with Doorly's[4] research which examined brain deformation metrics in relation to TBI lesions, the results presented here are generally of a larger magnitude. This is likely a result of the modeling techniques used. Doorly[4] used a MADYMO computational model to simulate the impacts and used the resulting dynamic response as input to the model. The MADYMO model uses deformable characteristics for the head under contact, whereas the physical model used in this research (Hybrid III) is a non-deformable steel skull with a deformable layer surrounding it to represent the skin. This difference may be the source of the larger magnitude response as a result of a stiffer system in comparison with Doorly's[4] data. However, when comparing to the research reconstructed using the Hybrid III physical models and finite element modelling to do impact reconstruction, the current results are comparable to the range representative of TBI. Zhang et al[45], Willinger and Baumgartner[42], and Kleiven[21] reported values for mTBI in the range of 0.18 to 0.26 MPS, and the current results are often well in excess of that. These comparisons highlight the importance of interpreting comparative results in light of the methodologies used. In comparison with the Hybrid III literature, much of Doorly's[4] data may seem at odds with the mTBI research (0.15 for SDH), but that is possibly a result of the deformable condition of the skull in MADYMO simulations leading to a lower dynamic response value for the corresponding injury. When comparing the present results with vascular tolerance data presented in the literature the current results are well within the range. The values in table 16 show some vascular tissue tolerances as well as general brain tissue tolerances. In comparison with the vascular tolerances, which are typically the source of many brain bleeds (TBI) the values are between 0.2 and 0.55 strain. These values fit nicely with the data presented from these reconstructions with 0.2 to 0.3 strain for the low end of the TBI continuum of injury. Interestingly there was found to be damage to general brain tissue with strains as low as 0.1 which implies that it may be possible to incur damage similar to those of a concussion at values lower than those found by Zhang et al[45], Willinger and Baumgartner[43], and Kleiven[21].

Table 11. Subdural hematoma thresholds from finite element modelling research[3]

Threshold	Dependent Variable
55 - 308 kPa	Pressure
0.14 - 0.53	Max. Principal Strain
5 - 17 kPa	Von Mises
1.8 - 4.75 kPa	Shear Stress
0.17 - 0.50	Shear Strain
147 - 348 s^{-1}	Strain Rate
14 - 24 s^{-1}	Product of Strain and Strain Rate

Table 12. Contusion thresholds from finite element modelling research[3]

Threshold	Dependent Variable
93 - 123 kPa	Pressure
0.16 - 0.23	Max. Principal Strain
5 - 8 kPa	Von Mises
2.22 - 3.81 kPa	Shear Stress
0.25 - 0.40	Shear Strain
119 - 265 s^{-1}	Strain Rate
14.7 - 56.3 s^{-1}	Product of Strain and Strain Rate

Table 13. Subarachnoid hemmorrhage thresholds from finite element modelling research[3]

Threshold	Dependent Variable
270 kPa	Pressure
0.34	Max. Principal Strain
12.2 kPa	Von Mises
4.3 kPa	Shear Stress
0.4	Shear Strain
197 s^{-1}	Strain Rate
36.3 s^{-1}	Product of Strain and Strain Rate

Table 14. Epidural hematoma thresholds from TBI reconstruction research[3]

Threshold	Dependent Variable	Reference
139 - 281 kPa	Pressure	Doorly[3]
173 - 235 kPa	Pressure	Ward et al[36]
0.16 - 0.23	Max. Principal Strain	Doorly[3]
4.8 - 7.9 kPa	Von Mises	Doorly[3]
2.3 - 3.81 kPa	Shear Stress	Doorly[3]
0.24 - 0.40	Shear Strain	Doorly[3]
129 - 141 s^{-1}	Strain Rate	Doorly[3]
14.5 - 19.0 s^{-1}	Product of Strain and Strain Rate	Doorly[3]

Table 15. mTBI thresholds from reconstruction research

mTBI Threshold (50% risk)	Dependent Variable	Reference
0.21 - 0.26	Max. Principal Strain	Kleiven[16]
0.19	Max. Principal Strain	Zhang et al[39]
48.5 s^{-1}	Strain Rate	Kleiven[16]
10.1 s^{-1}	Product of Strain and Strain Rate	Kleiven[16]
8.4 kPa	Von Mises	Kleiven[16]
7.8 kPa	Von Mises	Zhang et al[39]
18 kPa	Von Mises	Willinger and Baumgartner[36]
65.8 kPa	Pressure	Kleiven[16]
90.0 kPa	Pressure	Zhang et al[39]

When examining the low end values presented in table 10 using the ranking system, the different TBI lesions occur (from low to high magnitude) in the following order: subdural hematoma, contusion, subarachnoid hemorrhage, epidural hematoma, and parenchymal hemorrhage. This order is represented exactly by shear stress and average maximum principal strain metrics. This order is also in evidence when examining the number of the types of TBI lesions accumulated from the reconstructions. The subdural hematoma was the lesion with the highest occurrence (19), followed by contusion (7), subarachnoid hemorrhage (6), epidural hematoma (2), and parenchymal hemorrhage (1). This ordering represents a possible validation for the influence of magnitude of response on the creation of certain TBI lesions as the most common injury would be the one with the lowest threshold to injury, and in this case it would be subdural hematoma.

Statistical comparisons were conducted to establish if the model's regional TBI responses differed from the average and peak cerebrum responses. They show that in general across the majority of the brain deformation metrics that there was a significant difference between the cerebrum and ROI. The cerebrum values were however normally larger than those in the TBI regions of interest and were located for the most part along the tentorium and falx. This phenomenon was reported for the same model by Doorly[4], with normal restrictions along those membranes causing higher stresses and strains the probable cause. Doorly[4] felt that the reason why these areas sustained no injury could be attributed to these regions being more resistant to those types of motions. While this is possible, it is also possible that the model needs further refinement and validation in these regions of the brain. As the current validation for finite element brain models are for pressures and brain motion only in the cerebrum[13,28], further validation data against cadavers is required for these regions before motions in these areas can be accurately modeled.

Table 16. Listing of measured brain tissue tolerances from anatomical testing

Injury Threshold Value	Tissue Type	Method	Reference
20 Mpa stress, 0.2 strain, no dependence on strain rate	Cerebral blood vessels	Cerebral cadaver arteries	Chalupnik et al. (1971)
Documented strain rate dependence of tissue	Parasagittal Bridging veins	Cadaver bridging veins	Lowenhielm (1974)
0.51 to 0.55 strain, no dependence on strain rate	Parasagittal Bridging veins	Cadaver bridging veins	Lee and Hault (1989)
0.05 to 0.10 strain	General to brain tissue	Analytical tissue model based on animal and physical models	Margulies and Thibault (1992)
0.1	White matter axons	Squid axon stretch	Thibault (1993)
0.19 strain, 6-11 kPa Von Mises stress and 0.8-1.0 kJ/m^3 strain energy density for contusions	Cortex	Cadaver tissue	Schreiber (1997)
8-16 kPa for DAI	CNS tissue	Sheep model	Anderson et al. (1999)
0.14 to 0.34 strain	White matter axons	Male guinea pig optic nerve stretch	Bain and Meaney (2000)
0.31 strain, no dependence on strain rate	Cerebral blood vessels	Human cerebral blood vessels from surgery	Monson et al. (2003)
Documented no dependence on strain rate	Hippocampal tissue culture	Rat hippocampal tissue culture deformation	Cater et al. (2006)

Conclusions

While this work shows a comprehensive dataset (Tables 5 through 9; Figures 7 through 15) illustrating the deformation in the brain using several injury metrics, overall no measurement was found to effectively differentiate between the different types of brain lesion. This is probably due to the large amount of variability in the human population. It may be possible to gain further insight into the nature of the continuum of injury found here if more subjects could be added to the current research. If the minimum values were taken as the low end thresholds for these types of injuries, there is no statistical consistency as to which lesion would be at the bottom of the continuum (Table 10).

While not significant, when using a rank order based on table 10 to identify which lesion was produced at the lowest magnitude, the following hierarchy of response was identified: subdural hematoma, contusion, subarachnoid hemorrhage, and epidural hematoma. This order was further validated by the number of each injury which was found for the reconstruction cases, with subdural hematoma being the most present, and epidural hematoma the least. Although since epidural hematoma is commonly associated with skull fractures, the lack of skull fractures in this work may be one reason for the low number. As a result, this study has successfully reconstructed 20 TBI cases which resulted in the analysis of several different types of TBI. With the availability of more data from which to make comparisons this data may be useful as a starting point to recognize where brain deformation may indicate TBI injuries as opposed to mTBI injuries.

As there were no significant differences between lesion type, each lesion and brain deformation metric was compared to the literature to examine if these results agree with the current research into TBI. It was found that many of the reconstructions conducted had results which were close to those already described in the literature; although the literature concerning brain deformation thresholds and TBI is very sparse. When there was disagreement between the values from this study to previous work, the magnitudes were generally larger than those in the literature. The high values from this study may be a result of the use of a rigid steel headform (Hybrid III) which would not deform under impact, likely resulting in a stiffer response. Doorly and Gilchrist[5] and Doorly's[4] research is the best literature available for comparison, however both sources used input curves from

MADYMO, which uses a deformable representation of the human head, and likely a less stiff response, which could result in lower values.

Limitations

Limitations of this study revolve around the accuracy of the reconstruction and the modeling process. The reconstructions conducted within the laboratory use non biofidelic physical models that produce acceleration loading curves that may not be similar to the response of a non-rigid system such as the head. The input parameters (velocity, mass, location) are all approximate and may not accurately represent the event, while using multiple conditions for each injury simulation may cover the actual event; it is unlikely an exact representation of what occurred to cause the injury will be simulated. The influence of the musculature on the impact was difficult to ascertain and is thus a limitation to this study. While simple to reconstruct injury scenarios were chosen for this study, it is unlikely that each simulation will be exact to the individual who was injured.

The finite element method has limitations inherent to its use. The finite element model (UCDBTM) is an approximation of the material characteristics, constitutive properties, and geometries of the human head and brain system. While validations for finite element models of the human brain in general have been conducted, a complete verification of its predictions for human response has not been accomplished. As a result the deformation of the brain represented by the simulation can only be taken as an estimate and not an absolute.

References

1. Adamec J, Jelen K, Kubovy P, Lopot F, Schuller E: Forensic biomechanical analysis of falls from height using numerical human body models. **J Forensic Sci 55(6)**:1615-1623, 2010

2. Bain AC, Meaney DF: Tissue-level thresholds for axonal damage in an experimental model of central nervous system white matter injury. **J Biomech Eng 16**:615-622, 2000

3. Chalupnik JD, Daly CH, Merchant HC: Material properties of cerebral blood vessels. Final report on contract No. NIH-69-2232, report No. ME 71-11, Univ. of Washington, 1971, Seattle.

4. Doorly MC: Investigations into head injury criteria using numerical reconstruction of real life accident cases [PhD thesis]. Dublin, Ireland, University College Dublin; 2007.

5. Doorly MC, Gilchrist MD: The use of accident reconstruction for the analysis of traumatic brain injury due to head impacts arising from falls. **Comput Meth Biomech Biomed Eng 9(6)**:371-377, 2006

6. Doorly MC, Gilchrist MD: Three-dimensional multibody dynamics analysis of accidental falls resulting in traumatic brain injury. **IJCrash 14(5)**:503-509, 2009

7. Forero Rueda MA, Gilchrist MD: Comparative multibody dynamics analysis of falls from playground climbing frames. **Forensic Sci Int 191**:52-57, 2009

8. Forero Rueda MA, Cui L, Gilchrist MD: Finite element modeling of equestrian helmet impacts exposes the need to address rotational kinematics in future helmet designs. **Comput Meth Biomech Biomed Eng 14(12)**:1021-1031, 2011

9. Galbraith JA, Thibault LE, Matteson DR: Mechanical and electrical responses of the squid giant axon to simple elongation. **J Biomech Eng 115(1)**:13-22, 1993

10. Gilchrist MD, O’Donoghue D: Simulation of the development of frontal head impact injury. **Comput Mech 26(3)**:229-235, 2000.

11. Gilchrist MD, O’Donoghue D, Horgan T: A two-dimensional analysis of the biomechanics of frontal and occipital head impact injuries. **IJCrash 6(2)**:253-262, 2001

12. Goldsmith W: Current controversies in the stipulation of head injury criteria. Letter to the editor. **J Biomech 14**:883-884, 1981

13. Hardy WN, Foster CD, Mason MJ, Yang KH, King AI, Tashman S. Investigation of head injury mechanisms using neutral density technology and high-speed biplanar x-ray. **Stapp Car Crash J 45**:337-368, 2001

14. Hardy WN, Khalil TB, King AI: Literature review of head injury biomechanics. **Int J Impact Eng 15(4)**:561-568, 1994

15. Horgan TJ: A finite element model of the human head for use in the study of pedestrian accidents [PhD Thesis]. Dublin, Ireland, University College Dublin; 2005.

16. Horgan TJ, Gilchrist MD: The creation of three-dimensional finite element models for simulating head impact biomechanics. **IJCrash 8(4)**:353-366, 2003

17. Horgan TJ, Gilchrist MD: Influence of FE model variability in predicting brain motion and intracranial pressure changes in head impact simulations. **IJCrash 9(4)**:365-379, 2004

18. Hoshizaki TB, Brien SE: The science and design of head protection in sport. **Neurosurg 55**:956-967, 2004

19. Kang HS, Willinger R, Diaw BM, Chinn B: Modeling of the human head under impact conditions: A parametric study. Proceedings of the 41st **Stapp Car Crash Conference**, SAE paper No. 973338, 1997

20. King AI, Yang KH, Zhang L, Hardy W, Viano DC: Is head injury caused by linear or rotational acceleration. Proceedings of the **IRCOBI conference**, Lisbon, Portugal, 2003

21. Kleiven S: Predictors for traumatic brain injuries evaluated through accident reconstruction. **Stapp Car Crash J 51**:81-114, 2007

22. Kleiven S, Von Holst H: Consequences of size following trauma to the human head. **J Biomech 35**:135-160, 2002

23. Lee MC, Haut RC: Insensitivity of tensile failure properties of human bridging veins to strain rate: implications in biomechanics of subdural hematoma. **J Biomech 22(6-7)**:537-542, 1989

24. Lovenhielm P: Dynamic properties of the parasagittal bridging veins. **Z. Rechtsmed 74**:55-62, 1974

25. Mendis K, Stalnaker R, Advani S: A constitutive relationship for large deformation finite element modeling of brain tissue. **J Biomech Eng 117(4)**:279-285, 1995

26. Miller R, Margulies S, Leoni M, Nonaka M, Chen Z, Smith D, et al: Finite element modeling approaches for predicting injury in an experimental model of severe diffuse

axonal injury. Proceedings of the 42nd **Stapp Car Crash Conference**, SAE paper No. 983154, 1998

27. Monson KL, Goldsmith W, Barbaro NM, Manle GT: Axial mechanical properties of fresh human cerebral blood vessels. **J Biomed Eng 125(2)**:288-294, 2003

28. Nahum AM, Smith R, Ward CC: Intracranial pressure dynamics during head impact. Proceedings 21st **Stapp Car Crash Conference**, SAE paper No. 770922, 1977

29. Newman JA: Head injury criteria in automotive crash testing. Proceedings of the 20th **Stapp Car Crash Conference**, SAE paper 801317, 1980

30. Newman JA: A generalized acceleration model for brain injury threshold (GAMBIT). Proceedings of **IRCOBI conference**: 121-131, 1986

31. O'Connor C, Colantonio A, Polatajko H: Long term symptoms and limitations of activity of people with traumatic brain injury: a ten-year follow-up. **Psych Rep 97**:169-179, 2005

32. O'Riordain K, Thomas PM, Phillips JP, Gilchrist MD: Reconstruction of real world head injury accidents resulting from falls using multibody dynamics. **Clin Biomech 18**:590-600, 2003

33. Post A, Hoshizaki TB, Gilchrist MD, Brien S: Analysis of the influence of independent variables used for reconstruction of a traumatic brain injury event. **J Sport Eng Tech 226(3/4)**:290-298, 2012

34. Padgaonkar AJ, Kreiger KW, King AI: Measurement of rotational acceleration of a rigid body using linear accelerometers. **J Appl Mech 42**:552-556, 1975

35. Ruan JS: Impact biomechanics of head injury by mathematical modeling [PhD thesis]. Detroit, Michigan, Wayne State University, 1994.

36. Schreiber DI, Bain AC, Meaney DF: In vivo thresholds for mechanical injury to the blood-brain barrier. Proceedings of the **Stapp Car Crash Conference**, 277-291, SAE paper 973335, 1997

37. Sosin DM, Sniezek JE, Thurman DJ: Incidence of Mild and Moderate Brain Injury in the United States, 1991. **Brain Inj 10(1)**:47-54, 1996

38. Styrke J, Stalnacke B, Sojka P, Bjornstig U: Traumatic brain injuries in a well-defined population: Epidemiological aspects and severity. **J Neurotrauma 24**:1425-1436, 2007

39. Versace J: A review of the severity index. In proceedings of the 15th **Stapp Car Crash conference**, SAE paper No. 710881, 1971

40. Viano DC. Lovsund P: Biomechanics of brain and spinal-cord injury: Analysis of neuropathologic and neurophysiologic experiments. **J Crash Prev Inj Cont 1**:35-43, 1999

41. Ward C, Chan M, Nahum AM: Intracranial pressure – a brain injury criterion. Proceedings of the 24th **Stapp Car Crash Conference**, SAE paper 751163, 1980

42. Willinger R, Baumgartner D: Numerical and physical modelling of the human head under impact – towards new injury criteria. **Int J Vehicle Des 32**:94-115, 2003

43. Willinger R, Taled L, Pradoura P: Head biomechanics from finite element model to the physical model. Proceedings of the **IRCOBI Conference**, 1995.

44. Yogandandan N, Li J, Zhang J, Pintar FA, Gennarelli TA: Influence of rotational acceleration-deceleration pulse shapes on regional brain strains. **J Biomech 41**:2253-2262, 2008

45. Zhang L, Yang KH, King AI: A proposed injury threshold for mild traumatic brain injury. **J Biomech Eng 126**:226-236, 2004

46. Zhou C, Khalil TB, King AI. A new model for comparing responses of the homogeneous and inhomogeneous human brain. Proceedings of the 39th **Stapp Car Crash Conference**, 121-136, 1995

Disclosure:

Funding was received by Dr. Hoshizaki for this work from the Canadian Institutes of Health Research

Conflict of interest statement:

There are no conflicts of interest with respect to this research

Study 2

The influence of acceleration loading curve characteristics on traumatic brain injury

Andrew Post[a], T. Blaine Hoshizaki[a], Michael D. Gilchrist[b,a], Susan Brien[c,a], Michael Cusimano[d], and Shawn Marshall[e]

Human Kinetics, University of Ottawa, Ottawa, Canada[a]

School of Mechanical & Materials Engineering, University College Dublin, Dublin, Ireland[b]

Hull Hospital, Gatineau, Canada[c]

St. Michael's Hospital, Toronto, Canada[d]

Ottawa General Hospital, Ottawa, Canada[e]

Word count: 3,082

Abstract

To reduce the incidence and severity of brain trauma an understanding of the biomechanical mechanism of injury is essential. Once the mechanism of brain injury has been identified, prevention technologies could then be developed to aid in their prevention. The past research has shown incidence of brain injury is linked to how the kinematics of a brain injury producing event affects the internal structures of the brain. As a result it is essential that an attempt be made to describe how the characteristics of the acceleration loading curves influence specific traumatic brain injury lesions. As a result, the purpose of this study was to examine the influence of the characteristics of linear and rotational loading curves and how they account for the variance in predicting the outcome of TBI lesions, namely contusion, subdural hematoma (SDH), subarachnoid hemorrhage (SAH), and epidural hematoma (EDH) using a principal components analysis (PCA). Monorail impacts were conducted that simulated falls that caused the TBI lesions. From these reconstructions, the characteristics of the loading curves were determined and used for a PCA analysis. The results indicated that peak resultant acceleration variables did not account for any of the variance in predicting TBI lesions. The majority of the variance was accounted for by duration of the resultant and component acceleration loading curves. In addition, the component curves characteristics in x, y, and z accounted for the majority of the remainder of the variance after duration.

Keywords: Traumatic brain injury, principle components analysis, kinematics

Introduction

Understanding the mechanism of injury for brain trauma is very important in developing prevention technologies and strategies to prevent impacts associated with those injuries. The inability to obtain direct measures on human subjects to study the underlying mechanics of brain injury has led to employing animal, physical, and numerical models (Ommaya et al., 1971; Zhang et al., 2004). Several researchers have published review articles summarizing brain injury mechanism research using these methods (King et al., 2003; Hardy et al., 1994; Viano et al., 1989). This research describes the mechanism of brain injury as linked to damaging levels of brain tissue deformation caused by linear and rotational acceleration loading (Viano et al., 1989; Kleiven, 2007).

These linear and rotational loading curves affect tissue compression, tension and shearing which can be measured using computational models of the human brain (Gurdjian and Webster, 1947; Kleiven, 2007; Post and Hoshizaki, 2012). The response of tissue to anatomical testing methods also suggests that the brain is sensitive to rates and direction of loading (Darvish et al., 2001; Hrapko et al., 2006). Strain dependent nature of brain tissue has also been reported by Nicolle et al. (2004). In addition, other researchers have observed that during high speed impacts neural tissue behaves differently at high frequency when compared to low frequency (Rashid et al, 2012a/b). The method of loading of the brain tissue for tolerance testing has also been documented to produce varying failure rates (Lee and Hault, 1989; Monson et al., 2003) and Arbogast and Margulies (1997) as well as Donnelly and Medige (1997) demonstrated that brain material response was dependent on loading rate, particularly in the brainstem.

The mechanical response of the brain is linked to the kinematics of the event, which is typically measured using linear and rotational acceleration response (Post and Hoshizaki, 2012). As a result, how the tissue in the brain is loaded, where it is loaded, and the magnitude of that loading is dependent on these kinematic variables. How this loading affects brain tissue is determined by the characteristics of the tissue itself. Researchers have investigated the influence of loading curve shape and direction on tissue deformation metrics associated with brain injury (Willinger and Baumgartner, 2003; Zhang et al., 2004; Kleiven 2007). Kleiven (2006) used a finite element model to evaluate the influence of kinematic dependent variables on intracranial strains causing mTBI. Using pure rotational and translational pulses of sinusoidal shape with magnitudes reflecting severities thought to be associated with concussion, Kleiven found that pure rotational pulses showed the best correlation with strain in the FE model. When comparing the translational pulses to strain, the head injury criterion (HIC) and head impact power showed the best correlation (Kleiven 2006). Kleiven did not however discuss the influence of the curve characteristics on the intracranial strains, but simply identified the level of correlation between peak values. In an attempt to examine the influence of time to peak on maximum principal strain and Von Mises stress, Post et al. (2012a) produced artificial acceleration loading curves and found that dissimilar shaped curves with identical peak values and area produced different magnitudes of brain deformation. These results suggest that peak resultant values are not the sole contributor to injurious brain deformation. They concluded from their research that while it is evident that various characteristics of the acceleration loading curve, such as slope and total duration, are influential in the production of brain deformation, an examination of loading curves causing a brain injury was necessary as the next step. The same authors attempted a more refined analysis of hockey helmet impacts to examine how the kinematic variables influenced the magnitude of stress and strain within a finite element model of the human brain (Post et al., 2012b). They found that rotational acceleration loading curve characteristics had a stronger relationship with maximum principal strain and von Mises stress than linear acceleration (Post et al., 2012b). The authors of these two studies did not, however, have reconstructions of actual injuries with which to examine the influence of the kinematic variables, and were thus limited to discussing possible trends between linear and rotational acceleration and brain deformation metrics.

The purpose of this study was to examine the influence of the characteristics of linear and rotational loading curves and how they account for the variance in predicting the outcome of TBI lesions incurred from falls using a principal components analysis. The TBI lesions that were analyzed were: contusion, subdural hematoma (SDH), subarachnoid hemorrhage (SAH), and epidural hematoma (EDH).

Methods

Head injury reconstructions

Twenty adult subjects who incurred a non-fatal TBI lesion from simple falls were recruited for this research. Each subject signed informed consent and all procedures concerning the contact and use of data followed approved ethical guidelines. The subjects were recruited from the Hull Hospital (Gatineau, Quebec, Canada), Ottawa General Hospital (Ottawa, Ontario, Canada), and the National Department of Neurosurgery at Beaumont Hospital, Dublin, Ireland. For the subjects to be recruited they had to have incurred a TBI lesion from a simple fall, where there was no contact with another person or object before or during the fall. In addition, each subject had no previous head injury or neurological defect.

For each case, CT and/or MRI scans were conducted within 24 hours of incurring the injury from the falling event. Each CT/MRI scan was analyzed for the presence of a TBI lesion by the radiologist and neurosurgeon at the hospital. In many cases the medical imaging was confirmed by surgical interventions. For the purpose of the laboratory reconstruction, injury report forms filled out by the patient and/or eyewitnesses of the event were used to ascertain the initial conditions of each fall simulation. The form gave information such as: establishing likely starting body position, impact surface, and location of impact on the head (which was also confirmed by CT scan in many cases by the presence of an extradural hematoma). The process of reconstructing the falling event was conducted in two parts. First, a MAthematical DYnamic MOdels (MADYMO) simulation was run of the incident to establish the possible inbound velocities of the head when it made contact with the surface accounting for the most likely body positions. Second, a Hybrid III headform and neckform attached to a monorail device was used to simulate the impact, with the surface defined by the report form and velocity by the MADYMO reconstruction.

MADYMO reconstructions

Mathematical dynamic models is a tool that has been commonly used to reconstruct the kinematics of the human body for falling scenarios. This software has a particular strength in that it has a variety of ellipsoid pedestrian models which have joint parameters similar to those of a human (O'Riordain et al., 2003). This tool allows for the simulation of the events leading up to the head contact to the ground (in this case) that makes it possible to approximate the head impact velocity while taking into account the motions of the body as the fall takes place. The ellipsoid pedestrian models used in this research were validated using various impactors that were designed to determine the risk to pedestrians from vehicle impacts.

For each fall reconstruction, a series of MADYMO simulations were conducted using an ellipsoid pedestrian model that was closest to the anthropometry of the human subject. The model was placed within the accident environment in a similar position to the starting position as described in the accident reports forms and eyewitness reports (Adamec et al., 2010). As report forms inherently have some variability in their accuracy concerning the actual event, a sensitivity analysis of each case was run with a series of possible impact scenarios conducted (Figure 1) (O'Riordain et al., 2003; Forero Rueda and Gilchrist, 2009; Adamec et al., 2010). For each injury reconstruction, a minimum of three MADYMO simulations were conducted to ensure that the contact head velocity at impact was properly framed with a slowest possible and fastest possible value. These velocities were then used as the target velocities for the Hybrid III headform drops using a monorail drop rig (Table 1).

Table 1. Impact velocities and surfaces of the reconstructions

Case #	Velocity (m/s)	Surface	TBI Lesion
1	3.0 - 4.0	Concrete	Subdural Hematoma
2	4.7 - 5.2	Concrete	Subdural Hematoma
3	5.1 - 6.1	Concrete	Subdural Hematoma; Epidural Hematoma; Contusion
4	4.1 - 5.4	Concrete	Subarachnoid Hemorrhage
5	3.9 - 6.2	Wood	Subdural Hematoma; Subarachnoid Hemorrhage
6	2.2 - 3.3	Carpet	Subdural Hematoma
7	3.9 - 6.2	Concrete	Subdural Hematoma; Subarachnoid Hemorrhage; Contusion
8	3.3 - 4.8	Concrete	Subdural Hematoma
9	4.8 - 6.2	Concrete	Subdural Hematoma; Subarachnoid Hemorrhage;
10	3.6 - 4.9	Concrete	Subarachnoid Hemorrhage; Contusion
11	3.7 - 5.8	Concrete	Subdural Hematoma; Contusion
12	3.6 - 4.8	Concrete	Epidural Hematoma
13	4.8 - 6.2	Wood	Subdural Hematoma
14	3.8 - 6.0	Concrete	Subdural Hematoma; Contusion
15	4.8 - 5.8	Concrete	Parenchymal Hemorrhage; Contusion
16	5.1 - 5.6	Concrete	Subdural Hematoma
17	4.5 - 4.8	Concrete	Subdural Hematoma
18	3.5 - 4.2	Concrete	Subdural Hematoma
19	4.7 - 5.1	Concrete	Subdural Hematoma
20	5.4 - 6.1	Metal bar	Subdural Hematoma

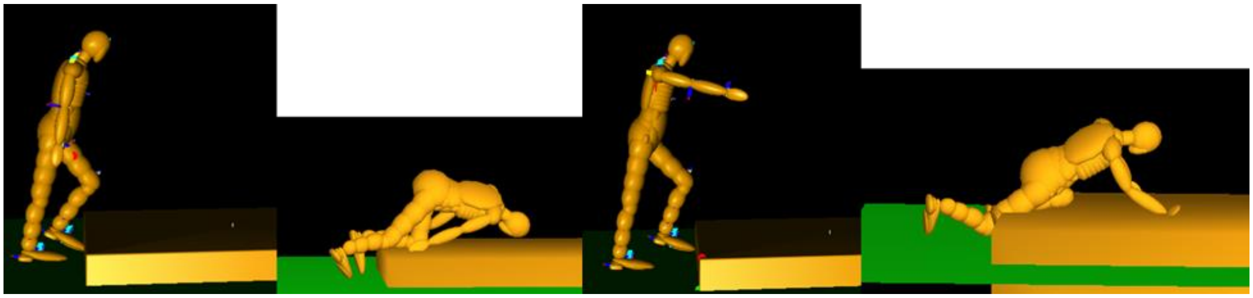

Figure 1. Two MADYMO reconstructions of two extremes for a falling simulation: (left) trip with no arms to brace the fall; and (right) arms held out to brace against the fall

Equipment

The physical reconstructions used the monorail drop rig outfitted with a Hybrid III headform and neckform (Figure 2). The monorail was 4.7 m high and had a drop carriage to which the Hybrid III 50% headform and neckform was affixed. Upon release, the headform dropped vertically on ball bushings until contact with the impacting surface. The release mechanism was a pneumatic piston to ensure a clean drop, and the contact velocity was determined by photoelectric time gate within 2.6 cm of impact. The impact location on the headform was determined by the accident reports and CT/MRI scans (Figure 3). The impact surfaces were determined from the injury report forms and are described in table 1 for each case. For each velocity three impacts were conducted per subject.

Figure 2. Physical reconstruction using a Hybrid III headform and neckform for a fall onto a carpet with underlay covering a concrete anvil

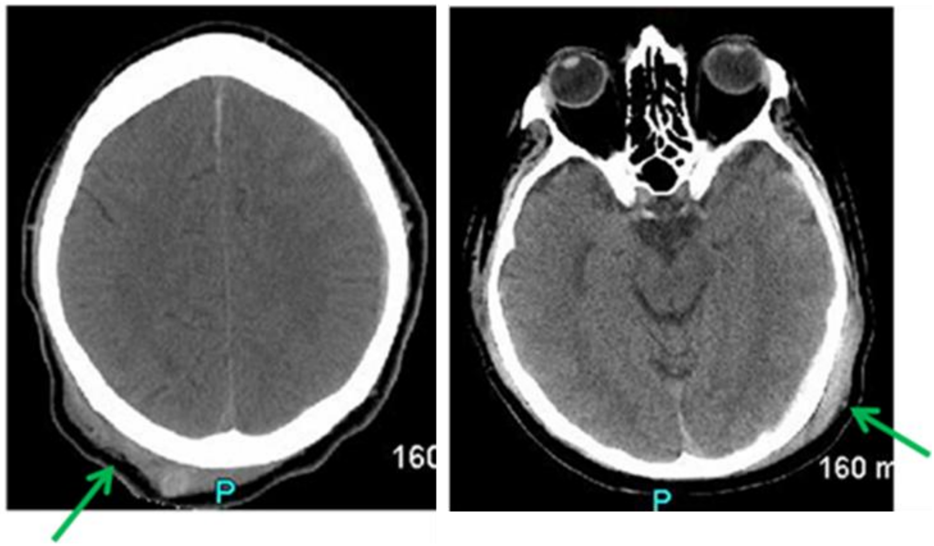

Figure 3. CT scans showing the impact location on the skull as shown by extradural hematoma (designated by arrows)

The Hybrid III 50% headform was outfitted with a 3-2-2-2 accelerometer array (Padgaonkar et al., 1975) and sampled at 20 kHz. The accelerometers used were Endevco 7264C-2KTZ-2-300. The x-axis was defined as facing forward from the head centre of gravity, the y-axis to the left of the head and the z-axis vertically upwards. The resulting signal was filtered using SAE J211 class 1000 filter. All signals were collected using a DTS prolab module and stored on a computer.

Curve characteristic analysis

The linear and rotational acceleration curve characteristics producing the specific lesion type (contusion, subdural hematoma, subarachnoid hemorrhage, epidural hematoma) was evaluated using a principal component analysis (PCA) approach. The influence of peak value, slope to peak, total duration, and time to peak (Figure 4) on outcome TBI lesion was conducted. The integral of the linear and rotational acceleration time curve for the resultant and all components was also calculated.

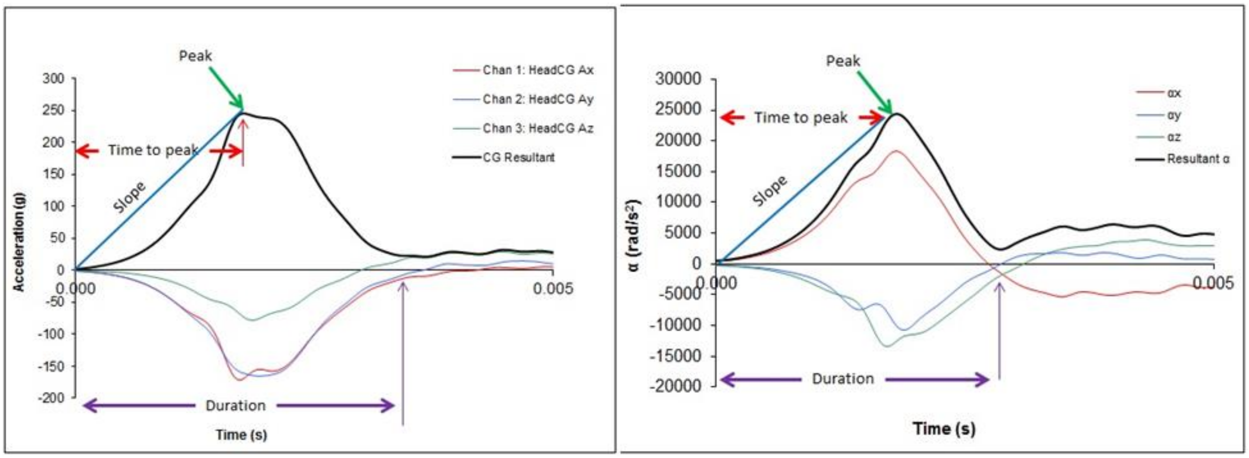

Figure 4. Linear (right) and rotational (left) acceleration loading curve characteristic breakdown using resultant acceleration curves as an example.

Results

Contusion

The principal components analysis with varimax (orthogonal rotation) disclosed a 4 component solution, which accounted for 93 % of the variance (table 2). Component 1 consisted of the time to peak components of the characteristic of the loading curves leading to contusion lesions, which accounted for 37 % of the total variance. Component 2, which accounted for 23.8 % of the total variance, consisted of the peak, slope and integrals of the x-axis linear and y-axis rotational components of the loading curves. The third component comprised of y-axis linear peak, slope and integral accounted for an additional 21.1 % of the total variance. Finally, component 4 represented z-axis peak, slope and integral in linear acceleration, which accounted for 11.1 % of the total variance.

Table 2. Table showing the total variance explained for the contusion injuries and the results of the rotated component matrix

Component 1	Rotated Matrix Output	Component 2	Rotated Matrix Output	Component 3	Rotated Matrix Output	Component 4	Rotated Matrix Output
R lin time	0.956	X lin peak	0.924	Y lin peak	0.988	Z lin peak	0.937
R ang time	0.899	X lin slope	0.934	Y lin slope	0.979	Z lin slope	0.859
X lin time	0.950	X lin integral	0.888	Y lin integral	0.985	Z lin integral	0.887
X ang time	0.943	Y ang peak	0.934				
Y lin time	0.951	Y ang slope	0.932				
Y ang time	0.891	Y ang integral	0.925				
Duration	0.954						
Variance accounted for	37.00%		23.80%		21.10%		11.10%
Cumulative	37.00%		60.80%		81.90%		93.00%

*R = Resultant; lin = linear; ang = angular; time = time to peak; peak = peak magnitude

Subdural hematoma

For subdural hematoma, the PCA identified a 4 component solution that accounted for 85.1 % of the total variance (table 3). Component one consisted of time to peak variables and total duration which accounted for 36.3 % of the total variance. Component 2 comprised of x-axis rotational loading curve peak magnitude, slope, and integral, which accounted for 18.7 % of the total variance. The third component consisted of x-axis linear acceleration peak, slope, and integral, as well as y-axis peak and integral, accounting for 18.2 % of the total variance. Finally, component 4 consisted of z-axis peak, slope, and integral, accounting for a further 12 % of the total variance.

Table 3. Table showing the total variance explained for the SDH injuries and the results of the rotated component matrix

Component 1	Rotated Matrix output	Component 2	Rotated Matrix output	Component 3	Rotated Matrix output	Component 4	Rotated Matrix output
R lin time	0.982	X ang peak	0.953	X lin peak	0.94	Z ang peak	0.937
R ang time	0.984	X ang slope	0.906	X lin slope	0.898	Z ang slope	0.938
X lin time	0.982	X ang intergr	0.962	X lin integral	0.938	Z ang integra	0.872
X ang time	0.964			Y ang peak	0.904		
Y lin time	0.971			Y ang integra	0.96		
Y ang time	0.979						
Z lin time	0.979						
Duration	0.951						
Variance accounted	36.3%		18.7%		18.2%		12.0%
Cumulative	36.3%		54.9%		73.2%		85.1%

*R = Resultant; lin = linear; ang = angular; time = time to peak; peak = peak magnitude

Subarachnoid hemorrhage

For subarachnoid hemorrhage, the PCA also identified a 4 component solution, which accounted for 93.1 % of the total variance (table 4). The first component consisted of the time to peak variables for the resultant, x, and y-axis as well as the total duration of the pulse, which accounted for 36.3 % of the total variance. The second component consisted of x-axis linear, and y-axis rotational loading curve peak, slope, and integral values, accounting for 23.9 % of the total variance. The third component consisted of x-axis rotational peak and slope as well as and z-axis peak, slope, and integral, which accounted for 21.8 % of the variance. Finally, the fourth component consisted of z-axis linear peak and slope, accounting for 11.1 % of the variance.

Table 4. Table showing the total variance explained for the SAH injuries and the results of the rotated component matrix

Component 1	Rotated Matrix Output	Component 2	Rotated Matrix Output	Component 3	Rotated Matrix Output	Component 4	Rotated Matrix Output
R lin time	0.953	X lin peak	0.949	X ang peak	0.85	Z lin peak	0.9
R ang time	0.904	X lin slope	0.957	X ang slope	0.851	Z lin slope	0.902
X lin time	0.941	X lin integral	0.884	Z ang peak	0.898		
X ang time	0.922	Y ang peak	0.953	Z ang slope	0.898		
Y lin time	0.957	Y ang slope	0.959	Z and integra	0.885		
Y ang time	0.875	Y ang int	0.922				
Duration	0.942						
Variance accounted	36.30%		23.90%		21.80%		11.10%
Cumulative	36.30%		60.20%		81.90%		93.10%

*R = Resultant; lin = linear; ang = angular; time = time to peak; peak = peak magnitude

Epidural hematoma

For the epidural hematoma, the PCA identified a 2 component solution, which accounted for 94.6 % of the total variance (table 5). The first component consisted of the resultant linear and rotational time to peak values, as well as x and y-axis linear and rotational time to peak. The first component also consisted of y-axis rotational acceleration peak, and z-axis rotational acceleration slope values, as well as total duration of the pulse. Overall, the first component accounted for 57.4 % of the total variance. The second component consisted of the x and y-axis linear acceleration peak, slope, and integral, as well as the z-axis rotational integral, accounting for a further 37.2 % of the total variance.

Table 5. Table showing the total variance explained for the EDH injuries and the results of the rotated component matrix

Component 1	Rotated Matrix Output	Component 2	Rotated Matrix Output
R lin time	0.893	X lin peak	0.971
R ang time	0.877	X lin slope	0.973
X lin time	0.886	X lin integral	0.974
X ang time	0.868	Y lin peak	0.939
Y lin time	0.904	Y lin slope	0.952
Y ang peak	0.937	Y lin integral	0.926
Y ang time	0.864	Z ang integral	0.992
Z ang time	0.862		
Z ang slope	0.864		
Duration	0.919		
Variance accounted for	57.40%		37.20%
Cumulative	57.40%		94.60%

*R = Resultant; lin = linear; ang = angular; time = time to peak; pea

Discussion

Contusion

The results of the PCA identified time to peak resultant and components in the x and y-axis characteristics of the linear and rotational acceleration curves as the best predictors for contusions. The total duration of the pulse was found to be important. The influence of the z-axis on the variance was low, probably as a result of there being no crown impacts in this dataset. When examining the components, only the x-axis rotational characteristics and the y-axis linear and rotational characteristics accounted for part of the variance and not the resultant characteristics such as peak, slope or integral. These results indicate that resultant loading curve characteristics, other than linear and rotational time to peak, had little influence on the variance of the dataset producing a contusion.

Subdural hematoma

Like the contusion result, the PCA identified time based variables such as time to peak for the linear and rotational loading curves in x and y component as well as resultant accounted for a large part of the variance. Total duration was also found to be influential. Interestingly, the results show more variance was accounted for by the rotational components in x, y, and z-axes (30 % +) than the x-axis linear curve characteristics. These results would suggest that the rotational acceleration characteristics accounted for more variance than the linear acceleration characteristics. The lack of resultant loading curve characteristics accounting for very much of the total variance is likely a result of the components being more closely associated with the event. This is in agreement with previous literature that has identified subdural hematoma as a rotationally influenced lesion as opposed to a linear dominant injury similar to other forms of TBI (Kleiven, 2003).

Subarachnoid hemorrhage

As with contusion and subdural hematoma, the PCA for subarachnoid hemorrhage indicated a large amount of the variance to be accounted for by time to peak and total duration characteristics. The remaining components involve x and z-axis linear curve characteristics and x, y, and z-axis rotational curve characteristics. Like subdural hematoma, a large amount of the variance, after the time based characteristics, is accounted for by rotational loading curve peak, slope, and integral. This indicates a rotational influence for the risk of subarachnoid hemorrhage which is based within the x, y, and z components and not the characteristics of the resultant loading curves.

Epidural hematoma

There was a low sample size of reconstructions that produced an epidural hematoma ($n = 2$). As a result the PCA extracted 2 components which accounted for 94.6 % of the total variance. The first component was time based, which was similar to the other TBI lesions. The second component was mostly x and y-axis linear dynamic response characteristics. Overall, after the linear and rotational time to peak values in x, y, and z-axes, the characteristics of the linear acceleration loading curve appeared to account for more variance in the cases involving epidural hematoma.

Conclusion

In conclusion, the PCA showed that both linear and rotational acceleration accounted for variance in the dynamic response that incurred contusion, SDH, SAH, or EDH. Of particular interest was that the resultant curve characteristics of slope, integral, or peak did not appear to account for any of the variance. This result suggests that using components of the linear and rotational acceleration loading curve in x, y, and z-axes may account for more variance in the production of these TBI than the resultant values alone. This reinforces the usefulness of tools such as finite element modeling of the human brain to measure brain deformation responses using the components of linear and rotational acceleration as this method can quantify the influence these curve characteristics have on the outcome.

The fact that the results show that time of the pulse and time to peak variables have importance when it comes to TBI, reinforces the use of integrations such as Gadd severity index (GSI) and the Head injury criterion (HIC) as they attempt to use duration to influence the predictions of injury risk (Gadd, 1966; Versace, 1971). However, the GSI and HIC are not particularly predictive of injury (Goldsmith, 1981), which may be in part due to time based considerations only accounting for around 38 % of the variance of TBI as well as no rotational components. The reconstructions in this study led to extremely short duration time to peak (0.0017 s) and duration (0.03) dynamic response curves. The intervention of protective devices (helmets, crash pads etc) serve to lengthen this response, but may as a result create longer pulses which have been associated with the occurrence of mTBI (Wright et al., 2012). As a result it would be interesting for future research to investigate mTBI dynamic response and examine curve characteristics which may differentiate between TBI and mTBI.

Limitations

Limitations of this study revolve around the accuracy of the reconstruction and the modeling process from the previous work simulating brain injuries. The reconstructions conducted within the laboratory use Hybrid III physical models which have been validated for forehead impact, however the impacts in other locations may produce magnitudes of response which are dissimilar to human responses. As a result the headform used may produce acceleration loading curves which may not be similar to the response of a non-rigid system such as the human head. The input parameters (velocity, mass, location) are all calculated and may not accurately represent the actual event, while using multiple conditions for each injury simulation may include the actual event; it is unlikely a precise representation of the event causing the injury will be simulated. The influence of the musculature on the impact will also be difficult to ascertain and is thus also a limitation to this study. While simple injury scenarios were chosen for this study, it is unlikely that each simulation was exact to the individual who was injured. The variables chosen to reflect the characteristics of the acceleration loading curve do not reflect all possible combinations of time and peak variable. As such it is possible that a curve characteristic not analyzed here could account for a larger amount of the variance.

Acknowledgements

Funding was provided for this research by the Canadian Institutes of Health Research

Conflict of interest statement

There are no conflicts of interest with the submitted research.

References

1. Arbogast, K.B., Margulies, S.S., 1998. Material characterization of the brainstem from oscillatory shear tests. Journal of biomechanics 31(9), 801-807.

2. Darvish, K.K., Crandall, J.R., 2001. Nonlinear viscoelastic effects in oscillatory shear deformation of brain tissue. Medical Engineering and Physics 23(9), 633-645.

3. Donnelly, B.R., Medige, J., 1997. Shear properties of human brain tissue. Journal of Biomechanical Engineering 119(4), 423-432.

4. Gadd, C.W., 1966. Use of a weighted impulse criterion for estimating injury hazard. In Proceedings of the 10th Stapp Car Crash Conference, SAE paper No. 660793.

5. Goldsmith, W., 1981. Current controversies in the stipulation of head injury criteria. Letter to the editor. Journal of Biomechanics 14, 883-884.

6. Gurdjian, E.S., Webster, J.E., 1947. The mechanism and management of injuries to the head. Journal of the American Medical Association 134(13), 1072-1077.

7. Hardy, W.N., Khalil, T.B., King, A.I., 1994. Literature review of head injury biomechanics. International Journal of Impact Engineering 15(4), 561-568.

8. Hrapko, M., van Dommelen, J.A.W., Peters, G.W.M., Wismans, J.S., 2006. The mechanical behaviour of brain tissue: Large strain response and constitutive modeling. Biorheology 43(5), 623-636.

9. King, A.I., Yang, K.H., Zhang, L., Hardy, W., Viano, D.C., 2003. Is head injury caused by linear or rotational acceleration. In Proceedings of the IRCOBI Conference, Lisbon, Portugal.

10. Kleiven, S., 2006. Evaluation of head injury criteria using a finite element model validated against experiments on localized brain motion, intracerebral acceleration, and intracranial pressure. International Journal of Crashworthiness 11 (1), 65-79.

11. Kleiven, S., 2007. Predictors for traumatic brain injuries evaluated through accident reconstruction. Stapp Car Crash Journal 51, 81-114.

12. Lee, M.C., Hault, R.C., 1989. Insensitivity of tensile failure properties of human bridging veins to strain rate: implications in biomechanics of subdural hematoma. Journal of Biomechanics 22(6-7), 537-542.

13. Monson, K.L., Goldsmith, W., Barbaro, N.M., Manle, G.T., 2003. Axial mechanical properties of fresh human cerebral blood vessels. Journal of Biomedical Engineering 125(2), 288-294.

14. Nicolle, S., Lounis, M., Willinger, R., 2004. Shear properties of brain tissue over a frequency range relevant for automotive impact situations: New experimental results. Stapp Car Crash Journal 48, 239-258.

15. Ommaya, A.K., Grubb, R.L., Naumann, R.A., 1971. Coup and contrecoup injury: Observations in the mechanics of visible brain injuries in the rhesus monkey. Journal of Neurosurgery 35- 503-516.

16. Padgaonkar, A.J., Kreiger, K.W., King, A.I., 1975. Measurement of rotational acceleration of a rigid body using linear accelerometers. Journal of Applied Mechanics 42, 552-556.

17. Post, A., Hoshizaki, T.B., 2012. Mechanical properties describing brain impact injuries: A review. Trauma 14(4), 327-349.

18. Post, A., Hoshizaki, T.B., Gilchrist, M.D., 2012a. Finite element analysis of the effect of loading curve shape on brain injury predictors. Journal of Biomechanics 45, 679-683.

19. Post, A., Walsh, E.S., Hoshizaki, T.B., Gilchrist, M.D., 2012b. Analysis of loading curve characteristics on the production of brain deformation metrics. Journal of Sports Engineering and Technology 226(3/4), 200-207.

20. Rashid, B., Destrade, M., Gilchrist, M.D., 2012a. Mechanical characterization of brain tissue in compression at dynamic strain rates. Journal of the Mechanical Behavior of Biomedical Materials 10, 23-38.

21. Rashid, B., Destrade, M., Gilchrist, M.D., 2012b. Mechanical characterization of brain tissue in tension at dynamic strain rates. Journal of the Mechanical Behavior of Biomedical Materials, in press.

22. Versace, J., 1971. A review of the severity index. In Proceedings of the 15th STAPP Car Crash Conference, SAE paper No. 710881.

23. Viano, D.C., King, A.I., Melvin, J.W., Weber, K., 1989. Injury biomechanics research: An essential element in the prevention of trauma. Journal of Biomechanics 22(5), 403-417.

24. Willinger, R., Baumgartner, D., 2003. Numerical and physical modelling of the human head under impact – towards new injury criteria. International Journal of Vehicle Design 32, 94-115.

25. Wright, R., Post, A., Hoshizaki, T.B., Ramesh, K.T., 2012. A computational approach to estimate axonal damage under inertial loading of the head. Journal of Neurotrauma, in press

26. Zhang, L., Yang, K.H., King, A.I., 2004. A proposed injury threshold for mild traumatic brain injury. Journal of Biomechanical Engineering 126, 226-236.

Study 3

The influence of dynamic response and brain deformation metrics on the occurrence of subdural hematoma in different regions of the brain

Andrew Post[1] PhD, T. Blaine Hoshizaki[1] PhD, Michael D. Gilchrist[2,1] PhD, Susan Brien[3,1] MD, Michael Cusimano[4] MD, and Shawn Marshall[5] MD

Human Kinetics, University of Ottawa, Ottawa, Ontario, Canada[1]

School of Mechanical & Materials Engineering, University College Dublin, Dublin, Ireland[2]

Hull Hospital, Gatineau, Quebec, Canada[3]

St. Michael's Hospital, Toronto, Ontario, Canada[4]

Ottawa General Hospital, Ottawa, Ontario, Canada[5]

Key Words: Traumatic brain injury; subdural hematoma, injury reconstruction, falling injuries

Running Title: Analysis of SDH location in the brain

Abstract

Object: The purpose of this study is to examine how the dynamic response and brain deformation of the head and brain representing a series of injury reconstructions of which subdural hematoma was the outcome influences the location of the lesion in the lobes of the brain. *Methods:* Sixteen falling cases in which SDH was the outcome were reconstructed using a monorail drop rig and Hybrid III headform. The location of the SDH in one of the four lobes of the brain (frontal, parietal, temporal, occipital) was confirmed by CT/MRI scan examined by a neurosurgeon. *Results:* The results indicated that there were minimal differences found between locations of SDH for linear acceleration. Rotational acceleration peak resultant and x-axis component was larger for the parietal lobe in comparison to the other lobes. There were also some differences between the parietal lobe and the other lobes in the z axis component. Maximum principal strain, VMS, shear strain, and product of strain and strain rate all had differences in magnitude depending on which lobe the SDH was present. The parietal lobe consistently had the largest magnitude response, followed by the frontal lobe and the occipital lobe. *Conclusion:* In conclusion, the results indicated that there are differences in magnitude for rotational acceleration and brain deformation metrics which may identify the location of SDH in the brain.

Introduction:

Of all traumatic brain injuries (TBI), subdural hematoma (SDH) and diffuse axonal injury (DAI) are the most lethal[9]. The high mortality of SDH in particular has led to an increased need to develop a better understanding of the mechanism and tolerance for this type of brain trauma. Early work in understanding SDH was conducted by Gennarelli et al[8] who discovered that rotational acceleration dominant motions could create this type of TBI lesion. Specifically, it was found that SDH was produced from short duration high magnitude rotational pulses. Using a brain model, Zhou et al.[34] proposed that subdural hematoma was more likely to be produced from an occipital impact than with a frontal impact. The anterior-posterior rotational movement theory to creating a hematoma was tested on cadaver specimens by Lovenhielm[20] and peak resultant rotational acceleration thresholds of 4.5 krad/s^2 were proposed. However, due to the complex nature of brain tissue it is likely that the use of linear or rotational acceleration alone in the description of TBI thresholds will underestimate the risk of injury[30].

The directional nature (anisotropy) of brain tissue in response to loading has been investigated by several researchers using physical and anatomical models[10,12,27]. Investigators researching subdural hematoma using finite element modeling have found that antero-posterior motion can cause higher strain on the brain tissues and vasculature than lateral motions[34]. However, this study used a tied interface between the skull and brain, and is limited as SDH is thought to result from relative brain skull motion[16]. In 2003, Kleiven[16] used a finite element modeling approach to investigate the directional sensitivity of subdural hematoma. He found the largest skull-brain motion, and therefore the greatest strains in the brain tissue and vasculature were found in the antero-posterior rotational motions, with near zero for translational motions. These results supported the antero-posterior theory of directional sensitivity for subdural hematoma. While lateral tests were conducted, Kleiven[16] found that the relative brain skull motion and strains were lower for corresponding rotational impulses, and even lower for translational pulses. Using a finite element model of the human brain, Zhou et al[34] found that antero-posterior motions potentially cause higher strains in regions associated with SDH than lateral direction motions. Doorly and Gilchrist[5], Doorly[4], Willinger and Baumgartner[32], and Post et al[26] also examined the incidence of SDH using injury reconstruction and found that large magnitude brain deformations were required to incur this type of injury.

While SDH has been described in terms of global brain deformation responses, and gross directional kinematics, there have not been any attempts to discover which metrics differentiate between the presence of SDH in the different lobes of the brain. This is important as currently SDH is viewed as a focal TBI with no difference in their causation although they can be present in different parts of the brain. This presence in certain parts of the brain is likely caused by the characteristics of the event (velocity, mass, impact location, etc.) which is described by the dynamic response and resulting brain deformation. Investigations into this phenomenon would provide important insights into the mechanism of injury for subdural hematoma. As a result, the purpose of this research was to investigate how the dynamic response and brain deformation metrics of the head influences the location of acute focal subdural hematoma in the brain.

Materials and Methods

Sixteen adult subjects were selected by physicians at the Hull hospital in Gatineau, the General Hospital in Ottawa, both in Canada as well as the National Department of Neurosurgery at Beaumont Hospital, Dublin, Ireland who incurred a non-fatal subdural hematoma from a fall. Brain injury identification and assessment were conducted by the radiologists and neurosurgeons at the hospital according to CT and MRI scans. For all cases, medical examination and medical imaging was carried out within 24 hours of the injury event. These medical images were confirmed in many cases through ensuing surgical interventions. The conditions surrounding the fall were assessed based upon accident report forms and eyewitness accounts. The report forms established starting points for reconstructive parameters of the incident such as: impact vector, location of impact on the head, and velocity of impact. To simplify the reconstructive parameters, only simple falls were used for this study, and in all cases the impact surface was a rigid structure such as cement. The process of reconstructing the brain injury event consisted of first using MAthematical DYnamic Models (MADYMO) to simulate the fall to ascertain the head impact velocity, then using a Hybrid III headform to conduct the impacts. Once the three-dimensional acceleration loading curves were generated from the Hybrid III impacts, they were used as input to the University College Dublin Brain Trauma Model (MADYMO) for brain deformation analyses.

MADYMO reconstructions

Mathematical dynamic models is a tool which has been used primarily in the automotive industry for pedestrian impacts but has found use in other applications such as injury reconstructions and injury biomechanics. This tool allows for approximate simulations of the events leading up to an incident (such as a fall in this case) to calculate the kinematics surrounding an event[1,6]. Mathematical dynamic models has a particular strength in that it has a wide variety of human body models, which includes a series of human ellipsoid pedestrian models which have joint parameters which are similar to those of a human[24]. These pedestrian models were validated using various impactors that were designed to determine the risk to pedestrians from vehicle impacts.

For the fall reconstructions using MADYMO simulations, an ellipsoid pedestrian model was chosen that was the closest match to the human subject's anthropometrics (Figure 1). The model was then placed within the environment which was modeled after the descriptions of the event from the injury report forms and/or video. The fall simulation was then conducted based upon the initial fall parameters (body position, initial velocity) which were described in the reports[1]. As there was some uncertainty surrounding the nature of the fall in some cases (other body parts contacting the ground first for example) a sensitivity analysis was conducted based upon the possible parameters leading to the head contact with the hard surfaces[1,7,24]. This sensitivity analysis comprised running simulations without any body part bracing the fall, and various arm or leg positions which may have lowered the head velocity upon contact with the object which caused the SDH. The lowest head contact velocity was used for the physical model simulations as these were designated the 'best possible scenario' for the simulations.

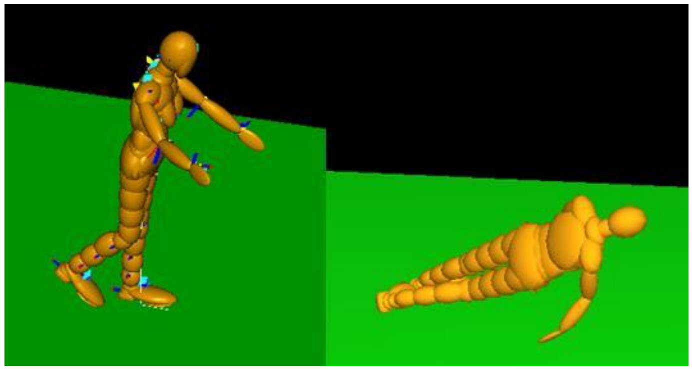

Figure 1. MADYMO simulation of a fall forwards and to the right; (left) initial position of the ellipsoid pedestrian model; (right) position just prior to head contact

Laboratory reconstruction

As all the subjects in this study were victims of severe falls, a guided monorail device equipped with an instrumented Hybrid III head and neck form was used for the injury reconstructions.

Monorail

To simulate falling impacts a monorail was used (Figure 2). The monorail consisted of a 4.7 m long rail to which the headform was attached through a special jig. The headform runs along the rails on ball bushings to reduce the effects of friction on inbound velocity and is released by pneumatic piston. A Hybrid III 50th percentile headform and neck was used for these reconstructions because it allowed for the measurement of the three-dimensional dynamic headform response. The impact velocity was measured using a photoelectric time gate placed within 0.02 m of the impact. The anvil at the base of the monorail was steel and was changed to represent the surface the head contacted as was described by the injury report. In the case of this research, the majority of cases were impacting concrete (Table 1). The base of the monorail was 0.67 m high, 0.30 m wide, and 0.38 m deep and was fixed to the floor.

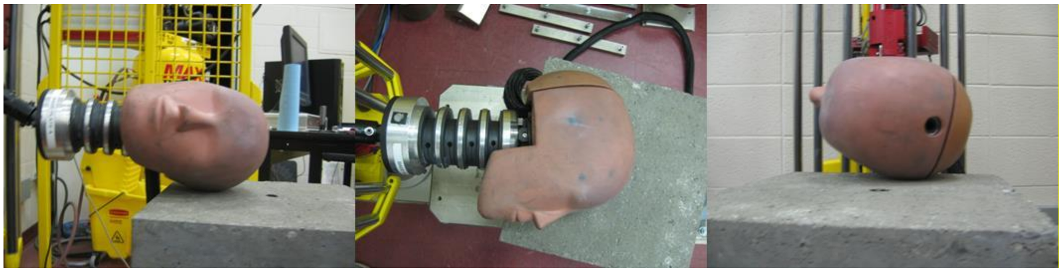

Figure 2. Hybrid III head and neckform setup for a reconstruction of a fall to concrete

Table 1. Impact velocities, surfaces, and resulting injuries for each case

Case #	Velocity (m/s)	Surface	TBI Lesion
1	3.0 - 4.0	Concrete	Subdural Hematoma
2	4.7 - 5.2	Concrete	Subdural Hematoma
3	5.1 - 6.1	Concrete	Subdural Hematoma; Epidural Hematoma; Contusion
4	4.1 - 5.4	Concrete	Subarachnoid Hemorrhage
5	3.9 - 6.2	Wood	Subdural Hematoma; Subarachnoid Hemorrhage
6	2.2 - 3.3	Carpet	Subdural Hematoma
7	3.9 - 6.2	Concrete	Subdural Hematoma; Subarachnoid Hemorrhage; Contusion
8	3.3 - 4.8	Concrete	Subdural Hematoma
9	4.8 - 6.2	Concrete	Subdural Hematoma; Subarachnoid Hemorrhage;
10	3.6 - 4.9	Concrete	Subarachnoid Hemorrhage; Contusion
11	3.7 - 5.8	Concrete	Subdural Hematoma; Contusion
12	3.6 - 4.8	Concrete	Epidural Hematoma
13	4.8 - 6.2	Wood	Subdural Hematoma
14	3.8 - 6.0	Concrete	Subdural Hematoma; Contusion
15	4.8 - 5.8	Concrete	Parenchymal Hemorrhage; Contusion
16	5.1 - 5.6	Concrete	Subdural Hematoma
17	4.5 - 4.8	Concrete	Subdural Hematoma
18	3.5 - 4.2	Concrete	Subdural Hematoma
19	4.7 - 5.1	Concrete	Subdural Hematoma
20	5.4 - 6.1	Metal bar	Subdural Hematoma

Hybrid III

A 50^{th} percentile adult headform (mass 4.54 ± 0.01kg) and neck was instrumented for measurement of three-dimensional dynamic response according to Padgaonkar's 3-2-2-2 accelerometer array[25] (Figure 2). The accelerometers used were Endevco 7264C-2KTZ-2-300.

Laboratory reconstruction procedure

Upon identification of a brain injury suitable for reconstruction, the parameters from the injury report were utilized to identify starting points for the laboratory reconstructions. The MADYMO simulations were used to determine the head impact velocities (Table 1). The impact site was identified from images of the impact location on the subject's head or CT scans where swelling would identify the site of impact on the skull (Figure 3). Three impacts were conducted per scenario. The impact surface was changed to reflect the impact surface and thus its characteristics (Table 1).

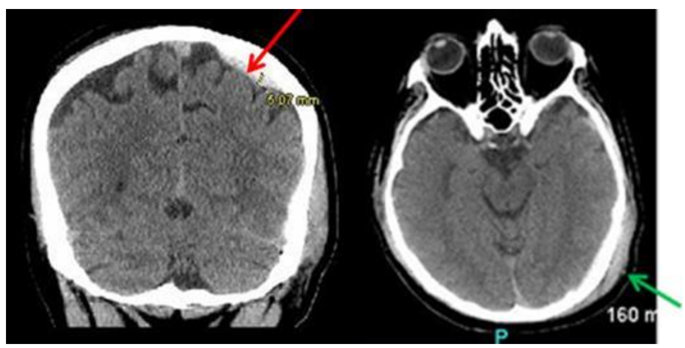

Figure 3. CT of the subject's head post-impact. SDH indicated by red arrow, impact site shown by green arrow.

The impacts were sampled at 20 kHz and recorded using DTS TDAS PRO software. All data was filtered using a SAE J211 class 1000 filter. This reconstruction provided a three-dimensional description of the kinematics of the impact event which created each subdural hematoma. The x-axis was defined as facing forward from the head centre of gravity, the y-axis to the left of the head and the z-axis vertically upwards. These loading curves were then used as input to the finite element model of the human brain.

Finite element model

The finite element model used for this research was the University College Dublin Brain Trauma Model (UCDBTM)[13,14]. The geometry of the model was based upon CT scans of a male cadaver, and as such does not represent the typical 50 percentile of the human male. The model was comprised of the dura, cerebrospinal fluid (CSF), pia, falx, tentorium, grey and white matter, cerebellum, and brain stem. The UCDBTM had approximately 26,000 elements and was validated against Nahum et al's[23] and Hardy et al's[11] cadaver impact research. Real life reconstructions were conducted to further validate the model and were found to be in good agreement with lesions on CT scans for TBI incidents[5,26].

The material properties of the model are presented in tables 2 and 3. The brain characteristics were derived from Zhang et al[33]. A linear viscoelastic material model combined with large deformation theory was used to model the brain tissue[13,14,29,34]. The compressive behaviour of the brain was considered elastic, and the shear characteristics of the brain were defined as:

$$G(t) = G_\infty + (G_0 - G_\infty)e^{-\beta t}$$

where G_∞ is the long term shear modulus, G_0 is the short term shear modulus and β is the decay factor[13]. The hyperelastic model used for the brain in shear is represented by:

$$C_{10}(t) = 0.9C_{01}(t) = 620.5 + 1930e^{-t/0.008} + 1103e^{-t/0.15} \text{ (Pa)}$$

where C_{10}, and C_{01} are temperature dependent material parameters, and t is seconds[13]. The brain skull interaction was accomplished by modeling the CSF as solid elements with a high bulk modulus and low shear modulus, the contact definitions allowed for no separation and used a friction coefficient of 0.2[21].

Table 2. Material characteristics of the UCDBTM

Material	Poisson's Ratio	Density (kg/m^3)	Young's Modulus (MPa)
Dura	0.45	1130	31.5
Pia	0.45	1130	11.5
Falx	0.45	1140	31.5
Tentorium	0.45	1140	31.5
CSF	0.5	1000	-
Grey Matter	0.49	1060	Hyperelastic
White Matter	0.49	1060	Hyperelastic

Table 3. Material characteristics of the brain tissue used for the UCDBTM

	Shear Modulus (kPa)			
Material	G_0	G_∞	Decay Constant (s^{-1})	Bulk Modulus (GPa)
White Matter	12.5	2.5	80	2.19
Grey Matter	10	2	80	2.19
Brain Stem	22.5	4.5	80	2.19
Cerebellum	10	2	80	2.19

The CT scans from the hospital were used to create the regions of interest (ROI) in the UCDBTM which represented each SDH. The UCDBTM was first scaled to the size of the brain of the subject for each case based on measurements taken from the CT scans[17]. The region which was identified by neurosurgeon as the SDH was then matched to the UCDBTM. The elements which encompassed the volume of the blood on the CT were selected to represent the ROI of the SDH (Figure 4).

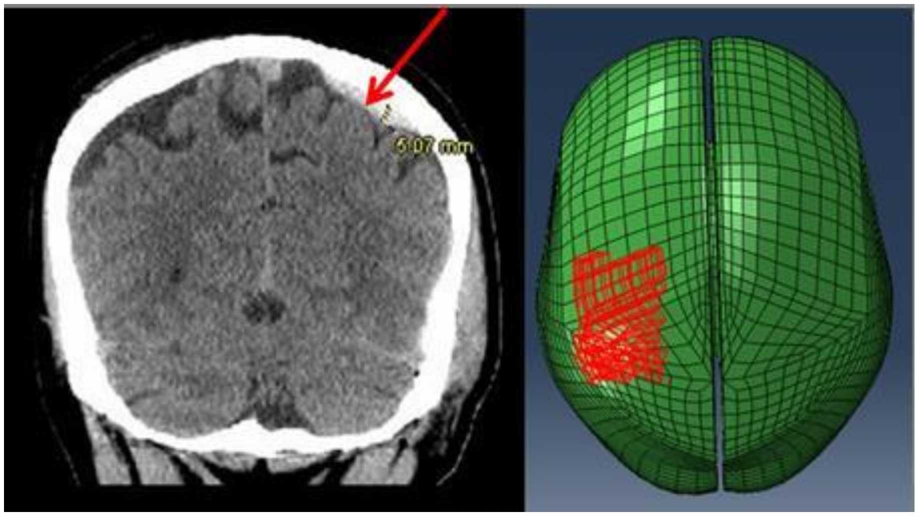

Figure 4. UCDBTM region of interest (right) representing the volume of the SDH

Data Analysis

The resulting curves from the simulations were compiled and analyzed separately in x, y and z-axes of linear and rotational acceleration. The peak values in all three component axes were then associated with the region of the brain in which the SDH occurred, specifically the: frontal, parietal, or occipital lobes (Figure 5). For the UCDBTM finite element modeling, the brain deformations were measured using the following metrics: maximum principal strain (MPS), von Mises stress (VMS), pressure, shear strain, shear stress, strain rate, and product of strain and strain rate. In addition, the average MPS and VMS was computed for the SDH region of interest as well as the entire cerebellum. While it is acknowledged that these measures do not measure the damaged bridging veins which are generally associated with SDH, these metrics define the nature of the deformation in the regions in which the vasculature may be present. As a result the metrics used here indicate a global, or macro level, response of the brain in those regions, and for further analysis a local, or micro, model of the vasculature of the SDH ROI may be warranted[18]. In addition, as it was important to discern if the SDH ROI deformations were significantly different from the cerebellum, a t-test was conducted to establish if there were any significant differences between the responses. An ANOVA was conducted across different lobes of the brain for each response variable. This was conducted to examine if there were differences in responses between the presences of SDH for between each lobe of the brain.

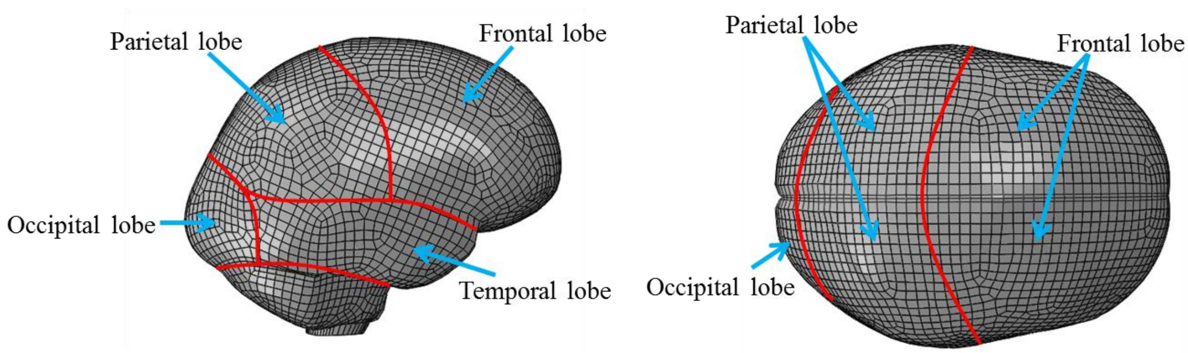

Figure 5. The segmentation of the different lobes of the brain as shown on the UCDBTM

Results:

The results are presented for resultant and component accelerations in tables 4 and 5 and brain deformation parameters in tables 6 through 8. The impact locations from the injury reconstructions for each of the subdural hematoma cases are shown in figures 6 through 8. Overall there were 8 SDH present in the frontal lobe, and 4 in each of the occipital and parietal lobes. For the finite element modeling, the magnitudes of deformation in the ROI was found to be significantly different from the values in the rest of the cerebrum for each case when compared using the t-test (p<0.05).

Table 4. Linear acceleration resultant and components for each SDH region. Standard deviations in brackets.

Lobe	# Cases	Resultant Linear (g)	Linear component (g) x	y	z
Frontal	8	372.4 (155.9)	245.1 (158.1)	195.3 (165.6)	106.7 (60.9)
Parietal	4	462.4 (166.3)	306.1 (222.8)	245.7 (184.3)	106.5 (57.7)
Occipital	4	311.8 (65.6)	282.6 (84.8)	64.3 (72.2)	82.5 (31.8)

Table 5. Rotational acceleration resultant and components for each SDH region. Standard deviations in brackets.

Lobe	# Cases	Resultant Rotational (krad/s^2)	Rotational component (krad/s^2) x	y	z
Frontal	8	30.7 (13.1)	19.2 (15.9)	18.0 (11.6)	11.5 (7.82)
Parietal	4	53.9 (11.3)	32.6 (21.1)	30.2 (21.7)	28.6 (14.1)
Occipital	4	22.4 (6.35)	6.80 (6.60)	19.5 (7.63)	4.72 (4.50)

Table 6. Pressure, von Mises stress, and shear stress response for the region of interest representing SDH in the lobes of the UCDBTM. Standard deviations in brackets.

	Pressure (kPa)	VMS (kPa)	Shear stress (kPa)
Frontal	672.3 (294.2)	10.7 (2.6)	5.4 (2.3)
Parietal	776.2 (292.7)	12.9 (2.4)	5.2 (0.7)
Occipital	996.4 (414.8)	9.0 (3.9)	3.8 (1.7)

Table 7. Maximum principal strain, shear strain, strain rate and product of strain and strain rate response for the region of interest representing SDH in the lobes of the UCDBTM. Standard deviations in brackets.

	MPS	Shear strain	Strain rate (s^{-1})	Product of strain and strain rate (s^{-1})
Frontal	0.327 (0.07)	0.491 (0.125)	75.7 (35.4)	26.5 (16.3)
Parietal	0.388 (0.08)	0.539 (0.07)	85.9 (45.8)	36.3 (24.3)
Occipital	0.264 (0.08)	0.361 (0.125)	52.9 (22.6)	15.3 (11.4)

Table 8. Average maximum principal strain and von Mises stress for the region of interest representing SDH in the lobes of the UCDBTM. Standard deviations in brackets.

	Average	
	MPS	VMS (kPa)
Frontal	0.135 (0.05)	4.7 (1.6)
Parietal	0.134 (0.03)	4.4 (1.1)
Occipital	0.115 (0.02)	3.9 (1.0)

Figure 6. Frontal lobe SDH impact locations on the Hybrid III

Figure 7. Parietal lobe SDH impact locations on the Hybrid III

Figure 8. Occipital lobe SDH impact locations on the Hybrid III

Subdural hematoma dynamic response by lobular region

When comparing the results between where the subdural hematomas occurred it was found that for linear acceleration there was significance between the occipital lobe SDH and the parietal lobe SDH for the y component only ($p < 0.05$). For all other linear acceleration resultant values and components there was no difference between the SDH's in each lobe ($p > 0.05$) (table 4). For rotational acceleration the resultant and z axis values were significant between the parietal lobe and all other lobes ($p < 0.05$), however all other lobes were not statistically different ($p > 0.05$). There was also significance found between the parietal lobe and the occipital lobe SDH's for the x-axis rotational acceleration component ($p < 0.05$) (table 5).

Acceleration component influence on subdural hematoma regions

Frontal lobe

For the frontal lobe subdural hematoma's the x-axis linear acceleration was significantly different from the z component ($p < 0.05$), while y-axis was not significant from the z or x-axis components ($p > 0.05$). For the rotational acceleration components, there was no significant difference between the accelerations in the x, y, or z-axis ($p > 0.05$).

Parietal lobe

For the parietal lobe subdural hematoma the x-axis linear acceleration component was significantly larger in magnitude than the z-axis component ($p < 0.05$). All other component comparisons were not significantly different ($p > 0.05$). For the rotational acceleration components, none of the axes produced a significantly different response ($p > 0.05$).

Occipital lobe

For the occipital lobe subdural hematoma the x-axis linear acceleration component was significantly larger in magnitude than the y or z-axes ($p < 0.05$). All other component comparisons were not significantly different ($p > 0.05$). For the rotational acceleration components, the y-axis component was of significantly larger magnitude than the y or x-axes components.

Subdural hematoma brain deformation by lobular region

The results of the focal subdural hematoma reconstructions are presented in tables 6, 7, and 8. In total, there were 8 frontal lobe SDH's, 4 parietal lobe SDH's, and 4 occipital lobe SDH's. There was no temporal lobe SDH's in the reconstructed cases. Shear stress, strain rate, average MPS, and average VMS showed no significant difference between the SDH in the different lobes of the brain ($p>0.05$). The pressure response was significantly lower in the frontal lobe when compared to the occipital and parietal ($p<0.05$). The von Mises stress response was lower in the occipital and frontal lobes when compared to the parietal ($p<0.05$). Maximum principal strain was larger in the parietal lobe than the other two lobes ($p<0.05$). Shear strain had lower values for the occipital lobe ($p<0.05$) with the other two lobes not significantly different from each other ($p>0.05$). The product of strain and strain rate had lower values for the occipital lobe when compared with the parietal lobe responses, but were not different from the frontal lobe responses. Overall, the lowest magnitude response was in the occipital lobe for 6 of the 8 peak brain deformation metrics. In addition, the largest magnitudes occurred in the parietal lobe SDH's for 5 of the 8 peak brain deformation metrics.

Discussion:

Subdural hematoma dynamic response by lobular region

When examining the results by lobe region, the resultant linear acceleration was not found to show any difference between the subdural hematomas in different regions of the brain. There was also no significance between the components of linear acceleration for the SDH's in the regions of the brain, except in the occipital lobe SDH and the parietal lobe SDH for the y component. This may indicate that these measures may be less sensitive to the types of motions which produced the injury to these distinct regions. The variance in response is likely influenced by human variability as well as the differing impact sites which caused the injury that is reflected in the large standard deviations. However, while not significant, when looking at pure magnitude of responses in peak resultant linear acceleration causing SDH in the distinct regions, the following hierarchy occurs: occipital (311.8 g), frontal (372.4 g), and parietal (462.4 g).

When examining the subdural hematoma regions by peak resultant rotational acceleration, the parietal lobe incurred larger rotations than the other lobes. The x-axis rotations show a difference between the parietal and occipital lobes. Also, the z-axis rotations were larger for the parietal lobe. All other components showed no significant differences. The statistical significance upon examination of these distinct regions suggests that rotational acceleration may be more sensitive to differentiating between the lobe likely to be injured. This is consistent with literature indicating that subdural hematoma is a rotationally influenced injury[8]. When examining the magnitudes of peak resultant rotational acceleration for each injury region, the order from lowest magnitude to largest is the same as linear acceleration: occipital (22,4 krad/s^2), frontal (30,7 krad/s^2), and parietal (53,9 krad/s^2). Since both peak resultant linear and rotational acceleration measures suggest this trend, it is possible that the occipital regions incur the lowest response to injury, while the frontal and parietal regions require larger responses to produce a subdural hematoma.

Acceleration component influence on subdural hematoma regions

When examining the lobes separately to discover how the components of x, y, and z-axes might influence the occurrence of subdural hematoma, certain interesting relationships result. When using linear acceleration components as the injury metric, the x axis linear acceleration indicated a trend where they are larger in magnitude than the other axes except for the y axis in the parietal lobe. This suggests that translational motions in the x-axis may be a significant contributor to SDH in general, and perhaps the y-axis rotations for the parietal region.

The components of rotational acceleration do not show similar significance when looking at the influence of the x, y, and z-axes. For the frontal, and parietal lobe SDH's there is no significance between the components in terms of rotational acceleration, however the magnitudes for these regions in all axes were high. The y-axis component of rotational acceleration was also significantly larger than the x and z-axes for the occipital lobe SDH's. The sample size for occipital lobe SDH's was small (4 cases) and may be by chance that all impacts were through the back of the head, but may also be enough to indicate a trend.

When examining the results in comparison with the literature, the results presented fit within the ranges found from previous research on subdural hematoma. While higher in magnitude than this research, Huang et al[15] found values of 97.4 krad/s^2 and 71.2 krad/s^2 for SDH in the parasagittal and midsagittal plane respectively using finite element modeling reconstructions. Auer et al[2] reconstructed fatal pedestrian collisions and found linear acceleration thresholds for SDH to be in a range between 100 to 600 g. Kleiven[16] reconstructed an SDH injury using a finite element model and found that a peak resultant rotational acceleration threshold to be around 34 krads/s^2. Using MADYMO to reconstruct SDH injuries reported magnitudes of peak resultant linear acceleration range between 236.5 to 366.5 g and 7.4 to 49.2 krad/s^2 for rotational acceleration[4,5,6]. The average values for Doorly's[4] reconstructions were 296 g and 20 krad/s^2. For the present research, the average results for the subdural hematomas were 362.4 g and 32 krad/s^2. The higher results of this research in comparison to Doorly's[4] may be a result of using a stiff Hybrid III headform as opposed to a deformable head like that used in Doorly's MADYMO simulations.

Subdural hematoma brain deformation by lobular region

Maximum principal strain, VMS, shear strain and product of strain and strain rate for focal subdural hematoma was consistent with values reported in the literature. The maximum principal strain values for SDH for injury reconstructions in the literature were in the region of 0.14 to 0.53 which was similar to those reported in this study[4,5]. Also, the magnitudes found in this study are in agreement with the strain measures to induce a TBI reported in anatomical studies[3,19,22,28]. The von Mises stress values are also within the range reported by computational SDH reconstructions[4,5] (5 – 17 kPa) as well as the thresholds described by Willinger and Baumgartner[32] and Schrieber et al[28] (6.1 – 10.8 kPa). Shear strain is a parameter not commonly used in brain injury reconstruction research for SDH, however, a point for comparison exists in Doorly and Gilchrist[5] and Doorly[4] (0.17 – 0.50), which is similar to the magnitudes found in this study (0.36 – 0.539). Finally, the product of strain and strain rate response in this study (15.3 – 36.3 s^{-1}) is consistent with the literature on SDH reconstructions (14 – 24 s^{-1})[4,5]. Only the pressure responses found in this study were inconsistent with the literature with values much larger than those presented in previous research[4,5,31]. This difference may be a result of the large variation in pressure response that was generated for each of the impacts. Overall, the subdural hematoma reconstructions conducted in this research were consistent with the literature, which suggests there is agreement with the general magnitudes of response resulting in a SDH. However, the previous literature did not examine the magnitudes in relation to focal SDH location.

Conclusions:

In summary, peak resultant linear acceleration was not found to show any difference between any of the subdural hematoma regions. There was also no significance between the components of linear acceleration, except for the y component for the parietal lobe SDH. For rotational acceleration more differences were found, with peak resultant values higher for the parietal lobe than for the other lobes, and x and z-axis components also showing some discrimination between the presence of SDH by region. These results indicate that peak linear acceleration may not be as sensitive as rotational acceleration when examining the lobe in which SDH was present. Also, overall the peak rotational accelerations (resultant and component) were very high. This is a result consistent with previous literature in which rotational acceleration was identified as being a key component in the creation of an SDH[8]. When examining the results by magnitude, a trend occurs for both peak linear and rotational acceleration (from low to high): occipital, frontal, and parietal. This indicates that there are aspects of the dynamic response which may be producing the lesions in these particular lobes. When conducting this analysis using a finite element model of the human brain, it was found that the brain deformation metrics shear stress, strain rate, average MPS, and average VMS had no significant difference between the lobes. This suggests that these measures may be insensitive to predicting where in the brain the SDH is likely to occur. For the other metrics, MPS, VMS, pressure, shear strain, and product of strain and strain rate all had significant differences between SDH lobe locations. Of those metrics, MPS, VMS, shear strain and product of strain and strain rate had the highest magnitude response for the SDH in the parietal lobe and the lowest magnitude for the occipital lobe, with the frontal lobe responses somewhere in between. Only the pressure responses differed from this trend with occipital lobe responses being the highest and frontal being the lowest. These results show that there is sensitivity in the brain tissue to deformation based on magnitude of response, where the largest magnitudes would incur a SDH in the parietal lobe, followed by the frontal lobe and then the occipital lobe.

Limitations

Limitations of this study revolve around the accuracy of the reconstruction and the modeling process from the previous work simulating brain injuries. The reconstructions conducted within the laboratory used non biofidelic physical models that produce acceleration loading curves which may not be similar to the response of a non-rigid system such as the head. The input parameters (velocity, mass, location) are all approximate and may not accurately represent the event. While using multiple conditions for each injury simulation may cover the response of the actual event; it is unlikely a precise representation of what occurred to cause the injury will be simulated. The influence of the musculature on the impact will also be difficult to ascertain and is thus a limitation to this study. While simple to reconstruct injury scenarios were chosen for this study, it is unlikely that each simulation was exact to the individual who was injured.

Disclosure:

Funding was received by Dr. Hoshizaki for this work from the Canadian Institutes of Health Research

Conflict of interest statement:

There are no conflicts of interest with respect to this research

References

1. Adamec J, Jelen K, Kubovy P, Lopot F, Schuller E: Forensic biomechanical analysis of falls from height using numerical human body models. **J Forensic Sci 55(6)**:1615-1623, 2010

2. Auer C, Schonpflug M, Beier G, Eisenmenger W: An analysis of brain injuries in real work pedestrian traffic accidents by computer simulation reconstruction. Proceedings of the **International Society of Biomechanics** XVIIIth Congress: July 8-13; Zurich, Switzerland, 2001

3. Bain AC, Meaney DF: Tissue-level thresholds for axonal damage in an experimental model of central nervous system white matter injury. **J Biomech Eng 16**:615-622, 2000

4. Doorly MC: Investigations into head injury criteria using numerical reconstruction of real life accident cases [PhD thesis]. Dublin, Ireland, University College Dublin; 2007.

5. Doorly MC, Gilchrist MD: The use of accident reconstruction for the analysis of traumatic brain injury due to head impacts arising from falls. **Comput Meth Biomech Biomed Eng 9(6)**:371-377, 2006

6. Doorly MC, Gilchrist MD: Three-dimensional multibody dynamics analysis of accidental falls resulting in traumatic brain injury. **IJCrash 14(5)**:503-509, 2009

7. Forero Rueda MA, Gilchrist MD: Comparative multibody dynamics analysis of falls from playground climbing frames. **Forensic Sci Int 191**:52-57, 2009

8. Gennarelli TA, Abel JM, Adams H, Graham D: Differential tolerance of frontal and temporal lobes to contusion induced by rotational acceleration. Proceedings of the 23rd **Stapp Car Crash Conference**, SAE paper No.791022, 1979

9. Gennarelli TA, Thibault LE: Biomechanics of acute subdural hematoma. **J Trauma 22(8)**:680-686, 1982

10. Gennarelli TA, Thibault LE, Tomel G, Wiser R, Graham D, Adams J: Directional dependence of axonal brain injury due to centroidal and non centroidal acceleration. Proceedings of the **Stapp Car Crash Conference**, 49-53, New Orleans, LA, 1987

11. Hardy WN, Foster CD, Mason MJ, Yang KH, King AI, Tashman S. Investigation of head injury mechanisms using neutral density technology and high-speed biplanar x-ray. **Stapp Car Crash J 45**:337-368, 2001

12. Hodgson VR, Thomas LM, Khalil TB: The role of impact location in reversible cerebral concussion. Proceedings of the 27th **Stapp Car Crash Conference**, SAE paper No. 831618, 1983

13. Horgan TJ, Gilchrist MD: The creation of three-dimensional finite element models for simulating head impact biomechanics. **IJCrash 8(4)**:353-366, 2003

14. Horgan TJ, Gilchrist MD: Influence of FE model variability in predicting brain motion and intracranial pressure changes in head impact simulations. **IJCrash 9(4)**:365-379, 2004

15. Huang HM, Lee MC, Chiu TW, Chen CT, Lee SY: Three-dimensional finite element analysis of subdural hematoma. **J Trauma: Inj Infect Crit Care 47(3)**:253-259, 1999

16. Kleiven S: Influence of impact direction to the human head in prediction of subdural hematoma. **J Neurotrauma 20(4)**:365-379, 2003

17. Kleiven S, Von Holst H: Consequences of size following trauma to the human head. **J Biomech 35**:135-160, 2002

18. Kraft RH, Mckee, PJ, Dagro AM, Grafton ST: Combining the finite element method with structural connectome-based analysis for modeling neurotrauma: Connectome neurotrauma mechanics. **PLoS Comput Bio 8(8)**:1-15, 2012

19. Lee MC, Haut RC: Insensitivity of tensile failure properties of human bridging veins to strain rate: implications in biomechanics of subdural hematoma. **J Biomech 22(6-7)**:537-542, 1989

20. Lovenhielm P: Dynamic properties of the parasagittal bridging veins. **Z. Rechtsmed 74**:55-62, 1974

21. Miller R, Margulies S, Leoni M, Nonaka M, Chen Z, Smith D, et al: Finite element modeling approaches for predicting injury in an experimental model of severe diffuse axonal injury. Proceedings of the 42nd **Stapp Car Crash Conference**, SAE paper No. 983154, 1998

22. Monson KL, Goldsmith W, Barbaro NM, Manle GT: Axial mechanical properties of fresh human cerebral blood vessels. **J Biomed Eng 125(2)**:288-294, 2003

23. Nahum AM, Smith R, Ward CC: Intracranial pressure dynamics during head impact. Proceedings 21st **Stapp Car Crash Conference**, SAE paper No. 770922, 1977

24. O'Riordain K, Thomas PM, Phillips JP, Gilchrist MD: Reconstruction of real world head injury accidents resulting from falls using multibody dynamics. **Clin Biomech 18**:590-600, 2003

25. Padgaonkar AJ, Kreiger KW, King AI: Measurement of rotational acceleration of a rigid body using linear accelerometers. **J Appl Mech 42**:552-556, 1975

26. Post A, Hoshizaki TB, Gilchrist MD, Brien S: Analysis of the influence of independent variables used for reconstruction of a traumatic brain injury event. **J Sport Eng Tech 226(3/4)**:290-298, 2012

27. Prange MT, Meaney DF, Margulies SS: Defining brain mechanical properties: Effects of region, direction and species. Proceedings 44th **Stapp Car Crash Conference**, 2002.

28. Schreiber DI, Bain AC, Meaney DF: In vivo thresholds for mechanical injury to the blood-brain barrier. Proceedings of the **Stapp Car Crash Conference**, 277-291, SAE paper 973335, 1997

29. Shuck LZ, Advani SH: Rheological response of human brain tissue in shear. **J Basic Eng 94(4)**:905-912, 1972

30. Ueno K, Melvin JW: Finite element model study of head impact based on Hybrid III head acceleration: The effects of rotational and translational accelerations. **J Biomech Eng 117(3)**:319-328, 1995

31. Ward C, Chan M, Nahum AM: Intracranial pressure – a brain injury criterion. Proceedings of the 24th **Stapp Car Crash Conference**, SAE paper 751163, 1980

32. Willinger R, Baumgartner D, Human head tolerance limits to specific injury mechanisms. **IJCrash 8(6)**:605-617, 2003

33. Zhang L, Yang K, Dwarampudi R, Omori K, Li T, Chang K, et al, Recent advances in brain injury research: A new human head model development and validation. **Stapp Car Crash J 45**:369-393, 2001

34. Zhou C, Khalil TB, King AI. A new model for comparing responses of the homogeneous and inhomogeneous human brain. Proceedings of the 39th **Stapp Car Crash Conference**, 121-136, 1995

PART III – Global discussion and conclusions

The research for this thesis was separated into three studies as presented. The first study conducted reconstructions of traumatic brain injury events and examined thresholds for injury using the University College Dublin Brain Trauma Model. The second study used the results of the first study to examine the effect of the linear and rotational acceleration loading curves on the creation of the TBI lesions. Finally, the third study examined the subdural hematoma lesions more closely; examining how the components of linear and rotational acceleration influenced where in the cranium the SDH was present.

The first study employed medical imaging to examine the discrete regions of brain tissue damaged from the impacts. The resulting brain deformation metrics from the FE model identified ranges in which these injuries would likely occur. While there was considerable variance in the response, which would be expected due to human variation, the results were consistent with previously published research (Doorly 2007; Kleiven 2007). Notably, assuming there to be a continuum of injury within TBI, the results suggested that the lesion hierarchy from lowest response to highest was: subdural hematoma, contusion, subarachnoid hematoma, and finally epidural hematoma. To date there has not been a dataset that has been able to shed any light on the continuum of TBI, most likely as a result of low numbers of subjects available and limited reconstruction techniques. Through the use of MADYMO, physical reconstruction, and finite element modeling this study has shown that the careful synthesis of using multiple techniques may produce more accurate reconstructions for future research. In addition to the research involving TBI lesions, this study also established the University College Dublin Brain Trauma Model as a suitable tool for accident reconstruction and brain injury investigations. In conclusion, the first study established a methodology for accurately reconstructing TBI from falls that was used to establish new thresholds for injury based on lesion type. The results suggested that there may be a continuum of injury severity that needs to be investigated with more subjects to achieve statistical significance due to human variation.

The second study was a continuation of the first study. The first study conducted reconstructions that employed MADYMO, physical, and finite element models to demonstrate the accuracy of the methodology when compared with other published research. The second study examined the characteristics of the loading curves in linear and rotational acceleration that were generated from using the Hybrid III and was used as input for the FE model to calculate the brain deformations. Using a principal component analysis the results showed that duration and time to peak variables were important in predicting TBI. These results are consistent with the use of these variables for helmet standards which resulted in a reduction of TBI in sport (Hoshizaki and Brien 2004). Of interest was that peak resultant variables accounted for very little of the variance in the creation of TBI. The result that x and y components of linear and rotational acceleration account for much of the variance after time-based results show that component curve characteristics are important when researching brain injury. This reinforces research conducted by the current authors and others indicating that the use of finite element modeling is the next step to examining brain injury as FE allows for the interpretation of the components of the loading curve and their interaction with brain tissue (King et al. 2003; Post and Hoshizaki 2012). In conclusion study 2 established that there are aspects of the acceleration loading curves which account for the variation in TBI results (namely SDH, EDH, SAH, and contusion). In particular, there were differences in the characteristics of the curves which accounted for the most variance between the different lesion types.

The third study examined how resultant and component peak variables contribute where a subdural hematoma may occur in the cranium. This study also served to further validate the reconstruction of SDH by comparing the linear and rotational results to previous research (Huang et al., 1999; Auer et al., 2001; Kleiven, 2003; Doorly, 2007). In terms of validation, the results of the reconstructions were well within the expected values for incurring a SDH from the literature, though there was not a great deal of information on this lesion. In addition there was no literature that compared the components of x, y, and z-axes in linear and rotational acceleration for SDH cases resulting from an impact. Overall, when examining the magnitude of the results there was a trend indicating a separation between where in the brain the SDH occurred for both peak resultant linear and rotational acceleration as well as brain deformation. The trend revealed that temporal SDH's occurred at lower magnitudes, followed by occipital, frontal, and finally parietal regions. When examining the components, the x and y-axis linear acceleration may have an influence on the parietal region SDH's, however the variation in impact sites made it difficult to achieve any further significance from the results. For rotational acceleration, the frontal and parietal SDH's resulted from large magnitude rotational accelerations in all axes, while the occipital lobe incurred large rotational accelerations in the y-axis. These results demonstrated the importance of both linear and rotational acceleration in the creation of injury (Gennarelli et al., 1972). In conclusion study 3 examined the kinematics and brain stress and strain linked to SDH events and found that there is an order of magnitude effect on the presence of this type of brain injury in different lobes of the brain.

Conclusion

All three studies completed for this thesis dealt with aspects of traumatic brain injury prediction. The first study reconstructed TBI events and achieved validation of the methodology through comparisons to literature for dynamic response and brain deformations using finite element modeling. The second study examined how the acceleration loading curves' characteristics influenced the outcome TBI lesion. The third study refined the analysis to a single TBI lesion, namely subdural hematoma. This was conducted in an attempt to further understand the nature of the injury and how acceleration loading curves influenced the region in which the SDH occurred. As a result of this avenue of research, this thesis has provided further information on how to accomplish an accurate reconstruction of traumatic brain injury. It has also supplied information relating to threshold parameters in dynamic response and brain deformation metrics for TBI. Dynamic response curve characteristics were analyzed for all lesions and important links were found between duration of the pulse and time to peak variables for incurring a TBI. This analysis also found that component parameters were more important than resultant variables and that the different characteristics accounted for differing variances in each TBI lesion. Finally, when examining where in the brain subdural hematoma occurs, it was found that there was a trend indicating a continuum based on magnitude. Overall, this research has provided information regarding methodologies and mechanisms of traumatic brain injury. In the future this data could be used to aid in the design of improved sporting equipment, vehicle design, and safer environments. More specifically, this research has provided a new baseline of brain injury metrics from which improvements in helmet technology, car, and play structure safety can be compared. The principal components analysis has identified which kinematic variables account for the largest variance in the results that can be used to help develop new injury metrics that may have better predictive capacity for traumatic brain injuries. The curve characteristics identified by the PCA could also be further investigated to identify how to control these dependent variables and lower the corresponding risk of injury. The research into subdural hematoma has shown that the components of the linear and rotational acceleration loading curves have an effect on the result. This data and procedure can be used to inform future protective devices and standards to consider including the x, y, and z-axis components as opposed to just the resultant peak magnitudes as these may not be fully reflective of the mechanism of injury.

PART IV – Statement of contribution

List of collaborators:

Andrew Post (PhD student) was involved in all aspects of this thesis, from conception to data collection and analysis. All writing was done by the student.

T. Blaine Hoshizaki was involved as the thesis supervisor and was involved in a supervisory role in all aspects of the thesis.

Michael D. Gilchrist provided finite element modeling support and was a committee member for the thesis. He also provided a section of the data from his student's TBI reconstructions (Doorly, 2007).

Susan Brien was involved in the acquisition of subjects for the thesis from the Hull Hospital in Hull Canada. She also provided analysis of the medical imaging results.

Shawn Marshall was involved in the acquisition of subjects for the thesis from the General Hospital in Ottawa Canada.

D. G. E. Robertson was involved as a committee member for this thesis.

References:

Adams, J.H., Graham, D.I., and Gennarelli, T.A. (1981). Acceleration induced head injury in the monkey. II. Neuropathology. Acta Neuropathol 7, 26-28.

Adams, J.H., Graham, D.I., and Gennarelli, T.A. (1983). Head injury in man and experimental animals: Neuropathology. Acta Neurochirurgica, Suppl. 32, 15-30.

Adams, J.H., Graham, D.I., Scott, D., Parker, L.S., and Doyle, D. (1980). Brain damage in fatal non-missle head injury. Journal of Clinical Pathology, 33, 1132-1145.

Al-Bsharat, A.S., Hardy, W.N., Yang, K.H., Khalil, T.B., Tashman, S., and King, A.I. (1999). Brain/skull relative displacement magnitude due to blunt head impact: New experimental data and model. Proceedings of the 43rd Stapp Car Crash Conference, San Diego, California, USA, SAE 99SC22.

Antranik.org. (2011). Protection for the Brain: Meninges, CSF, Blood-Brain Barrier. Retrieved with permission from http://antranik.org/protection-for-the-brain-meninges-csf-blood-brain-barrier/ , July 16, 2013.

Arbogast, K.B. and Margulies, S.S. (1998). Material characterization of the brainstem from oscillatory shear tests. Journal of biomechanics, 31(9), 801-807.

Auer, C., Schonpflug, M., Beier, G., and Eisenmenger, W. (2001). An analysis of brain injuries in real work pedestrian traffic accidents by computer simulation reconstruction. Proceedings of the International Society of Biomechanics XVIIIth Congress, Zurich, Switzerland, July 8-13.

Bain, A.C., and Meaney, D.F. (2000). Tissue-level thresholds for axonal damage in an experimental model of central nervous system white matter injury. Journal of Biomechanical Engineering 16, 615-622.

Bandak, F. (1994). On the mechanics of impact neurotrauma: A review and critical synthesis. Journal of Neurotrauma, 12(4), 635-649.

Bandak, F.A., and Eppinger, R.H. (1994). A three-dimensional FE analysis of the human brain under combined rotational and translational accelerations. Proceedings 38th Stapp Car Crash Conference, 145-163.

Basser, P.J. and Jones, D.K. (2002). Diffusion-tensor MRI: theory, experimental design and data analysis – a technical review. NMR in Biomedicine, 15, 456-467.

Bigler, E.D. (2001). Quantitative magnetic resonance imaging in traumatic brain injury. Journal of Head Trauma and Rehabilitation, 16(2), 117-134.

Bradshaw, D.R., Ivarsson, J., Morfey, C.L., Viano, D.C., (2001). Simulation of acute subdural hematoma and diffuse axonal injury in coronal head impact. Journal of Biomechanics, 34 (1), 85-94.

Bradshaw, D.R.S. and Morfey, C.L. (2001). Pressure and shear responses in brain injury models. Proceedings of the 17th Int. Technical Conference on the Enhanced Safety of Vehicles, Amsterdam, The Netherlands.

Breen, N., Woods, J., Bury, G., Murphy, A.W., and Brazier, H. (2000). A national census of ambulance response times to emergency calls in Ireland. J. Accid. Emerg. Med., 17, 392-395.

Brolinson, P.G., Manoogian, S., McNeely, D., Goforth, M., Greenwald, R., and Duma, S. (2006). Analysis of linear head accelerations from collegiate football impacts. In: Proceedings of the IRCOBI Conference; Isle of Man, 353-355.

Brooks, C., Gabella, B., Hoffman, R., Sosin, D., and Whiteneck, G. (1997). Traumatic brain injury: designing and implementing a population-based followup system. Arch Phys Med Rehabil, 78(8), 26-30.

Canadian Institute for Health Information (2006). Head injuries in Canada: A decade of change (1994-1995 to 2003-2004), August 2006.

Cassidy, J.D., Carroll, L.J., Peloso, P.M. (2004). Incidence, risk factors and prevention of mild traumatic brain injury: results of the WHO Collaborating Centre Task Force on Mild Traumatic Brain Injury. Journal of Rehabilitative Medicine, 43, 28-60.

Cater, H.L., Sundstrom, L.E., Morrison, III. B. (2006). Temporal development of hippocampal cell death is dependent on tissue strain but not strain rate. Journal of biomechanics, 39, 2810-2818.

Centers for Disease Control and Prevention (1997) Traumatic Brain Injury—Colorado, Missouri, Oklahoma, and Utah, 1990-1993. MMWR Morbidity and Mortality Weekly Report, Jan. 10; 46(1): 8-11.

Chalupnik, J.D., Daly, C.H., and Merchant, H.C. (1971). Material properties of cerebral blood vessels. Final report on contract No. NIH-69-2232, report No. ME 71-11, Univ. of Washington, Seattle.

Chan, H.S. (1974). Mathematical model for closed head impact. Proceedings of the 18th Stapp Car Crash Conference, Ann Arbor, Michigan, USA, SAE 741191.

Claessens, M., Sauren, F., and Wismans, J. (1997). Modeling of the human head under impact conditions: A parametric study. In: Proceedings 41st Stapp Car Crash Conference, SAE paper no. 973338, 315-328.

Colgan, N.C., Cronin, M.M., Gobbo, O.L., O'Mara, S.M., O'Connor, W.T., and Gilchrist, M.D. (2010a). Qantitative MRI analysis of brain volume changes due to controlled cortical impacts. Journal of Neurotrauma, 27, 1265-1274.

Colgan, N.C., Gilchrist, M.D., and Curran, K.M. (2010b). Applying DTI white matter orientations to finite element head models to examine diffuse TBI under high rotational accelerations. Progress in Biophy.

Committee on Medical Aspects of Automotive Safety. (1971). Rating the severity of tissue damage – I. The abbreviated scale. JAMA 215, 277-280.

Courville, C.B. (1950). The mechanism of coup-contrecoup injuries of the brain: A critical review of recent experimental studies in the light of clinical observations. From: Bulleting of the Los Angeles Neurological Society, 15(2), 72-86.

Darvish, K.K., and Crandall, J.R. (2001). Nonlinear viscoelastic effects in oscillatory shear deformation of brain tissue. Medical Engineering and Physics, 23(9), 633-645.

Dawson, S.L., Hirsch, C.S., Lucas, F.V. and Sebek, B.A. (1980). The contracoup phenomenon: reappraisal of a classic problem. Human pathology, 11, 155-166.

Denny-Brown, D. and Russell, W.R. (1941). Experimental cerebral concussion. Brain, 64, 93-164.

Donnelly, B.R. and Medige, J. (1997). Shear properties of human brain tissue. Journal of Biomechanical Engineering, 119(4), 423-432.

Doorly, M.C. (2007). Investigations into head injury criteria using numerical reconstruction of real life accident cases. PhD thesis, University College Dublin.

Doorly, M.C. and Gilchrist, M.D. (2006). The use of accident reconstruction for the analysis of traumatic brain injury due to head impacts arising from falls. Computer Methods in Biomechanics and Biomedical Engineering, 9(6), 371-377.

Duma, S.M., Manoogian, S.J., Bussone, W.R., Brolinson, P.G., Goforth, M.W., Donnenwerth, J.J., Greenwald, R.M, Chu, J.J., and Crisco, J.J. (2005). Analysis of real-time head accelerations in collegiate football players. Clinical Journal of Sport Medicine, 15(1), 3-8.

DiMasi, F., Eppinger, R.H., and Bandak, F.A. (1995). Computational analysis of head impact response under car crash loadings. In: Proceedings 39th Stapp Car Crash Conference.

Edburg, S., Rieker, J., and Angrist, A. (1963). Study of impact pressure and acceleration in plastic skulll models. Lab. Invest., 12, 1305-1311.

Ewing, C.L. (1975). Injury criteria and human tolerance for the neck. Air-craft Crashworthiness, University Press of Virginia, Charlottesville, VA.

European Transport Safety Council (1999). Exposure data for travel risk assessment.

Fijalkowski, R.J., Yoganandan, N., Zhang, J., and Pintar, F.A. (2009). A finite element model of region-specific response for mild diffuse brain injury. Stapp Car Crash Journal, 53, 193-213.

Forero Rueda, M.A., Cui, L., and Gilchrist, M.D. (2011). Finite element modeling of equestrian helmet impacts exposes the need to address rotational kinematics in future helmet designs. Computer Methods in Biomechanics and Biomedical Engineering, 14(12), 1021-1031.

Franklyn, M., Fildes, B., Zhang, L., Yang, K., and Sparke, L. (2005). Analysis of finite element models for head injury investigation: Reconstruction of four real-world impacts. Stapp Car Crash Journal, 49, 1-32.

Fréchède, B. and McIntosh, A.S. (2009). Numerical reconstructions of real-life concussive football impacts. Medicine and Science in Sports and Exercise, 41(2), 390-398.

Gadd, C.W. (1966). Use of a weighted impulse criterion for estimating injury hazard. In Proceedings of the 10th STAPP Car Crash Conference, SAE paper No. 660793.

Gavett, B.E., Stern, R.A., and McKee, A.C. (2011) Chronic traumatic encephalopathy: A potential late effect of sport-related concussive and subconcussive head trauma. Clinical Sports Medicine, 30, 179-188.

Gennarelli, T. (1983). Head injury in man and experimental animals: Clinical aspects. Acta Neurochirurgica, 32, 1-13.

Gennarelli, T.A., Abel, J.M., Adams, H., and Graham, D. (1979). Differential tolerance of frontal and temporal lobes to contusion induced by rotational acceleration. In Proceedings of the 23rd Stapp Car Crash Conference, SAE paper No.791022.

Gennarelli, T.A., Adams, J.H., and Graham, D.I. (1981). Acceleration induced head injury in the monkey. I. The model, its mechanical and physiological correlates. Acta Neuropathol, 7, 23-25.

Gennarelli, T.A. and Thibault, L.E. (1982). Biomechanics of acute subdural hematoma. Journal of Trauma, 22(8), 680-686.

Gennarelli, T.A., Thibault, L.E., Adams, J.H., Graham, D.I, Thompson, C.J., and Marcincin, R.P. (1983). Diffuse axonal injury and traumatic coma in the primate. Ann Neurol, 12, 564-574.

Gennarelli, T.A., Thibault, L.E., and Ommaya, A. (1971). Comparison of translational and rotational accelerations in experimental cerebral concussion. In Proceedings of the 15th Stapp car Crash Conference.

Gennarelli, T.A., Thibault, L.E., and Ommaya, A. (1972). Pathophysiological responses to rotational and translational accelerations of the head. In Proceedings of the 16th Stapp Car Crash Conference, SAE paper No. 720970.

Gennarelli, T.A., Thibault, L.E., Tomel, G., Wiser, R., Graham, D., Adams, J. (1987). Directional dependence of axonal brain injury due to centroidal and non centroidal acceleration. In: Proceedings of the Stapp Car Crash Conference, New Orleans, LA, 49-53.

Gilchrist, M.D. and O'Donoghue, D. (2000). Simulation of the development of frontal head impact injury. Computational Mechanics, 26(3), 229-235.

Gilchrist, M.D., O'Donoghue, D., and Horgan, T. (2001). A two-dimensional analysis of the biomechanics of frontal and occipital head impact injuries. International Journal of Crashworthiness, 6(2), 253-262.

Goldsmith, W. (1981). Current controversies in the stipulation of head injury criteria. Letter to the editor. Journal of Biomechanics, 14, 883-884.

Gross, A.G. (1958). A new theory on the dynamics of brain concussion and brain injury. Journal of Neurosurgery, 29, 725-732.

Gurdjian, E.S. (1970). Movements of the brain and brain stem from impact induced linear and rotational acceleration. Transactions of the American Neurological Association, 95, 248-249.

Gurdjian, E.S. and Gurdjian, E.S. (1975). Re-evaluation of the biomechanics of blunt impact injury of the head. Surgery, Gynecology and Obstetrics, 140(6), 845-850.

Gurdjian, E.S. and Gurdjian, E.S. (1976). Cerebral contusions: Re-evaluation of the mechanism of their development. The Journal of Trauma, 16(1), 35-51.

Gurdjian, E.S. and Gurdjian, E.S. (1980). Acute head injury: A review. Surgery Annual, 12, 223-241.

Gurdjian, E.S., Hodgson, V.R., Thomas, L.M., and Patrick, L.M. (1968). Significance of relative movements of scalp, skull, and intracranial contents during impact injury to the head. Journal of Neurosurgery, 29(1), 70-72.

Gurdjian, E.S. and Lissner, H.R. (1944). Mechanisms of head injury as studied by the cathode ray occiloscope: Preliminary report. Journal of Neurology, Neurosurgery and Psychiatry, 1, 393-399.

Gurdjian, E.S. and Lissner, H.R.(1961). Photoelastic confirmation of the presence of shear strains at the craniospinal junction in closed head injury. Journal of Neurosurgery, 18(1), 58-60.

Gurdjian, E.S., Lissner, H.R., and Evans, F.G. (1961). Intracranial pressure and acceleration accompanying head impacts in human cadavers. Surgery, Gynecology & Obstetrics, 113(4), 185-190.

Gurdjian, E.S., Lissner, H.R., Latimer, F.R., Haddad, B.F., and Webster, J.E. (1953). Quantitative determination of acceleration and intracranial pressure in experimental head injury: Preliminary report. Neurology, 3, 417-423.

Gurdjian, E.S., Lissner, H.R., and Patrick, L.M. (1963). Concussion-mechanism and pathology. Proceeings of the 7th Stapp Car Crash Conference, Warrendale, Pennsylvania, 470-482.

Gurdjian, E.S., Lissner, H.R., Hodgson, V.R., and Patrick, L.M. (1966a). Mechanisms of head injury. Clinical Neurosurgery, 12, 112-128.

Gurdjian, E.S., Roberts, V.L., and Thomas, L.M. (1966b). Tolerance curves of acceleration and intracranial pressure and protective index in experimental head injury. Journal of Trauma, 6, 600-604.

Gurdjian, E.S. and Webster, J.E. (1947). The mechanism and management of injuries to the head. Journal of the American Medical Association, 134(13), 1072-1077.

Haddad, B.F., Lissner, H.R., Webster, J.E., and Gurdjian, E.S. (1955). Experimental concussion: Relation of acceleration to physiologic effect. Neurology, 5(11), 798-800.

Hardy, W.N., Khalil, T.B., and King, A.I. (1994). Literature review of head injury biomechanics. Int. J. Impact Engineering, 15(4), 561-568.

Hardy, W.N., Foster, C.D., Mason, M.J., Yang, K.H., King, A.I., and Tashman, S. (2001). Investigation of head injury mechanisms using neutral density technology and high-speed biplanar x-ray. Stapp Car Crash Journal, The Stapp Association, Ann Arbor, Michigan.

Ho, J., Kleiven, S. (2007). Dynamic response of the brain with vasculature: A three-dimensional computational study. Journal of Biomechanics.

Ho, J., Kleiven, S. (2009). Can sulci protect the brain from traumatic injury? Journal of Biomechanics, 42(13), 2074-2080.

Hodgson, V.R., Thomas, L.M., and Khalil, T.B. (1983). The role of impact location in reversible cerebral concussion. In Proceedings of the 27th Stapp Car Crash Conference, SAE paper No. 831618.

Holbourn, A.H.S. (1943). Mechanics of head injuries. The Lancet.

Horgan, T.J. (2005). A finite element model of the human head for use in the study of pedestrian accidents. PhD Thesis, University College Dublin, Dublin Ireland.

Horgan, T.J. and Gilchrist, M.D. (2003). The creation of three-dimensional finite element models for simulating head impact biomechanics. IJCrash, 8 (4), 353-366.

Horgan, T.J., and Gilchrist, M.D. (2004). Influence of FE model variability in predicting brain motion and intracranial pressure changes in head impact simulations. IJCrash, 9 (4), 401-418.

Hoshizaki, T.B. and Brien, S.E. (2004). The science and design of head protection in sport. Neurosurgery, 55, 956-967.

Hrapko, M., van Dommelen, J.A.W., Peters, G.W.M., and Wismans, J.S. (2006). The mechanical behaviour of brain tissue: large strain response and constitutive modeling. Biorheology, 43(5), 623-636.

Huang, H.M., Lee, M.C., Chiu, W.T., Chen, C.T., and Lee, S.Y. (1999). Three-dimensional finite element analysis of subdural hematoma. The Journal of Trauma: Injury, Infection and Critical Care, 47(3), 538-544.

Human Tolerance to Impact Conditions as Related to Motor Vehicle Design, SAE J885a. SAE Information Report, October 1966, SAE Handbook.

Kang, H.S., Willinger, R., Diaw, B.M., and Chinn, B. (1997). Modeling of the human head under impact conditions: A parametric study. Proceedings, 41st Stapp Car Crash Conference. SAE paper No. 973338.

Kendall, M., Post, A., Rousseau, P., Oeur, A., Gilchrist, M.D., and Hoshizaki, T.B. (2012). A comparison of dynamic impact response and brain deformation metrics of head impact reconstructions for three mechanisms of head injury in ice hockey. Proceedings of IRCOBI, Dublin, IRL, Sept 10-14.

Kenner, V.H. and Goldsmith, W. (1972). Dynamic loading of a fluid filled spherical shell. Int. J. Mech. Sci., 1, 557-569.

King, A.I., Ruan, J.S., Zhou, C., Hardy, W.N., and Khalil, T.B. (1995). Recent advances in biomechanics of brain injury research: A review. Journal of Neurotrauma, 12(4), 651-658.

King, A.I., Yang, K.H., Hardy, W.N., Al-Bsharat, A.S., Deng, B., Begeman, P.C., and Tashman, S. (1999). Challenging problems and opportunities in impact biomechanics. Proceedings Summer Bioengineering Conference, American Society of Mechanical Engineers, New York, 269-270.

King, A.I., Yang, K.H., Zhang, L., Hardy, W., and Viano, D.C. (2003). Is head injury caused by linear or rotational acceleration. IRCOBI conference, Lisbon, Portugal.

Kleiven, S., and Hardy, W.N. (2002). Correlation of an FE model of the human head with experiments on localized motion of the brain – Consequences for injury prediction. In: 46th Stapp Car Crash Journal, 123-144.

Kleiven, S. (2003). Influence of impact direction to the human head in prediction of subdural hematoma. Journal of Neurotrauma, 20(4), 365-379.

Kleiven, S. (2006). Evaluation of head injury criteria using a finite element model validated against experiments on localized brain motion, intracerebral acceleration, and intracranial pressure. International Journal of Crashworthiness 11 (1), 65-79.

Kleiven, S. (2007). Predictors for traumatic brain injuries evaluated through accident reconstruction. Stapp Car Crash Journal, 51, 81-114.

Kleiven, S., and Von Holst, H. (2002). Consequences of size following trauma to the human head. Journal of Biomechanics, 35, 135-160.

Kopecky, J.A. and Ripperger, E.A. (1969). Closed brain injuries: An engineering analysis. Journal of Biomechanics, 2, 29-34.

Lee, M.C. and Haut, R.C. (1989). Insensitivity of tensile failure properties of human bridging veins to strain rate: implications in biomechanics of subdural hematoma. Journal of Biomechanics 22 (6-7), 537-542.

Levin, H.S., Li, X., McCauley, S.R., Hanten, G., Wilde, E.A., and Swank, P. (2012). Neuropsychological outcome of mTBI: A principal components analysis approach. Journal of Neurotrauma, Epub ahead of print, doi: 10.1089/neu.2012.2627.

Li, J., Zhang, J., Yoganandan, H., Pintar, F., Gennarelli, T. (2007). Regional brain strains and role of falx in lateral impact-induced head rotational acceleration. Biomedical Sciences and Instrumentation, 43, 24-29.

Lindenburg, R. (1960). The mechanism of cerebral contusions. Arch. Pathol., 69, 440.

Lovenhielm, P. (1974a). Dynamic properties of the parasagittal bridging veins. Z. Rechtsmed, 74, 55-62.

Lovenhielm, P. (1974b). Strain tolerance of the Vv. Cerebri Sup. (bridging veins) calculated from head-on collision tests with cadavers. Z. Rechtsmedzin 75, 131-144.

Lubock, P. and Goldsmith, W. (1980). Experimental cavitation studies in a model head-neck system. Journal of Biomechanics, 13, 1041-1052.

Margulies, S.S., and Thibault, L.E. (1992). A proposed tolerance criterion for diffuse axonal injury in man. Journal of Biomechanics 25(8), 917-923.

Mao, H., Jin, X., Zhang. L., Yang, K.H., Igarashi, T., Noble-Haeusslein, L.J., and King, A.I. (2010). Finite element analysis of controlled cortical impact-induced cell loss. Journal of Neurotrauma, 27, 877-888.

Marieb, E.N. (1998). Human anatomy and physiology, 4th ed. Benjamin/Cummings Science Publishing, California.

McKee, A.C., Gavett, B.E., Stern, R.A., Nowinski, C.J., Cantu, R.C., Kowall, N.W., Perl, D.P., Hedley-White, T., Price, B., Sullivan, C., Morin, P., Lee, H., Kubilus, C.A., Daneshvar, D.H., Wulff, M., and Budson, A.E. (2010). TDPE-43 proteinopathy and motor neuron disease in chronic traumatic encephalopathy. Journal of Neuropathology and Experimental Neurology, 69(9), 918-929.

Meaney, D.F. and Smith, D.H. (2011). Biomechanics of concussion. Clinical Sports Medicine, 30(1), 19-31.

Meaney, D.F. and Thibault, L.E. (1990). Physical model studies of cortical brain deformation in response to high strain rate inertial loading. Proceedings IRCOBI Conference, Lyon, France, 11, 215-224.

Meaney, D., Thibault, L., and Gennarelli, T. (1994). Rotational brain injury tolerance criteria as a function of vehicle crash parameters. In Proceedings of the 1994 International IRCOBI Conf. on the Biomechanics of Impacts, 51-62.

Mendis, K., Stalnaker, R., and Advani, S. (1995). A constitutive relationship for large deformation finite element modeling of brain tissue. Journal of Biomechanical Engineering, 117(4), 279-285.

Miller, R., Margulies, S., Leoni, M., Nonaka, M., Chen, Z., Smith, D., and Meaney, D. (1998). Finite element modeling approaches for predicting injury in an experimental model of severe diffuse axonal injury. In Proceedings of the 42nd Stapp Car Crash Conference, SAE paper No. 983154.

Monson, K.L., Goldsmith, W., Barbaro, N.M. and Manle, G.T. (2003). Axial mechanical properties of fresh human cerebral blood vessels. Journal of Biomedical Engineering, 125(2), 288-294.

Morrison III,B., Cater, H.L., Wang, C.C.B., Thomas, F.C., Hung, C.T., Ateshian, G.A., and Sundstrom, L.E. (2003). A tissue level tolerance criterion for living brain developed in an in vitro model of traumatic mechanical loading. In 47th Stapp Car Crash Journal, SAE paper no. 2003-22-00066.

Nahum, A.M. and Smith, R. (1976). An experimental model for closed head impact injury. In Proceedings of the 20th STAPP Car Crash Conference, SAE paper No. 760825.

Nahum, A.M., Smith, R., and Ward, C.C. (1977). Intracranial pressure dynamics during head impact. Proceedings 21st Stapp Car Crash Conference. SAE paper No. 770922.

Nahum, A.M., Ward, C., Raasch, F., Adams, S., and Schneider, D. (1980). Experimental studies of side impacts to the human head. Proceedings of the 24th Stapp Car Crash Conference, Troy, Michigan, USA, SAE 801301.

Nahum, A.M., Ward, C., Schneider, D., Raasch, F., and Adams, S. (1981). A study of impacts to the lateral protected and unprotected head. Proceedings of the 25th Stapp Car Crash Conference, San Francisco, California, USA, SAE 811006.

National Institute of Health. (1999). NIH Consensus Development Panel on Rehabilitation of Persons with Traumatic Brain Injury. JAMA, 282, 974-983.

Newman, J.A. (1980). Head injury criteria in automotive crash testing. In Proceedings of the 20th STAPP Car Crash Conference, SAE paper No. 801317.

Newman, J. (1986). A generalized acceleration model for brain injury threshold (GAMBIT). In Proceedings International Conf. on the Biomechanics of Impact (IRCOBI), 121-131.

Newman, J., Beusenberg, M., Fournier, E., Shewchenko, N., Whitnall, C., King, A., Yang, K., Zhang, L., McElhaney, J., Thibault, L., and McGinnis, G. (1999). A new biomechanical assessment of minor traumatic brain injury. In International IRCOBI Conference on the Biomechanics of Impact, 17-36, Barcelona, Spain.

Newman, J., Barr, C., Beusenberg, M., Fournier, E., Shewchenko, N., Welbourne, E., and Withnall, C. (2000a). A new biomechanical assessment of mild traumatic brain injury: Part 2 – results and conclusions. In International IRCOBI Conference on the Biomechanics of Impact, 223-233, Montpellier, France.

Newman, J.A., Beusenberg, M.C., Shewchenko, N., Withnall, C., and Fournier, E. (2005). Verification of biomechanical methods employed in a comprehensive study of mild traumatic brain injury and the effectiveness of American football helmets. Journal of Biomechanics, 38, 1469-1481.

Newman, J., Shewchenko, N., and Welbourne, E. (2000b). A proposed new biomechanical head injury assessment function – the maximum power index. In 44th Stapp Car Crash Conf., SAE paper No. 2000-01-SC16.

Nicolle, S., Lounis, M., and Willinger, R. (2004). Shear properties of brain tissue over a frequency range relevant for automotive impact situations: New experimental results. Stapp Car Crash Journal, 48, 239-258.

Nuscholtz, G.S, Kaiker, P.S. and Gould, W.S. (1987). Two factors critical in the pressure response of the impacted head. Aviation, Space and Environmental Medicine, 58(12), 1157-1161.

Nuscholtz, G.S., Lux, P., Kaiker, P.S., and Janicki, M.A. (1984). Head impact response – skull deformation and rotational acceleration. Proceedings of the 28th Stapp Car Crash Conference. SAE paper No. 841657.

O'Donoghue, D. (1999). Biomechanics of frontal and occipital head impact injuries: A plane strain simulation of coup and contrecoup contusion. Master's thesis, University College Dublin, Belfield, Dublin 4, Ireland.

Oeur, A., Post, A., Hoshizaki, T.B., and Gilchrist, M. (2011). The Correlation Between Brain Deformation Metrics and Acceleration Using a Linear and Non-Linear Impact Protocol. XXIIIrd International Society of Biomechanics Congress, Brussels, Belgium.

Oka, K., Rhoton, A.L., Barry, M., and Rodriguez, R. (1985). Microsurgical anatomy of the superficial veins of the cerebrum. Neurosurgery, 17(5), 711-748.

Omalu, B.I., DeKosky, S.T., Minster, R.L., Kamboh, M.I., Hamilton, R.L., and Wecht, C.H. (2005). Chronic traumatic encephalopathy in a national football league player. Neurosurgery, 57, 128-134.

Ommaya, A.K. (1968). The mechanical properties of tissues of the nervous system. Journal of Biomechanics, 2, 1-12.

Ommaya, A.K. and Gennarelli, T.A (1974). Cerebral concussion and traumatic unconsciousness: Correlation of experimental and clinical observations on blunt head injuries. Brain, 97, 633-654.

Ommaya, A.K., Grubb, R.L., and Naumann, R.A. (1971). Coup and contrecoup injury: Observations on the mechanics of visible brain injuries in the rhesus monkey. Journal of Neurosurgery, 35, 503-516.

Ommaya, A.K. and Hirsch, A.E. (1971). Tolerance of cerebral concussion from head impact and whiplash in primates. Journal of Biomechanics, 4, 13-22.

Ommaya, A.K., Yarnell, P., Hirsch, A.E., and Harris, E.H. (1967). Scaling of experimental data on cerebral concussion in sub-human primates to concussion threshold for man. Proceedings of the 11th Stapp Car Crash Conference, Warrendale, Pennsylvania, SAE 970906.

Ono, K., Kikuchi, M., Nakamura, H., Kobayashi, H., and Nakamura, N. (1980). Human head tolerance to sagittal impact reliable estimation deduced from experimental head injury subhuman primates and human cadaver skull. In Proceedings of the 24th STAPP Car Crash Conference, SAE paper No. 801303.

O'Riordan, K., Thomas, P.M., Phillips, J.P., and Gilchrist, M.D. (2003). Reconstruction of real world head injury accidents resulting from falls using multibody dynamics. Clinical Biomechanics, 18, 590-600.

Padgaonkar, A.J., Kreiger, K.W., and King, A.I. (1975). Measurement of rotational acceleration of a rigid body using linear accelerometers. J. Appl. Mech., 42, 552-556.

Pellman, E.J., Viano, D.C., Tucker, A.M., and Casson, I.R. (2003). Concussion in professional football: Location and direction of helmet impacts – part 2. Neurosurgery, 53(6), 1328-1341.

Petrucelli, E., States, J.D., and Hames, L.N. (1981). The abbreviated injury scale: Evolution, usage and future adaptability. Accident Analysis and Prevention 13(1), 29-35.

Pincemaille, Y., Trosseille, X., Mack, P., Tarriere, C., Breton, F., and Renault, B. (1989). Some new data related to human tolerance obtained from volunteer boxers. Proceedings of the 33rd Stapp Car Crash Conference. SAE paper No. 892435.

Post, A. and Hoshizaki, T.B. (2012). Mechanisms of brain impact injuries and their prediction: A review. Trauma, 14(4), 327-349.

Post, A., Hoshizaki, T.B. and Gilchrist, M. (2012). Finite element analysis of the effect of loading curve shape on brain injury predictors. Journal of Biomechanics, 45, 679-683.

Prange, M.T., Meaney, D.F., and Margulies, S.S. (2002). Defining brain mechanical properies: Effects of region, direction and species. In: Proceedings 44th Stapp Car Crash Conference.

Prasad, P. and Mertz, H.J. (1985). The position of the United States Delegation to the ISO working group 6 on the use of HIC in the automotive environment. SAE peper No. 851246.

Rashid, B., Destrade, M., Gilchrist, M.D. (2012a). Mechanical characterization of brain tissue in compression at dynamic strain rates. Journal of the Mechanical Behavior of Biomedical Materials, 10, 23-38.

Rashid, B., Destrade, M., Gilchrist, M.D. (2012b). Mechanical characterization of brain tissue in tension at dynamic strain rates. Journal of the Mechanical Behavior of Biomedical Materials, in press.

Ruan, J.S. (1994). Impact biomechanics of head injury by mathematical modeling. PhD thesis, Wayne State University.

Ruan, J.S., Khalil, T.B., and King, A.I. (1993). Finite element modeling of direct head impact. Proceedings of the 37th Stapp Car Crash Conference, San Antonio, Texas, USA, SAE 933114.

Schnebel, B., Gwin, J.T., Anderson, S., and Gatlin, R. (2007). In vivo study of head impacts in football: A comparison of National Collegiate Athletic Association Division I versus high school impacts. Neurosurgery, 60(3), 490-495.

Shively, S., Scher, A.I., Perl, D.P., and Diaz-Arrastia, R. (2012). Dementia resulting from traumatic brain injury: What is the pathology? Archives of Neurology, 69(10), 1245-1251.

Shugar, T.A. (1975). Transient structural response of the linear skull-brain system. Proceedings of the 19th Stapp Car Crash Conference, San diego, California, USA, SAE 751161.

Shugar, T. and Katona, M. (1975). Development of a finite lement head injury model. ASCE, Journal of Engineering mechanics, EM3 (E101/173), 223-239.

Silva, V.D. (2006). Mechanics and Strength of Materials. New York, NY, Springer Berlin Heidelberg.

Singh, M., Jeong, J., Hwang, D., Sungkarat, W., and Gruen, P. (2010). Novel diffusion tensor imaging methodology to detect and quantify injured regions and affected brain pathways in traumatic brain injury. Magnetic Resonance Imaging, 28, 22-40.

Sosin, D.M., Sniezek, J.E., & Thurman, D.J. (1996) Incidence of Mild and Moderate Brain Injury in the United States, 1991. Brain Injury, 10(1): 47-54.

Stalhammar, D. (1975a). Experimental brain damage from fluid pressures due to impact acceleration – 1. Design of experimental procedure. Acta. Neurol. Scand., 52 7-26.

Stalhammar, D. (1975b). Experimental brain damage from fluid pressures due to impact acceleration – 2. Pathophysiological observations. Acta. Neurol. Scand., 52, 27-37.

Stalhammar, D. and Olsson, Y. (1975). Experimental brain damage from fluid pressures due to impact acceleration – 3. Morphological observations. Acta. Neurol. Acand., 52, 38-55.

Steiner, L.A. and Andrews, P.J.D. (2006). Monitoring the injured brain: ICP and CBF. Br. J. Anaesthesia, 97, 26-38.

Styrke, J., Stalnacke, B., Sojka, P., and Bjornstig, U. (2007). Traumatic brain injuries in a well-defined population: Epidemiological aspects and severity. Journal of Neurotrauma, 24, 1425-1436.

Suh, W., Yang, W., and McElhaney, J.H. (1972). Rarefaction of liquids in a spherical shell due to local radial loads with application to brain damage. Journal of Biomechanics, 5, 181-189.

Sundgren, P.C., Dong, Q., Gomez-Hassan, D., Mukherji, S.K., Maly, P., and Welsh, R. (2004). Diffusion tensor imaging of the brain: review of clinical applications. Neuroradiology, 46, 339-350.

Takhounts, E.G., Eppinger, R.H., Campbell, J.Q., Tannous, R.E., Power, E.D., and Shook, L.S. (2003). On the development of the SIMon finite element head model. 47th Stapp Car Crash Journal.

Takhounts, E.G., Ridella, S.A., Hasija, V., Danelson, K., Stitzel, J., Rowson, S., and Duma, S. (2008). Investigation of traumatic brain injuries using the next generation of simulated injury monitor (SIMon) finite element head model. Stapp Car Crash Journal, 52, 1-31.

Thomas, L.M., Roberts, V.L., and Gurdjian, E.S. (1966). Experimental intracranial pressure gradients in the human skull. Journal of Neurology, Neurosurgery and Psychiatry, 29, 404-411.

Thomas, L.M., Roberts, V.L., and Gurdjian, E.S. (1967). Impact-induced pressure gradients along three orthogonal axes in the human skull. Journal of Neurosurgery, 26(3), 316-321.

Trosseille, X., Tarriére, C., Lavaste, F., Guillon, F., and Domont, A. (1992). Development of a F.E.M. of the human head according to a specific test protocol. Proceedings of the 36th Stapp Car Crash Conference, Seattle, Washington, USA, SAE 922527.

Turquier, F., Kang, H.S., Trosseille, X., Willinger, R., Lavaste, F., Tarriere, C., and Domont, A. (1996). Validation study of a 3D finite element head model against experimental data. Proceedings of the 40th Stapp Car Crash Conference, Albuquerque, New Mexico, USA, SAE 962431.

Unterharnscheidt, F. and Higgins, L.S. (1969). Neuropathologic effects of translational and rotational acceleration of the head in animal experiments. In:"The Late Effects of Head Injury." Edited by A.E. Walker, W.F Caveness and M. Critchley. Springfield: Thomas, 158-167.

Unterharnscheidt, F. and Sellier, K. (1966). Closed brain injuries: mechanics and pathomorphology. In: "head Injury Conference Proceedings." Edited by W.F Caveness and A.E. Walker. Philadelphia: Lippincott, 321-341.

Versace, J. (1971). A review of the severity index. In Proceedings of the 15th STAPP Car Crash Conference, SAE paper No. 710881.

Viano, D., Holst, H. v., and Gordon, E. (1997). Serious brain injury from traffic related causes: Priorities for primary prevention. Accident Analysis and Prevention, 29(6), 811-816.

Viano, D.C., King, A.I., Melvin, J.W., and Weber, K. (1989). Injury biomechanics research: An essential element in the prevention of trauma. Journal of Biomechanics, 22(5), 403-417.

Viano, D.C. and Lovsund, P. (1999). Biomechanics of brain and spinal-cord injury: Analysis of neuropathologic and neurophysiologic experiments. Journal of Crash Prevention and Injury Control, 1, 35-43.

Voo, L., Kumaresan, S., Pintar, F.A., Yoganandan, N., and Sances Jr., A. (1996). Finite-element models of the human head. Med. & Biol. Eng. & Comput., 34, 375-381.

Walsh, E.S., Rousseau, P., and Hoshizaki, T. B. (2011). The influence of impact location and angle on the dynamic impact response of a hybrid III headform. Sports Engineering.

Ward, C. and Thompson,R.B. (1975). The development of a detailed finite element brain model. Proceedings of the 19th Stapp Car Crash Conference, San Diego, California, USA, SAE 751163.

Ward, C.C., and Nahum, A. (1979). Correlation between brain injury and intracranial pressure in experimental head impacts. Proceedings of the international Conf. on Biomechanics of Trauma, IRCOBI, Gotenborg, Sweden.

Ward, C. (1982). Finite element models of the head and their use in brain injury research. Proceedings of the 26th Stapp Car Crash Conference, Ann Arbor, Michigan, USA, SAE 821154.

Willinger, R., Taled, L., and Pradoura, P. (1995). Head biomechanics from finite element model to the physical model. Proceedings of the 1995 IRCOBI Conference.

Willinger, R., and Baumgartner, D. (2003a). Human head tolerance limits to specific injury mechanisms. International Journal of Crashworthiness 8(6), 605-617.

Willinger, R., and Baumgartner, D. (2003b). Numerical and physical modelling of the human head under impact – towards new injury criteria. Int. J. Vehicle Design, Vol 32, 94-115.

Yanagida, Y., Fujiwara, S., and Mizoi, Y. (1989). Differences in the intracranial pressure caused by a "blow" and/or a "fall" – an experimental study using physical models of head and neck. Forensic Science International, 41, 135-145.

Yang, K.H., Hu, J., White, N.A., and King, A.I. (2006). Development of numerical models for injury biomechanics research: A review of 50 years of publications in the Stapp Car Crash Conference. Stapp Car Crash Journal, 50, 429-490.

Yogandandan, N., Li, J., Zhang, J., Pintar, F.A., and Gennarelli, T.A. (2008). Influence of rotational acceleration-deceleration pulse shapes on regional brain strains. Journal of biomechanics, 41, 2253-2262.

Zhang, L., Yang, K.H., Dwarampudi, R., Omori, K., Li, T., Chang, K., Hardy, W.N., Khalil, T.B., and King, A.I. (2001). Recent advances in brain injury research: a new human head model development and validation. Stapp Car Crash Journal 45, 369-394.

Zhang, L., Yang, K., and King, A.I. (2001). Biomechanics of neurotrauma. Neurology Research, 23(2-3), 144-156.

Zhang, L., Yang, K.H., and King, A.I. (2004). A proposed injury threshold for mild traumatic brain injury. Journal of Biomechanical Engineering, 126, 226-236.

Zhang, J., Yoganandan, N., Pintar, F.A., and Gennarelli, T.A. (2006). Role of translational and rotational accelerations on brain strain in lateral head impact. Biomedical Science and Instrumentation, 42, 501-506.

Zhou, C., Khalil, T.B., King, A.I. (1995). A new model for comparing responses of the homogeneous and inhomogeneous human brain. In: Proceedings of the 39th Stapp Car Crash Conference, 121-136.

APPENDIX I

This appendix shows the reconstruction parameters for each case in the thesis research. In some cases the MADYMO simulations produced impact velocities which resulted in linear accelerations above 800 g. When this point was reached the ensuing increases in velocity were not collected to protect the equipment.

Case 1

Case #1 involved an 85 year old gentleman who had weighed 165 lbs, was 183 cm tall and had no previous record of head injury. He fell stepping up a normal sized step onto his concrete veranda. As he stepped his toe caught the veranda edge and fell straight headfirst into the concrete floor. Witnesses said he did not put his hands out to slow the velocity of impact.

The gentleman did not lose consciousness or display signs of confusion, but did incur a subdural hematoma in the left – frontal region of the cerebrum.

Mathematic Dynamic Models (MAYDMO) reconstructions

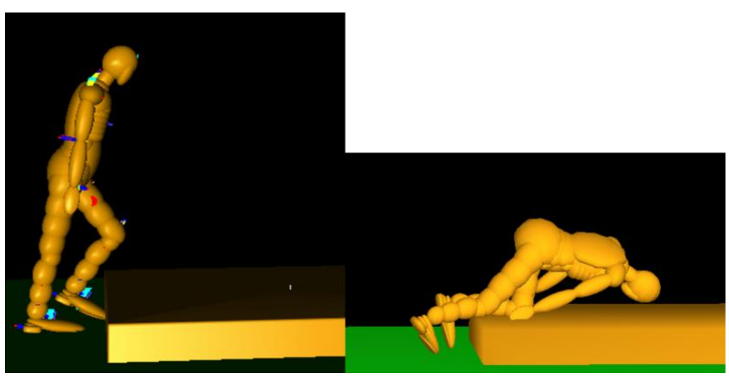

Figure 1. Simulation 1; Initial walking velocity 1.0 m/s

Impact velocity 4.0 m/s

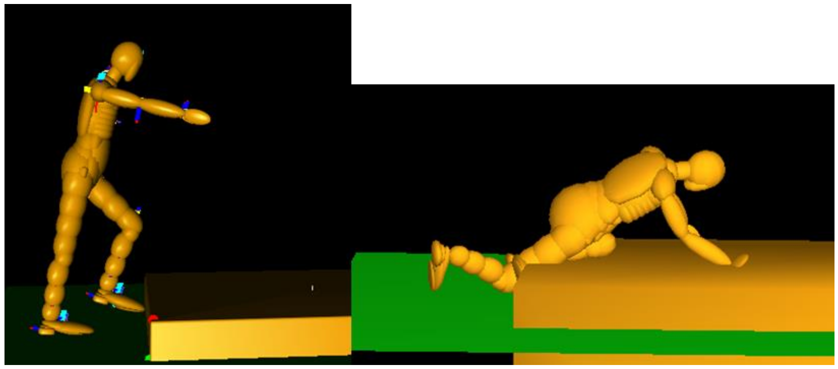

Figure 2. Simulation 2; Initial walking velocity 1.0 m/s

Impact velocity: 3.0 m/s

Medical imaging (CT scans)

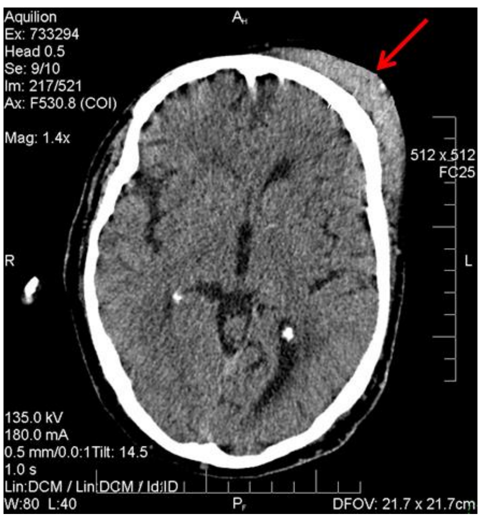

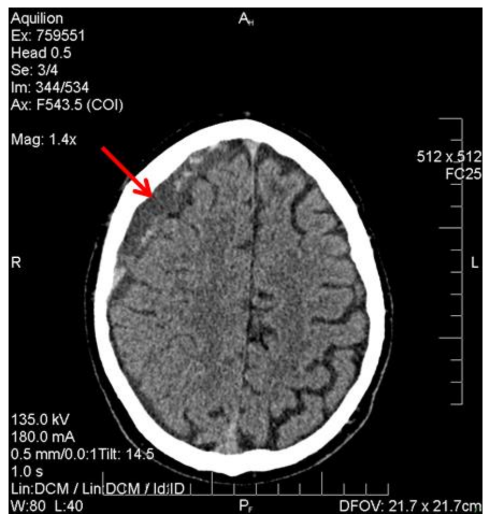

Figure 3. Impact site shown on left as designated by red arrow and large surface hematoma. Subdural hematoma identified on right as indicated by red arrow.

Physical reconstruction

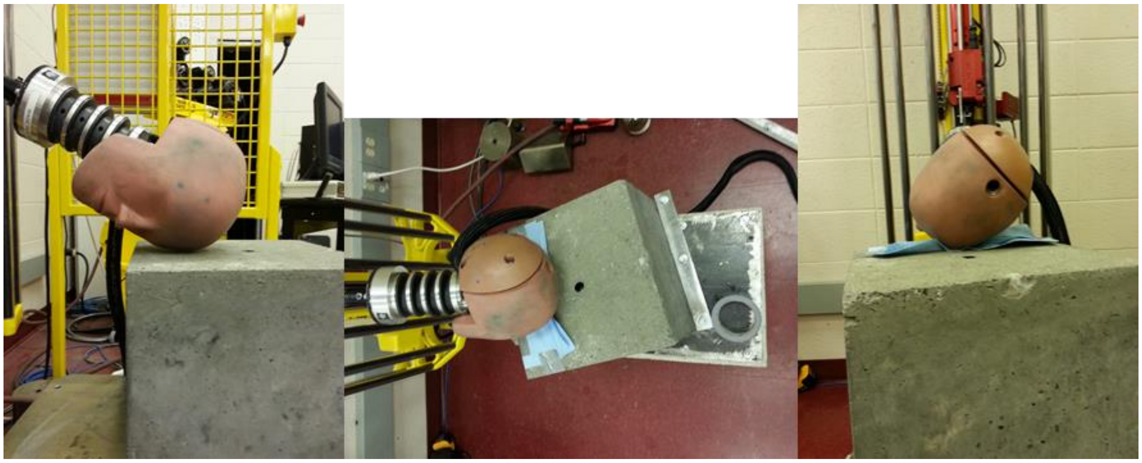

Figure 4. Hybrid III physical reconstruction of case 1.

Table 1. Dynamic response peak resultant values for the reconstruction

	Acceleration	
Velocity (m/s)	Linear (g)	Rotational (rad/s^2)
3.0	258.4 (11.7)	25083 (660.4)
4.0	410.1 (7.2)	40694 (1219)

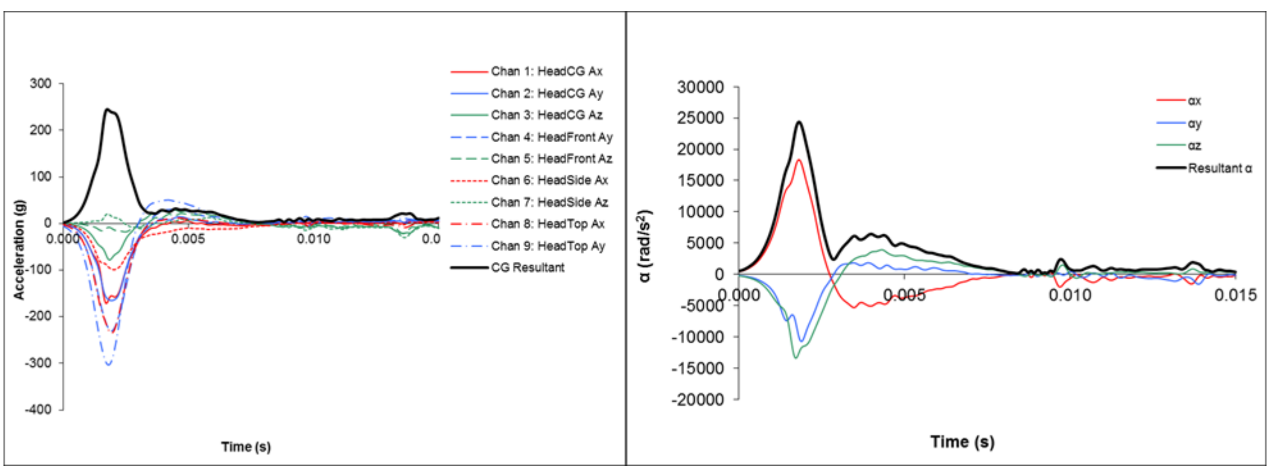

Figure 5. Sample dynamic response curves for the physical reconstruction of case 1. Linear acceleration presented on the left, rotational on the right.

Finite element model region of interest and sizing

The brain was measured to be 12.3 cm wide at the widest point (ear to ear), 15.8 cm long from front to back of the head, and 13.5 cm high from brainstem to top of the head. When using a global scaling tool, the model was scaled to the closest dimensions in the x, y, and z axes. The resulting UCDBTM dimensions were 13.4 cm wide x 16.9 cm long x 13.8 cm high.

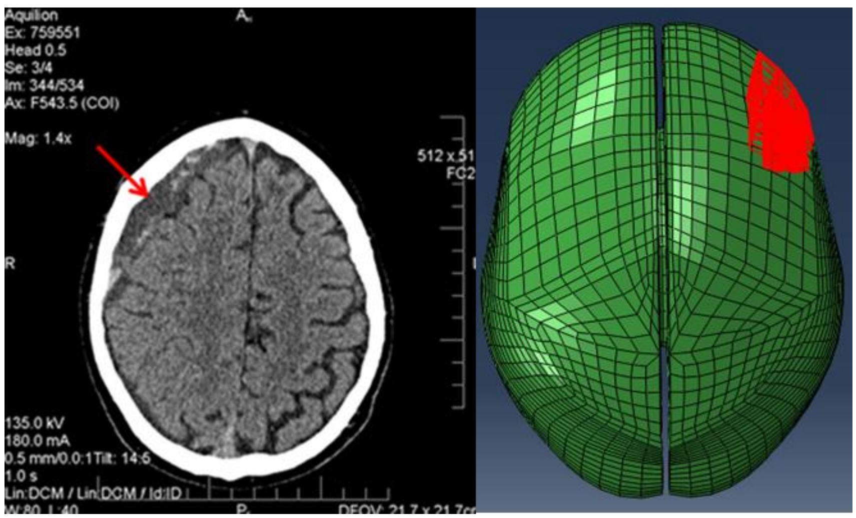

Figure 6. CT scan showing region of SDH on left, corresponding region of interest for the UCDBTM on right.

Finite element modeling results

Table 2. UCDBTM results for the subdural hematoma region. Bold signifies significance between the SDH region and the cerebrum ($p < 0.05$).

Velocity (m/s)	Pressure (Pa)	MPS	VMS (Pa)	Shear stress (Pa)	Shear Strain	Strain rate (s^{-1})	Product (s^{-1})	Avg MPS	Avg VMS (Pa)
3.0	404128 (23212)	0.283 (0.023)	9714 (237.7)	4228 (526.1)	0.439 (0.05)	45.8 (2.0)	13.0 (1.6)	0.079 (0.01)	3798 (198.4)
Significance	**0.007**	**0.001**	**0.001**	**0.001**	**0.001**	**0.001**	**0.001**	**0.026**	0.052
4.0	662675 (46722)	0.385 (0.01)	12972 (130.1)	6055 (164.9)	0.630 (0.017)	68.1 (1.6)	26.2 (0.22)	0.106 (0.009)	4439 (22.5)
Significance	**0.002**	**0.001**	**0.001**	**0.001**	**0.001**	**0.001**	**0.001**	**0.003**	**0.001**

Table 3. UCDBTM results for the cerebrum

Velocity (m/s)	Pressure (Pa)	MPS	VMS (Pa)	Shear stress (Pa)	Shear Strain	Strain rate (s^{-1})	Product (s^{-1})	Avg MPS	Avg VMS (Pa)
3.0	2161899 (597675)	0.736 (0.02)	24296 (567.9)	10801 (346.9)	1.16 (0.05)	125.9 (4.8)	92.7 (5.7)	0.101 (0.003)	3456 (86.8)
4.0	3435110 (668148)	0.974 (0.04)	33970 (1918)	17958 (1205)	1.79 (0.09)	161.1 (6.8)	157.0 (10.5)	0.142 (0.003)	4967 (21.5)

Case 2

Case #2 involved a 75 year old gentleman who weighed 200 lbs, was 180 cm tall and had no record of previous head injury. He lost his footing on ice covered concrete at the entrance to his garage, slipped and fell backwards and hit his head.

The gentleman did not lose consciousness, but was dizzy and saw stars. He incurred a subdural hematoma to the frontal region of the cerebrum.

Mathematic Dynamic Models (MAYDMO) reconstructions

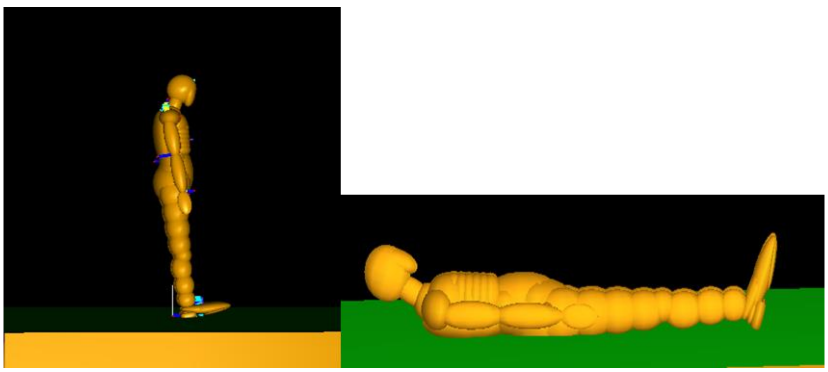

Figure 1. Simulation 1

Impact velocity: 5.2 m/s

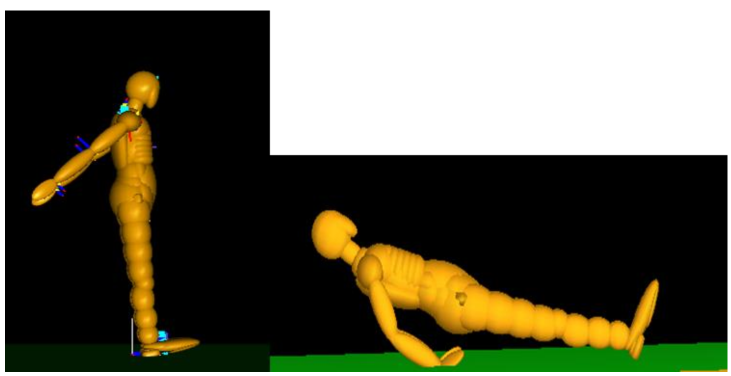

Figure 2. Simulation 2

Impact velocity: 4.69 m/s

Medical imaging (CT scans)

Figure 3. Subdural hematoma as evidenced in upper left part of the skull identified by red arrow.

Physical reconstruction

Impact site for case 2 was taken from the Neurotrauma impact report forms and not from the medical imaging.

Figure 4. Hybrid III physical reconstruction of case 2.

Table 1. Dynamic response peak resultant values for the reconstruction

	Acceleration	
Velocity (m/s)	Linear (g)	Rotational (rad/s^2)
4.69	477.3 (103.2)	32078 (3117)
5.2	496.4 (9.73)	36826 (1218)

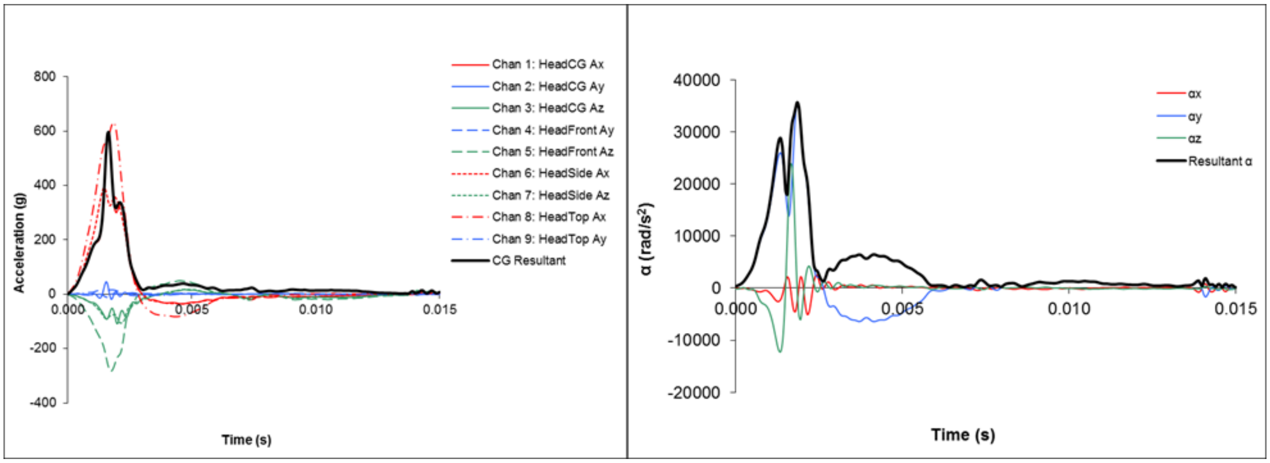

Figure 5. Sample dynamic response curves for the physical reconstruction of case 2. Linear acceleration presented on the left, rotational on the right.

Finite element model region of interest and sizing

The brain was measured to be 13.1cm wide at the widest point (ear to ear), 16.0cm long from front to back of the head, and 12cm high from brainstem to top of the head. When using a global scaling tool, the model was scaled to the closest dimensions in the x, y, and z axes. The resulting UCDBTM dimensions were 12.7cm wide x 16.4cm long x 13.1cm high.

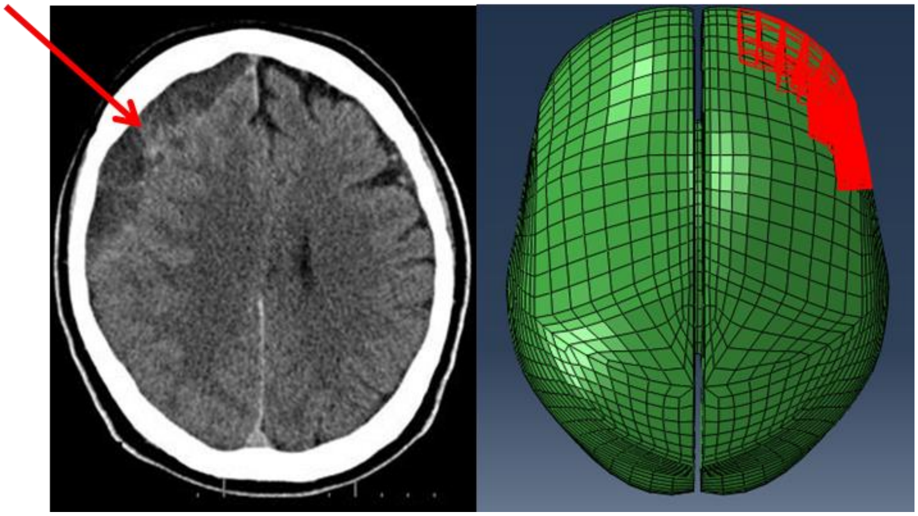

Figure 6. UCDBTM region of interest representing the region of the subdural hematoma (red)

Finite element modeling results

Table 2. UCDBTM results for the subdural hematoma region. Bold signifies significance between the SDH region and the cerebrum ($p < 0.05$).

Velocity (m/s)	Pressure (Pa)	MPS	VMS (Pa)	Shear stress (Pa)	Shear Strain	Strain rate (S^{-1})	Product (S^{-1})	Avg MPS	Avg VMS (Pa)
4.69	1115715 (163994)	0.346 (0.01)	10911 (364.1)	5039 (117.1)	0.529 (0.01)	108.4 (2.36)	37.5 (1.0)	0.093 (0.003)	3344.7 (174.6)
Significance	**0.005**	**0.022**	**0.023**	**0.028**	**0.028**	0.399	0.214	0.714	0.677
5.2	928662 (92984)	0.388 (0.004)	12235 (137.0)	5875 (119.0)	0.61 (0.009)	122.6 (2.32)	47.6 (1.4)	0.107 (0.001)	4228 (633.1)
Significance	0.115	**0.002**	**0.002**	**0.004**	**0.002**	**0.002**	**0.004**	**0.006**	**0.048**

Table 3. UCDBTM results for the cerebrum

Velocity (m/s)	Pressure (Pa)	MPS	VMS (Pa)	Shear stress (Pa)	Shear Strain	Strain rate (S^{-1})	Product (S^{-1})	Avg MPS	Avg VMS (Pa)
4.69	2534862 (72333)	0.676 (0.08)	23265 (3369)	11766 (1990)	1.13 (0.18)	158.0 (78.8)	111.2 (70.2)	0.100 (0.03)	3181 (690.9)
5.2	2387394 (872103)	0.882 (0.04)	31127 (1568)	15443 (1035)	1.38 (0.07)	290.8 (15.4)	256.9 (25.3)	0.079 (0.004)	2884 (138.8)

Case 3

Case #3 involved a 59 year old lady who weighed 180 lbs, was 157 cm tall and had no previous record of head injury. She fell sideways off a small ladder (feet were 2 ft off the ground) and hit the centre of the side of her head on concrete/terrazzo flooring.

The lady lost consciousness for about one minute, was confused and suffered from amnesia for about 80 minutes. She had a GCS score of 14. The medical scans showed an epidural hematoma at the occipital region as well as a small subdural and frontal contusion.

Mathematic Dynamic Models (MAYDMO) reconstructions

Figure 1. Simulation 1

Impact velocity: 6.11 m/s

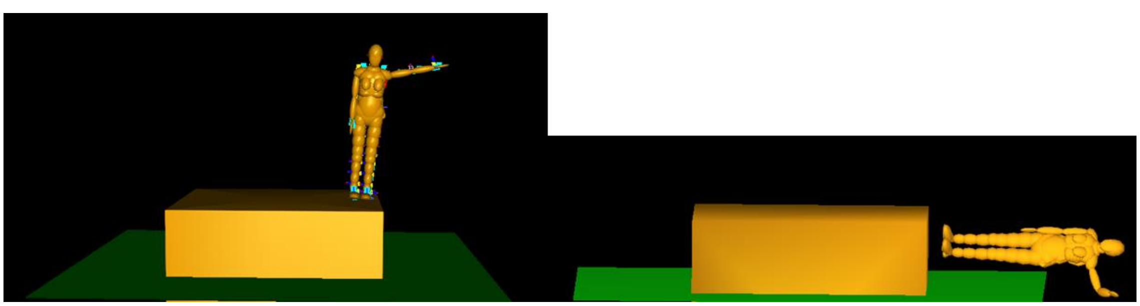

Figure 2. Simulation 2

Impact velocity: 5.1 m/s

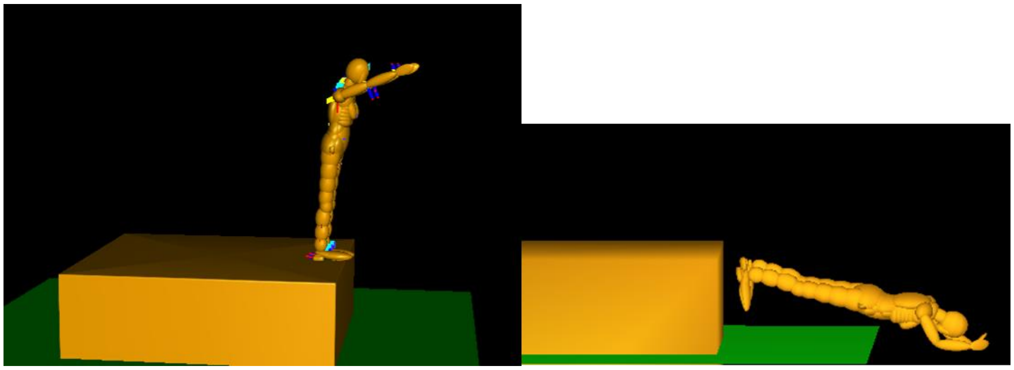

Figure 3. Simulation 3

Impact velocity: 5.4 m/s

Medical imaging (CT scans)

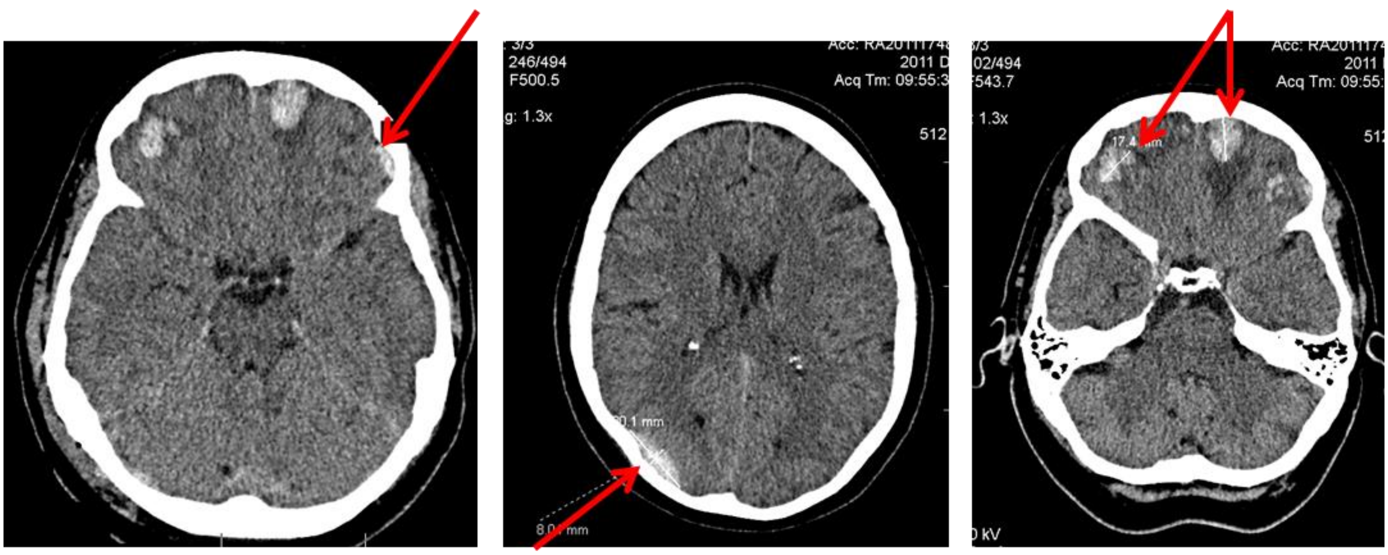

Figure 4. Medical images showing: (left) subdural hematoma, (centre) epidural hematoma, and (right) contusions

Physical reconstruction

Impact site for case 3 was taken from the Neurotrauma impact report forms and not from the medical imaging. Only the 5.1 m/s condition was conducted as the accelerations were approaching the sensor tolerances at that velocity. To go higher would have damaged the equipment.

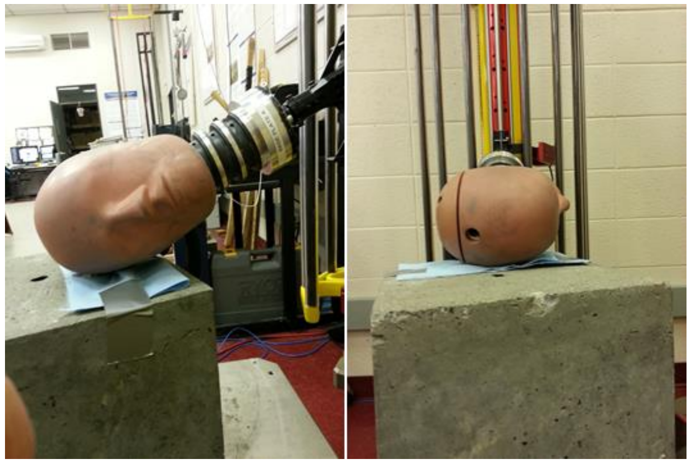

Figure 5. Hybrid III physical reconstruction of case 3.

Table 1. Dynamic response peak resultant values for the reconstruction

	Acceleration	
Velocity (m/s)	Linear (g)	Rotational (rad/s^2)
5.1	610.9 (39.9)	56188 (961.2)

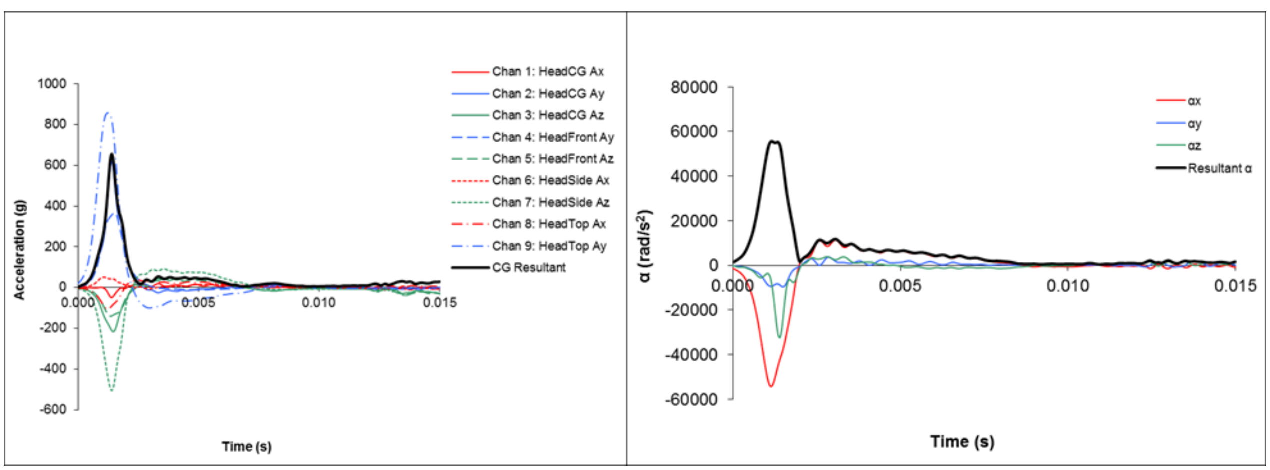

Figure 6. Sample dynamic response curves for the physical reconstruction of case 3. Linear acceleration presented on the left, rotational on the right.

Finite element model region of interest and sizing

The brain was measured to be 12cm high from brainstem to top of the head, 16cm long from front to back and 12.8cm wide from ear to ear. The UCDBTM was scaled to the closest dimensions which were: 12.7cm wide x 16.4cm long x 13.1cm high.

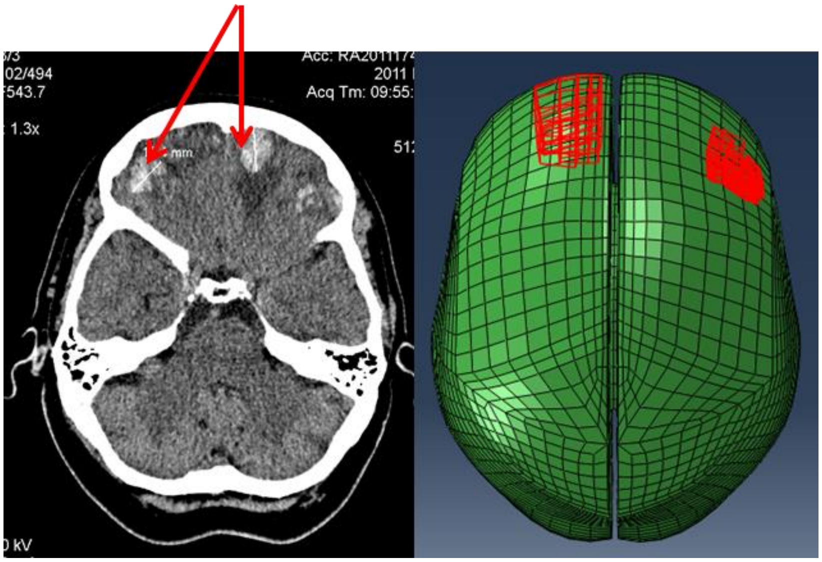

Figure 7. UCDBTM region of interest representing the region of the contusions (red)

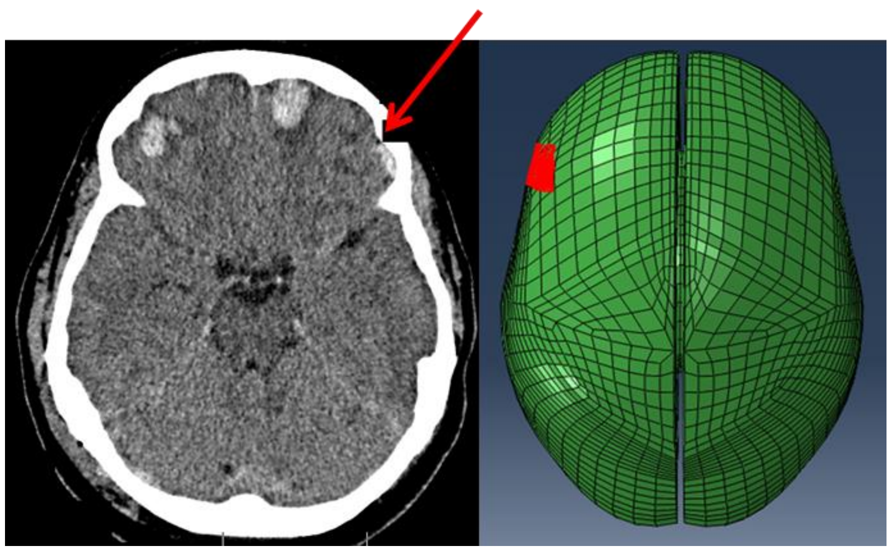

Figure 8. UCDBTM region of interest representing the region of the subdural hematoma (red)

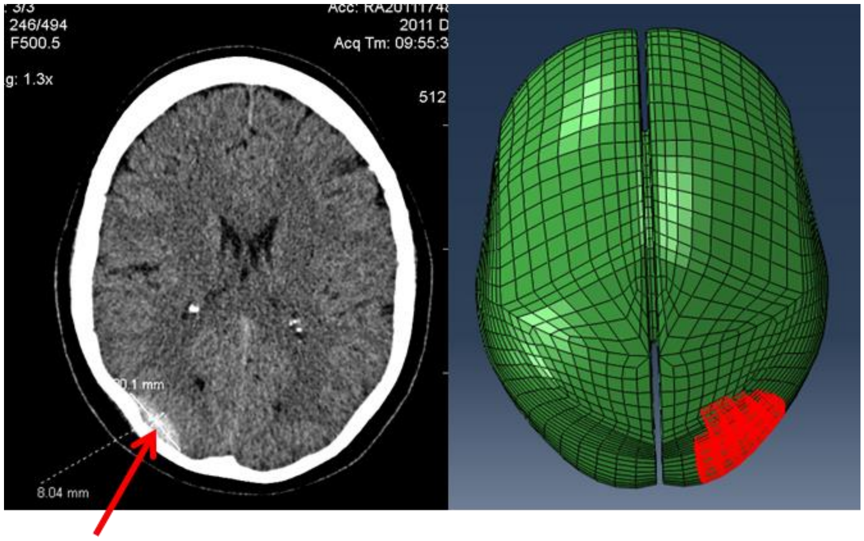

Figure 9. UCDBTM region of interest representing the region of the epidural hematoma (red)

Finite element modeling results

Table 2. UCDBTM results for the contusion region. Bold signifies significance between the contusion region and the cerebrum ($p < 0.05$).

Velocity (m/s)	Pressure (Pa)	MPS	VMS (Pa)	Shear stress (Pa)	Shear Strain	Strain rate (S^{-1})	Product (S^{-1})	Avg MPS	Avg VMS (Pa)
5.1	878273 (34352)	0.288 (0.01)	9916 (381.8)	4708 (133.9)	0.442 (0.02)	110.9 (4.1)	32.0 (2.7)	0.085 (0.003)	3700 (843.4)
Significance	0.068	**0.001**	**0.000**	**0.004**	**0.000**	0.099	**0.031**	**0.017**	0.099

Table 3. UCDBTM results for the subdural hematoma region. Bold signifies significance between the SDH region and the cerebrum ($p < 0.05$).

Velocity (m/s)	Pressure (Pa)	MPS	VMS (Pa)	Shear stress (Pa)	Shear Strain	Strain rate (S^{-1})	Product (S^{-1})	Avg MPS	Avg VMS (Pa)
5.1	531408 (14037)	0.431 (0.01)	16007 (396.0)	7762 (79.0)	0.757 (0.01)	129.3 (10.8)	55.7 (4.0)	0.222 (0.03)	8297 (422.8)
Significance	**0.049**	**0.001**	**0.001**	**0.009**	**0.002**	0.175	**0.045**	0.069	**0.019**

Table 4. UCDBTM results for the epidural hematoma region. Bold signifies significance between the EDH region and the cerebrum ($p < 0.05$).

Velocity (m/s)	Pressure (Pa)	MPS	VMS (Pa)	Shear stress (Pa)	Shear Strain	Strain rate (S^{-1})	Product (S^{-1})	Avg MPS	Avg VMS (Pa)
5.1	702452 (4188)	0.264 (0.01)	10294 (452.3)	4522 (173.1)	0.361 (0.02)	36 (13.6)	9.57 (3.88)	0.089 (0.005)	3835 (205.1)
Significance	0.058	**0.001**	**0.001**	**0.006**	**0.001**	0.051	**0.029**	**0.004**	**0.004**

Table 5. UCDBTM results for the cerebrum.

Velocity (m/s)	Pressure (Pa)	MPS	VMS (Pa)	Shear stress (Pa)	Shear Strain	Strain rate (S^{-1})	Product (S^{-1})	Avg MPS	Avg VMS (Pa)
5.1	3157955 (1063810)	1.02 (0.02)	35575 (484.5)	16664 (1424)	1.74 (0.07)	212.7 (63.2)	216.8 (59.7)	0.144 (0.01)	5171 (337.0)

Case 4

Case #4, an adult male fell onto the floor at home. The medical scans showed contusion and subarachnoid hemorrhage. No further information was available, concrete was the assumed surface compliance.

Mathematic Dynamic Models (MAYDMO) reconstructions

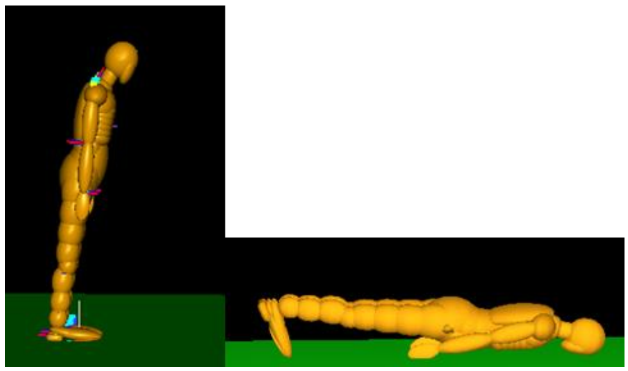

Figure 1. Simulation 1

Head impact velocity: 4.87 m/s

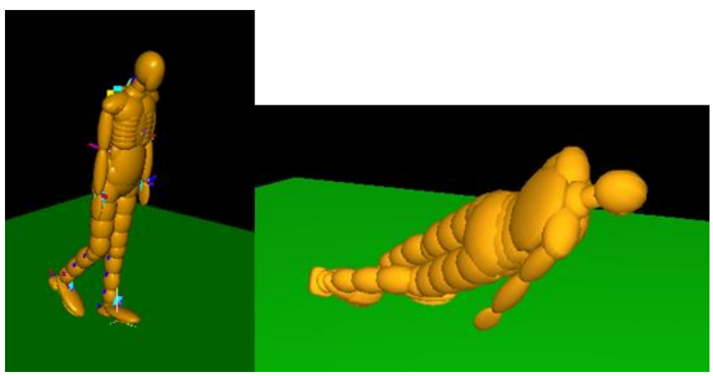

Figure 2. Simulation 2

Impact velocity: 5.35 m/s

Figure 3. Simulation 3

Head impact velocity: 4.1 m/s

Medical imaging (CT scans)

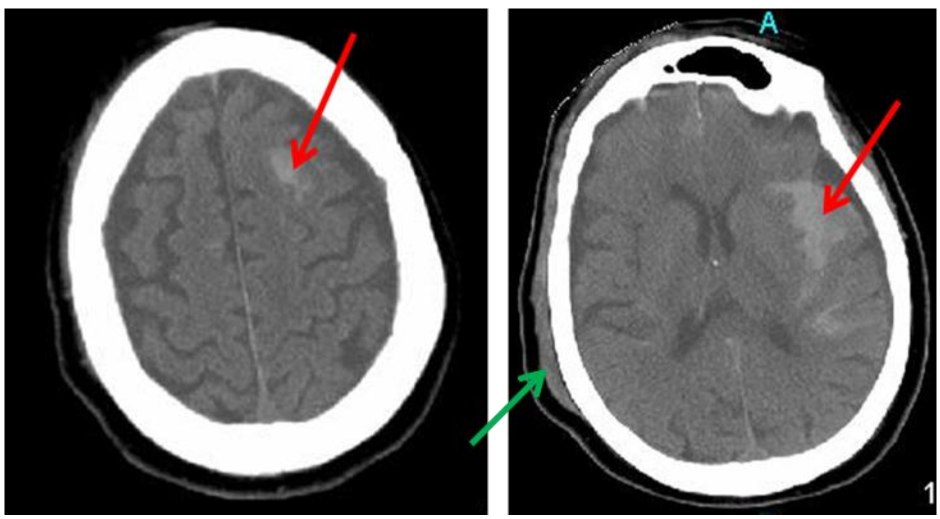

Figure 4. Medical images showing: (left) contusion, and (right) subarachnoid hemorrhage (red arrows). Impact site indicated by green arrow.

Physical reconstruction

Only the 4.1 and 4.8 m/s condition was conducted as the accelerations were approaching the sensor tolerances at that velocity. To go higher would have damaged the equipment.

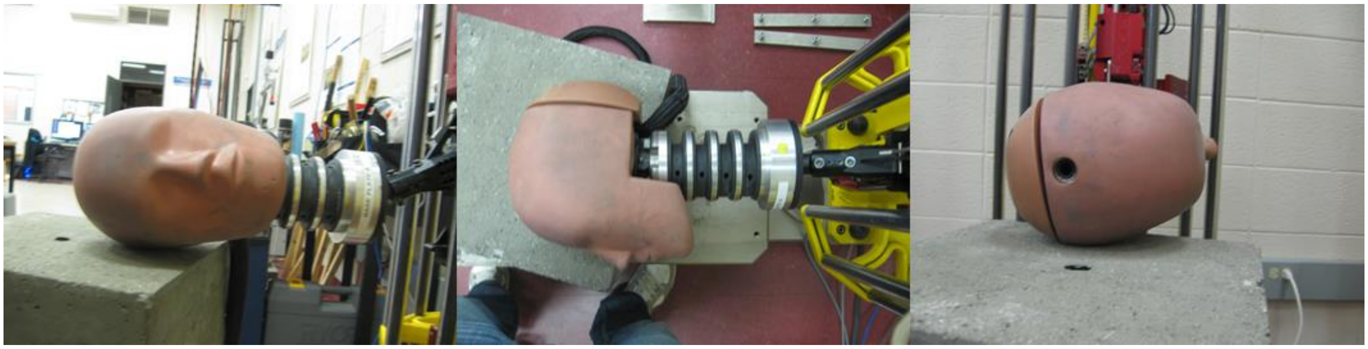

Figure 5. Hybrid III physical reconstruction of case 4.

Table 1. Dynamic response peak resultant values for the reconstruction

	Acceleration	
Velocity (m/s)	Linear (g)	Rotational (rad/s^2)
4.1	387.7 (1.97)	47686 (1160)
4.8	518.5 (8.64)	65856 (1846)

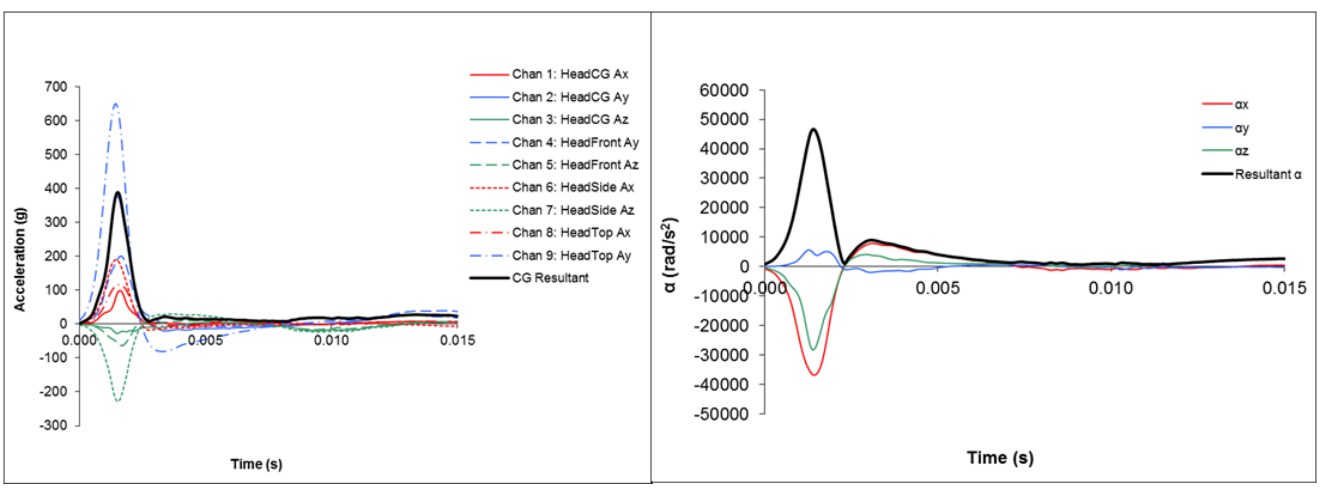

Figure 6. Sample dynamic response curves for the physical reconstruction of case 4. Linear acceleration presented on the left, rotational on the right.

Finite element model region of interest and sizing

The brain was measured to be 12.5 cm high from brainstem to top of the head, 16 cm long from front to back and 13 cm wide from ear to ear. The UCDBTM was scaled to the closest dimensions which were: 12.3 cm high, 15.3 cm long, and 12.1 cm wide.

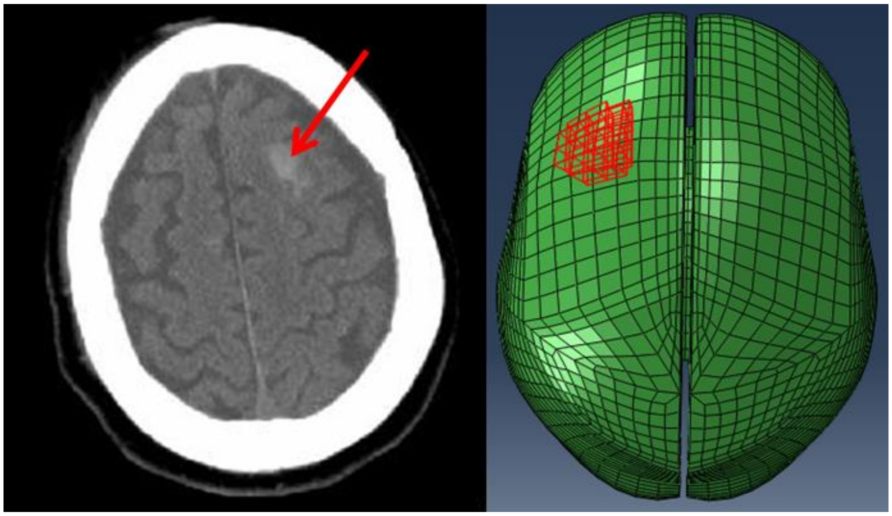

Figure 7. UCDBTM region of interest representing the region of the contusion (red)

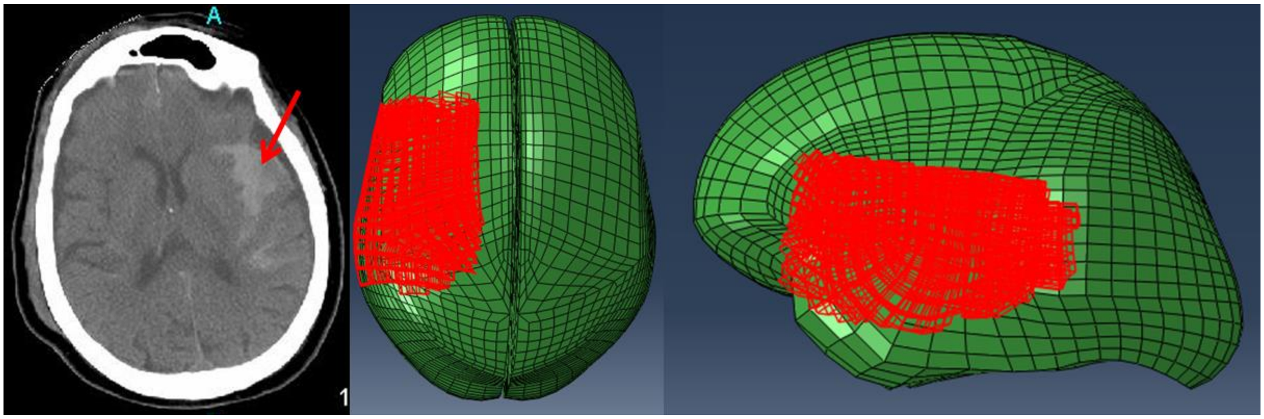

Figure 8. UCDBTM region of interest representing the region of the subarachnoid hemorrhage (red)

Finite element modeling results

Table 2. UCDBTM results for the contusion region. Bold signifies significance between the contusion region and the cerebrum ($p < 0.05$).

Velocity (m/s)	Pressure (Pa)	MPS	VMS (Pa)	Shear stress (Pa)	Shear Strain	Strain rate (s^{-1})	Product (s^{-1})	Avg MPS	Avg VMS (Pa)
4.1	311944 (66984)	0.2 (0.004)	6611 (130.6)	2799 (97.0)	0.224 (0.01)	55.5 (1.02)	11.1 (0.4)	0.069 (0.002)	2736 (330.0)
Significance	**0.014**	**0.002**	**0.001**	**0.001**	**0.001**	**0.011**	**0.011**	**0.001**	**0.010**
4.8	1651420 (2165255)	0.242 (0.004)	7980 (76.2)	3545 (133.0)	0.282 (0.005)	67.1 (1.15)	16.2 (0.55)	0.087 (0.003)	3608 (66.5)
Significance	0.476	**0.000**	**0.000**	**0.001**	**0.000**	0.079	**0.041**	**0.001**	**0.013**

Table 3. UCDBTM results for the subarachnoid hemorrhage region. Bold signifies significance between the SAH region and the cerebrum ($p < 0.05$).

Velocity (m/s)	Pressure (Pa)	MPS	VMS (Pa)	Shear stress (Pa)	Shear Strain	Strain rate (s^{-1})	Product (s^{-1})	Avg MPS	Avg VMS (Pa)
4.1	2118524 (474444)	0.442 (0.04)	14019 (917.0)	5822 (69.5)	0.594 (0.007)	92.1 (5.82)	40.9 (6.0)	0.113 (0.005)	3958 (139.0)
Significance	0.423	**0.013**	**0.001**	**0.001**	**0.002**	**0.043**	**0.029**	**0.040**	**0.013**
4.8	2464190 (330127)	0.492 (0.03)	15935 (439.1)	7048 (121.7)	0.665 (0.01)	109.3 (3.6)	53.7 (2.89)	0.131 (0.007)	4578 (154.3)
Significance	0.343	**0.001**	**0.000**	**0.003**	**0.001**	0.218	**0.074**	0.051	**0.019**

Table 4. UCDBTM results for the cerebrum.

Velocity (m/s)	Pressure (Pa)	MPS	VMS (Pa)	Shear stress (Pa)	Shear Strain	Strain rate (s^{-1})	Product (s^{-1})	Avg MPS	Avg VMS (Pa)
4.1	2148868 (420860)	0.761 (0.04)	25889 (154.5)	10197 (240.6)	1.07 (0.03)	149.9 (16.5)	114.4 (18.4)	0.135 (0.004)	4796 (50.4)
4.8	27144388 (211084)	0.858 (0.02)	29430 (165.0)	13591 (683.5)	1.28 (0.01)	155.6 (47.0)	134.0 (43.0)	0.156 (0.004)	5476 (362.2)

Case 5

Case #5, an adult male fell backwards after losing footing and hit right occiput on wooden deck. The medical scans showed left frontal/temporal subarachnoid hemorrhage and subdural hematoma. No further information was available.

Mathematic Dynamic Models (MAYDMO) reconstructions

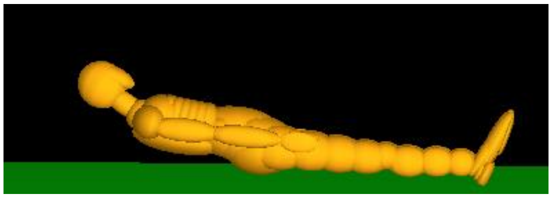

Figure 1. Simulation 1, impact only

Impact velocity: 6.2 m/s

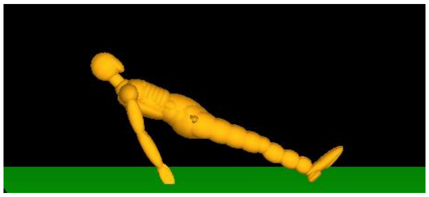

Figure 2. Simulation 2, impact only

Impact velocity: 4.68 m/s

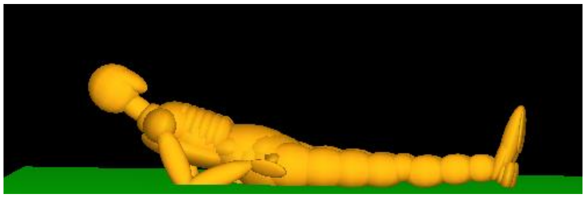

Figure 3. Simulation 3, impact only (gluteus makes initial contact)

Impact velocity: 3.91 m/s

Medical imaging (CT scans)

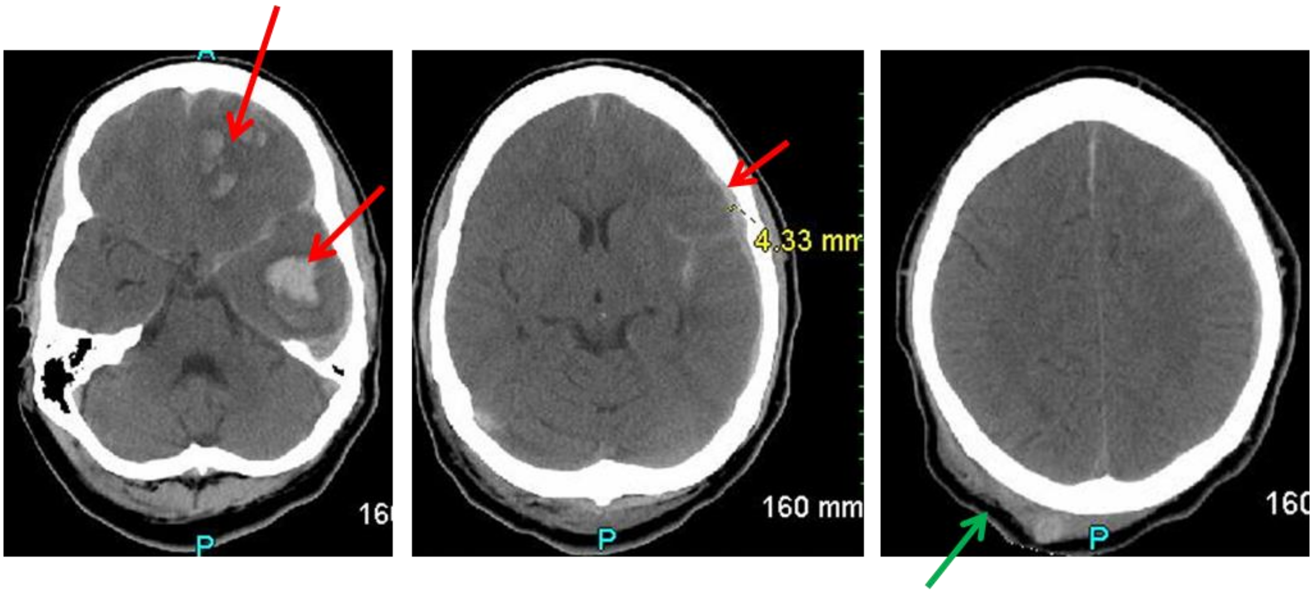

Figure 4. Medical images showing: (left) frontal and temporal subarachnoid hemorrhages, and (right) subdural hematoma (red arrows). Impact site indicated by green arrow.

Physical reconstruction

Only the 3.9 and 4.6 m/s condition was conducted as the accelerations were approaching the sensor tolerances at that velocity. To go higher would have damaged the equipment.

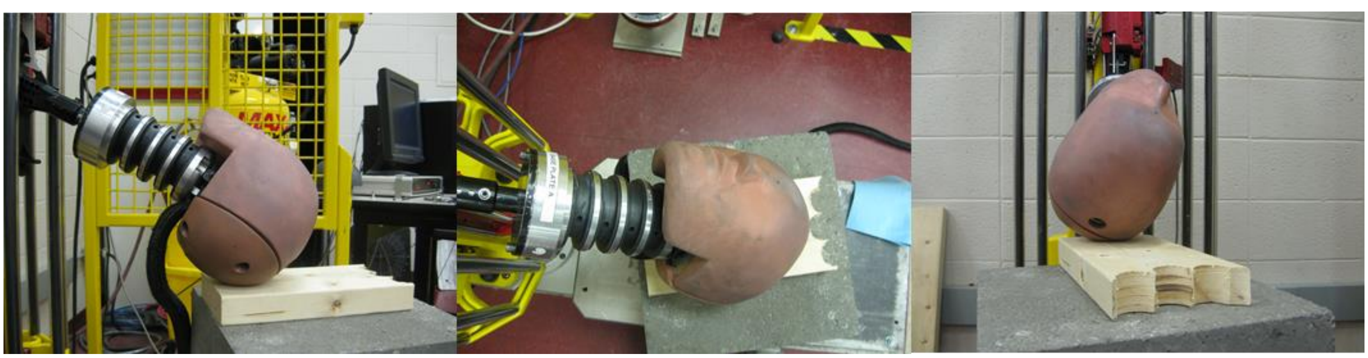

Figure 5. Hybrid III physical reconstruction of case 5.

Table 1. Dynamic response peak resultant values for the reconstruction

	Acceleration	
Velocity (m/s)	Linear (g)	Rotational (rad/s^2)
3.9	258.7 (3.1)	16817 (106.2)
4.7	372.9 (5.1)	23968 (279.2)

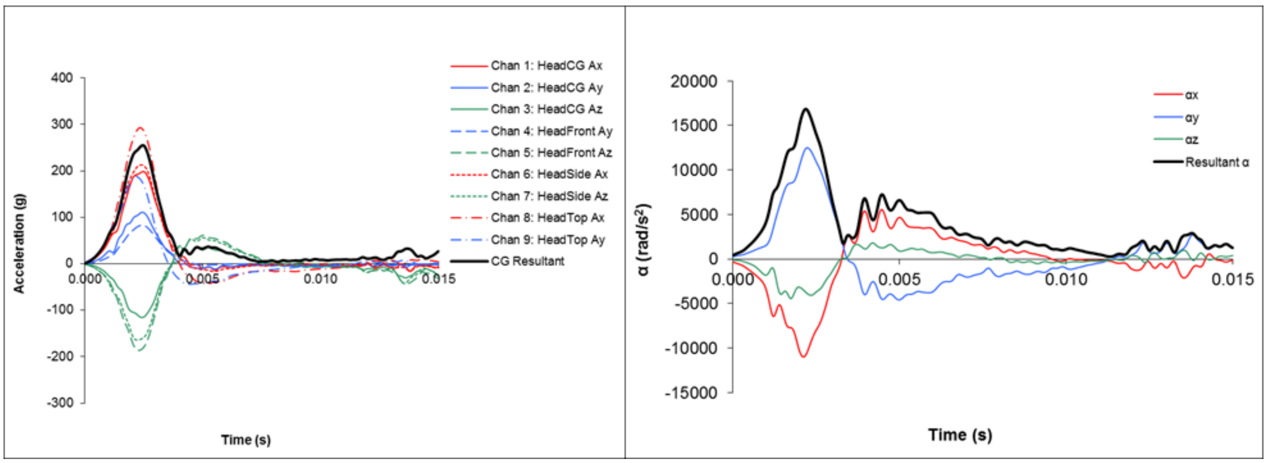

Figure 6. Sample dynamic response curves for the physical reconstruction of case 5. Linear acceleration presented on the left, rotational on the right.

Finite element model region of interest and sizing

The brain was measured to be 12 cm high from brainstem to top of the head, 15.8 cm long from front to back and 12.75 cm wide from ear to ear. The UCDBTM was scaled to the closest dimensions which were: 12.3 cm high, 15.3 cm long, and 12.1 cm wide.

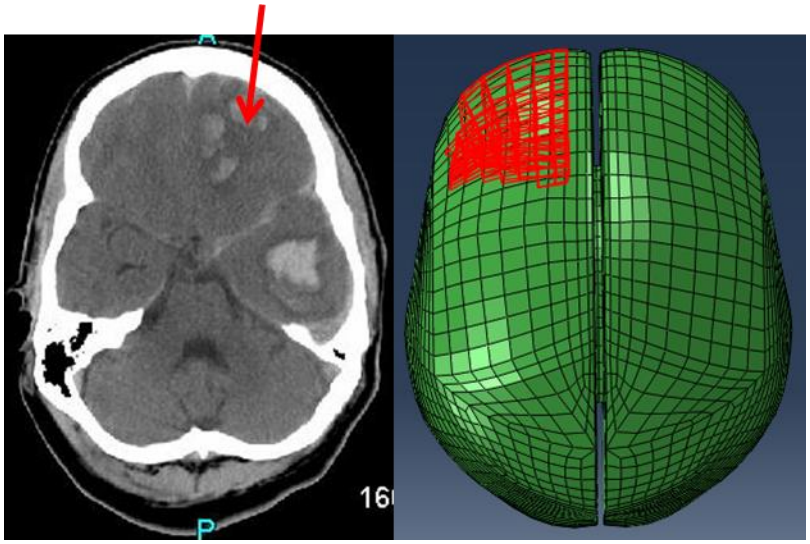

Figure 7. UCDBTM region of interest representing the region of the frontal subarachnoid hemorrhage (red)

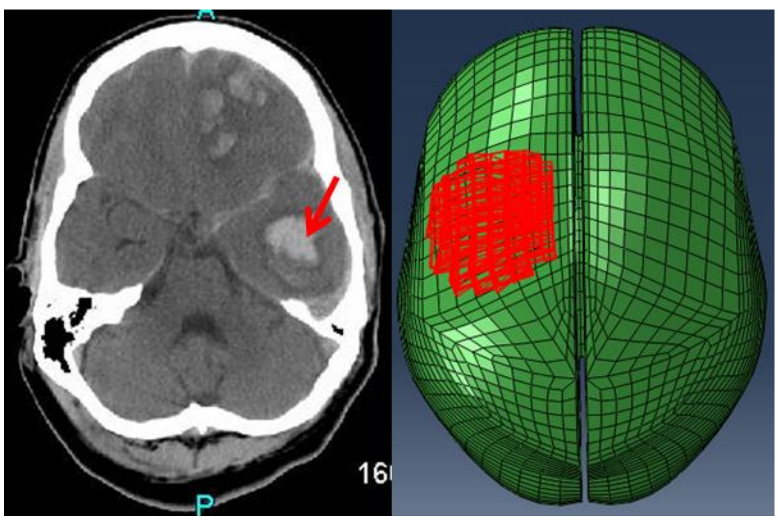

Figure 8. UCDBTM region of interest representing the region of the temporal subarachnoid hemorrhage (red)

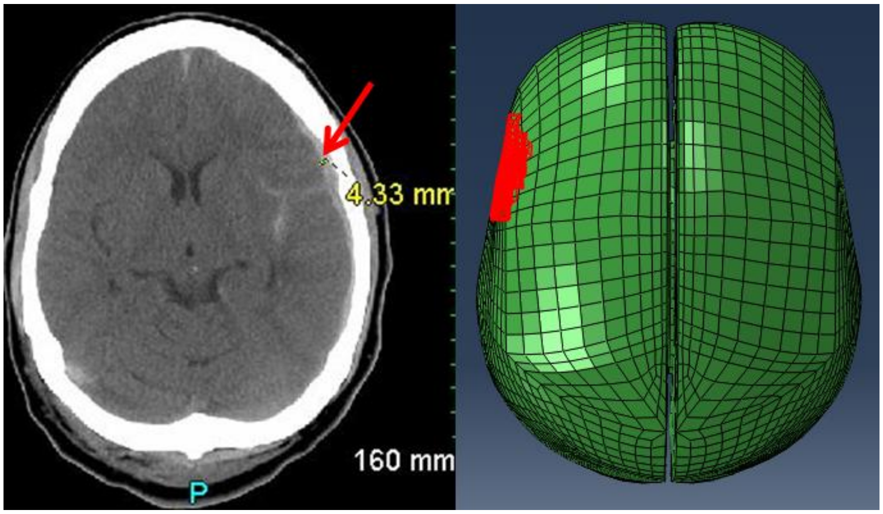

Figure 9. UCDBTM region of interest representing the region of the subdural hematoma (red)

Finite element modeling results

Table 2. UCDBTM results for the subdural hematoma region. Bold signifies significance between the SDH region and the cerebrum ($p < 0.05$).

Velocity (m/s)	Pressure (Pa)	MPS	VMS (Pa)	Shear stress (Pa)	Shear Strain	Strain rate (s^{-1})	Product (s^{-1})	Avg MPS	Avg VMS (Pa)
3.9	873194 (35604)	0.23 (0.001)	8354 (136.0)	3908 (77.9)	0.381 (0.008)	39.1 (1.16)	9.0 (0.26)	0.154 (0.01)	4595 (320.7)
Significance	0.125	**0.001**	**0.001**	0.081	**0.001**	**0.001**	**0.001**	**0.005**	**0.014**
4.7	1161935 (89066)	0.283 (0.005)	10106 (109.9)	4819 (101.3)	0.458 (0.003)	50.6 (2.5)	14.4 (0.97)	0.184 (0.014)	5643 (266.2)
Significance	**0.016**	**0.002**	**0.001**	**0.003**	**0.000**	**0.015**	**0.006**	**0.009**	**0.008**

Table 3. UCDBTM results for the frontal subarachnoid hemorrhage region. Bold signifies significance between the FSAH region and the cerebrum ($p < 0.05$).

Velocity (m/s)	Pressure (Pa)	MPS	VMS (Pa)	Shear stress (Pa)	Shear Strain	Strain rate (s^{-1})	Product (s^{-1})	Avg MPS	Avg VMS (Pa)
3.9	873949 (40926)	0.298 (0.005)	10491 (161.9)	5811 (87.0)	0.520 (0.01)	49.7 (15.9)	14.9 (4.9)	0.103 (0.002)	4004 (97.8)
Significance	0.114	**0.001**	**0.001**	0.375	**0.008**	0.528	**0.030**	**0.002**	**0.001**
4.7	1427159 (265100)	0.374 (0.003)	12611 (136.8)	6989 (102.1)	0.688 (0.01)	83.1 (0.59)	31.1 (0.44)	0.117 (0.001)	4950 (38.0)
Significance	0.184	**0.003**	**0.001**	**0.005**	**0.012**	0.098	**0.012**	**0.001**	**0.001**

Table 4. UCDBTM results for the temporal subarachnoid hemorrhage region. Bold signifies significance between the TSAH region and the cerebrum ($p < 0.05$).

Velocity (m/s)	Pressure (Pa)	MPS	VMS (Pa)	Shear stress (Pa)	Shear Strain	Strain rate (s^{-1})	Product (s^{-1})	Avg MPS	Avg VMS (Pa)
3.9	499232 (119346)	0.302 (0.005)	9435 (127.4)	4977 (173.0)	0.551 (0.028)	33.6 (0.5)	10.2 (0.3)	0.083 (0.002)	3152 (593.4)
Significance	0.069	**0.002**	**0.001**	0.181	0.063	**0.001**	**0.001**	**0.008**	0.565
4.7	938218 (166753)	0.391 (0.005)	12009 (173.9)	6479 (124.8)	0.719 (0.012)	65.2 (0.91)	25.5 (0.70)	0.092 (0.001)	3776 (993.3)
Significance	0.069	**0.003**	**0.002**	**0.002**	**0.002**	**0.038**	**0.009**	**0.002**	0.968

Table 5. UCDBTM results for the cerebrum.

Velocity (m/s)	Pressure (Pa)	MPS	VMS (Pa)	Shear stress (Pa)	Shear Strain	Strain rate (s^{-1})	Product (s^{-1})	Avg MPS	Avg VMS (Pa)
3.9	1214913 (252053)	0.555 (0.014)	18606 (341.7)	6874 (1541)	0.608 (0.005)	56.6 (0.62)	31.4 (1.13)	0.079 (0.001)	2926 (42.1)
4.7	1574105 (142926)	0.737 (0.03)	25076 (793.0)	7913 (187.7)	0.785 (0.008)	76.8 (3.13)	56.7 (4.55)	0.101 (0.001)	3751 (31.3)

Case 6

Case #6 involved a 74 year old male with no record of previous head injury. Fell out of bed and hit his head. The medical scans showed small subacute bilateral subdural hematoma. The bed height was assumed to be that of a common bed (0.635 m).

Mathematic Dynamic Models (MAYDMO) reconstructions

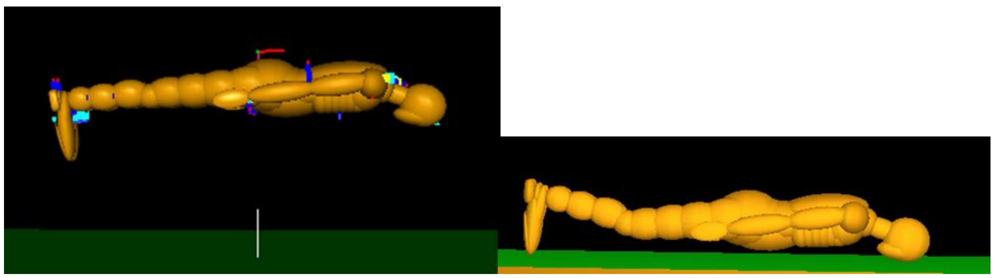

Figure 1. Simulation 1

Impact velocity: 3.33 m/s

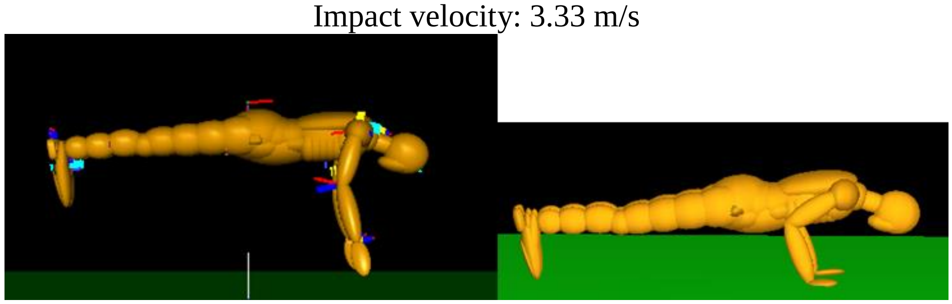

Figure 2. Simulation 2

Impact velocity: 2.24 m/s

Medical imaging (CT scans)

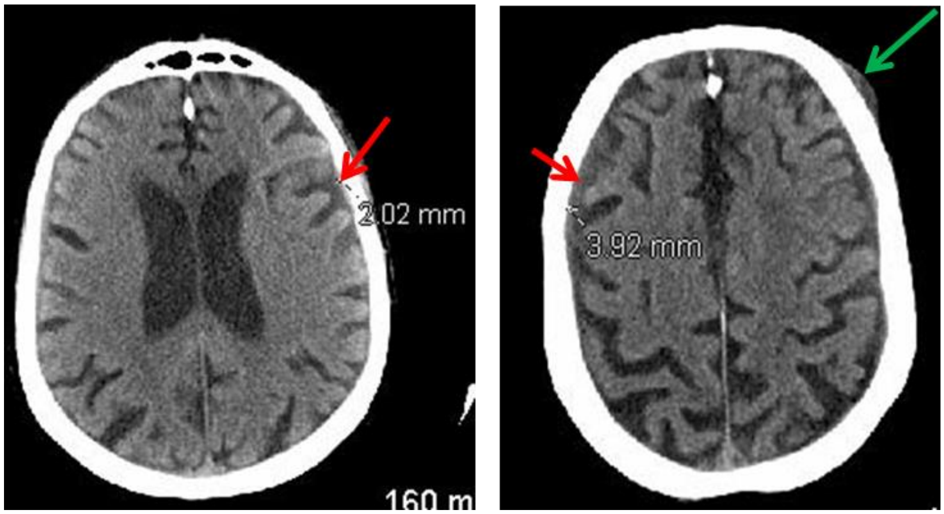

Figure 3. Medical images showing: (left) left subdural hematoma (right) right subdural hematoma (red arrows). Impact site indicated by green arrow.

Physical reconstruction

Figure 4. Hybrid III physical reconstruction of case 6.

Table 1. Dynamic response peak resultant values for the reconstruction

	Acceleration	
Velocity (m/s)	Linear (g)	Rotational (rad/s^2)
2.24	68.3 (5.7)	4865 (553.8)
3.33	156.7 (2.8)	13268 (244.2)

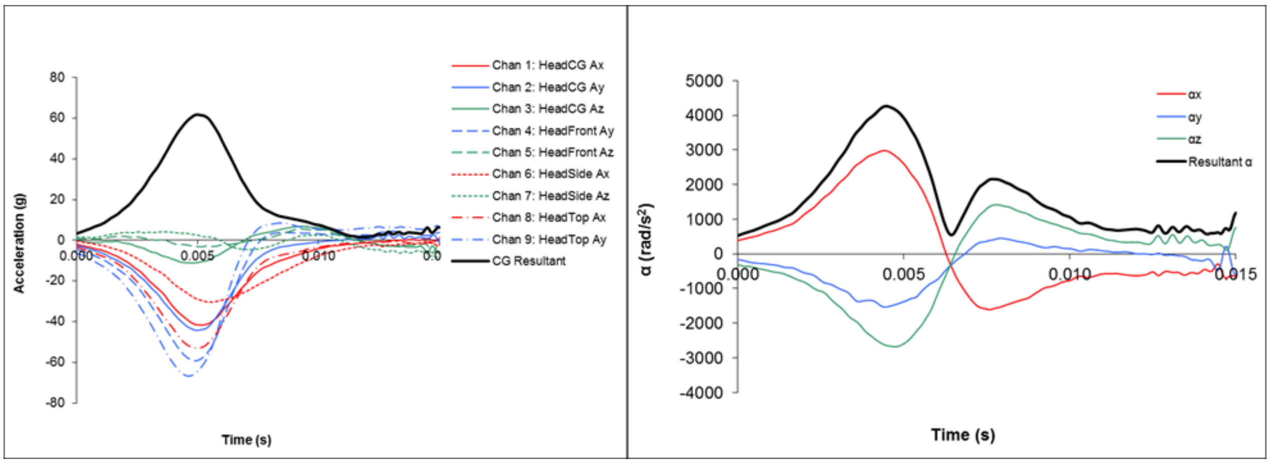

Figure 5. Sample dynamic response curves for the physical reconstruction of case 6. Linear acceleration presented on the left, rotational on the right.

Finite element model region of interest and sizing

The brain was measured to be 13 cm high from brainstem to top of the head, 15.8 cm long from front to back and 13.5 cm wide from ear to ear. The UCDBTM was scaled to the closest dimensions which were: 12.3 cm high, 15.3 cm long and 12.1 cm wide.

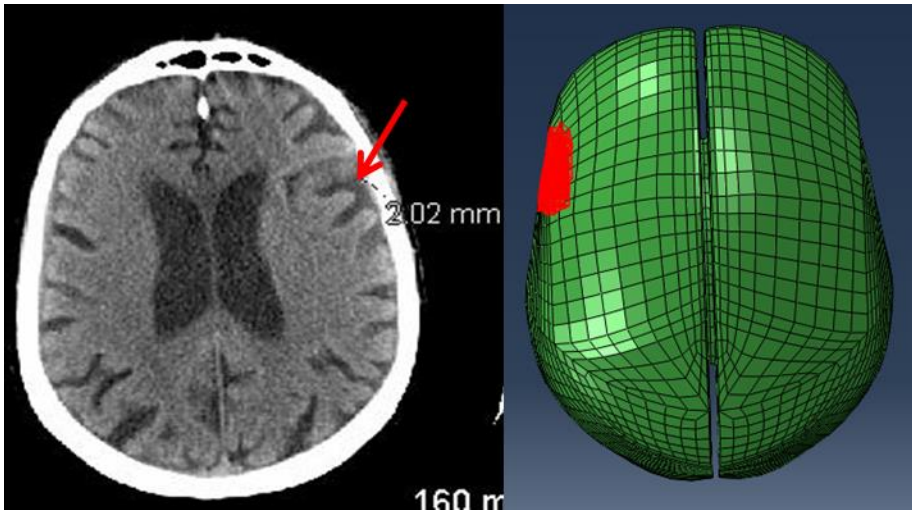

Figure 6. UCDBTM region of interest representing the region of the left subdural hematoma (red)

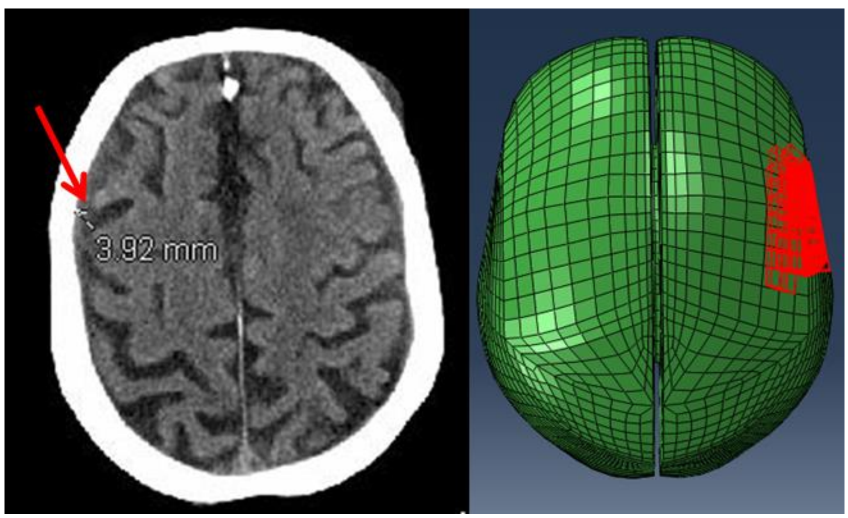

Figure 7. UCDBTM region of interest representing the region of the right subdural hematoma (red)

Finite element modeling results

Table 2. UCDBTM results for the left subdural hematoma region. Bold signifies significance between the SDH region and the cerebrum ($p < 0.05$).

Velocity (m/s)	Pressure (Pa)	MPS	VMS (Pa)	Shear stress (Pa)	Shear Strain	Strain rate (s^{-1})	Product (s^{-1})	Avg MPS	Avg VMS (Pa)
2.24	175257 (24095)	0.147 (0.008)	4361 (171.7)	1809 (94.9)	0.208 (0.01)	21.3 (1.1)	3.1 (0.33)	0.106 (0.007)	3157 (219.1)
Significance	**0.015**	**0.001**	**0.001**	**0.002**	**0.001**	**0.003**	**0.002**	**0.001**	**0.001**
3.33	347584 (39022)	0.255 (0.02)	8333 (270.8)	3755 (147.3)	0.407 (0.02)	53.2 (2.4)	13.6 (1.6)	0.154 (0.02)	5226 (334.1)
Significance	**0.032**	**0.001**	**0.001**	**0.001**	**0.001**	**0.002**	**0.001**	**0.005**	**0.000**

Table 3. UCDBTM results for the right subdural hematoma region. Bold signifies significance between the SDH region and the cerebrum ($p < 0.05$).

Velocity (m/s)	Pressure (Pa)	MPS	VMS (Pa)	Shear stress (Pa)	Shear Strain	Strain rate (s^{-1})	Product (s^{-1})	Avg MPS	Avg VMS (Pa)
2.24	123044 (12800)	0.125 (0.007)	3781 (175.3)	1520 (73.7)	0.17 (0.007)	15.8 (1.2)	2.0 (0.3)	0.094 (0.006)	2953 (212.6)
Significance	**0.009**	**0.001**	**0.001**	**0.001**	**0.001**	**0.001**	**0.001**	**0.001**	**0.001**
3.33	170883 (2802)	0.241 (0.003)	7775 (196.0)	2953 (92.1)	0.318 (0.01)	37.7 (1.0)	9.1 (0.3)	0.171 (0.004)	5572 (57.8)
Significance	**0.009**	**0.001**	**0.001**	**0.001**	**0.001**	**0.001**	**0.001**	**0.001**	**0.001**

Table 4. UCDBTM results for the cerebrum.

Velocity (m/s)	Pressure (Pa)	MPS	VMS (Pa)	Shear stress (Pa)	Shear Strain	Strain rate (s^{-1})	Product (s^{-1})	Avg MPS	Avg VMS (Pa)
2.24	522593 (145632)	0.272 (0.02)	8445 (571.3)	3085 (288.7)	0.356 (0.03)	31.6 (2.6)	8.6 (1.3)	0.052 (0.003)	1697 (91.7)
3.33	754373 (215497)	0.537 (0.01)	16831 (491.9)	6728 (97.4)	0.737 (0.02)	69.7 (3.1)	37.4 (2.5)	0.092 (0.002)	3053 (95.4)

Case 7

Case #7 involved a 44 year old male with no record of previous head injury. He was giving a presentation, passed out and hit his head on the occipital area on the floor. The medical scans showed a contusion in the frontal lobe, subdural hematoma in the occipital region and subarachnoid hemorrhage.

Mathematic Dynamic Models (MAYDMO) reconstructions

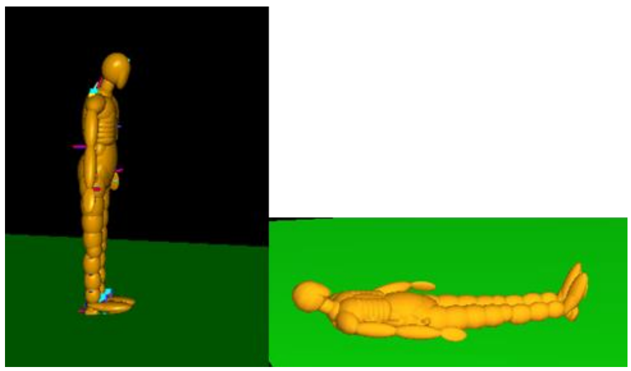

Figure 1. Simulation 1

Impact velocity: 6.2 m/s

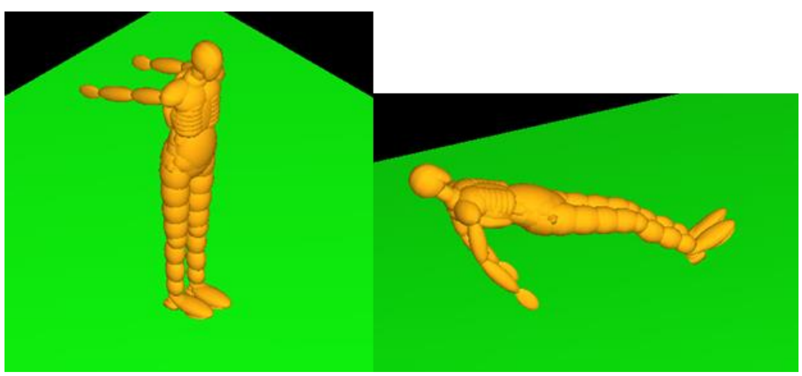

Figure 2. Simulation 2

Impact velocity: 5.0 m/s

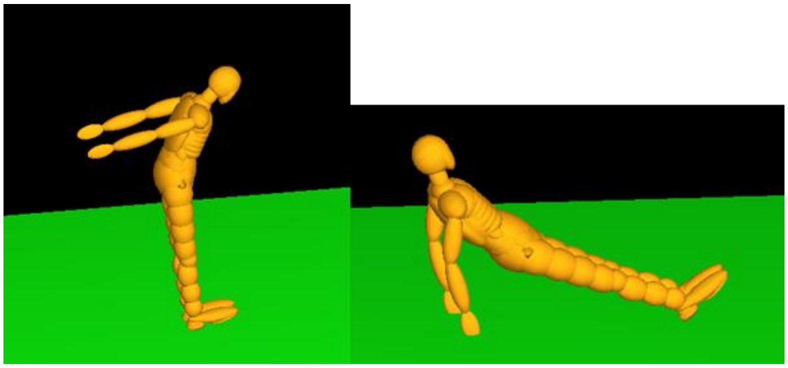

Figure 3. Simulation 3

Impact velocity: 3.9 m/s

Medical imaging (MRI scans)

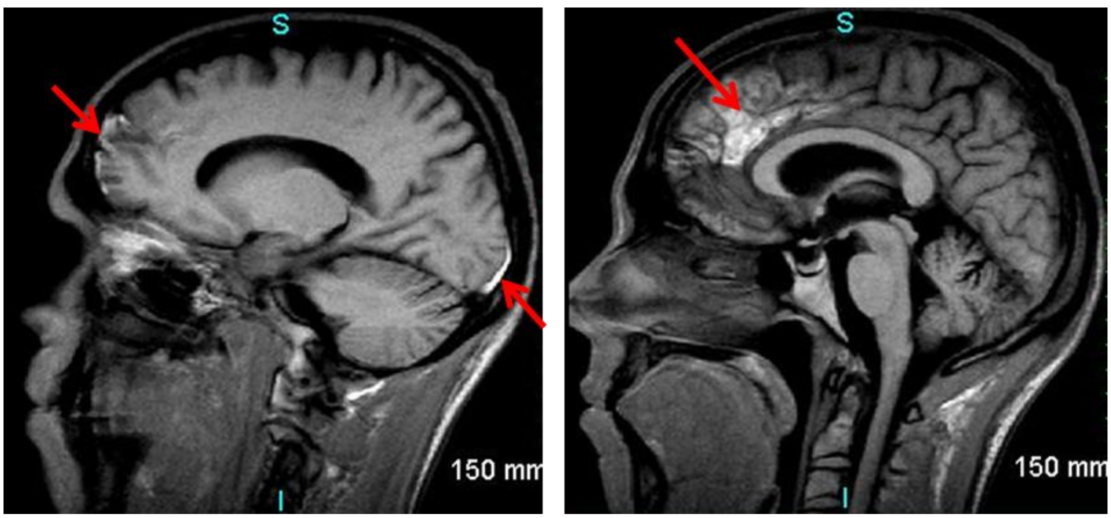

Figure 4. Medical images showing: (left) contusion in frontal lobe, and subdural hematoma in occipital region (right) subarachnoid hemorrhage (red arrows).

Physical reconstruction

The impact location was derived from the Neurotrauma injury report form. Only the 3.9 and 5.0 m/s condition was conducted as the accelerations were approaching the sensor tolerances at that velocity. To go higher would have damaged the equipment.

Figure 5. Hybrid III physical reconstruction of case 7.

Table 1. Dynamic response peak resultant values for the reconstruction

	Acceleration	
Velocity (m/s)	Linear (g)	Rotational (rad/s^2)
3.9	308.2 (2.7)	21287 (845.7)
5.0	472.5 (22.1)	33695 (372.0)

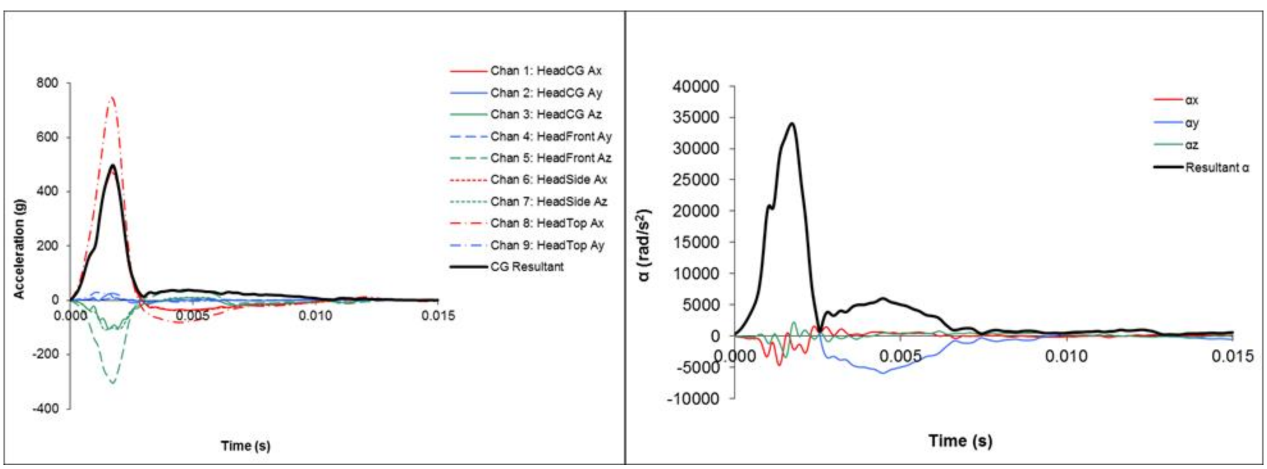

Figure 6. Sample dynamic response curves for the physical reconstruction of case 7. Linear acceleration presented on the left, rotational on the right.

Finite element model region of interest and sizing

The brain was measured to be 13.5 cm high from brainstem to top of the head, 17 cm long from front to back and 12.2 cm wide from ear to ear. The UCDBTM was scaled to the closest dimensions which were: 14.0 cm high, 17.6 cm long, and 13.1 cm wide.

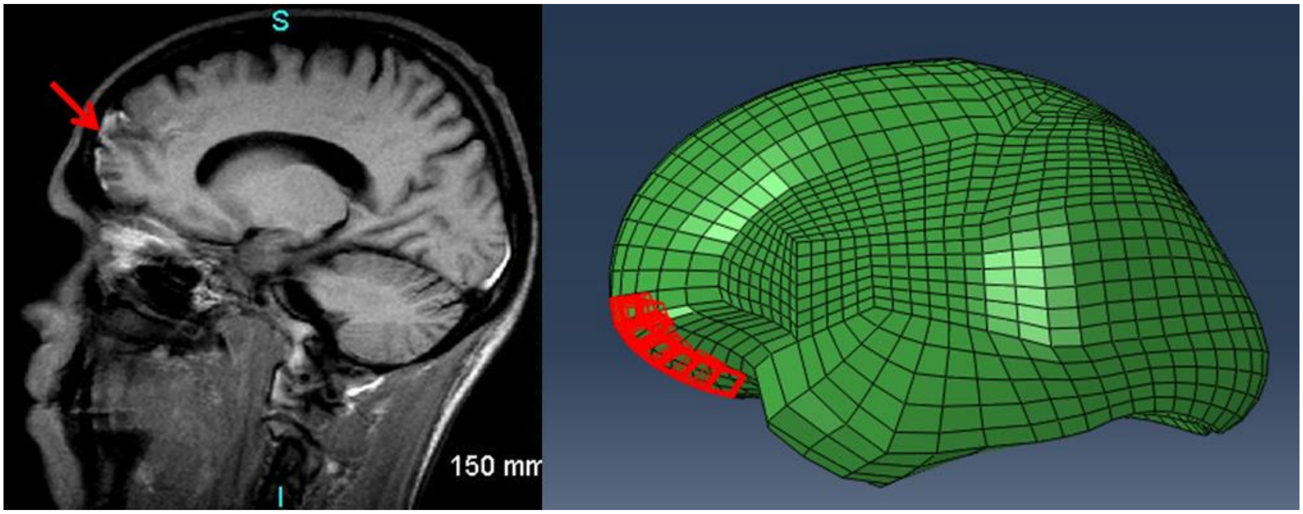

Figure 7. UCDBTM region of interest representing the region of the contusion (red)

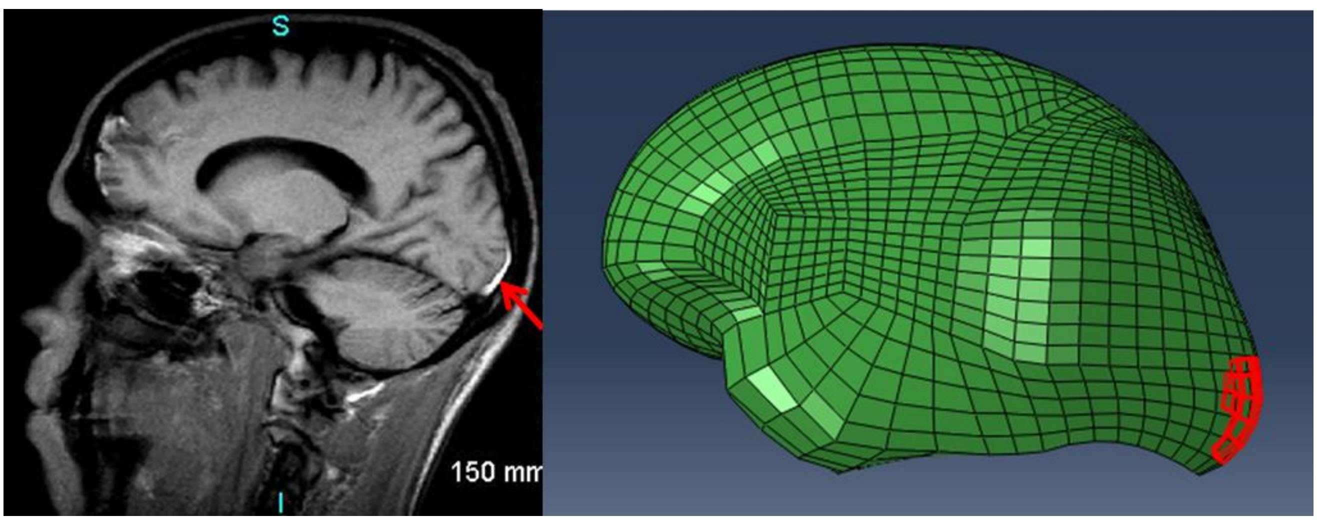

Figure 8. UCDBTM region of interest representing the region of the subdural hematoma (red)

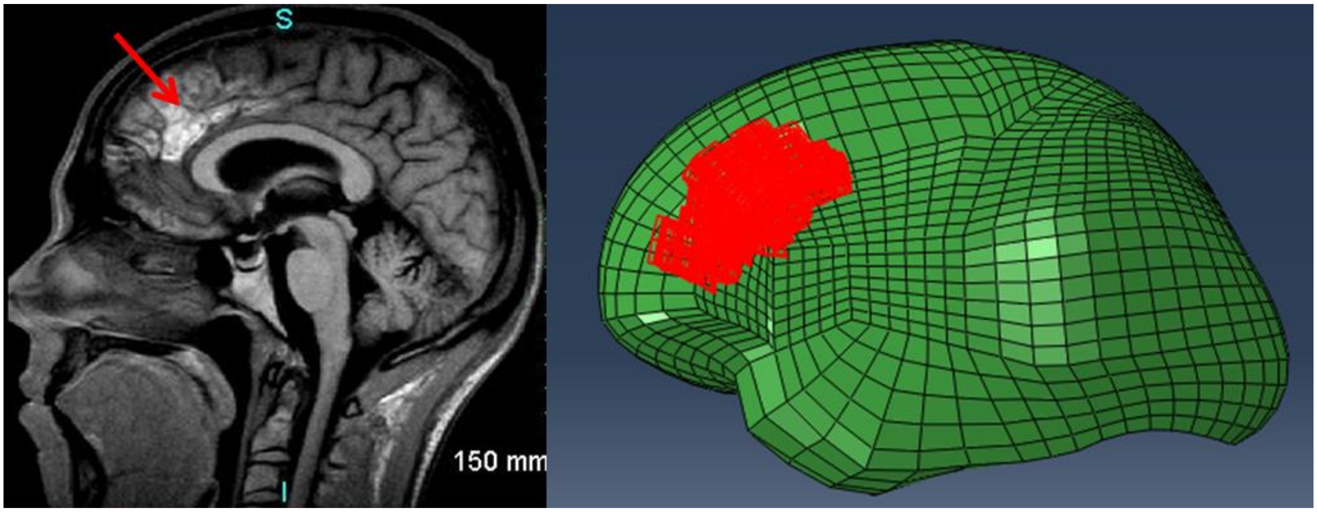

Figure 9. UCDBTM region of interest representing the region of the subarachnoid hemorrhage (red)

Finite element modeling results

Table 2. UCDBTM results for the contusion region. Bold signifies significance between the contusion region and the cerebrum ($p < 0.05$).

Velocity (m/s)	Pressure (Pa)	MPS	VMS (Pa)	Shear stress (Pa)	Shear Strain	Strain rate (s^{-1})	Product (s^{-1})	Avg MPS	Avg VMS (Pa)
3.9	1851790 (531107)	0.561 (0.014)	19536 (520.4)	10380 (327.3)	1.10 (0.03)	136.9 (4.6)	76.8 (3.1)	0.152 (0.002)	5545 (136.4)
Significance	0.553	**0.037**	0.210	1.000	1.000	**0.029**	0.122	**0.003**	**0.001**
5.0	2089370 (51595)	0.655 (0.033)	23797 (1097)	10172 (166.1)	1.08 (0.02)	168 (8.5)	110.3 (11.1)	0.209 (0.006)	7665 (218.5)
Significance	0.405	**0.001**	**0.004**	**0.001**	**0.001**	0.167	**0.009**	**0.001**	**0.001**

Table 3. UCDBTM results for the subdural hematoma region. Bold signifies significance between the SDH region and the cerebrum ($p < 0.05$).

Velocity (m/s)	Pressure (Pa)	MPS	VMS (Pa)	Shear stress (Pa)	Shear Strain	Strain rate (s^{-1})	Product (s^{-1})	Avg MPS	Avg VMS (Pa)
3.9	1071299 (147542)	0.204 (0.004)	6381 (205.7)	2989 (45.1)	0.307 (0.01)	31.5 (8.1)	6.4 (1.7)	0.110 (0.005)	3478 (357.0)
Significance	**0.004**	**0.001**	**0.001**	**0.001**	**0.001**	**0.001**	**0.001**	0.329	0.154
5.0	1700790 (386128)	0.326 (0.01)	10049 (636.3)	4444 (33.2)	0.465 (0.007)	120.5 (48.6)	39.6 (16.8)	0.12 (0.004)	4228 (88.9)
Significance	0.137	**0.001**	**0.001**	**0.001**	**0.001**	0.106	**0.001**	0.946	0.727

Table 4. UCDBTM results for the subarachnoid hemorrhage region. Bold signifies significance between the SAH region and the cerebrum ($p < 0.05$).

Velocity (m/s)	Pressure (Pa)	MPS	VMS (Pa)	Shear stress (Pa)	Shear Strain	Strain rate (s^{-1})	Product (s^{-1})	Avg MPS	Avg VMS (Pa)
3.9	947520 (113622)	0.423 (0.005)	13631 (50.4)	6537 (148.0)	0.63 (0.019)	65.1 (1.1)	27.5 (0.35)	0.119 (0.005)	3991 (128.1)
Significance	**0.002**	**0.001**	**0.001**	**0.001**	**0.001**	**0.003**	**0.001**	0.094	**0.008**
5.0	1122595 (155218)	0.507 (0.004)	16095 (236.0)	7389 (117.6)	0.757 (0.018)	54.2 (22.3)	27.4 (11.2)	0.159 (0.002)	6359 (1680)
Significance	**0.011**	**0.001**	**0.001**	**0.001**	**0.001**	**0.001**	**0.001**	**0.001**	0.103

Table 5. UCDBTM results for the cerebrum.

Velocity (m/s)	Pressure (Pa)	MPS	VMS (Pa)	Shear stress (Pa)	Shear Strain	Strain rate (s^{-1})	Product (s^{-1})	Avg MPS	Avg VMS (Pa)
3.9	2071552 (252607)	0.621 (0.03)	20038 (263.1)	10380 (327.3)	1.1 (0.03)	112.0 (12.0)	69.4 (5.8)	0.100 (0.014)	2980 (338.0)
5.0	2325030 (435841)	0.844 (0.02)	28531 (852.8)	12215 (375.1)	1.35 (0.03)	179.9 (8.7)	151.9 (10.0)	0.120 (0.007)	4289 (264.7)

Case 8

Case #8 involved a 74 year old female with no record of previous head injury. She lost her balance and fell, hitting her head on the pavement. The medical scans showed left frontoparietal temporal acute subdural hematoma.

Mathematic Dynamic Models (MAYDMO) reconstructions

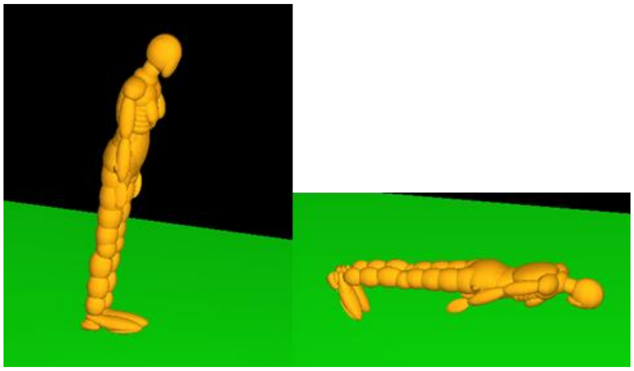

Figure 1. Simulation 1

Impact velocity: 4.53 m/s

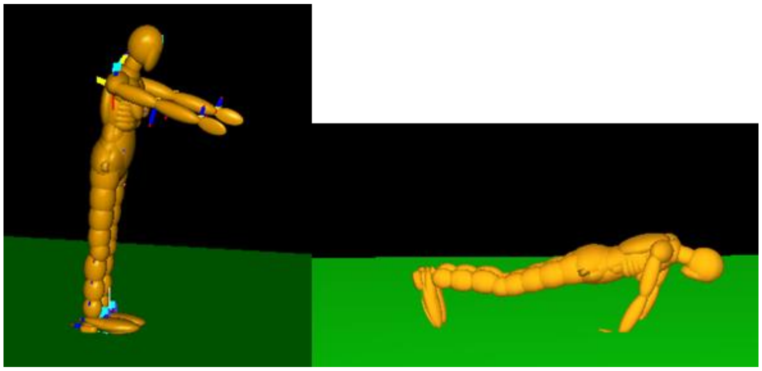

Figure 2. Simulation 2

Impact velocity: 3.3 m/s

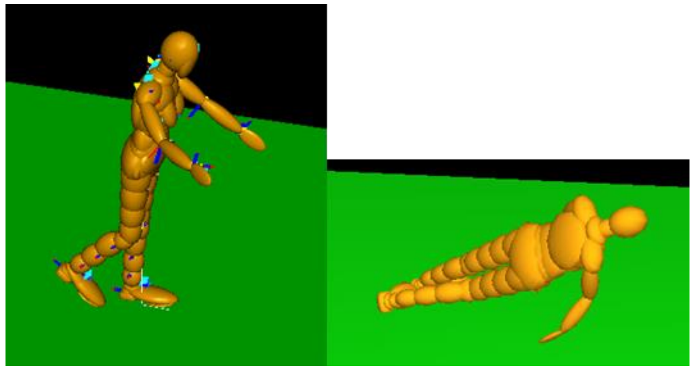

Figure 3. Simulation 3

Impact velocity: 4.8 m/s

Medical imaging (CT scans)

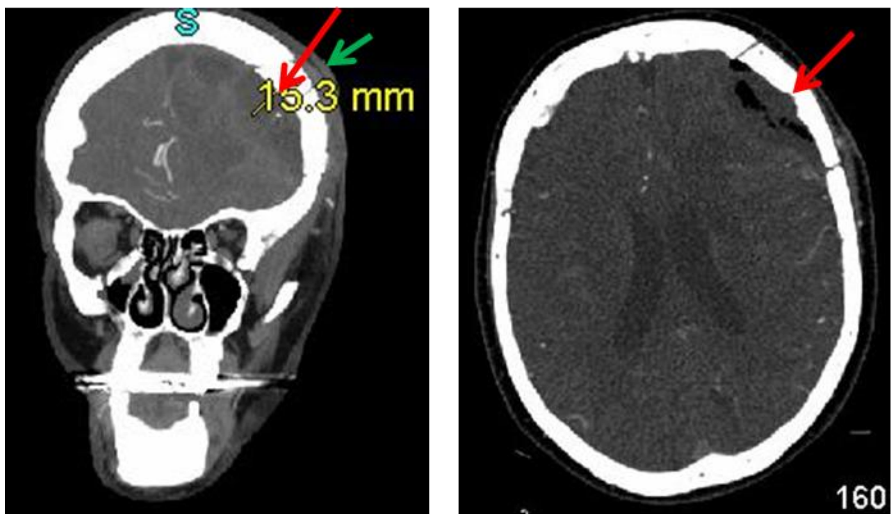

Figure 4. Medical images showing: subdural hematoma (red arrows). Impact site indicated by green arrow.

Physical reconstruction

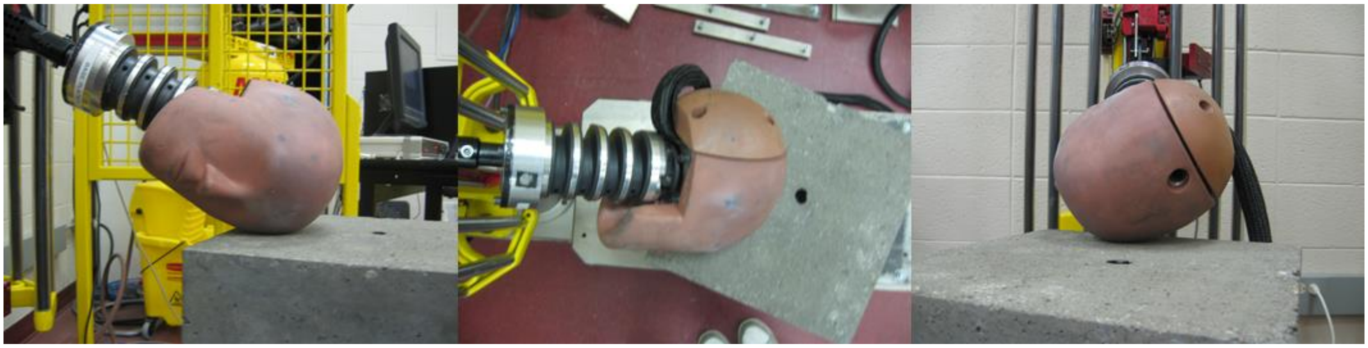

Figure 5. Hybrid III physical reconstruction of case 8.

Table 1. Dynamic response peak resultant values for the reconstruction

	Acceleration	
Velocity (m/s)	Linear (g)	Rotational (rad/s^2)
3.3	295.4 (1.0)	33614 (202.9)
4.5	490.8 (14.9)	55695 (1444.8)
4.8	500.7 (21.8)	57724 (2196.3)

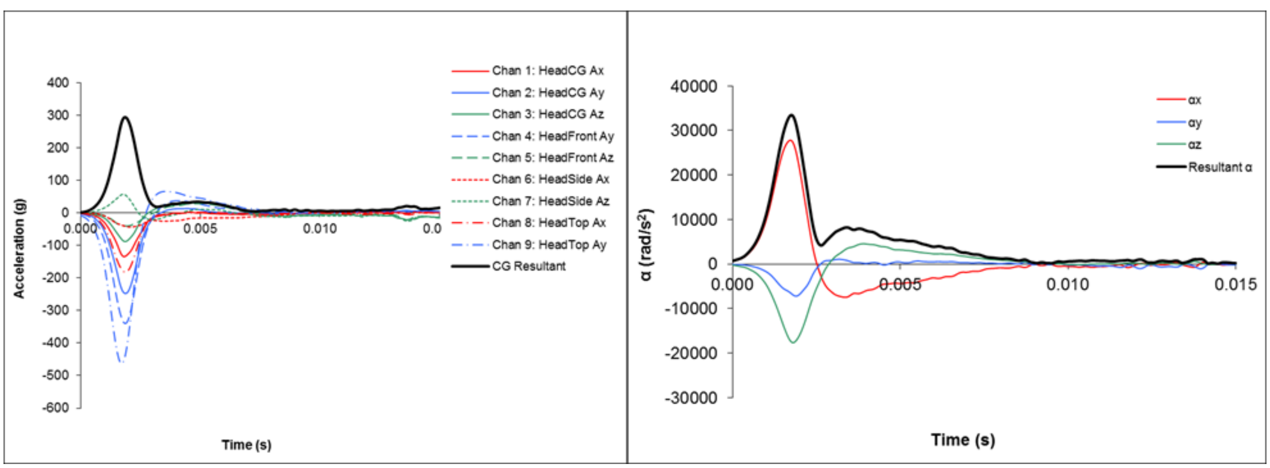

Figure 6. Sample dynamic response curves for the physical reconstruction of case 8. Linear acceleration presented on the left, rotational on the right.

Finite element model region of interest and sizing

The brain was measured to be 13 cm high from brainstem to top of the head, 15.5 cm long from front to back and 12.7 cm wide from ear to ear. The UCDBTM was scaled to the closest dimensions which were: 12.3 cm high, 15.3 cm long and 12.1 cm wide.

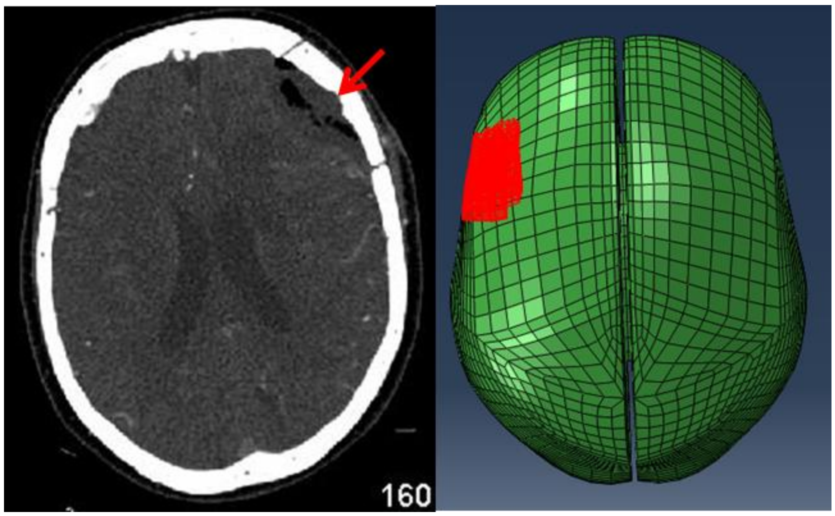

Figure 7. UCDBTM region of interest representing the region of the subdural hematoma (red)

Finite element modeling results

Table 2. UCDBTM results for the subdural hematoma region. Bold signifies significance between the SDH region and the cerebrum ($p < 0.05$).

Velocity (m/s)	Pressure (Pa)	MPS	VMS (Pa)	Shear stress (Pa)	Shear Strain	Strain rate (s^{-1})	Product (s^{-1})	Avg MPS	Avg VMS (Pa)
3.3	587120 (50032)	0.392 (0.009)	12804 (309.7)	4942 (219.9)	0.519 (0.015)	118.7 (2.8)	46.5 (2.2)	0.134 (0.002)	4596 (67.2)
Significance	0.154	**0.012**	**0.012**	**0.021**	**0.028**	**0.039**	**0.017**	**0.033**	**0.028**
4.5	1084661 (49653)	0.547 (0.024)	18187 (799.6)	6504 (236.2)	0.648 (0.016)	171.6 (17.2)	94.2 (13.7)	0.191 (0.007)	6598 (222.2)
Significance	0.052	**0.001**	**0.001**	**0.001**	**0.001**	**0.015**	**0.001**	**0.014**	**0.030**
4.8	1119598 (105372)	0.565 (0.018)	18697 (632.8)	6628 (325.9)	0.660 (0.007)	188.2 (5.9)	106.4 (6.7)	0.188 (0.004)	6480 (142.9)
Significance	0.123	**0.001**	**0.001**	**0.001**	**0.001**	**0.038**	**0.005**	**0.015**	**0.025**

Table 3. UCDBTM results for the cerebrum

Velocity (m/s)	Pressure (Pa)	MPS	VMS (Pa)	Shear stress (Pa)	Shear Strain	Strain rate (S^{-1})	Product (S^{-1})	Avg MPS	Avg VMS (Pa)
3.3	1128708 (238835)	0.853 (0.004)	28666 (101.1)	13438 (178.9)	1.34 (0.035)	157.9 (0.64)	157.9 (0.64)	0.115 (0.001)	3995 (30.4)
4.5	2150085 (430541)	109 (0.042)	40198 (1367)	17390 (500.1)	1.68 (0.03)	221.8 (6.5)	241.1 (14.0)	0.149 (0.004)	5623 (80.5)
4.8	2597114 (958025)	1.13 (0.02)	42154 (1438)	18184 (307.7)	1.73 (0.02)	226.9 (11.4)	257.3 (17.1)	0.160 (0.004)	5957 (53.9)

Case 9

Case #9 involved a 58 year old male with no record of previous head injury. Exited a vehicle, walked a few meters and fell onto the road, hitting his head. The medical scans indicated subdural hematoma and subarachnoid hemorrhage.

Mathematic Dynamic Models (MAYDMO) reconstructions

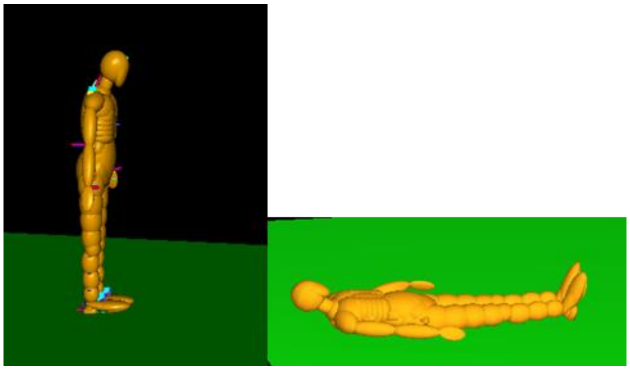

Figure 1. Simulation 1

Impact velocity: 6.2 m/s

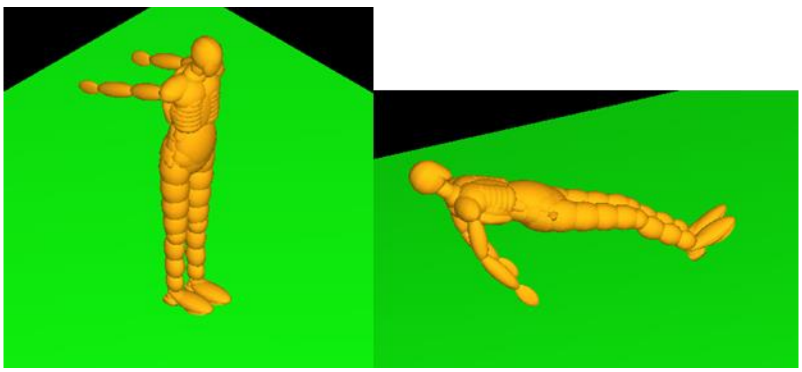

Figure 2. Simulation 2

Impact velocity: 5.0 m/s

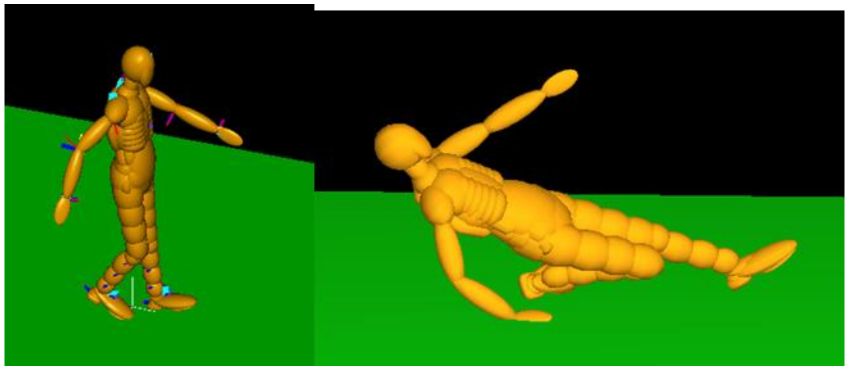

Figure 3. Simulation 3

Impact velocity: 4.8 m/s

Medical imaging (CT scans)

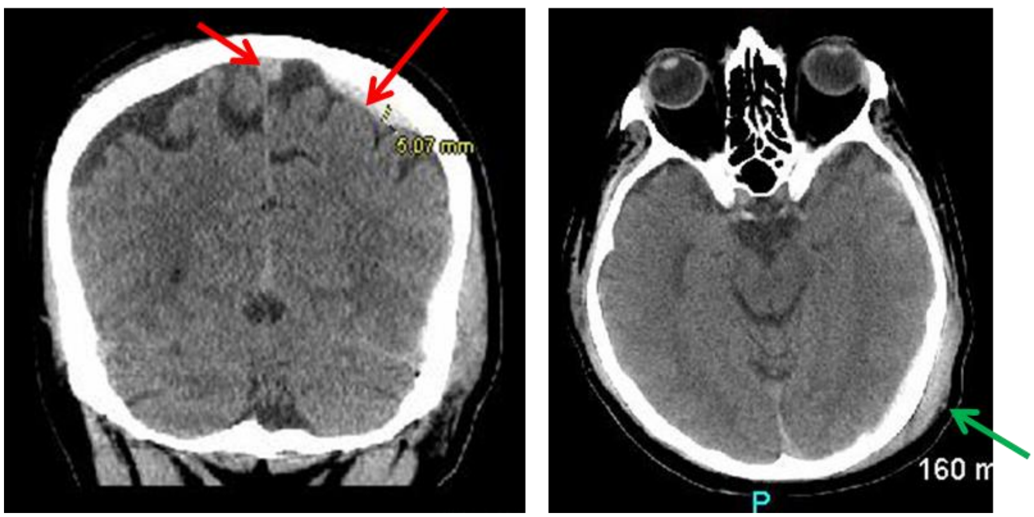

Figure 4. Medical images showing: (left) subdural hematoma on right and subarachnoid hemorrhage at crown (red arrows). Impact site indicated by green arrow (right).

Physical reconstruction

Only the 4.8 m/s condition was conducted as the accelerations were approaching the sensor tolerances at that velocity. To go higher would have damaged the equipment.

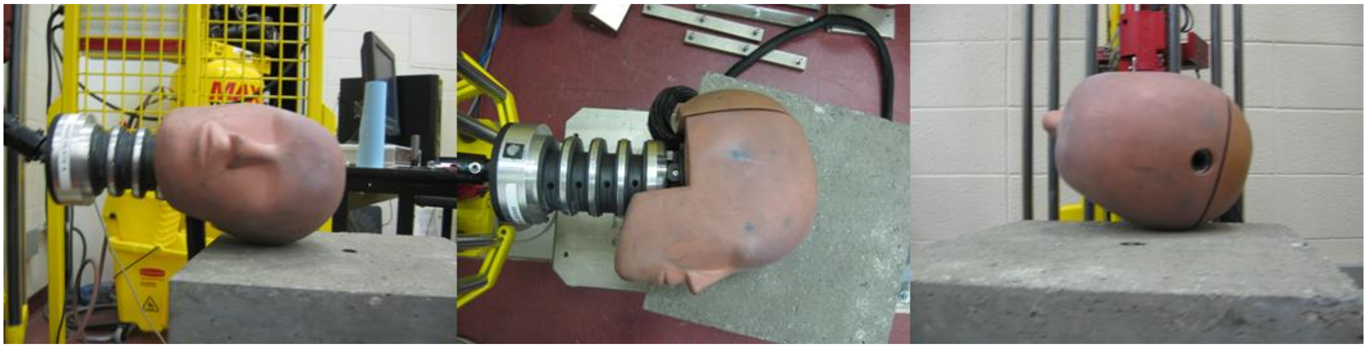

Figure 5. Hybrid III physical reconstruction of case 9

Table 1. Dynamic response peak resultant values for the reconstruction

	Acceleration	
Velocity (m/s)	Linear (g)	Rotational (rad/s^2)
4.8	532.8 (19.1)	63764 (1038.5)

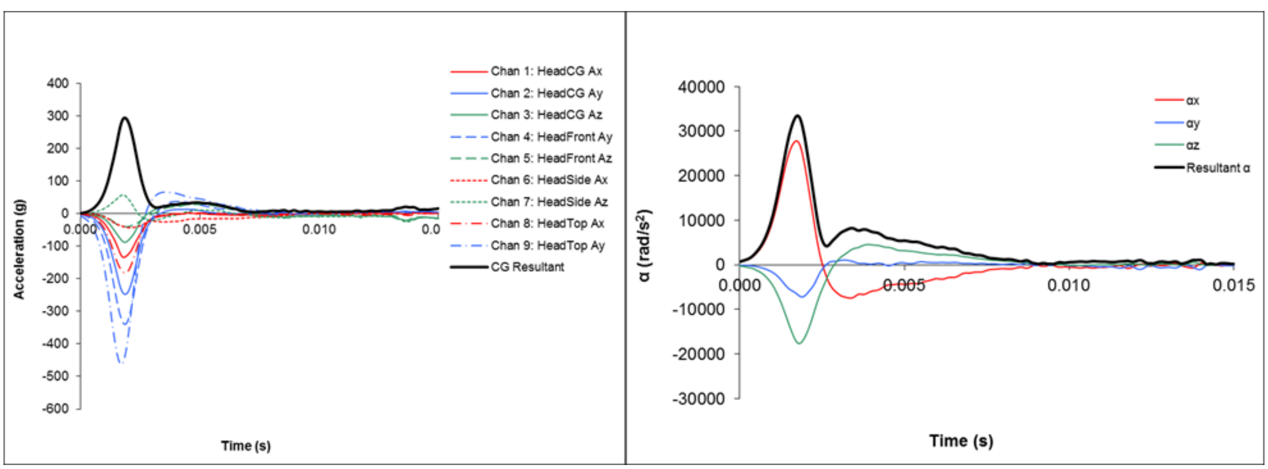

Figure 6. Sample dynamic response curves for the physical reconstruction of case 9. Linear acceleration presented on the left, rotational on the right.

Finite element model region of interest and sizing

The brain was measured to be 13 cm high from brainstem to top of the head, 15.7 cm long from front to back and 13.8 cm wide from ear to ear. The UCDBTM was scaled to the closest dimensions which were: 12.3 cm high, 15.3 cm long and 12.1 cm wide.

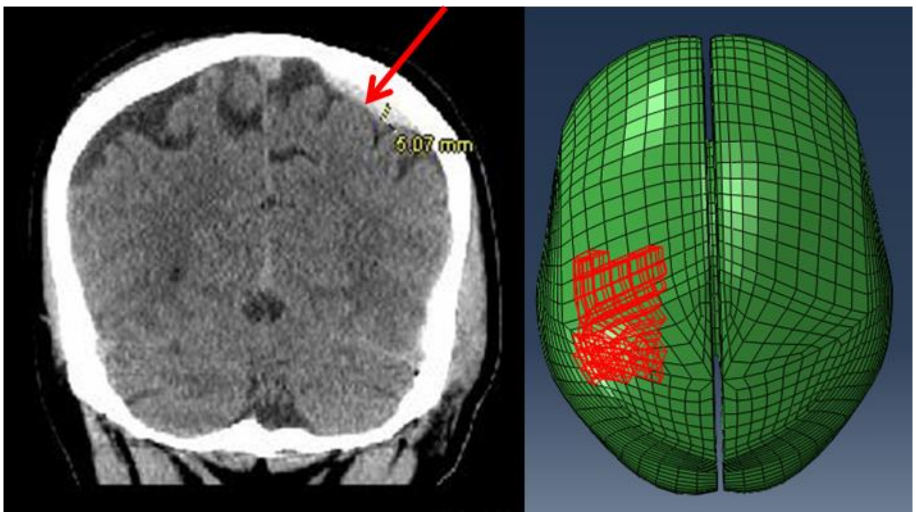

Figure 7. UCDBTM region of interest representing the region of the subdural hematoma (red)

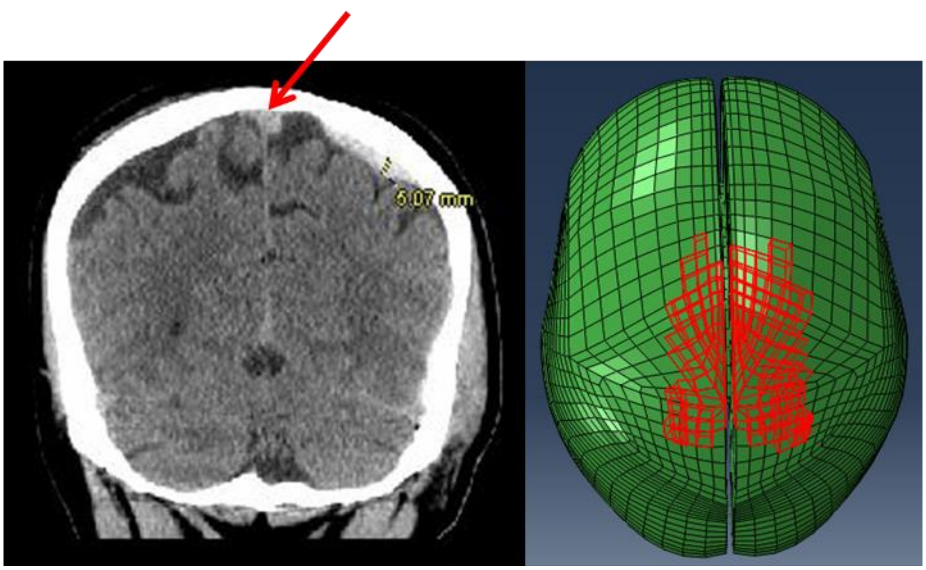

Figure 8. UCDBTM region of interest representing the region of the subarachnoid hemorrhage (red)

Finite element modeling results

Table 2. UCDBTM results for the subdural hematoma region. Bold signifies significance between the SDH region and the cerebrum ($p < 0.05$).

Velocity (m/s)	Pressure (Pa)	MPS	VMS (Pa)	Shear stress (Pa)	Shear Strain	Strain rate (s^{-1})	Product (s^{-1})	Avg MPS	Avg VMS (Pa)
4.8	793973 (52163)	0.444 (0.011)	14389 (255.4)	5901 (137.2)	0.621 (0.007)	134.5 (3.4)	59.7 (3.0)	0.148 (0.002)	4683 (468.1)
Significance	**0.016**	**0.001**	**0.001**	**0.001**	**0.001**	**0.018**	**0.002**	0.385	0.070

Table 3. UCDBTM results for the subarachnoid hemorrhage region. Bold signifies significance between the SAH region and the cerebrum ($p < 0.05$).

Velocity (m/s)	Pressure (Pa)	MPS	VMS (Pa)	Shear stress (Pa)	Shear Strain	Strain rate (s^{-1})	Product (s^{-1})	Avg MPS	Avg VMS (Pa)
4.8	1194823 (709179)	0.461 (0.008)	18873 (279.6)	10576 (113.4)	0.86 (0.012)	219.7 (3.7)	101.4 (3.4)	0.123 (0.002)	6512 (23.9)
Significance	0.088	**0.001**	**0.001**	**0.004**	**0.001**	0.074	**0.013**	**0.028**	**0.001**

Table 4. UCDBTM results for the cerebrum region.

Velocity (m/s)	Pressure (Pa)	MPS	VMS (Pa)	Shear stress (Pa)	Shear Strain	Strain rate (s^{-1})	Product (s^{-1})	Avg MPS	Avg VMS (Pa)
4.8	2531651 (745724)	0.834 (0.015)	29928 (621.0)	13873 (919.6)	1.27 (0.006)	187.1 (23.3)	156.2 (21.9)	0.143 (0.01)	5351 (42.5)

Case 10

Case #10 involved a 74 year old male with no record of previous head injury. He slipped on the ice and hit his head. The medical scans showed subarachnoid hemorrhage in prepontine basal cisterns, and frontal contusions.

Mathematic Dynamic Models (MAYDMO) reconstructions

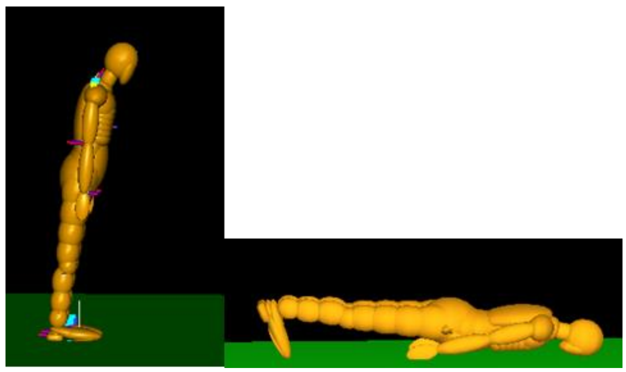

Figure 1. Simulation 1

Impact velocity: 4.87 m/s

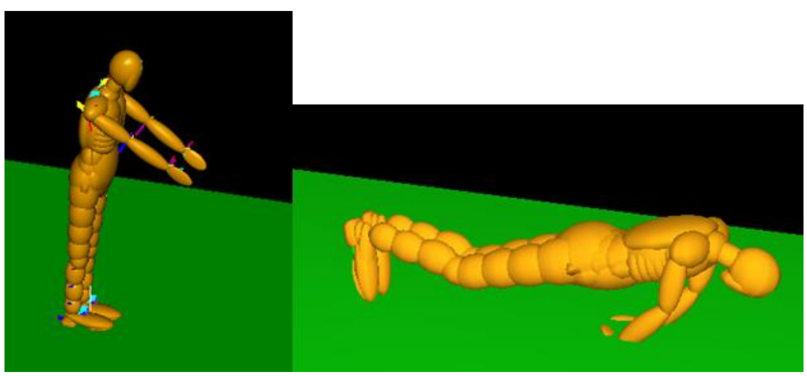

Figure 2. Simulation 2

Impact velocity: 3.6 m/s

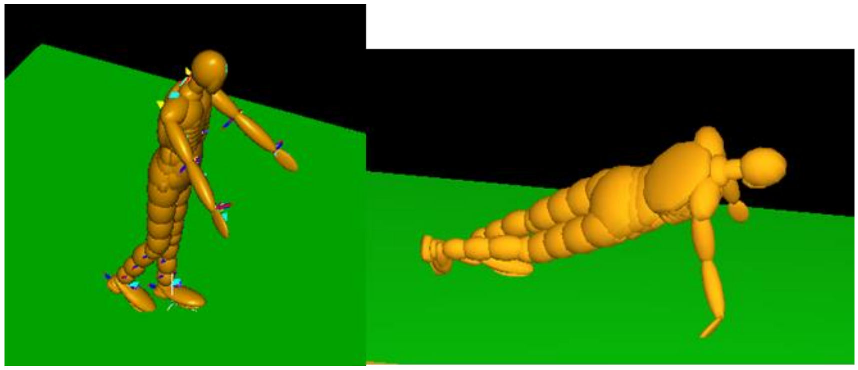

Figure 3. Simulation 3

Impact velocity: 3.8 m/s

Medical imaging (CT scans)

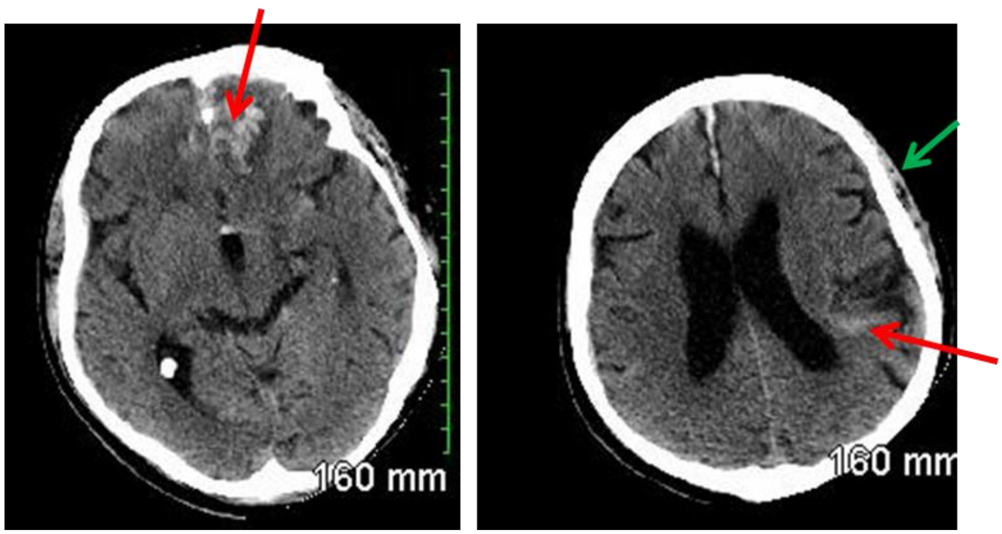

Figure 4. Medical images showing: (left) contusion in frontal lobe, (right) subarachnoid hemorrhage (red arrows). Impact site shown by green arrow.

Physical reconstruction

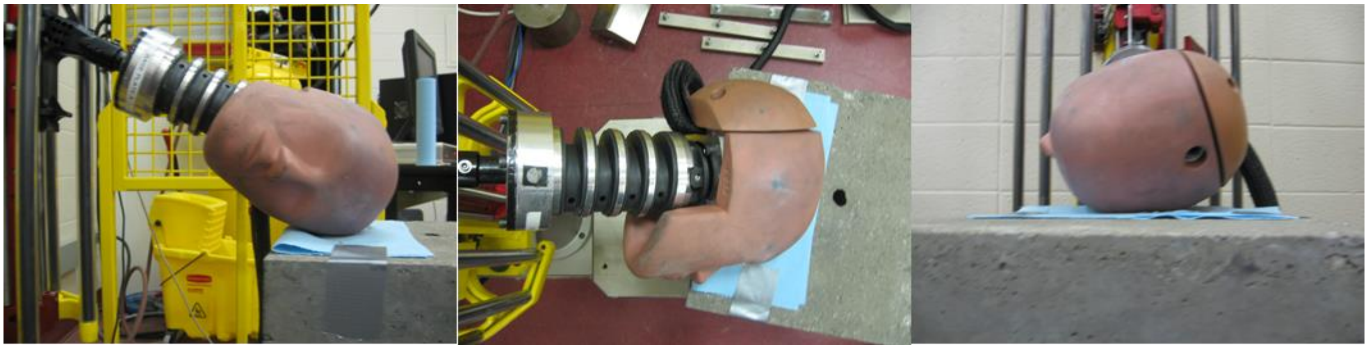

Figure 5. Hybrid III physical reconstruction of case 10

Table 1. Dynamic response peak resultant values for the reconstruction

	Acceleration	
Velocity (m/s)	Linear (g)	Rotational (rad/s^2)
3.6	357.6 (8.0)	38552 (1152)
3.8	386.4 (10.7)	41581 (1286)
4.9	623.1 (26.3)	65975 (2215)

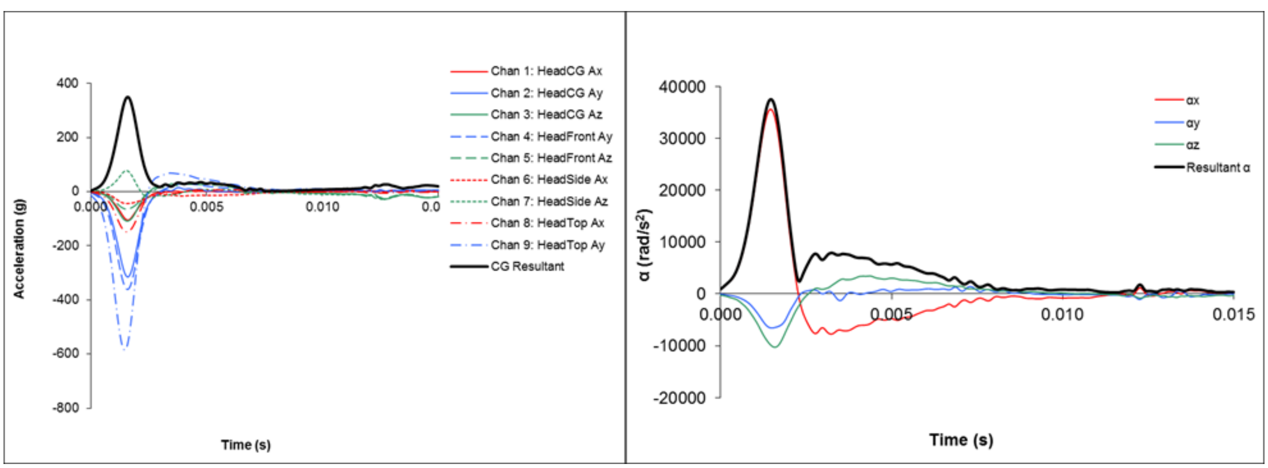

Figure 6. Sample dynamic response curves for the physical reconstruction of case 10. Linear acceleration presented on the left, rotational on the right.

Finite element model region of interest and sizing

The brain was measured to be 13 cm high from brainstem to top of the head, 16.5 cm long from front to back and 14 cm wide from ear to ear. The UCDBTM was scaled to the closest dimensions which were: 13.0 cm high, 16.4 cm long and 12.8 cm wide.

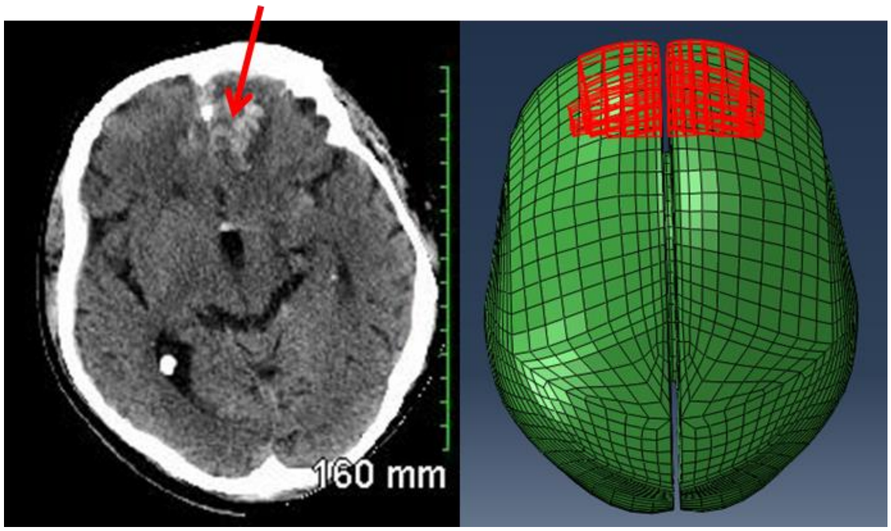

Figure 7. UCDBTM region of interest representing the region of the contusion (red)

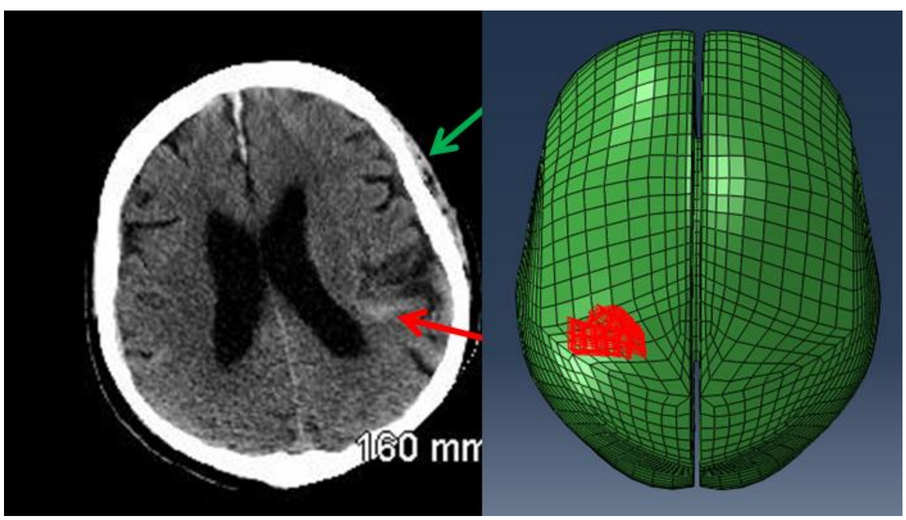

Figure 8. UCDBTM region of interest representing the region of the subarachnoid hemorrhage (red)

Finite element modeling results

Table 2. UCDBTM results for the contusion region. Bold signifies significance between the contusion region and the cerebrum ($p < 0.05$).

Velocity (m/s)	Pressure (Pa)	MPS	VMS (Pa)	Shear stress (Pa)	Shear Strain	Strain rate (s^{-1})	Product (s^{-1})	Avg MPS	Avg VMS (Pa)
3.6	617643 (14394)	0.242 (0.004)	8130 (228.3)	4439 (112.0)	0.465 (0.011)	36.7 (0.58)	8.9 (0.29)	0.070 (0.001)	2422 (37.2)
Significance	**0.012**	**0.001**	**0.001**	**0.001**	**0.001**	**0.009**	**0.003**	**0.001**	**0.001**
3.8	685397 (89951)	0.254 (0.002)	8530 (10.1)	4594 (18.0)	0.477 (0.008)	51.4 (22.7)	13.1 (5.9)	0.068 (0.007)	2391 (237.1)
Significance	**0.011**	**0.001**	**0.001**	**0.001**	**0.001**	**0.047**	**0.007**	**0.001**	**0.001**
4.9	1196140 (143220)	0.429 (0.013)	14331 (290.4)	7707 (75.2)	0.779 (0.005)	134.4 (11.3)	57.7 (6.5)	0.084 (0.001)	2977 (21.1)
Significance	**0.008**	**0.001**	**0.001**	**0.001**	**0.001**	0.142	**0.012**	**0.001**	**0.001**

Table 3. UCDBTM results for the subarachnoid hemorrhage region. Bold signifies significance between the SAH region and the cerebrum ($p < 0.05$).

Velocity (m/s)	Pressure (Pa)	MPS	VMS (Pa)	Shear stress (Pa)	Shear Strain	Strain rate (s^{-1})	Product (s^{-1})	Avg MPS	Avg VMS (Pa)
3.6	481864 (4194)	0.265 (0.005)	11475 (164.4)	4231 (96.6)	0.357 (0.015)	18.7 (1.2)	4.94 (0.39)	0.134 (0.01)	5918 (308.9)
Significance	**0.010**	**0.001**	**0.001**	**0.001**	**0.001**	**0.005**	**0.003**	0.055	**0.001**
3.8	523360 (13338)	0.277 (0.004)	12156 (260.0)	4466 (107.8)	0.374 (0.01)	19.7 (1.0)	5.4 (0.28)	0.138 (0.015)	5872 (50.1)
Significance	**0.007**	**0.001**	**0.001**	**0.001**	**0.001**	**0.010**	**0.006**	0.123	**0.001**
4.9	833037 (19886)	0.340 (0.016)	15589 (602.9)	6106 (174.6)	0.521 (0.02)	24.0 (0.95)	8.14 (0.5)	0.181 (0.02)	7290 (115.9)
Significance	**0.004**	**0.001**	**0.001**	**0.001**	**0.001**	**0.007**	**0.005**	0.126	**0.001**

Table 4. UCDBTM results for the cerebrum

Velocity (m/s)	Pressure (Pa)	MPS	VMS (Pa)	Shear stress (Pa)	Shear Strain	Strain rate (s^{-1})	Product (s^{-1})	Avg MPS	Avg VMS (Pa)
3.6	2647451 (802883)	0.933 (0.017)	35351 (835.8)	14973 (455.1)	1.51 (0.05)	148.2 (40.2)	137.9 (36.2)	0.118 (0.003)	4255 (51.1)
3.8	1988341 (494998)	0.963 (0.013)	36982 (910.5)	15398 (401.0)	1.54 (0.03)	128.1 (41.1)	123.1 (37.6)	0.121 (0.003)	4455 (45.1)
4.9	3514034 (795429)	1.17 (0.03)	45490 (2029)	18101 (816.1)	1.87 (0.04)	196.3 (57.7)	229.8 (68.6)	0.159 (0.006)	5800 (43.5)

Case 11

Case #11 involved a 54 year old female with no record of previous head injury. She was playing curling and slipped, fell backwards and hit her head. The medical scans showed large right temporal hemorrhagic contusion, subdural hematoma in the occipital region.

Mathematic Dynamic Models (MAYDMO) reconstructions

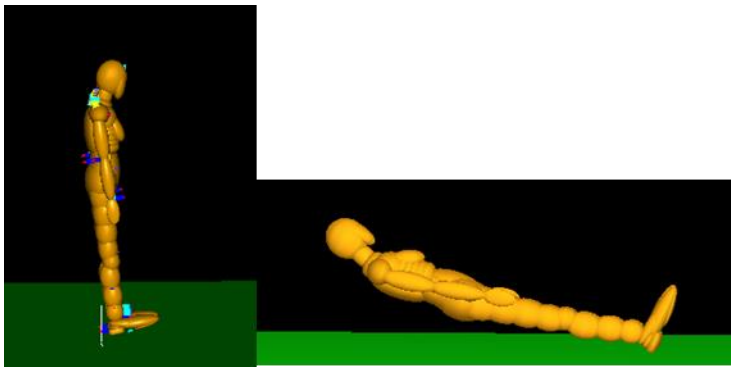

Figure 1. Simulation 1

Impact velocity: 5.76 m/s

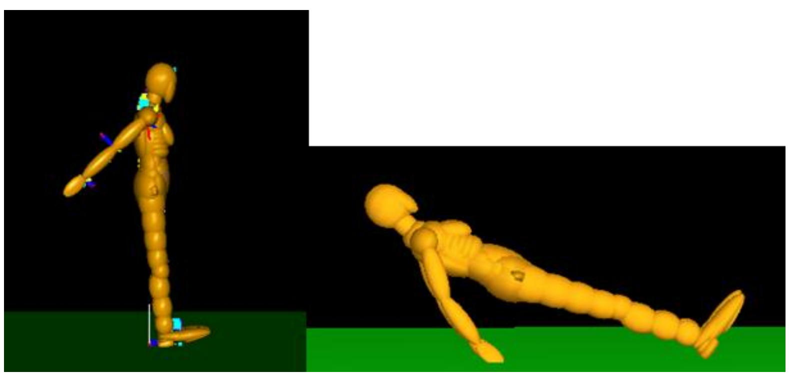

Figure 2. Simulation 2

Impact velocity: 4.21 m/s

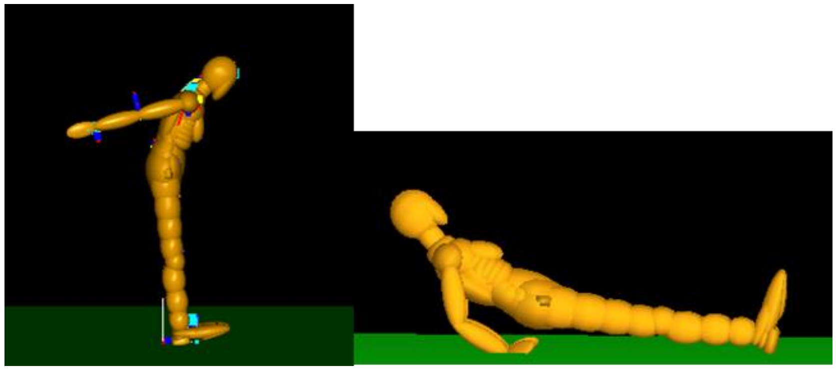

Figure 3. Simulation 3

Impact velocity: 3.7 m/s

Medical imaging (CT scans)

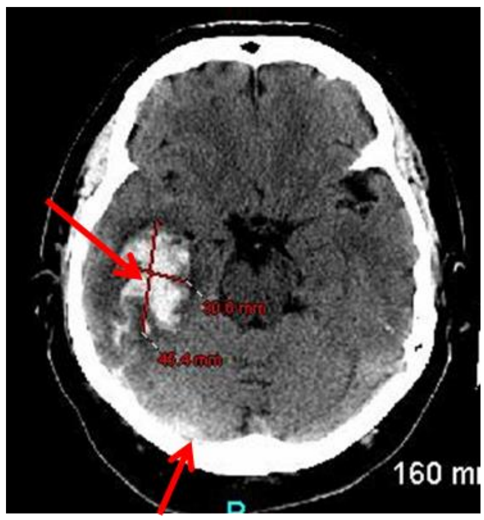

Figure 4. Medical images showing contusion (left arrow), and subdural hematoma in the occipital region (bottom arrow).

Physical reconstruction

The impact location was derived from the Neurotrauma injury report form. Only the 3.7 and 4.2 m/s condition was conducted as the accelerations were approaching the sensor tolerances at that velocity. To go higher would have damaged the equipment.

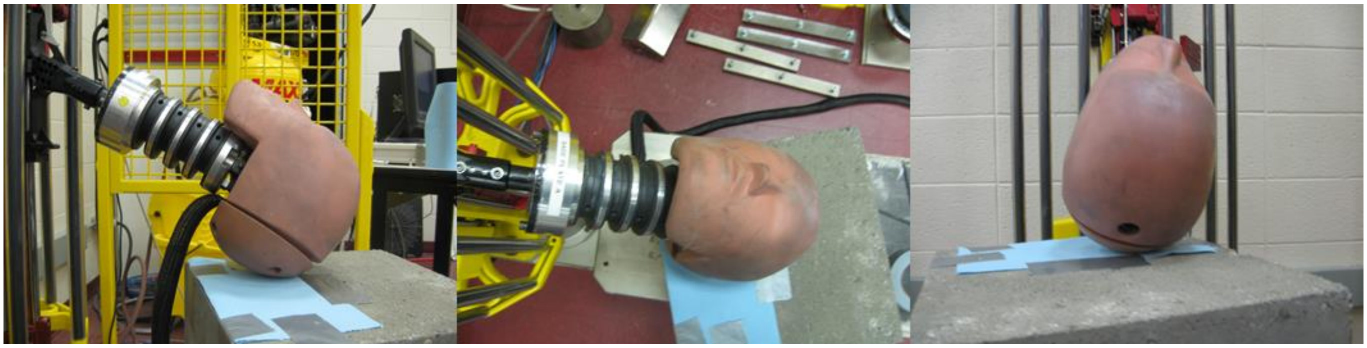

Figure 5. Hybrid III physical reconstruction of case 11

Table 1. Dynamic response peak resultant values for the reconstruction

	Acceleration	
Velocity (m/s)	Linear (g)	Rotational (rad/s^2)
3.7	268.4 (6.0)	14044 (487.7)
4.2	342.5 (2.5)	17986 (532.0)

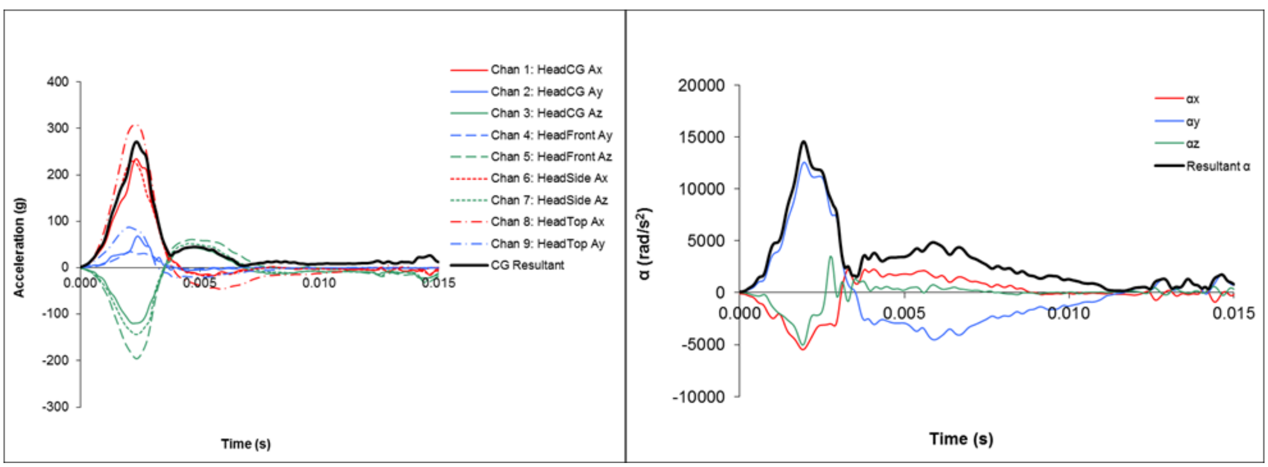

Figure 6. Sample dynamic response curves for the physical reconstruction of case 11. Linear acceleration presented on the left, rotational on the right.

Finite element model region of interest and sizing

The brain was measured to be 12 cm high from brainstem to top of the head, 16.4 cm long from front to back and 13.8 cm wide from ear to ear. The UCDBTM was scaled to the closest dimensions which were: 13.0 cm high, 16.4 cm long and 12.8 cm wide.

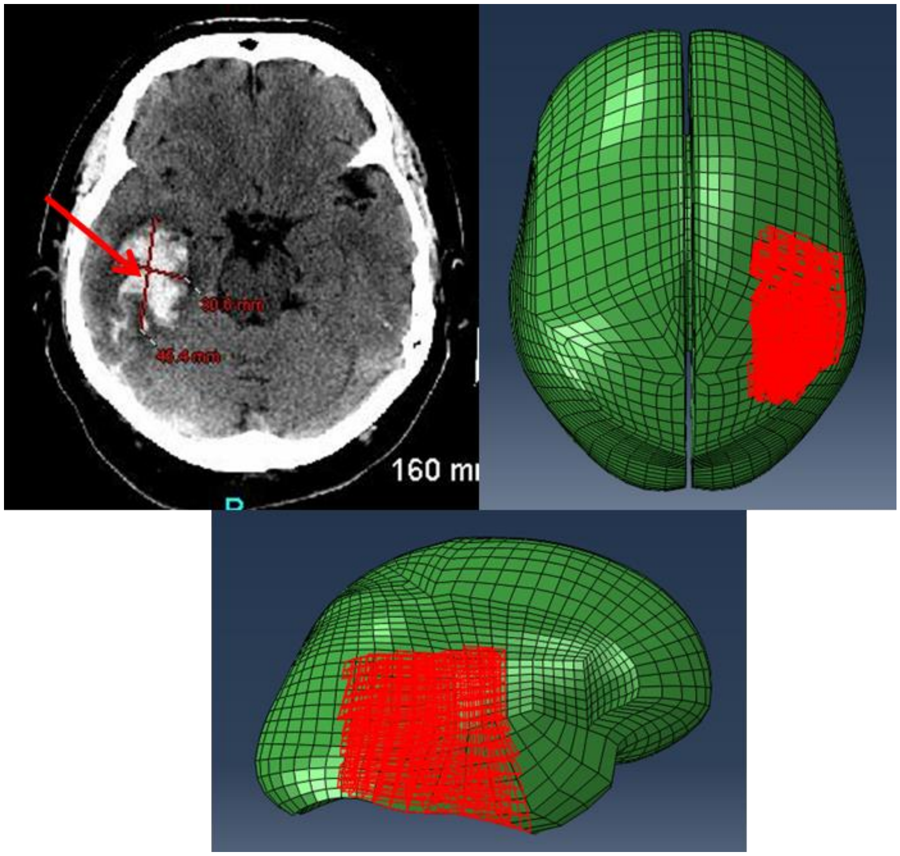

Figure 7. UCDBTM region of interest representing the region of the contusion (red)

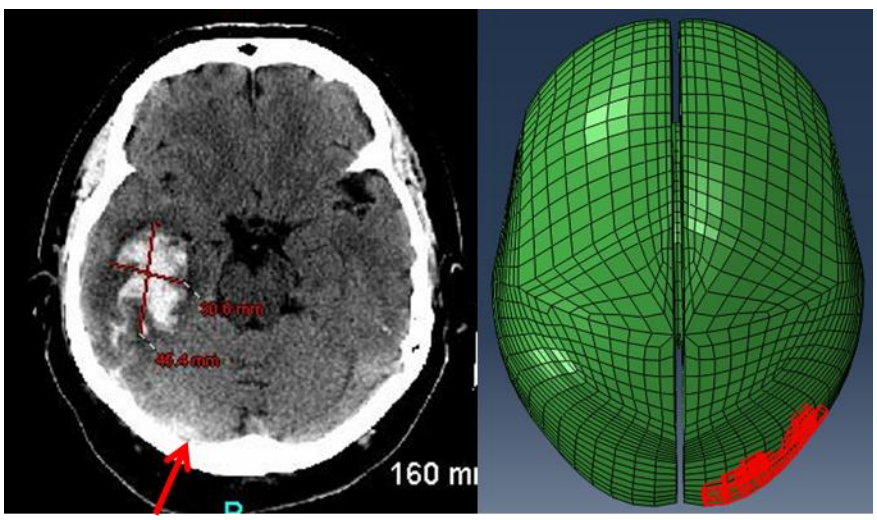

Figure 8. UCDBTM region of interest representing the region of the subdural hematoma (red)

Finite element modeling results

Table 1. UCDBTM results for the contusion region. Bold signifies significance between the contusion region and the cerebrum ($p < 0.05$).

Velocity (m/s)	Pressure (Pa)	MPS	VMS (Pa)	Shear stress (Pa)	Shear Strain	Strain rate (s^{-1})	Product (s^{-1})	Avg MPS	Avg VMS (Pa)
3.7	545972 (71542)	0.378 (0.014)	11622 (526.9)	5071 (3464)	0.441 (0.011)	66.2 (2.4)	25.0 (1.8)	0.080 (0.002)	2943 (52.5)
Significance	**0.006**	**0.004**	**0.001**	0.495	**0.001**	0.577	0.780	**0.018**	**0.010**
4.2	682552 (52519)	0.415 (0.022)	13060 (300.4)	5129 (233.1)	0.525 (0.038)	70.3 (10.2)	29.0 (3.1)	0.095 (0.022)	2950 (755.8)
Significance	**0.009**	**0.005**	**0.001**	**0.001**	**0.001**	**0.047**	0.631	0.705	0.529

Table 2. UCDBTM results for the subdural hematoma region. Bold signifies significance between the SDH region and the cerebrum ($p < 0.05$).

Velocity (m/s)	Pressure (Pa)	MPS	VMS (Pa)	Shear stress (Pa)	Shear Strain	Strain rate (s^{-1})	Product (s^{-1})	Avg MPS	Avg VMS (Pa)
3.7	692488 (128487)	0.228 (0.04)	7255 (395.4)	2949 (335.6)	0.288 (0.037)	43.5 (11.2)	9.7 (1.4)	0.090 (0.01)	2865 (57.1)
Significance	**0.038**	**0.001**	**0.001**	**0.001**	**0.001**	0.377	0.066	0.086	0.115
4.2	777051 (30557)	0.278 (0.019)	9412 (1105)	3016 (77.5)	0.315 (0.001)	54.5 (19.6)	15.3 (6.3)	0.107 (0.006)	3128 (503.8)
Significance	**0.012**	**0.001**	**0.001**	**0.001**	**0.001**	0.895	**0.035**	**0.007**	0.695

Table 3. UCDBTM results for the cerebrum.

Velocity (m/s)	Pressure (Pa)	MPS	VMS (Pa)	Shear stress (Pa)	Shear Strain	Strain rate (s^{-1})	Product (s^{-1})	Avg MPS	Avg VMS (Pa)
3.7	1021692 (135471)	0.462 (0.02)	15877 (279.4)	6577 (271.4)	0.671 (0.03)	58.1 (23.0)	27.1 (11.9)	0.076 (0.001)	2795 (18.8)
4.2	2028073 (489757)	0.524 (0.026)	17962 (840.9)	7345 (74.3)	0.763 (0.015)	52.9 (2.6)	27.8 (2.7)	0.090 (0.001)	3251 (48.2)

Case 12

Case #12 involved a 49 year old male with no record of previous head injury. He was carrying boxes when he slipped and hit his head on the pavement. The medical scans showed left parietal epidural hematoma.

Mathematic Dynamic Models (MAYDMO) reconstructions

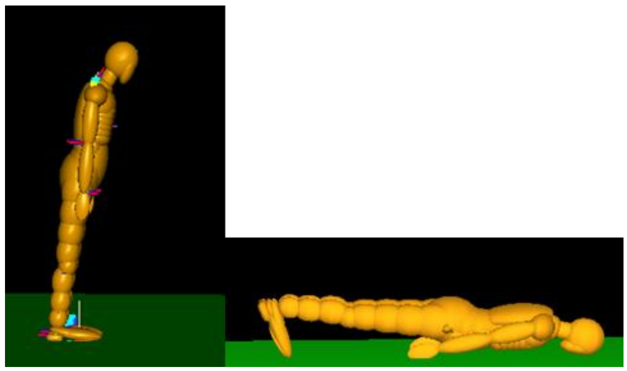

Figure 1. Simulation 1

Impact velocity: 4.87 m/s

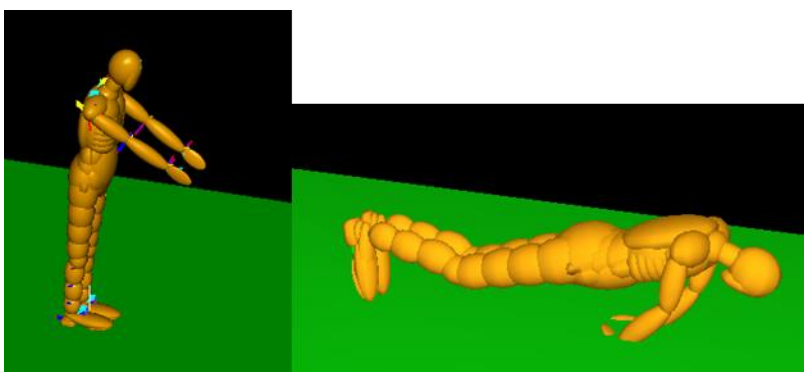

Figure 2. Simulation 2

Impact velocity: 3.6 m/s

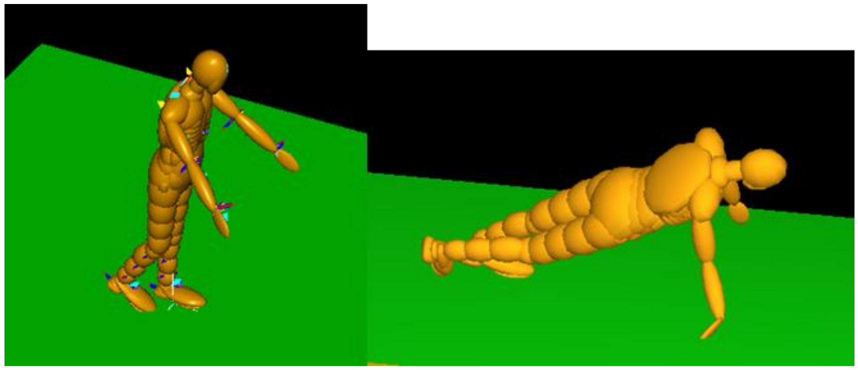

Figure 3. Simulation 3

Impact velocity: 3.8 m/s

Medical imaging (CT scans)

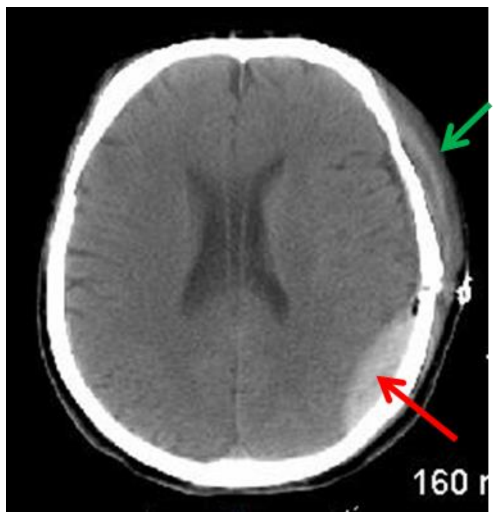

Figure 4. Medical images showing epidural hematoma (red arrow). Impact site indicated by green arrow.

Physical reconstruction

Figure 5. Hybrid III physical reconstruction of case 12

Table 1. Dynamic response peak resultant values for the reconstruction

	Acceleration	
Velocity (m/s)	Linear (g)	Rotational (rad/s^2)
3.6	327.5 (44.1)	33857 (788.1)
3.8	332.7 (3.9)	37555 (688.4)
4.9	501.8 (13.7)	55847 (703.7)

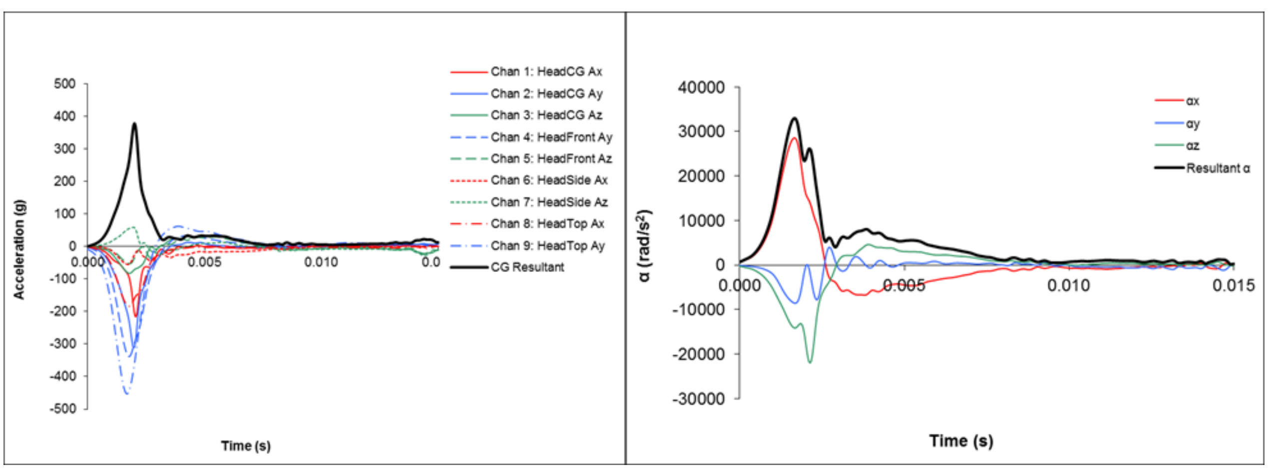

Figure 6. Sample dynamic response curves for the physical reconstruction of case 12. Linear acceleration presented on the left, rotational on the right.

Finite element model region of interest and sizing

The brain was measured to be 13 cm high from brainstem to top of the head, 15.9 cm long from front to back and 13.7 cm wide from ear to ear. The UCDBTM was scaled to the closest dimensions which were: 12.3 cm high, 15.3 cm long and 12.1 cm wide.

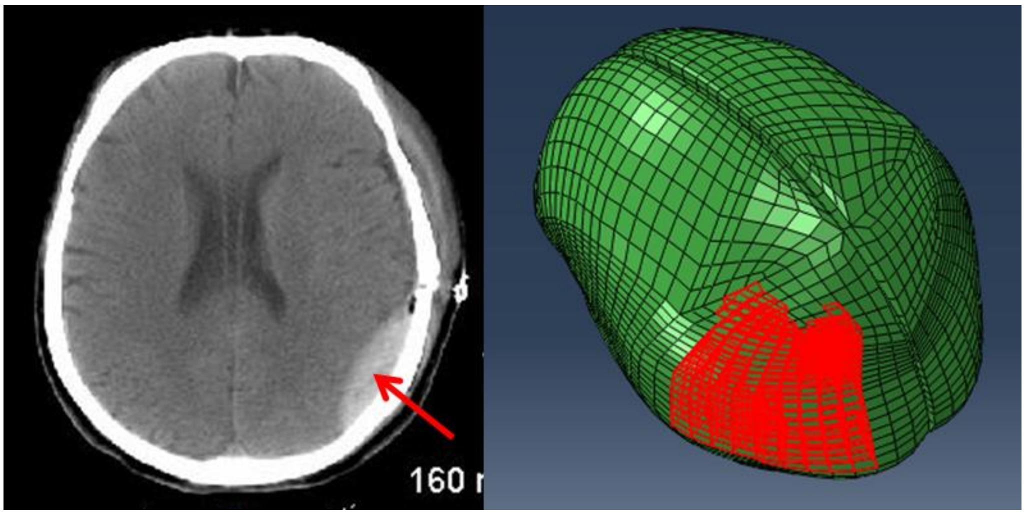

Figure 7. UCDBTM region of interest representing the region of the epidural hematoma (red)

Finite element modeling results

Table 2. UCDBTM results for the epidural hematoma region. Bold signifies significance between the EDH region and the cerebrum ($p < 0.05$).

Velocity (m/s)	Pressure (Pa)	MPS	VMS (Pa)	Shear stress (Pa)	Shear Strain	Strain rate (s^{-1})	Product (s^{-1})	Avg MPS	Avg VMS (Pa)
3.6	393708 (10391)	0.322 (0.006)	11167 (103.1)	4990 (45.2)	0.535 (0.004)	71.5 (1.4)	23.0 (0.9)	0.11 (0.001)	3982 (59.8)
Significance	0.181	**0.001**	**0.001**	**0.001**	**0.001**	**0.001**	**0.001**	**0.002**	**0.023**
3.8	432651 (10046)	0.333 (0.005)	11984 (132.0)	5253 (65.3)	0.558 (0.007)	74.1 (1.0)	24.7 (0.7)	0.118 (0.001)	4325 (42.4)
Significance	**0.002**	**0.001**	**0.001**	**0.001**	**0.001**	**0.001**	**0.001**	**0.001**	**0.001**
4.9	671264 (19033)	0.394 (0.004)	14751 (116.1)	6220 (107.5)	0.668 (0.012)	93.8 (1.0)	36.9 (0.8)	0.145 (0.001)	5295 (140.1)
Significance	**0.018**	**0.001**	**0.001**	**0.001**	**0.001**	**0.001**	**0.001**	**0.001**	**0.001**

Table 3. UCDBTM results for the cerebrum.

Velocity (m/s)	Pressure (Pa)	MPS	VMS (Pa)	Shear stress (Pa)	Shear Strain	Strain rate (s^{-1})	Product (s^{-1})	Avg MPS	Avg VMS (Pa)
3.6	2290206 (2027475)	0.861 (0.014)	29208 (233.5)	13858 (155.0)	1.36 (0.01)	162.5 (2.8)	139.8 (0.5)	0.121 (0.003)	4276 (129.4)
3.8	1832147 (354744)	0.899 (0.01)	31264 (620.0)	14744 (115.8)	1.46 (0.02)	169.8 (7.4)	152.7 (8.4)	0.129 (0.002)	4735 (37.0)
4.9	3437723 (1229842)	1.11 (0.025)	42786 (1080)	17819 (263.5)	1.7 (0.052)	232.0 (5.2)	2588.3 (11.7)	0.158 (0.001)	6007 (39.3)

Case 13

Case #13 involved a 45 year old male with no record of previous head injury. He slipped and hit the posterior aspect of his head from a standing position on his wooden dock. The medical scans showed subdural hematoma on the left side in the occipital region.

Mathematic Dynamic Models (MAYDMO) reconstructions

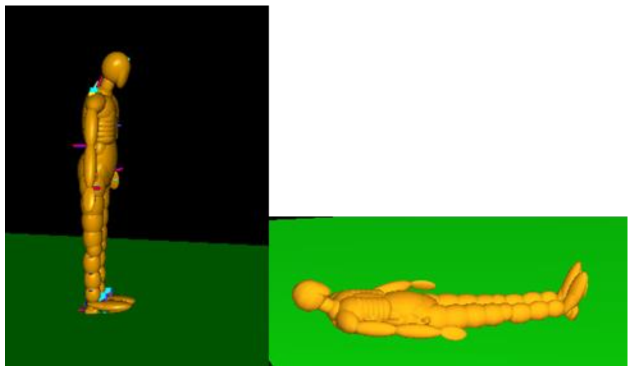

Figure 1. Simulation 1

Impact velocity: 6.2 m/s

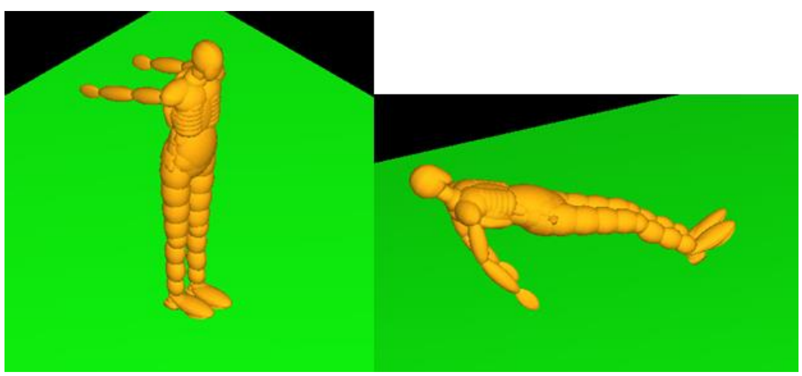

Figure 2. Simulation 2

Impact velocity: 5.0 m/s

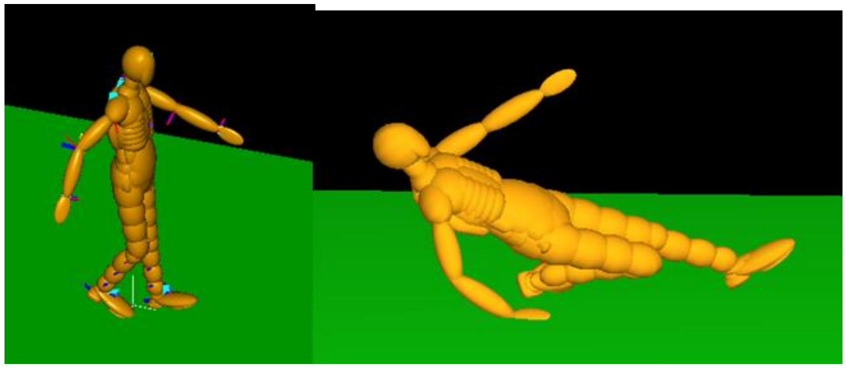

Figure 3. Simulation 3

Impact velocity: 4.8 m/s

Medical imaging (CT scans)

Figure 4. Medical images showing subdural hematoma (red arrow).

Physical reconstruction

The impact location was derived from the Neurotrauma injury report form. Only the 4.8 and 5.0 m/s condition was conducted as the accelerations were approaching the sensor tolerances at that velocity. To go higher would have damaged the equipment.

Figure 5. Hybrid III physical reconstruction of case 13.

Table 1. Dynamic response peak resultant values for the reconstruction

	Acceleration	
Velocity (m/s)	Linear (g)	Rotational (rad/s^2)
4.8	414.3 (7.7)	30799 (398.7)
5.0	449.5 (3.5)	33714 (489.3)

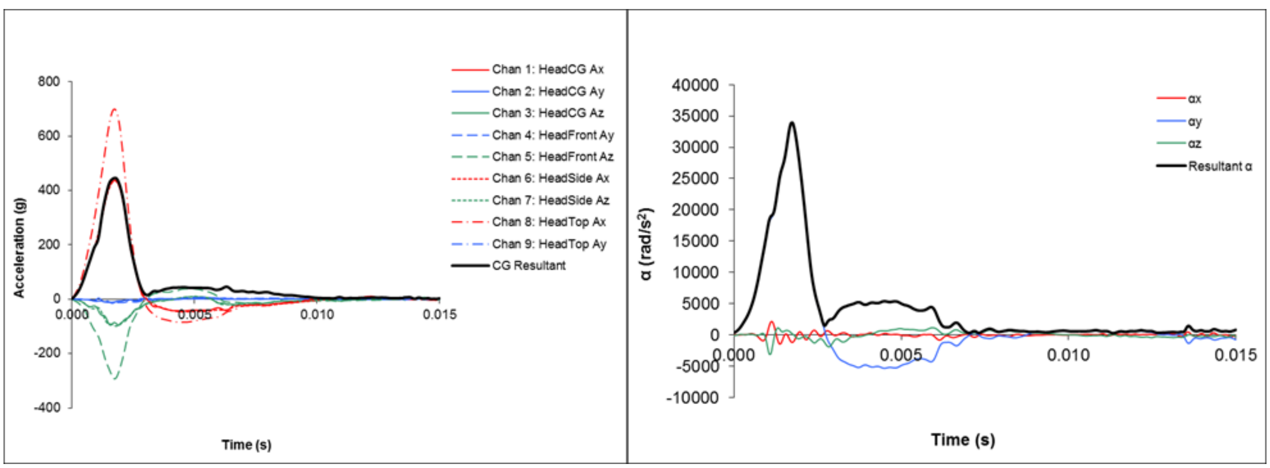

Figure 6. Sample dynamic response curves for the physical reconstruction of case 13. Linear acceleration presented on the left, rotational on the right.

Finite element model region of interest and sizing

The brain was measured to be 13 cm high from brainstem to top of the head, 17.5 cm long from front to back and 13 cm wide from ear to ear. The UCDBTM was scaled to the closest dimensions which were: 14.0 cm high, 17.6 cm long and 13.1 cm wide.

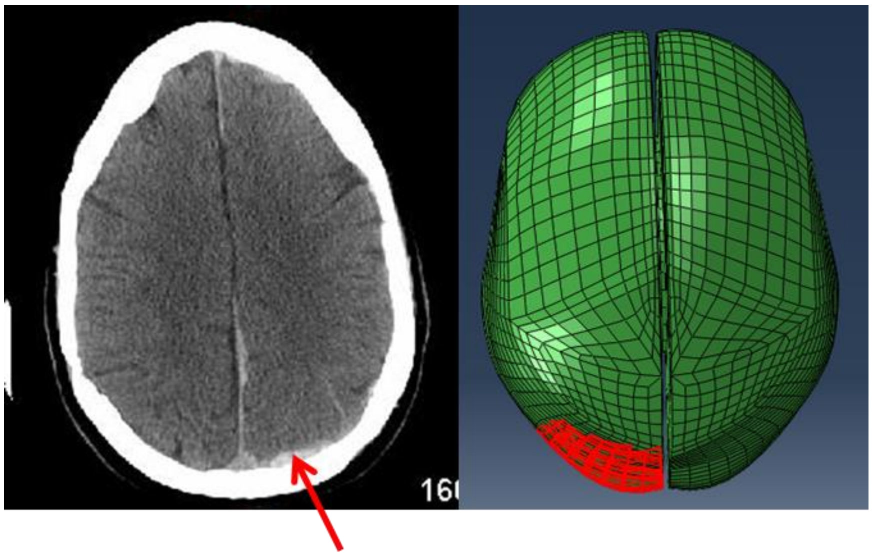

Figure 7. UCDBTM region of interest representing the region of the subdural hematoma (red)

Finite element modeling results

Table 2. UCDBTM results for the subdural hematoma region. Bold signifies significance between the SDH region and the cerebrum ($p < 0.05$).

Velocity (m/s)	Pressure (Pa)	MPS	VMS (Pa)	Shear stress (Pa)	Shear Strain	Strain rate (s^{-1})	Product (s^{-1})	Avg MPS	Avg VMS (Pa)
4.8	1600121 (45907)	0.391 (0.007)	15377 (254.2)	6566 (412.1)	0.564 (0.049)	85.1 (15.2)	33.3 (6.4)	0.148 (0.007)	5426 (115.9)
Significance	0.677	**0.001**	**0.001**	**0.001**	**0.001**	**0.001**	**0.001**	**0.003**	**0.001**
5.0	1669362 (111232)	0.417 (0.008)	14669 (562.2)	6541 (102.8)	0.552 (0.006)	104.5 (6.4)	43.6 (3.5)	0.157 (0.004)	5698 (108.6)
Significance	**0.007**	**0.001**	**0.001**	**0.001**	**0.001**	0.436	0.069	**0.006**	**0.001**

Table 3. UCDBTM results for the cerebrum.

Velocity (m/s)	Pressure (Pa)	MPS	VMS (Pa)	Shear stress (Pa)	Shear Strain	Strain rate (s^{-1})	Product (s^{-1})	Avg MPS	Avg VMS (Pa)
4.8	1374051 (873117)	0.791 (0.005)	26525 (290.0)	11422 (338.4)	1.25 (0.036)	161.6 (5.2)	127.9 (3.9)	0.117 (0.004)	5260 (138.3)
5.0	2901478 (408580)	0.842 (0.04)	27739 (937.6)	11902 (617.6)	1.24 (0.05)	135.4 (61.5)	112.4 (48.2)	0.115 (0.013)	4495 (36.2)

Case 14

Case #14 involved a 52 year old male with no record of previous head injury. He slipped and fell on the ice covered pavement hitting his head on the curb. The medical scans showed frontal contusion and subdural hematoma in the occipital lobe.

Mathematic Dynamic Models (MAYDMO) reconstructions

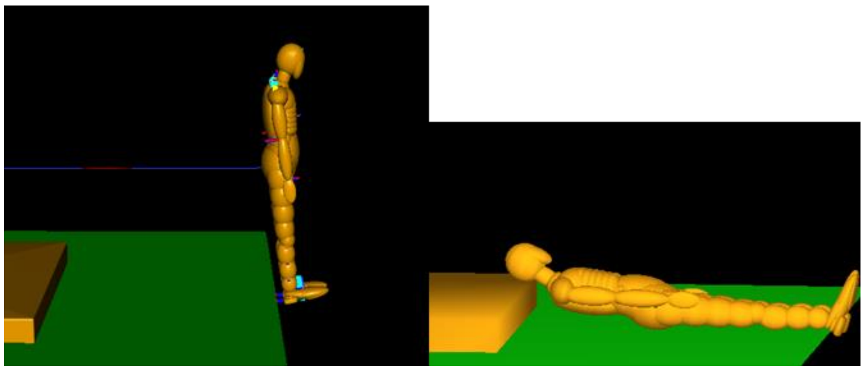

Figure 1. Simulation 1, curb height of 0.15 m.

Impact velocity: 6.0 m/s

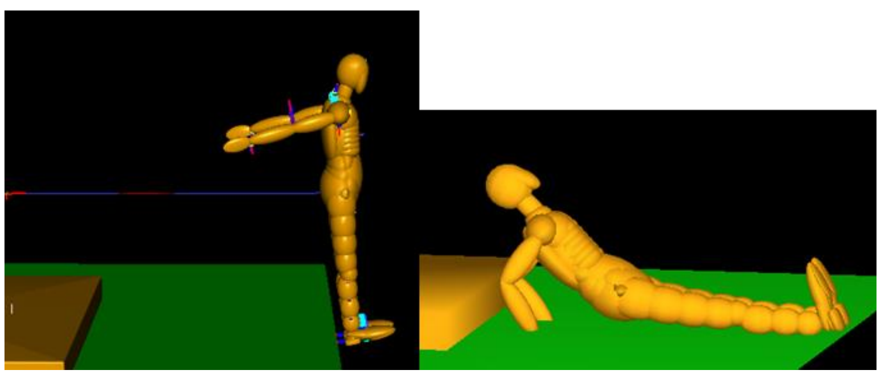

Figure 2. Simulation 2, curb height of 0.15 m.

Head Impact velocity: 3.8 m/s

Medical imaging (CT scans)

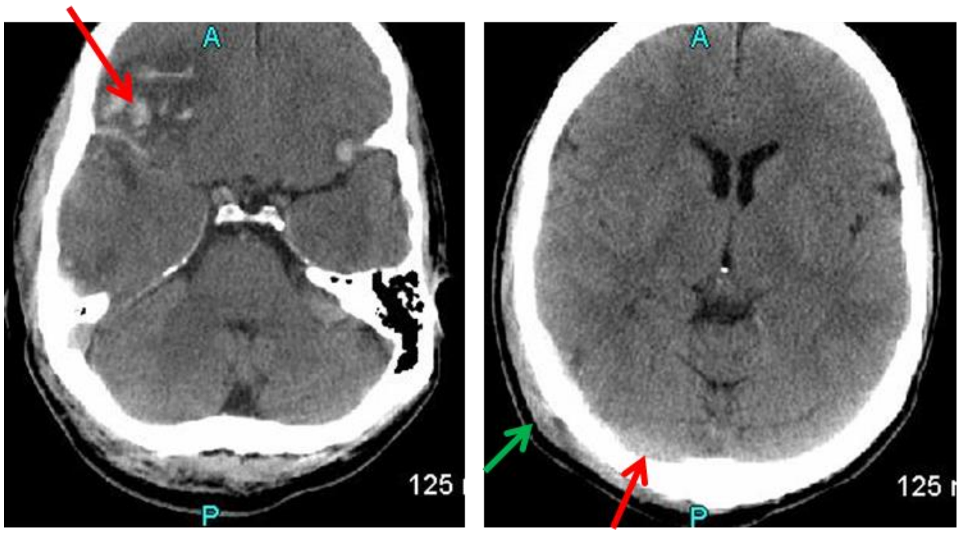

Figure 3. Medical images showing (left) contusion; (right) subdural hematoma (red arrow) and impact site (green arrow).

Physical reconstruction

Only the 3.8 m/s condition was conducted as the accelerations were approaching the sensor tolerances at that velocity. To go higher would have damaged the equipment.

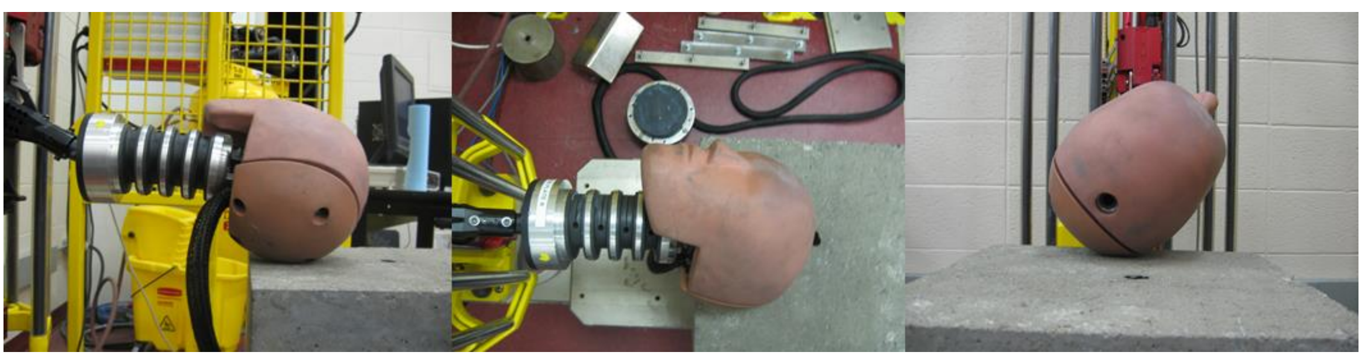

Figure 4. Hybrid III physical reconstruction of case 14.

Table 1. Dynamic response peak resultant values for the reconstruction

	Acceleration	
Velocity (m/s)	Linear (g)	Rotational (rad/s^2)
3.8	256.3 (18.7)	23353 (2619)

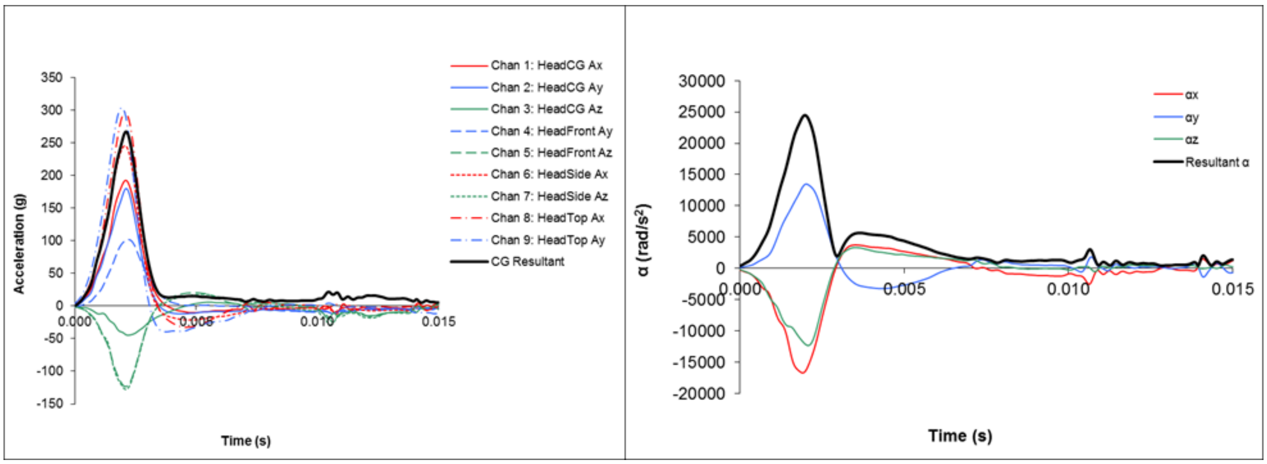

Figure 5. Sample dynamic response curves for the physical reconstruction of case 14. Linear acceleration presented on the left, rotational on the right.

Finite element model region of interest and sizing

The CT scans were of low quality and brain dimensions were not calculated. The UCDBTM was set to the dimensions of: 14.0 cm high, 17.6 cm long from front to back, and 13.1 cm wide.

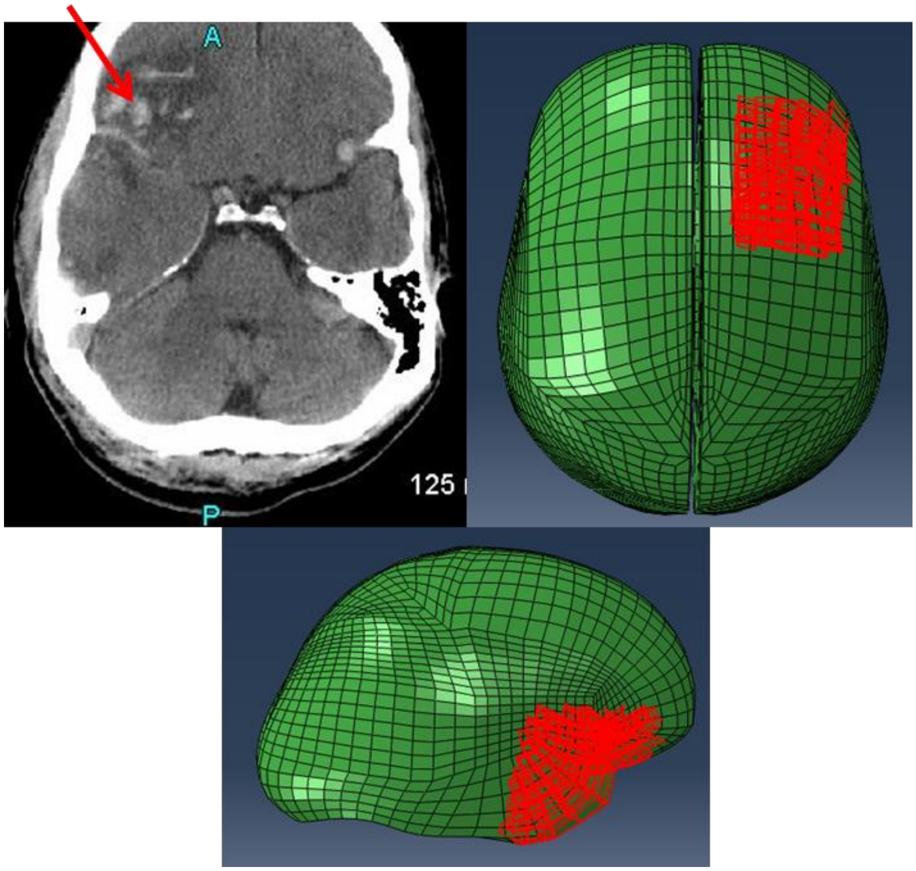

Figure 6. UCDBTM region of interest representing the region of the contusion (red)

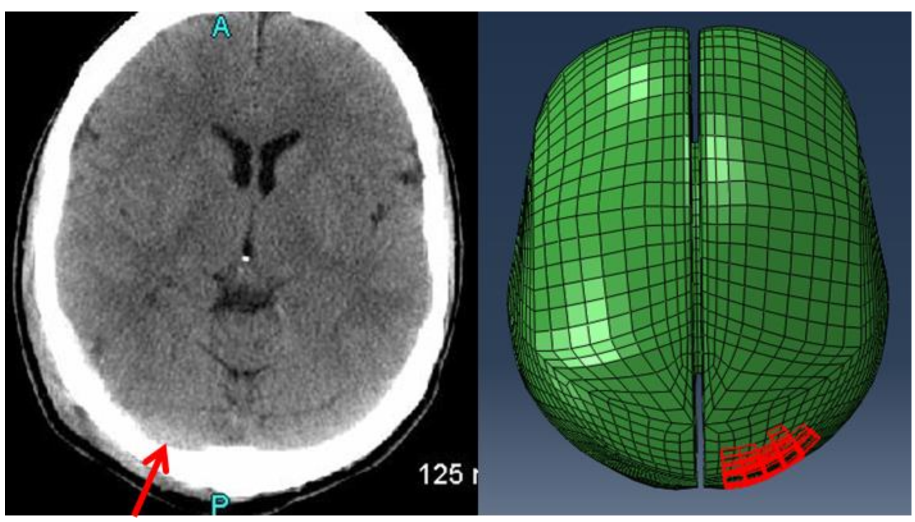

Figure 7. UCDBTM region of interest representing the region of the subdural hematoma (red)

Finite element modeling results

Table 2. UCDBTM results for the contusion region. Bold signifies significance between the contusion region and the cerebrum ($p < 0.05$).

Velocity (m/s)	Pressure (Pa)	MPS	VMS (Pa)	Shear stress (Pa)	Shear Strain	Strain rate (s^{-1})	Product (s^{-1})	Avg MPS	Avg VMS (Pa)
3.8	404932 (64342)	0.405 (0.014)	13225 (421.3)	6092 (324.6)	0.703 (0.032)	61.3 (2.1)	24.8 (1.7)	0.137 (0.001)	3553 (938.5)
Significance	**0.027**	**0.001**	**0.001**	**0.001**	0.058	0.419	0.131	**0.050**	0.809

Table 3. UCDBTM results for the subdural hematoma region. Bold signifies significance between the SDH region and the cerebrum ($p < 0.05$).

Velocity (m/s)	Pressure (Pa)	MPS	VMS (Pa)	Shear stress (Pa)	Shear Strain	Strain rate (s^{-1})	Product (s^{-1})	Avg MPS	Avg VMS (Pa)
3.8	621619 (37518)	0.232 (0.006)	6867 (149.5)	2682 (23.5)	0.285 (0.004)	51.5 (1.2)	11.9 (0.6)	0.114 (0.002)	3920 (73.1)
Significance	**0.041**	**0.001**	**0.001**	**0.001**	**0.001**	0.218	**0.033**	0.590	0.057

Table 4. UCDBTM results for the cerebrum

Velocity (m/s)	Pressure (Pa)	MPS	VMS (Pa)	Shear stress (Pa)	Shear Strain	Strain rate (s^{-1})	Product (s^{-1})	Avg MPS	Avg VMS (Pa)
3.8	2085556 (850052)	0.568 (0.01)	19901 (1372)	7895 (159.5)	0.758 (0.017)	77.1 (30.4)	43.8 (17.3)	0.108 (0.018)	3404 (329.4)

Case 15

Case #15 involved a 76 year old female with no record of previous head injury. She was standing on the step at the back door of her house, facing the door when she fell backwards. She then hit the back of her head on the vertical concrete/cement wall behind her. The fall resulted in an impact to the occipital bone, slightly to the left of the midline as evidenced by a laceration. The CT scans of the subject showed a large parenchymal haemorrhage of the right temporal lobe, and a small focal contusion on the cortical surface of the left frontal lobe.

Mathematic Dynamic Models (MAYDMO) reconstructions

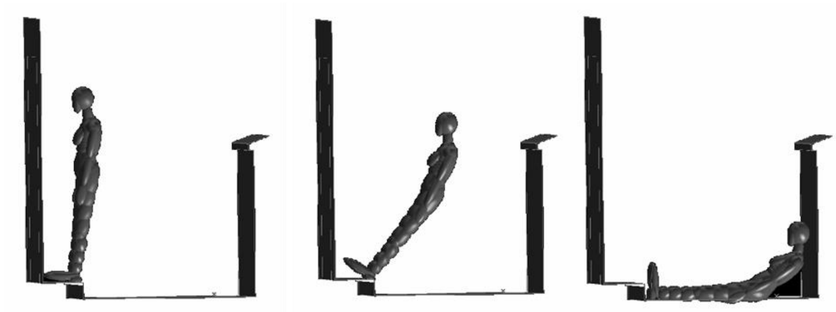

Figure 1. MADYMO Simulation results (From Doorly, 2007)

Impact velocity: 4.8 m/s

Medical imaging (CT scans)

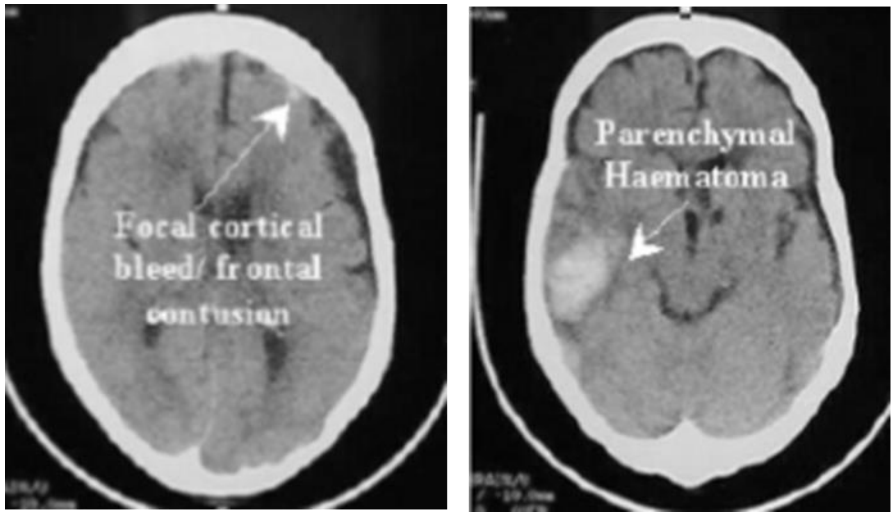

Figure 2. Medical images showing (left) contusion; (right) parenchymal hematoma (red arrow).

Physical reconstruction

The impact site was identified from Doorly's (2007) research on reconstructions of TBI incidents.

Figure 3. Hybrid III physical reconstruction of case 15.

Table 1. Dynamic response peak resultant values for the reconstruction

	Acceleration	
Velocity (m/s)	Linear (g)	Rotational (rad/s^2)
4.8	448.0 (15.1)	31668 (672.8)

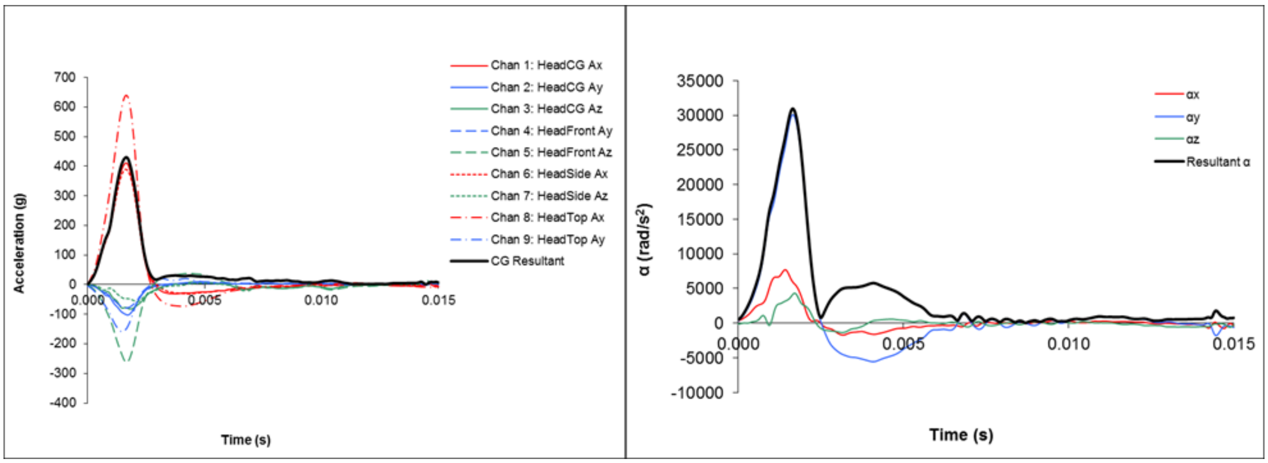

Figure 4. Sample dynamic response curves for the physical reconstruction of case 15. Linear acceleration presented on the left, rotational on the right.

Finite element model region of interest and sizing

The UCDBTM was set to the dimensions of: 14.0 cm high, 17.6 cm long from front to back, and 13.1 cm wide to match the dimensions used in Doorly's (2007) research.

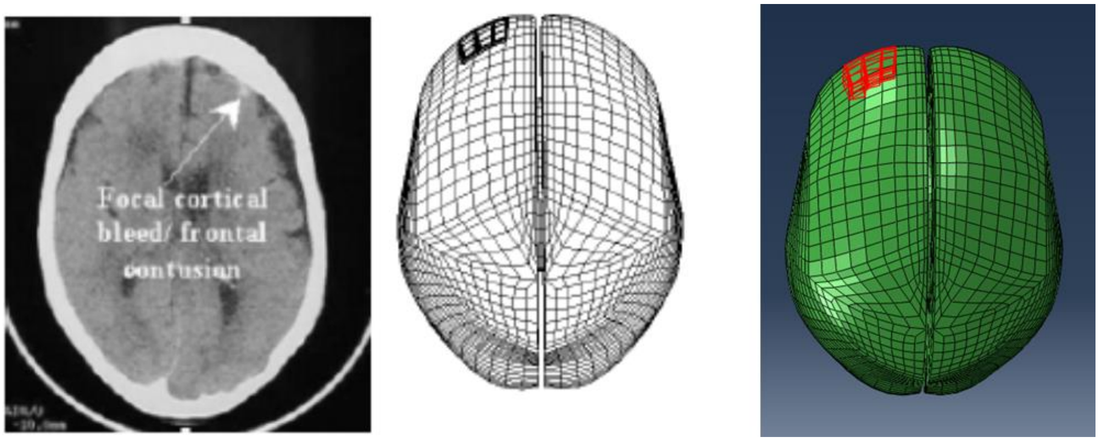

Figure 5. UCDBTM region of interest representing the region of the contusion for Doorly's (2007) FE reconstruction (middle) and the current reconstruction (red).

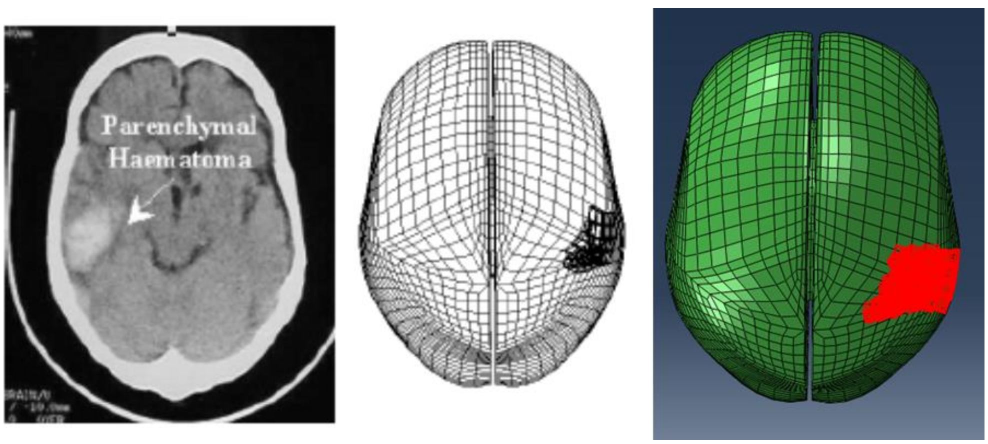

Figure 6. UCDBTM region of interest representing the region of the parenchymal hemorrhage for Doorly's (2007) FE reconstruction (middle) and the current reconstruction (red).

Finite element modeling results

Table 2. UCDBTM results for the contusion region. Bold signifies significance between the contusion region and the cerebrum ($p < 0.05$).

Velocity (m/s)	Pressure (Pa)	MPS	VMS (Pa)	Shear stress (Pa)	Shear Strain	Strain rate (s^{-1})	Product (s^{-1})	Avg MPS	Avg VMS (Pa)
4.8	1063102 (24508)	0.279 (0.012)	10136 (144.9)	4765 (179.6)	0.506 (0.024)	39.0 (2.4)	10.9 (1.1)	0.204 (0.008)	4181 (1567)
Significance	**0.007**	**0.001**	**0.001**	**0.001**	**0.001**	**0.007**	**0.005**	**0.002**	0.862

Table 3. UCDBTM results for the parenchymal hemorrhage region. Bold signifies significance between the parenchymal hemorrhage region and the cerebrum ($p < 0.05$).

Velocity (m/s)	Pressure (Pa)	MPS	VMS (Pa)	Shear stress (Pa)	Shear Strain	Strain rate (s^{-1})	Product (s^{-1})	Avg MPS	Avg VMS (Pa)
4.8	767545 (18245)	0.304 (0.007)	9876 (181.2)	4499 (50.2)	0.462 (0.006)	40.2 (4.6)	12.2 (1.4)	0.108 (0.006)	3725 (182.8)
Significance	**0.005**	**0.001**	**0.001**	**0.001**	**0.001**	**0.007**	**0.005**	**0.044**	0.139

Table 4. UCDBTM results for the cerebrum.

Velocity (m/s)	Pressure (Pa)	MPS	VMS (Pa)	Shear stress (Pa)	Shear Strain	Strain rate (s^{-1})	Product (s^{-1})	Avg MPS	Avg VMS (Pa)
4.8	3963774 (985452)	0.770 (0.031)	24187 (1498)	11374 (505.4)	1.25 (0.05)	133.9 (32.0)	103.7 (29.0)	0.134 (0.015)	4012 (198.8)

Case 16

Case #16 involved an 85 year old man who lost his balance while walking in the garden behind his house. He fell directly forward and hit his forehead on the ground, without using any body parts to break his fall. The impact surface was a concrete path and he hit no other objects during the fall. The CT scan showed a left side chronic subdural hematoma and a right acute subdural hematoma with a midline shift to the left.

Mathematic Dynamic Models (MAYDMO) reconstructions

Figure 1. MADYMO Simulation results (From Doorly, 2007)

Impact velocity: 5.1 m/s

Medical imaging (CT scans)

Figure 2. Medical images showing bilateral subdural hematomas (red arrows).

Physical reconstruction

The impact site was identified from Doorly's (2007) research on reconstructions of TBI incidents.

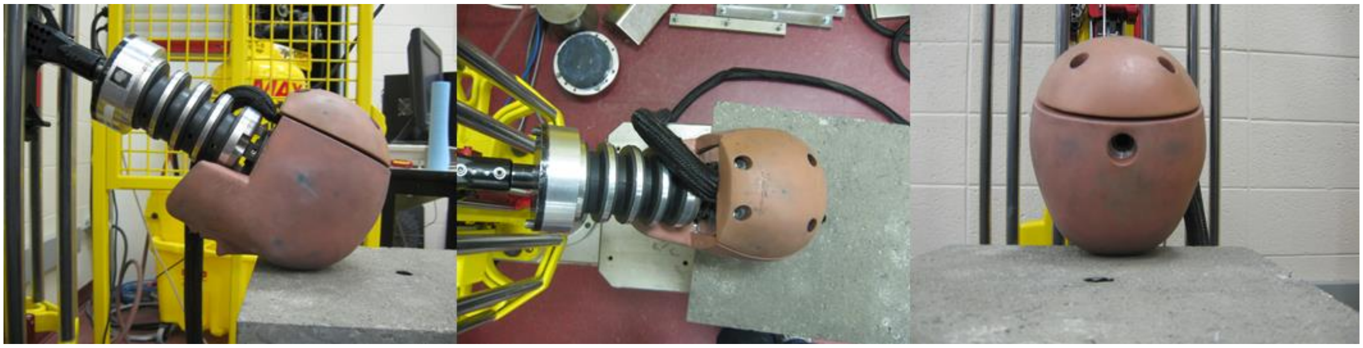

Figure 3. Hybrid III physical reconstruction of case 16.

Table 1. Dynamic response peak resultant values for the reconstruction

	Acceleration	
Velocity (m/s)	Linear (g)	Rotational (rad/s^2)
5.1	686.9 (50.5)	54930 (2681)

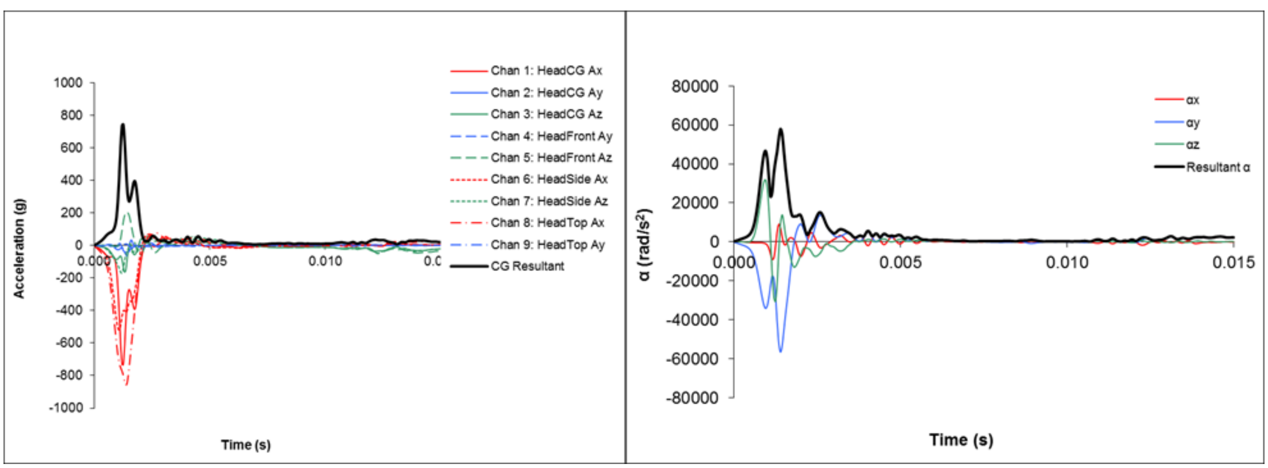

Figure 4. Sample dynamic response curves for the physical reconstruction of case 16. Linear acceleration presented on the left, rotational on the right.

Finite element model region of interest and sizing

The UCDBTM was set to the dimensions of: 14.0 cm high, 17.6 cm long from front to back, and 13.1 cm wide to match the dimensions used in Doorly's (2007) research.

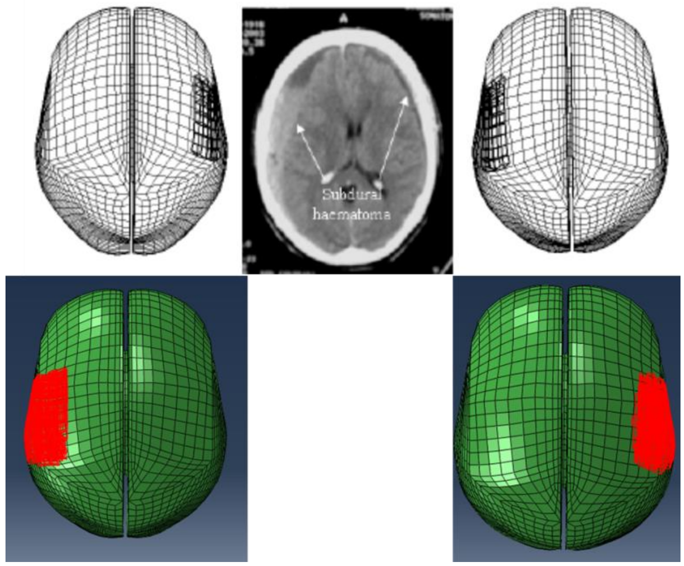

Figure 5. UCDBTM region of interest representing the region of the bilateral subdural hematomas for Doorly's (2007) FE reconstruction (top) and the current reconstruction (bottom).

Finite element modeling results

Table 2. UCDBTM results for the left subdural hematoma region. Bold signifies significance between the SDH region and the cerebrum ($p < 0.05$).

Velocity (m/s)	Pressure (Pa)	MPS	VMS (Pa)	Shear stress (Pa)	Shear Strain	Strain rate (s^{-1})	Product (s^{-1})	Avg MPS	Avg VMS (Pa)
5.1	1192431 (127075)	0.274 (0.043)	8702 (1159)	4574 (793.3)	0.493 (0.106)	40.4 (6.5)	11.0 (1.9)	0.095 (0.014)	3219 (530.1)
Significance	**0.005**	**0.001**	**0.001**	**0.009**	**0.001**	**0.001**	**0.003**	0.172	0.092

Table 3. UCDBTM results for the right subdural hematoma region. Bold signifies significance between the SDH region and the cerebrum ($p < 0.05$).

Velocity (m/s)	Pressure (Pa)	MPS	VMS (Pa)	Shear stress (Pa)	Shear Strain	Strain rate (s^{-1})	Product (s^{-1})	Avg MPS	Avg VMS (Pa)
5.1	1218123 (120029)	0.288 (0.012)	9104 (305.1)	4105 (126.2)	0.441 (0.019)	44.5 (16.3)	12.7 (4.2)	0.083 (0.02)	2958 (543.4)
Significance	**0.005**	**0.001**	**0.001**	**0.008**	**0.000**	**0.001**	**0.003**	0.097	**0.048**

Table 4. UCDBTM results for the cerebrum

Velocity (m/s)	Pressure (Pa)	MPS	VMS (Pa)	Shear stress (Pa)	Shear Strain	Strain rate (s^{-1})	Product (s^{-1})	Avg MPS	Avg VMS (Pa)
5.1	5756451 (1409988)	1.55 (0.225)	60858 (11543)	23036 (6739)	1.85 (0.163)	476.4 (63.9)	748.0 (198.2)	0.113 (0.013)	4105 (448.8)

Case 17

Case #17 involved an 84 year old woman who lost her balance while walking on a concrete footpath. She was walking downhill and became unbalanced and fell forwards and to the right without trying to use her arms to break her fall. She ended up falling on her head, hitting the right frontal area as evidenced by scratches and bruising of the skin. The impact surface was a smooth concrete footpath. The CT scan showed a left sided subdural hematoma resulting in midline shift.

Mathematic Dynamic Models (MAYDMO) reconstructions

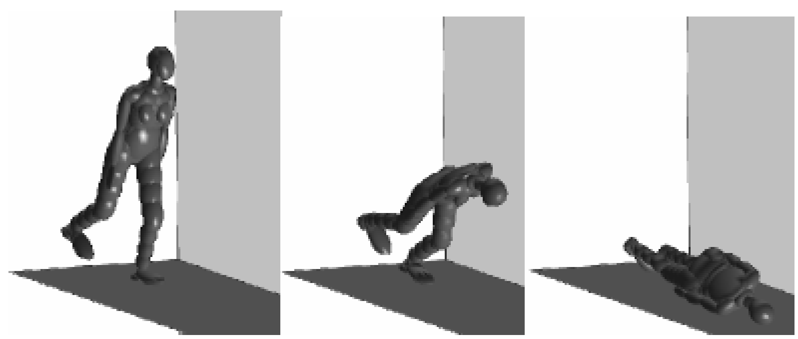

Figure 1. MADYMO Simulation results (From Doorly, 2007)

Impact velocities: 4.5 and 4.7 m/s

Medical imaging (CT scans)

Figure 2. Medical images showing the subdural hematoma (red arrow).

Physical reconstruction

The impact site was identified from Doorly's (2007) research on reconstructions of TBI incidents.

Figure 3. Hybrid III physical reconstruction of case 17.

Table 1. Dynamic response peak resultant values for the reconstruction

	Acceleration	
Velocity (m/s)	Linear (g)	Rotational (rad/s^2)
4.5	529.6 (32.3)	37840 (1698)
4.7	588.5 (9.3)	41281 (484.3)

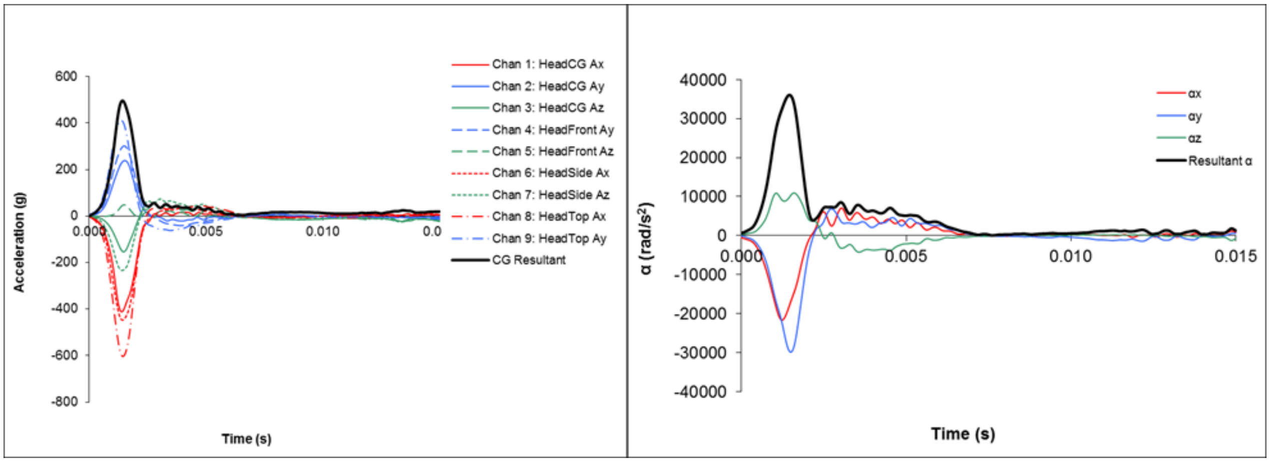

Figure 4. Sample dynamic response curves for the physical reconstruction of case 17. Linear acceleration presented on the left, rotational on the right.

Finite element model region of interest and sizing

The UCDBTM was set to the dimensions of: 14.0 cm high, 17.6 cm long from front to back, and 13.1 cm wide to match the dimensions used in Doorly's (2007) research.

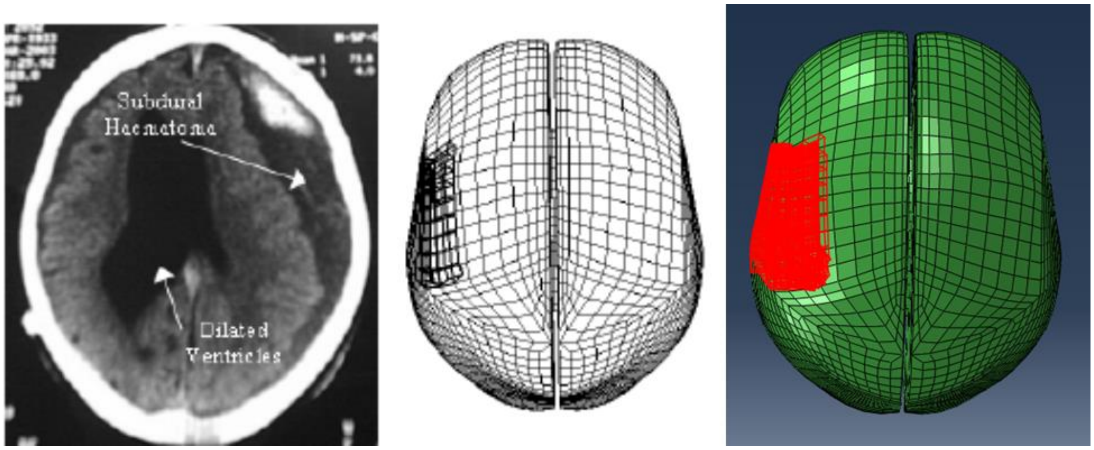

Figure 5. UCDBTM region of interest representing the region of the bilateral subdural hematomas for Doorly's (2007) FE reconstruction (middle) and the current reconstruction (right).

Finite element modeling results

Table 2. UCDBTM results for the subdural hematoma region. Bold signifies significance between the SDH region and the cerebrum ($p < 0.05$).

Velocity (m/s)	Pressure (Pa)	MPS	VMS (Pa)	Shear stress (Pa)	Shear Strain	Strain rate (s^{-1})	Product (s^{-1})	Avg MPS	Avg VMS (Pa)
4.5	921638 (19808)	0.391 (0.013)	12223 (409.7)	5026 (173.4)	0.544 (0.017)	62.5 (1.8)	24.5 (1.5)	0.106 (0.004)	3530 (110.1)
Significance	**0.002**	**0.001**	**0.001**	**0.001**	**0.001**	**0.001**	**0.001**	0.627	**0.010**
4.7	1069452 (34303)	0.401 (0.001)	12600 (102.3)	5333 (3.0)	0.568 (0.003)	70.1 (10.9)	28.1 (4.4)	0.109 (0.001)	3613 (38.4)
Significance	**0.001**	**0.001**	**0.001**	**0.001**	**0.001**	**0.001**	**0.001**	0.725	**0.008**

Table 3. UCDBTM results for the cerebrum

Velocity (m/s)	Pressure (Pa)	MPS	VMS (Pa)	Shear stress (Pa)	Shear Strain	Strain rate (s^{-1})	Product (s^{-1})	Avg MPS	Avg VMS (Pa)
4.5	5762044 (1136210)	1.14 (0.056)	42770 (1559)	16483 (407.1)	1.55 (0.07)	334.6 (31.2)	382.6 (53.6)	0.105 (0.003)	3998 (138.7)
4.7	6008800 (642589)	1.24 (0.015)	51551 (3855)	18352 (1134)	1.72 (0.081)	367.7 (12.3)	457.2 (20.6)	0.109 (0.001)	4194 (204.7)

Case 18

Case #18 involved an 84 year old woman who tripped on a path when heading to Mass. The heel of her shoe got caught in a crack and she fell forwards and to her right, hitting her right knee, arm, shoulder and impacting the right side of her face. The impact surface was the concrete footpath. The impact was deduced to have occurred to the right side of her face or head. The CT scan showed a right sided acute and chronic subdural hemorrhage with midline shift and subfalcine herniation.

Mathematic Dynamic Models (MAYDMO) reconstructions

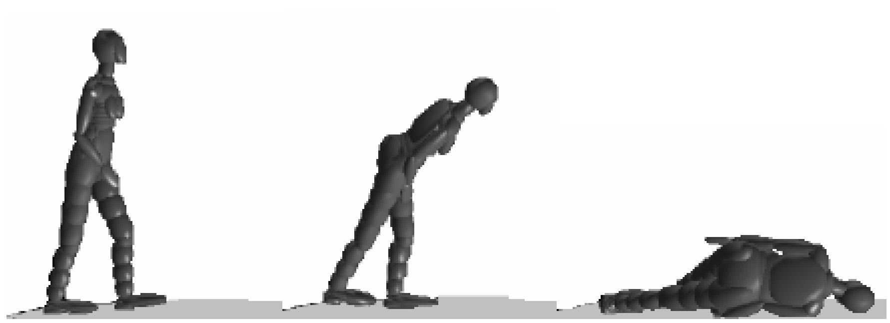

Figure 1. MADYMO Simulation results (From Doorly, 2007)

Impact velocities: 3.5 and 4.2 m/s

Medical imaging (CT scans)

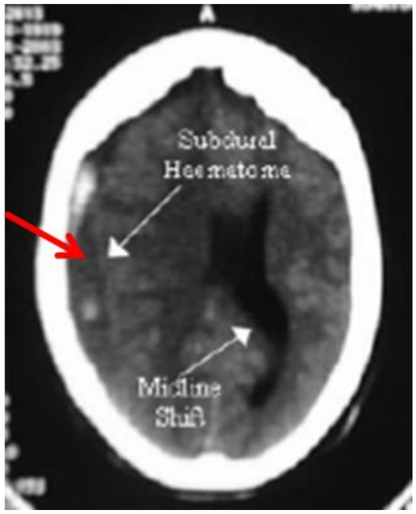

Figure 2. Medical images showing the subdural hematoma (red arrow).

Physical reconstruction

The impact site was identified from Doorly's (2007) research on reconstructions of TBI incidents.

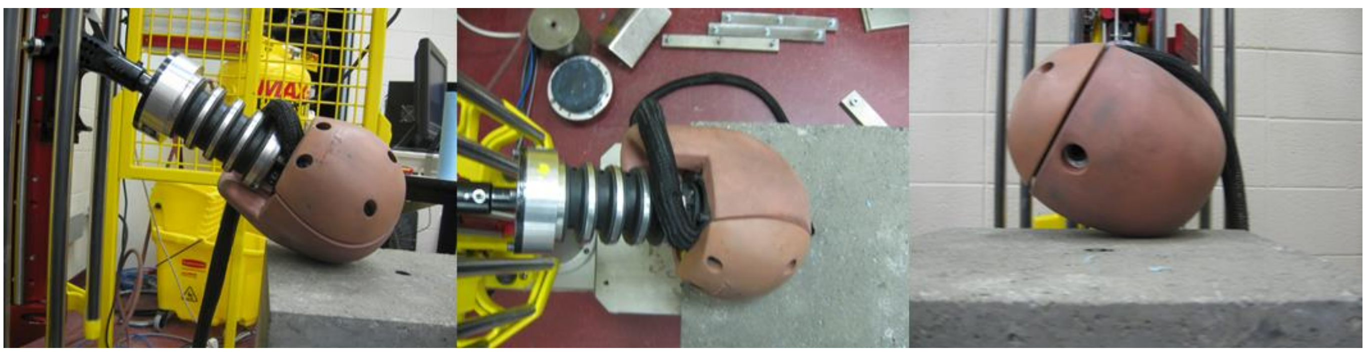

Figure 3. Hybrid III physical reconstruction of case 18.

Table 1. Dynamic response peak resultant values for the reconstruction

	Acceleration	
Velocity (m/s)	Linear (g)	Rotational (rad/s^2)
3.5	327.8 (14.1)	36320 (1678)
4.2	432.9 (10.3)	47370 (640.2)

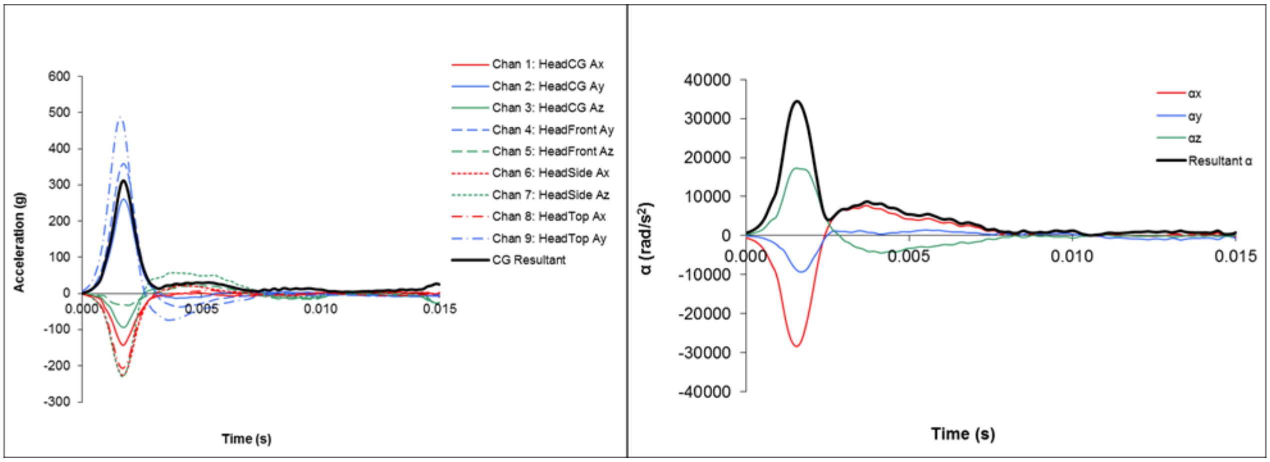

Figure 4. Sample dynamic response curves for the physical reconstruction of case 18. Linear acceleration presented on the left, rotational on the right.

Finite element model region of interest and sizing

The UCDBTM was set to the dimensions of: 14.0 cm high, 17.6 cm long from front to back, and 13.1 cm wide to match the dimensions used in Doorly's (2007) research.

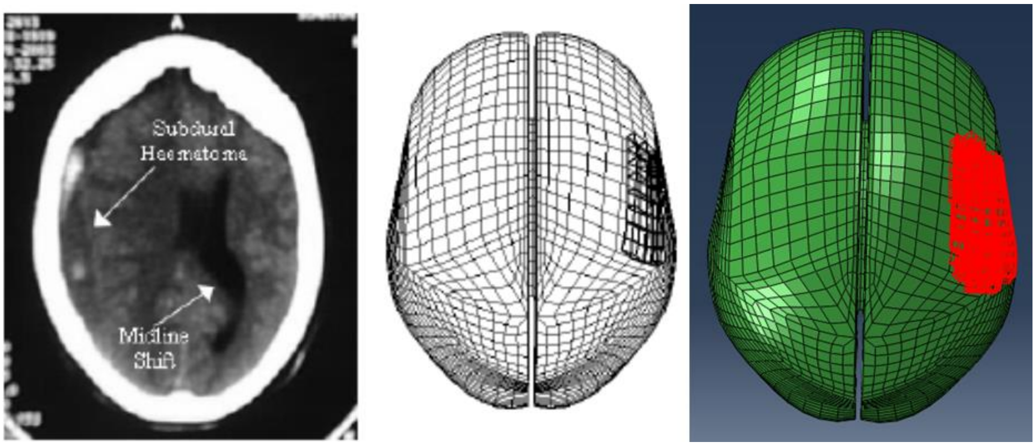

Figure 5. UCDBTM region of interest representing the region of the subdural hematoma for Doorly's (2007) FE reconstruction (middle) and the current reconstruction (right).

Finite element modeling results

Table 2. UCDBTM results for the subdural hematoma region. Bold signifies significance between the SDH region and the cerebrum ($p < 0.05$).

Velocity (m/s)	Pressure (Pa)	MPS	VMS (Pa)	Shear stress (Pa)	Shear Strain	Strain rate (s^{-1})	Product (s^{-1})	Avg MPS	Avg VMS (Pa)
3.5	651546 (11387)	0.481 (0.017)	15637 (572.9)	4617 (99.3)	0.483 (0.01)	137.5 (6.7)	66.2 (5.5)	0.113 (0.003)	3831 (90.9)
Significance	**0.005**	**0.001**	**0.001**	**0.001**	**0.001**	0.501	**0.031**	**0.004**	**0.001**
4.2	844054 (35858)	0.577 (0.006)	18808 (239.1)	5239 (28.0)	0.544 (0.013)	165.7 (1.7)	95.6 (1.8)	0.139 (0.003)	4697 (64.9)
Significance	**0.002**	**0.001**	**0.001**	**0.001**	**0.001**	**0.001**	**0.001**	**0.004**	**0.001**

Table 3. UCDBTM results for the cerebrum

Velocity (m/s)	Pressure (Pa)	MPS	VMS (Pa)	Shear stress (Pa)	Shear Strain	Strain rate (s^{-1})	Product (s^{-1})	Avg MPS	Avg VMS (Pa)
3.5	2867745 (679659)	1.00 (0.028)	37934 (1131)	14807 (257.5)	1.51 (0.025)	158.4 (48.6)	159.1 (49.1)	0.130 (0.004)	4821 (92.4)
4.2	4586402 (916154)	1.19 (0.02)	44374 (439.9)	16455 (308.4)	1.66 (0.068)	224.7 (3.9)	266.6 (5.1)	0.155 (0.004)	5807 (69.5)

Case 19

Case #19 involved a 76 year old man who fell coming back from the pub one evening. He tripped on a metal gate-stop and fell forwards and slightly to the left of centre ending up on his right side, with his right upper arm hitting the ground first. The impact site was the right side of his chin, the impact surface was concrete. The CT scan showed a right chronic subdural hematoma (which was deemed to not be a result of this fall) and a left subdural hematoma which was a result of the fall.

Mathematic Dynamic Models (MAYDMO) reconstructions

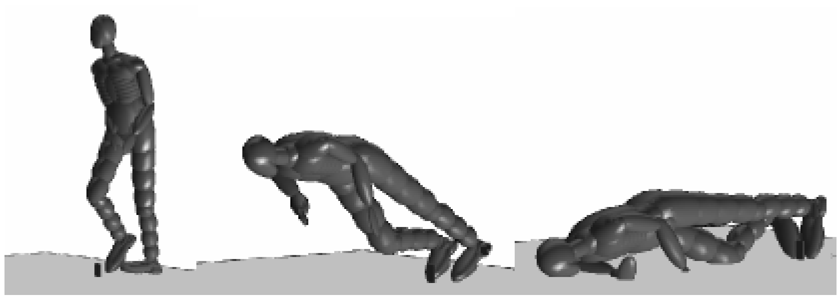

Figure 1. MADYMO Simulation results (From Doorly, 2007)

Impact velocities: 4.7 and 5.1 m/s

Medical imaging (CT scans)

Figure 2. Medical images showing the bilateral subdural hematomas (red arrow).

Physical reconstruction

The impact site was identified from Doorly's (2007) research on reconstructions of TBI incidents.

Figure 3. Hybrid III physical reconstruction of case 19.

Table 1. Dynamic response peak resultant values for the reconstruction

	Acceleration	
Velocity (m/s)	Linear (g)	Rotational (rad/s^2)
4.7	274.4 (12.4)	55520 (2941)
5.1	301.9 (12.3)	30424 (3375)

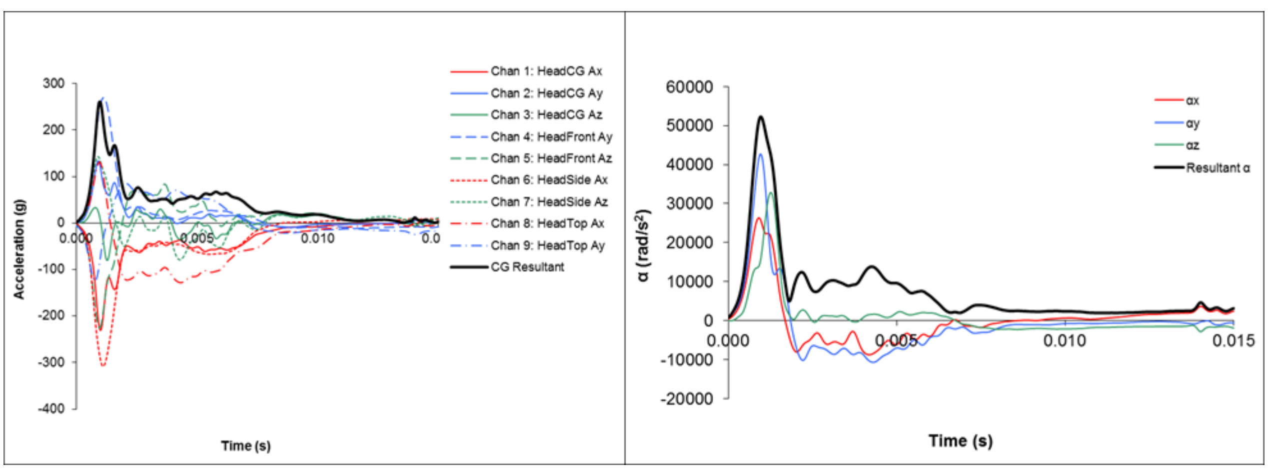

Figure 4. Sample dynamic response curves for the physical reconstruction of case 19. Linear acceleration presented on the left, rotational on the right.

Finite element model region of interest and sizing

The UCDBTM was set to the dimensions of: 14.0 cm high, 17.6 cm long from front to back, and 13.1 cm wide to match the dimensions used in Doorly's (2007) research.

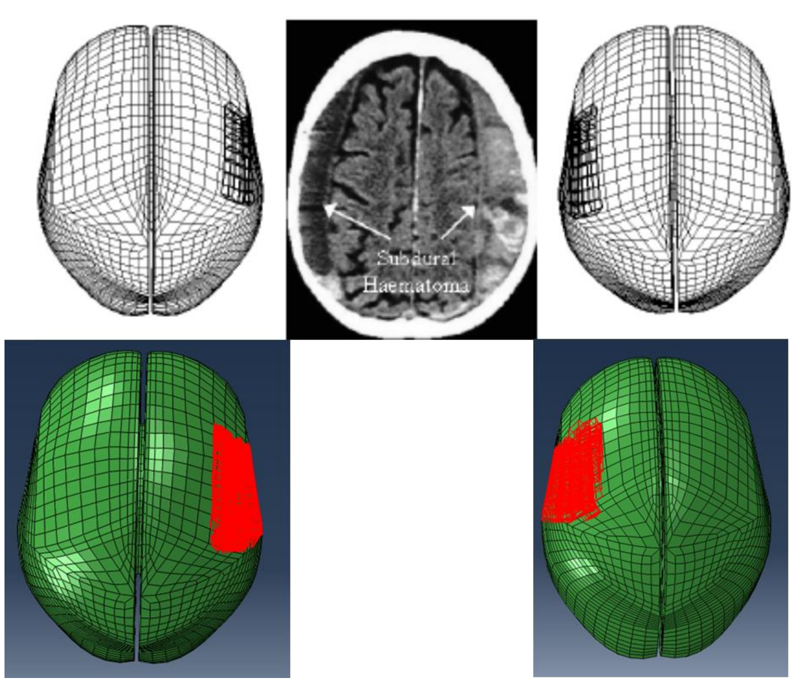

Figure 5. UCDBTM region of interest representing the region of the bilateral subdural hematomas for Doorly's (2007) FE reconstruction (top) and the current reconstruction (bottom).

Finite element modeling results

Table 2. UCDBTM results for the left subdural hematoma region. Bold signifies significance between the SDH region and the cerebrum ($p < 0.05$).

Velocity (m/s)	Pressure (Pa)	MPS	VMS (Pa)	Shear stress (Pa)	Shear Strain	Strain rate (s^{-1})	Product (s^{-1})	Avg MPS	Avg VMS (Pa)
4.7	846948 (102678)	0.303 (0.015)	11776 (109.1)	5038 (93.7)	0.592 (0.027)	39.6 (2.0)	12.0 (1.2)	0.139 (0.007)	4267 (123.8)
Significance	**0.004**	**0.001**	**0.001**	**0.001**	**0.001**	**0.002**	**0.001**	**0.010**	**0.001**
5.1	945825 (33239)	0.340 (0.006)	12467 (184.9)	5547 (87.1)	0.656 (0.008)	45.1 (0.9)	15.3 (0.6)	0.156 (0.002)	5023 (546.5)
Significance	**0.004**	**0.001**	**0.001**	**0.001**	**0.001**	**0.001**	**0.001**	**0.001**	**0.016**

Table 3. UCDBTM results for the right subdural hematoma region. Bold signifies significance between the SDH region and the cerebrum ($p < 0.05$).

Velocity (m/s)	Pressure (Pa)	MPS	VMS (Pa)	Shear stress (Pa)	Shear Strain	Strain rate (s^{-1})	Product (s^{-1})	Avg MPS	Avg VMS (Pa)
4.7	370441 (27923)	0.426 (0.013)	13421 (512.1)	5658 (107.6)	0.560 (0.020)	73.2 (28.3)	31.0 (11.6)	0.176 (0.006)	6220 (129.6)
Significance	**0.001**	**0.001**	**0.001**	**0.001**	**0.001**	0.198	**0.006**	**0.041**	**0.024**
5.1	378535 (14058)	0.472 (0.003)	14782 (156.6)	6240 (69.4)	0.608 (0.003)	100.7 (1.1)	47.5 (0.8)	0.194 (0.002)	6681 (106.3)
Significance	**0.001**	**0.001**	**0.001**	**0.001**	**0.001**	**0.001**	**0.001**	**0.001**	0.058

Table 4. UCDBTM results for the cerebrum

Velocity (m/s)	Pressure (Pa)	MPS	VMS (Pa)	Shear stress (Pa)	Shear Strain	Strain rate (s^{-1})	Product (s^{-1})	Avg MPS	Avg VMS (Pa)
4.7	1974118 (310823)	0.880 (0.017)	29886 (559.8)	12139 (743.1)	1.26 (0.076)	101.9 (15.5)	89.8 (14.8)	0.163 (0.005)	5740 (195.3)
5.1	2182314 (345762)	1.02 (0.07)	32819 (844.8)	13287 (352.8)	1.36 (0.02)	114.3 (0.8)	116.4 (7.3)	0.184 (0.001)	6360 (182.7)

Case 20

Case #20 involved an 87 year old woman who slipped on an icy ramp outside her house. She hit the front right of her head off the steel railing at the side of the path, fell forward and didn't hit her head again. The impact was considered to be right frontal. The CT scan showed a left sided subdural hematoma with the lateral ventricle shifted to the right side.

Mathematic Dynamic Models (MAYDMO) reconstructions

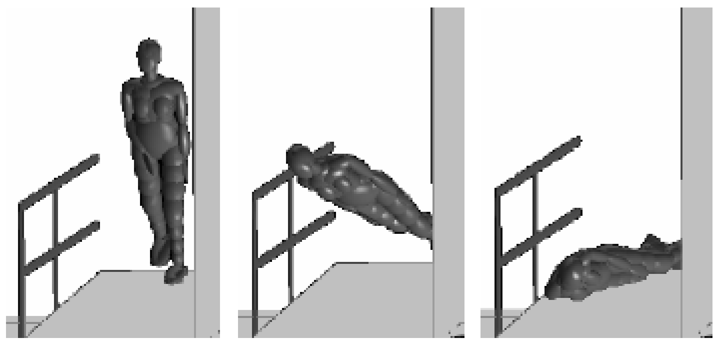

Figure 1. MADYMO Simulation results (From Doorly, 2007)

Impact velocities: 4.7 and 5.1 m/s

Medical imaging (CT scans)

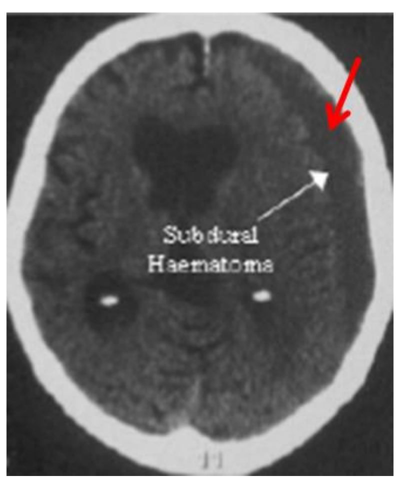

Figure 2. Medical images showing the subdural hematoma (red arrow).

Physical reconstruction

The impact site was identified from Doorly's (2007) research on reconstructions of TBI incidents.

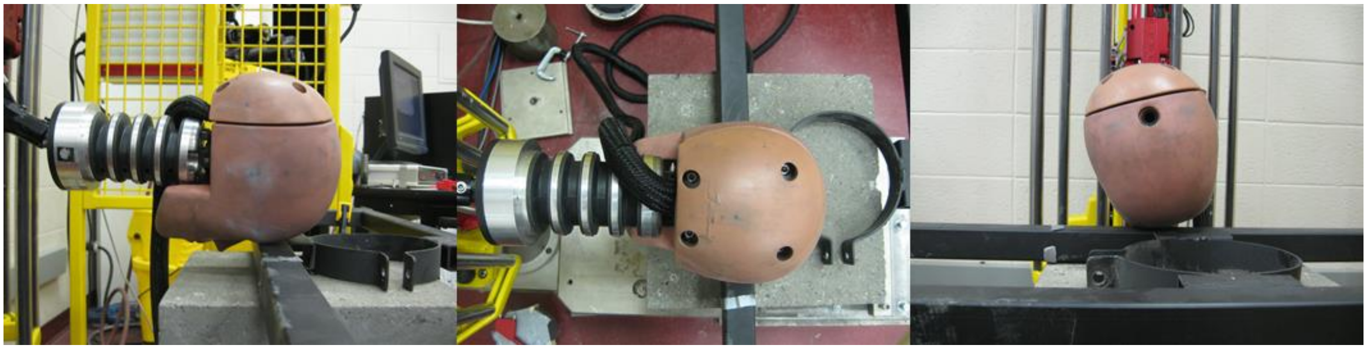

Figure 3. Hybrid III physical reconstruction of case 20.

Table 1. Dynamic response peak resultant values for the reconstruction

	Acceleration	
Velocity (m/s)	Linear (g)	Rotational (rad/s^2)
5.4	366.3 (17.2)	31607 (2807)

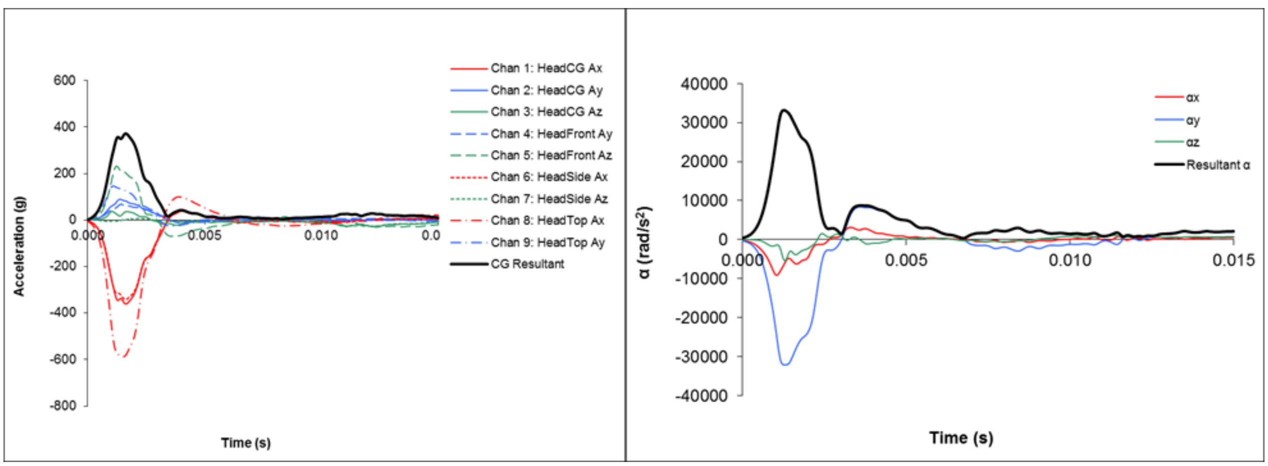

Figure 4. Sample dynamic response curves for the physical reconstruction of case 20. Linear acceleration presented on the left, rotational on the right.

Finite element model region of interest and sizing

The UCDBTM was set to the dimensions of: 14.0 cm high, 17.6 cm long from front to back, and 13.1 cm wide to match the dimensions used in Doorly's (2007) research.

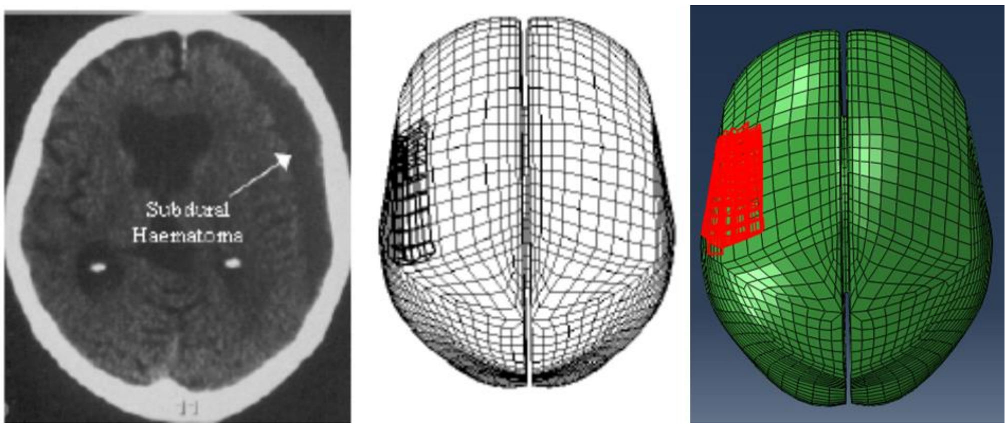

Figure 5. UCDBTM region of interest representing the region of the subdural hematoma for Doorly's (2007) FE reconstruction (middle) and the current reconstruction (right).

Finite element modeling results

Table 2. UCDBTM results for the subdural hematoma region. Bold signifies significance between the SDH region and the cerebrum ($p < 0.05$).

Velocity (m/s)	Pressure (Pa)	MPS	VMS (Pa)	Shear stress (Pa)	Shear Strain	Strain rate (s^{-1})	Product (s^{-1})	Avg MPS	Avg VMS (Pa)
5.4	718870 (66429)	0.347 (0.018)	9948 (621.2)	4212 (148.4)	0.452 (0.034)	44.7 (2.9)	15.5 (1.8)	0.100 (0.001)	3216 (43.1)
Significance	**0.001**	**0.001**	**0.001**	**0.001**	**0.001**	**0.001**	**0.001**	**0.001**	**0.001**

Table 3. UCDBTM results for the cerebrum

Velocity (m/s)	Pressure (Pa)	MPS	VMS (Pa)	Shear stress (Pa)	Shear Strain	Strain rate (s^{-1})	Product (s^{-1})	Avg MPS	Avg VMS (Pa)
5.4	2396950 (342024)	0.908 (0.046)	38514 (1304)	14553 (713.1)	1.44 (0.01)	75.3 (3.3)	68.4 (6.5)	0.138 (0.003)	5460 (125.7)

APPENDIX II

Neurotraumatic Injury Report

Patient Information

Age: ______ Gender: ☐ Male

Weight: ______ kg ☐ Female

Height: ______ cm Ethnicity: ____________________

Previous Head Injury: ☐ No ☐ Yes – Number _____

Pre-existing Medical Conditions

____

____

____

Diagnosis and General Description

Injury Diagnosis: __________________________

Incident Description: __________________________

____

____

____

____

Primary Impact Location

Please indicate the location of primary impact.

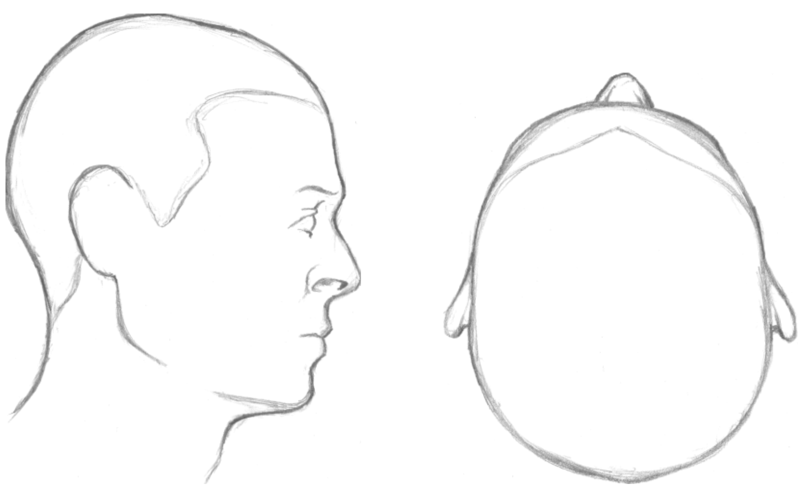

☐ Left ☐ Right

Documentation

Physician: __________________________

Hospital: __________________________

Date: (Y Y Y Y / M M / D D)

Glasgow Coma Scale

Eyes: ☐ 1 ☐ 2 ☐ 3 ☐ 4 ☐ Closed

Verbal: ☐ 1 ☐ 2 ☐ 3 ☐ 4 ☐ 5 ☐ Tube

Motor: ☐ 1 ☐ 2 ☐ 3 ☐ 4 ☐ 5 ☐ 6

Loss of Consciousness

☐ No ☐ Yes – Duration ________ minutes

Symptoms of Confusion

☐ No ☐ Yes – Duration ________ minutes

Fall

☐ N/A

Drop: ______ cm Initial Contact: ☐ Head ☐ Other

Impact Surface:

☐ Sand ☐ Grass ☐ Gravel ☐ Concrete

☐ Ice ☐ Steel ☐ Other: ____________

Collision

☐ N/A

Object: ______________________________

Weight: ______ kg Speed: ☐ Slow ☐ Moderate ☐ Fast

Material: _______________

Mode:

☐ Walk ☐ Run ☐ Bike ☐ Skate

☐ Ski ☐ Car ☐ Other: ____________

Helmet

☐ N/A

Make: ____________ Model: ____________

Size: ____________

Available for Analysis: ☐ No ☐ Yes

Supporting Documents (Please attach)

Injury Picture: ☐ No ☐ Yes

Incident Video: ☐ No ☐ Yes

MRI: ☐ No ☐ Yes

CT: ☐ No ☐ Yes

DTI: ☐ No ☐ Yes